FLOW AND HEAT TRANSFER IN CURVED DUCTS

by

Vanka Surya Pratap

Thesis submitted for the degree of
Doctor of Philosophy
in the Faculty of Engineering
University of London
and
for the Diploma of Membership
of Imperial College

Mechanical Engineering Department
Imperial College
London, S.W.7.

August, 1975

ABSTRACT

The partial-differential equations governing flow and heat-transfer phenomena in curved ducts are solved using a finite-difference calculation procedure. Both laminar and turbulent flows are considered; and the predicted distributions of flow variables are compared with experimental data. Primary importance is given to the computation of the developing regions of the flow and temperature fields, which are three-dimensional in nature. Predictions are also presented of the fully-developed flow and temperature fields.

The study is limited to situations in which the flow is predominantly along the axis of the duct, so that there are no regions of flow 'recirculation'. Such flow situations are divided in this thesis into two distinct categories, parabolic and partially-parabolic. The differential equations governing each flow category are solved using distinctly different calculation procedures, appropriate for the respective flow category. The two calculation procedures are described in detail and their distinctive features are pointed out. The calculation procedures are applied to predict flow and heat transfer in ducts with mild and strong curvatures.

The calculation of turbulent flows is made using a two-equation turbulence model. Two additional partial-differential equations are solved for the transport of the kinetic energy of turbulence and its volumetric rate of dissipation. The turbulent stresses are related to the mean-velocity gradients through a scalar viscosity, calculated from the above turbulence variables. Special practices are adopted for the calculation of flow region adjacent to the walls; these practices consist of empirically prescribing the momentum and heat fluxes for grid nodes adjacent to a wall, by making a simple Couette-flow analysis.

Computations are made for flow and heat transfer in mildly-curved ducts using the parabolic procedure; and the results are compared with experimental data reported in literature. Agreement in the case of laminar flows has been good both for the developing and the fully-developed regions of the flow and temperature fields. For turbulent flows, however, the agreement has not been as good as that for the laminar flow situation. It is inferred that the turbulence model presently employed incompletely accounts for the complex turbulence-structure which occurs in the presence of secondary flows, as in the present case.

A modest amount of experimental data is reported for the turbulent flow in a rectangular-sectioned curved

duct. The curvature of the duct was chosen to be large so as to make the flow partially-parabolic. Predictions are also made for the same flow situation and are compared with experimental data. The predictions using the partially-parabolic procedure display good agreement with experimental data, while the results using the parabolic procedure are observed to be qualitatively at variance with measurements, as expected.

The present study has been undertaken with the primary objective of verifying the calculation procedures for three-dimensional flow situations. The flow phenomena in curved ducts have been studied from this viewpoint; for this reason, detailed calculations have not been made of the effects of various flow parameters on the flow and heat-transfer characteristics.

PREFACE

The work reported in this thesis describes my research activities at Imperial College during the period of October 1972 and June 1975. These research activities centred mainly around the development and validation of finite-difference calculation procedures to predict three-dimensional flow and heat-transfer phenomena in curved ducts. The study was carried out under a research contract with the Science Research Council and was supervised by Professor D B Spalding.

Calculation of flow and heat-transfer phenomena in curved passages is of significant importance to the design of various industrial equipment. Curved passages are used in heat exchangers, turbomachinery, aircraft intakes and several other equipment. However, such calculations are complicated because of the three-dimensionality of the flows and also because they are frequently turbulent.

Recently some success has been made at Imperial College in developing generalised calculation procedures, of finite-difference variety for three-dimensional flow situations. Also, simultaneously, some progress has been made in developing 'universally applicable' turbulence models, to represent the turbulence structure.

My primary aim in this study was to first test and later develop further, the numerical procedure and turbulence models currently available, to calculate the flow in curved ducts.

I proceeded first to test the numerical procedure to calculate the laminar flow phenomena in curved ducts. I restricted my attention, throughout, to flows which are steady and have no recirculation in the longitudinal direction. The latter restriction I made to concentrate attention on flows which are 'parabolic' in nature. I performed some calculations, using the parabolic procedure of Patankar and Spalding (1972), of the laminar flow and heat transfer in helical coils. The computations agreed satisfactorily with experiments and thus encouraged further study.

I then proceeded to make calculations of the turbulent flow in curved pipes. For these calculations, the additional input needed was the turbulence model. First, I made a few calculations using a mixing-length hypothesis. These calculations, however, did not agree satisfactorily with experimental data and thus warranted a need for more-complex turbulence-models. On the suggestion of Professor Spalding, I therefore attempted to employ a two-equation k-ε turbulence model. This particular two-equation model was selected on the earlier experiences of its greater universality in two-dimensional

situations. The predictions using the two-equation turbulence model displayed better agreement with the experimental data; but the agreement was not as good as that observed for laminar flows. It therefore appeared that the turbulence model needs further refinements to account for the complex turbulence structure in curved pipes.

At this stage, I did not proceed further in refining the turbulence model, but instead decided to extend the study to predict flows in strongly-curved ducts. In strongly-curved ducts, the secondary flow (flow in the cross-sectional plane) is much larger, and the pressure variations across the duct are significant enough to invalidate the parabolic assumptions. The flow is partially-parabolic and can not be computed using the parabolic procedure. On Professor Spalding's suggestion, I therefore attempted to devise a calculation procedure for economic handling of partially-parabolic flows, the difference in this procedure from the parabolic one being that account is taken now of the transmission of downstream events upstream through the pressure. To this end, I worked on two different calculation schemes. In one procedure, two three-dimensional arrays were used for the pressure while in the other, only one three-dimensional pressure field was employed; the methods of calculation were also somewhat different. I tested the merits of these two procedures, in a few typical partially-parabolic flow

situations. These tests proved that the one-pressure method is superior, as it gave faster rates of convergence of the pressure field. I therefore selected the one-pressure method, and employed it, later, to predict flows in strongly-curved ducts. In this thesis, only the one-pressure method is reported.

While the development of the partially-parabolic procedure was in progress, I was also making plans to undertake an experimental program to obtain data suitable for the validation of the partially-parabolic procedure. During this period, I came to know through Dr S V Patankar and Professor J H G Howard that an experimental rig existed at the University of Waterloo Canada, that would suit my needs. On the invitation of Professor Howard, I therefore visited the University of Waterloo and over a period of four months, performed measurements of the turbulent flow in a strongly-curved rectangular duct.

After my return to England, in February 1974, I devoted my efforts to the application of the partially-parabolic calculation procedure to predict the flow situation studied experimentally. I made calculations also using the parabolic procedure and compared both the partially-parabolic and parabolic results with the experimental data. These comparisons showed that the partially-parabolic procedure is much needed to calculate

accurately the flow in strongly-curved ducts. In addition to the above predictions, I made a few calculations using the partially-parabolic procedure of the laminar flow in a strongly-curved circular pipe; but these are not presented in this thesis because of some doubts regarding the correctness of the experimental data. The above-described tasks marked the end of my research activities; in February 1975, I started preparing the thesis.

I now wish to thank all those who provided me with help and encouragement during the present study. First and foremost, I thank Professor Spalding for providing guidance, inspiration and encouragement to maintain a good pace of research. I have profited greatly from his suggestions and criticisms in several disciplines of research. To have worked in association with him, I consider it a privilege.

Throughout this study, Dr S V Patankar offered a number of suggestions and helped me both in technical and non-technical matters. I acknowledge with feelings of gratitude, the assistance and the homely atmosphere provided by him and the members of his family.

It is my duty to thank several persons who provided help during my experimental program. Professor Howard, who proposed the idea of my going to Canada, has

been very helpful in providing the necessary experimental facilities and in making various suggestions during the course of the work. During the measurements Dr V Parameswaran was actively associated with me and helped me in a number of ways. I wish to thank him for his help. The assistance provided by the laboratory staff at Waterloo, in particular by Don Bartlett and by Joe Verner, is also acknowledged.

Thanks are to Dr A D Gosman and Professor J H Whitelaw for acting as members of my thesis committee and for making a number of useful suggestions during the meetings. The assistance provided by Miss Colleen King and by Mrs Christine McKenzie in sorting the various administrative matters is acknowledged. Thanks are to Miss E M Archer for helping me in obtaining various technical reports.

Last but not the least, I acknowledge with deep respect the encouragement provided by my mother during my stay abroad, and in general, throughout my education career.

Finally, I cannot forget to thank Meena Maher for her excellent typing of the thesis.

London, August 1975. V S Pratap

LIST OF CONTENTS

LIST OF FIGURES

CHAPTER 1

INTRODUCTION

1.1 The problem considered

Fluid flow and heat transfer in curved ducts have been the subject of considerable interest, owing primarily to the applicability of this information to the design of heat-exchangers, refrigeration equipment and turbomachinery. The flow pattern in a curved duct differs from that in a straight one primarily through exhibiting a 'secondary flow' in the cross-sectional planes of the duct, as shown in Figure (1.1.1); this secondary flow is generated as a result of the centrifugal forces which act at right angles to the main flow direction. Because of the enhanced 'mixing' caused by the secondary flow, the rates of heat, mass and momentum transfer in curved ducts are significantly higher than the corresponding straight-tube values.

The present study describes the application of a finite-difference solution procedure to the partial-differential equations governing the three-dimensional flow and heat-transfer phenomena in curved ducts. The study has been restricted to flow situations which are steady and are characterised by a predominant flow direction along which there are no regions of flow

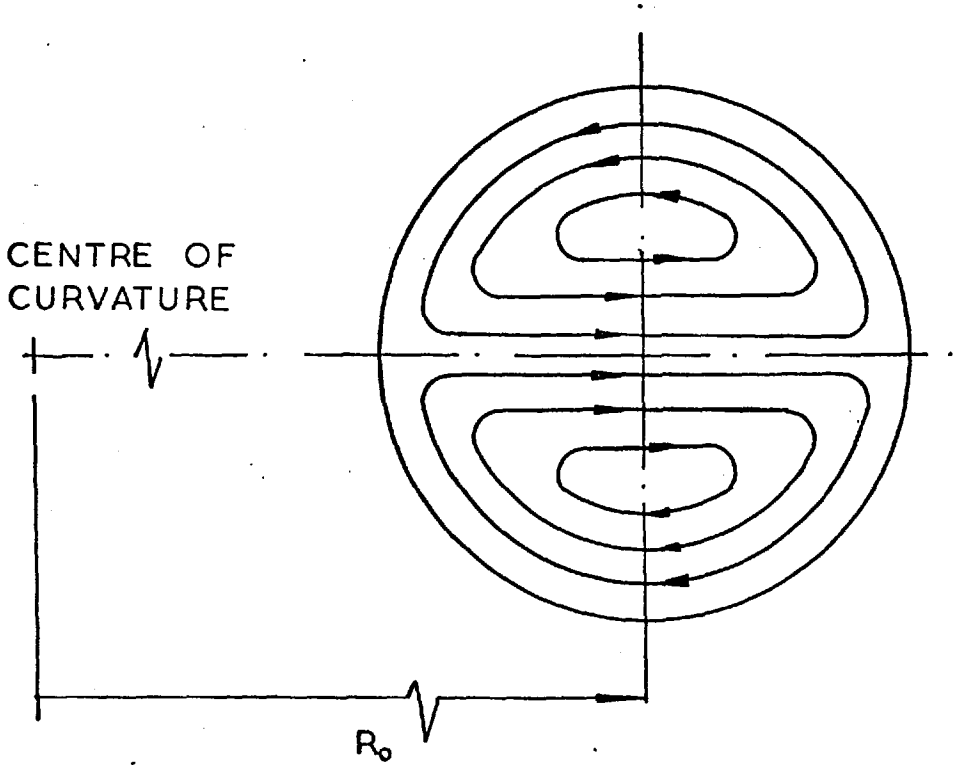

Fig. (1.1.1): General flow pattern in the cross-sectional plane of a curved pipe.

'recirculation'. The existence of a predominant flow direction ensures that:

(a) flow properties are convected only from upstream regions to downstream and not vice versa; and that

(b) at moderate and large Reynolds numbers, molecular actions, such as conduction, diffusion and viscous action, along that direction are small enough to be neglected.

These characteristics, simplify the equations governing the flow and make them easier to solve. In the present study, calculations have been made for both laminar and turbulent flow situations; the predicted results have been compared with experimental data and the capabilities of the calculation procedure are assessed. For turbulent flows, the additional 'stresses' due to turbulence have been represented through a two-equation turbulence model which comprised two additional partial-differential equations for the transport of the kinetic energy of turbulence and the volumetric rate of its dissipation.

1.2 Practical relevance of the present flow geometry

Because of the high rates of heat and mass transfer observed in curved ducts, many types of industrial equipment employ this geometry for their flow passages; further, a few environmental and physiological flows occur in passages which are curved in a somewhat

arbitrary manner. The ability to predict the detailed nature of the transfer processes in curved ducts would therefore lead to improved design of the equipment and to the better understanding of the natural phenomena. A short list of various flow situations where curved geometries are encountered is given below.

1) Flow passages of centrifugal compressors and gas turbines;
2) Heating and cooling coils of heat-exchangers, cryogenic and refrigeration equipment;
3) Intakes of jet aircraft;
4) Flow in bends of rivers and canals, where the purpose is to estimate:
   (a) the erosion of the banks due to the secondary flow and
   (b) the dispersion of the effluents in the stream;
5) Physiological flow systems in which it is desirable to understand the dispersion of a chemical substance into the coiled blood-vessels, the aorta being of primary importance.

1.3 Present method of calculation

The theoretical calculation of the flow and heat-transfer phenomena in curved ducts involves the simultaneous solution of a set of nonlinear partial-differential equations describing the transport processes

in three dimensions. If the flow is turbulent, methods also need to be devised to represent the additional stresses arising from turbulence. Because of the complicated nature of the equations it is impossible to obtain exact analytical solutions which are of the 'closed form' type.

In the present study, these equations have been solved by finite-difference calculation procedures. Two different calculation procedures have been employed; one to calculate the flow and heat transfer in mildly-curved ducts and the other for similar calculations in ducts with strong curvature. The two procedures are somewhat similar but the equations which they solve are distinctly different in their nature. The first set of equations, labelled here — parabolic, governs flow processes which are entirely 'one-way'; in these, the mechanisms of transmitting the downstream events to upstream namely, convection, diffusion and pressure transmission are completely absent so that the flow at any location is influenced solely by the events occurring upstream of that location. The second set of equations represents flow situations which are "partially-parabolic" in nature, so that the events at a downstream location <u>are</u> transmitted upstream but solely through the mechanism of pressure transmission. The two sets of equations which are similar in their structure differ in the manner in which the streamwise pressure gradient

is represented. The calculation procedure for partially -parabolic flows is more general than that for parabolic flows; it reduces to the latter in appropriate circumstances.

Both the above-mentioned calculation procedures are based on a numerical algorithm called SIMPLE (SIMPLE stands for Semi Implicit Method for Pressure-Linked Equations). Both procedures employ a marching integration procedure along the predominant flow direction and store velocities, temperatures etc. for only one cross-sectional plane at any time. The two procedures however differ in the following two respects.

(a) In the partially-parabolic calculation procedure, the pressure field is stored in a three-dimensional array whereas in the parabolic procedure only two dimensional storage is required for the pressure field.

(b) The partially-parabolic procedure performs several "marching-sweeps" over the flow domain, each time employing an improved guess for the three-dimensional pressure field; the parabolic procedure however, sweeps through the flow domain only once.

Calculation of turbulent flows

In the present study, the calculation of turbulent flows is made using a two-equation turbulence model. The turbulence model comprised two additional

equations for the transport of the kinetic-energy of turbulence and for the volumetric rate of its dissipation; the Reynolds stresses were related to the velocity gradients through a "turbulent viscosity" which was defined in terms of the above-mentioned properties of turbulence.

1.4 Main results

The present study comprised both experimental and theoretical investigations. In the experimental investigation, measurements were made of the flow in a strongly-curved duct with a view to collecting data suitable for validation of the partially-parabolic calculation procedure. The theoretical investigation comprised prediction of three different flow situations and comparison of the theoretical solutions with experimental data. The main achievements of the present study and the conclusions thereof are summarised below.

(a) The parabolic calculation procedure has been successfully applied to predict the laminar flow and heat transfer in mildly-curved circular pipes. The computed distributions of mean velocity, static pressure, temperature etc. display good agreement with experimental data.

(b) The predictions for turbulent flow in a curved pipe agree reasonably well with experiments but the agreement has not been as good as

that observed for the case of laminar flows. The turbulence model it is therefore concluded, requires modifications to account for the effects of secondary flow on the turbulence structure.

(c) A modest amount of experimental data has been collected which has been useful in validating the partially-parabolic calculation procedure.

(d) The partially-parabolic calculation procedure has been found to give good agreement with experimental data in a strongly-curved duct. The predictions obtained using the parabolic procedure, on the other hand, are qualitatively at variance with the measurements.

(e) The computing times required for the present calculations have been modest. In comparison with the parabolic procedure, the partially-parabolic procedure required larger computing times.

1.5 Layout of the thesis

The remaining sections of the thesis which describe the present study in more detail are arranged thus: in Chapter 2, a review is made of the previous experimental and analytical studies of the flow and heat transfer in curved ducts. In Chapter 3 the partial-differential equations governing the flow situations considered in the present study are described.

Chapter 3 describes a classification system for steady-flow situations based on the physical nature of the flow. The solution procedures are described in Chapter 4; and Chapter 5 describes the present practices for the modelling of the turbulence phenomena. The details of the experimental program are described in Chapter 6. The test rig, the measuring devices and the procedure adopted for making measurements are described; the experimental data obtained thereof are then presented.

The application of the numerical procedures to compute the various laminar and turbulent flow situations is explained in Chapters 7 and 8; the results of the computations are presented and compared with experimental data. Chapter 9 summarises the main contributions of the present study and lists the conclusions obtained thereof, along with a few suggestions for future work. The last part of the thesis provides a description of the nomenclature used, a list of the references and two appendices. The appendices provide supplementary details regarding the derivation of the governing differential equations and the data-reduction procedure for the measurements described in Chapter 6.

CHAPTER 2

PAST WORK

2.1 Introduction

Because of the practical importance of curved ducts, several experimental and theoretical investigations have been made of the flow and heat-transfer phenomena in curved ducts. The present chapter briefly reviews the relevant knowledge, so as to relate the present work to the earlier contributions. The chapter is divided into two main parts. The first reviews those investigations which, in particular, are concerned with flow and heat transfer in curved ducts; in this review, two flow-geometries are considered: (a) curved pipes of circular cross-section; and (b) curved ducts of rectangular cross-section. In the former geometry, studies of both laminar and turbulent flows are reviewed; while in the other attention is restricted to turbulent flows. The second section of the chapter reviews literature on generalised calculation-procedures which are suitable for prediction of flows in curved ducts. To this end, first the procedures are reviewed from the computational view point (i.e. mathematical formulation, numerical scheme employed, etc.); later the current status of the

"turbulence-models" is reviewed. The chapter is concluded by an evaluation of the available information of flow in curved ducts and an outline of the areas for future investigations.

2.2 Flow in circular-sectioned curved pipes

2.2.1 Experimental studies

Laminar flow

Measurements of the laminar flow and heat-transfer phenomena in curved pipes have been quite extensive; however, a large proportion of these measurements were restricted to the fully-developed regions, where the patterns of flow and heat transfer remain unchanged along the axial direction of the duct. In the investigations of the fully-developed regions, the measurements were mostly made of the friction factors and the overall heat-transfer rates; only in a few cases (Adler (1934) Hawes (1932) and Mori and Nakayama (1965)) have the distributions of velocity and temperature been measured. The experimental apparatuses and the techniques of measurement used in these investigations have been nearly the same, but the range of flow parameters such as the Reynolds number, radius ratio of the coil etc. differed in each case. A review of the various experimental investigations in fully-developed flow and temperature fields has recently been made by Srinivasan et al. (1968).

Experimental studies in the developing region of flow and temperature fields have been relatively less in number. Kulegan and Beij (1937) measured the pressure drop in the developing flow field and present an empirical relation for the axial variation of the friction factor.

The velocity-distributions in the developing flow field have been measured by Austin (1971) and by Olson (1971). In these investigations, the Reynolds number of the flow and the radius ratio of the coils have been nearly the same; but the techniques for measuring the velocity were different. Austin measured the velocities using hot-film anemometry whereas Olson employed a pulsed-wire technique. Measurements in the thermal entry region have been reported by Dravid et al. (1971) for the thermal boundary condition of axially-constant heat flux with isothermal periphery; the wall temperatures and heat transfer rates were measured at several axial stations and the heating was initiated only after the flow field became fully-developed. An interesting observation from this investigation has been that, in the thermal entrance region, the wall temperature and and the Nusselt number exhibit cyclic oscillations with distance along the duct axis; the oscillations however diminish in amplitude as the fully-developed state is reached. Such oscillations have been attributed by Dravid et al. to the convection effects of the secondary flow.

Oscillations of this kind had already been more tentatively reported by Seban and McLaughlin (1963), when the thermal boundary condition was that of constant heat flux around the periphery.

Turbulent flow

Measurements of turbulent flow in curved pipes have also been largely restricted to the fully-developed regions. The measured values of the fully-developed friction factors and heat-transfer rates have been expressed in terms of empirical functions of the flow parameters and the fluid properties. Ito (1959) and Srinivasan et al. (1968) provide a review of such correlations proposed by various investigators. The distributions of velocity in the fully-developed flow field have been measured by Adler (1934), Mori and Nakayama (1967) and Hogg (1968); the latter two authors also provide temperature distributions in the fully-developed thermal field for constant-heat-flux boundary conditions.

It has been observed that, when compared with laminar flows, turbulent flows are relatively less affected by the curvature of the duct; flow and temperature fields are less distorted and the friction factors and heat-transfer rates show relatively smaller increases over the straight-pipe values.

In the developing region of the turbulent flow field Hawthorne (1951) presents the contours of stagnation

pressure at several axial positions in a 180 degree bend; the inlet velocity distribution for these experiments varied linearly from zero at the bottom of the pipe to a maximum in the region close to the top wall. The measurements indicated that the secondary flow field in the bend develops in an oscillatory manner with a period of oscillation, in this case, approximately equal to 180 degrees. Squire (1954) made measurements similar to those of Hawthorne (1951) but, in his case, the flow field at inlet was that of a fully-developed, turbulent pipe-flow. The oscillatory nature of the secondary flow field was also suggested by these measurements. Further measurements in the developing flow have been reported by Detra (1953) and by Rowe (1966). The dimensions of the test section and the experimental apparatus in Rowe's experiments were the same as those employed in the experiments of Squire (1954); but Rowe's measurements also included the distributions of the flow angles. The thermal-entrance region in the turbulent flow in bends has been studied by Ede (1960, 1963, 1966). Measurements have been made of the rates of heat transfer in 90 and 180 degree bends for the constant-heat-flux boundary-condition. So far, no measurements have been made of the temperature distributions in the thermal entrance region.

Measurements have also been made of the flow in 'S' shaped ducts and in ducts with sinusoidal variations in curvature; such measurements have been reported by Horlock (1956) and more recently by Rowe (1966) and by Fish (1970). It has been observed in these investigations that the reversal of curvature increases the amount of secondary flows. Both Horlock (1956) and Rowe (1966) attribute this increase to the augmentation of the streamwise vorticity which is generated by the curvature of the duct.

2.2.2 Theoretical studies

In this section the previous theoretical studies in curved circular pipes are reviewed. For the reader's convenience, the various studies are categorised under three main headings, as follows.

Inviscid solutions

The applicability and methods of inviscid-flow analyses to calculate the flow in curved ducts have been reviewed by Hawthorne (1965, 1966). The objective of the inviscid-flow analyses has been to seek solutions to the equations of motion in which terms representing the effects of viscosity have been omitted. For the inviscid equations governing the flow in curved pipes, it has not been possible to obtain exact solutions for all ranges of curvature; hence, approximate solutions

have been obtained, from the assumption of small shear. In this, it is assumed that the stagnation pressure contours undergo negligible distortion around the bend. This approximation which is often referred to as the 'secondary-flow' approximation, was first employed by Squire and Winter (1951); they showed that, for such an approximation, the 'secondary' vorticity in the flow increases linearly with the bend angle. The same approximation was used in subsequent calculations by Detra (1953) and by Rowe (1966). Detra calculated the distribution of stagnation pressure at the exit of 21^{o} and 42^{o} bends and compared the results with measurements; the agreement was satisfactory; but difficulties were encountered in prescribing the correct distribution of the inlet-vorticity. The computations of Rowe (1966) were made for the developing flow in 180 degree bends and in 'S' shaped ducts. The computed distributions of stagnation pressure agreed satisfactorily with experimental data upto 45 degrees of the bend angle; but after this distance, the calculations displayed substantial discrepancies with the measurements.

Inviscid calculations of the oscillatory nature of the secondary flow field have also been presented, by Hawthorne (1951). The oscillatory nature of the secondary flow field was demonstrated through the solution of an equation for the angular displacement of the stagnation-pressure contours. The calculated period

of the first oscillation in a 180° bend agreed satisfactorily with the measured value. Hawthorne's analysis was also later extended to calculate the oscillatory nature of the flow in ducts with repeated reversals of curvature (Horlock (1956)).

Analysis of fully-developed flows

A number of theoretical studies have been made in which the complete equations governing the fully-developed flow in curved pipes have been solved either by analytical techniques or by finite-difference methods. Of these studies, we first review, those for laminar flows. The first calculations of laminar fully-developed flow in curved pipes were made by Dean (1927); Dean employed a perturbation technique to analyse the secondary flow field as a deviation from the Poiseuille flow. His solution is however applicable only to flows in which the Dean number, defined as $K = Re\sqrt{a/R}$ is smaller than about 17. For Dean numbers which are sufficiently large (<80) solutions of a different type have been proposed, by Adler (1934), Barua (1962) and Mori and Nakayama (1965). In these three solutions, a 'boundary-layer approximation' was made; first the flow cross-section was divided into a viscous, near-wall region and an inviscid core; equations were then solved separately for each flow region; and the flow conditions at the boundary of the two regions were matched. Using

a similar approach, Mori and Nakayama (1965) also calculated the fully-developed thermal field; and obtained expressions for the distribution of temperatures and heat-transfer rates. These authors analysed the temperature field for two different thermal boundary conditions, these being the constant-wall-temperature condition and the constant heat-flux condition.

The above-mentioned boundary-layer approximation is however valid only in flows with Dean number greater than about 80. In the intermediate range of Dean numbers, i.e. between 17 and 80, neither the analysis of Dean (1927) nor that based on the boundary-layer concept gives correct solutions to the equations. Solutions for flows in this intermediate range of Dean numbers have been obtained by McConalogue (1969), using Fourier-series expansions.

Solutions to the differential equations governing fully-developed flow and temperature fields have also been obtained using finite-difference numerical-schemes (Truesdell and Adler (1970), Austin and Seader (1973), Akiyama and Cheng (1971), Kalb and Seader (1972), Tarbell and Samuel (1973) and Greenspan (1973)). The schemes proposed by the above researchers differ in

(a) the dependent variables employed in the governing equations; and

(b) the way the finite-difference form of the differential equations is derived.

Numerical solutions of the temperature equation have been presented by Kalb and Seader (1972) and by Tarbell and Samuels (1973).

For the turbulent, fully-developed flow in curved pipes, two theoretical solutions have been reported (Ito (1959) and Mori and Nakayama (1967)); both solutions were based on the boundary-layer concept, akin to that adopted for calculating laminar flows. Numerical studies of the turbulent heat-transfer in curved pipes have not been reported yet.

Analysis of the developing region

Only a few theoretical solutions of the equations governing the developing flow and temperature fields have been reported. Singh (1974) calculated the development of the flow field, using a method based on asymptotic expansions. Solutions to the governing equations were obtained for two different inlet-conditions: (a) a uniform inlet pressure and (b) a uniform axial-velocity at the inlet. Yao and Berger (1975) analysed the developing flow field, using a method which was an extension of the method of Barua (1962) for the calculation of fully-developed flow field. Neither Singh (1974) nor Yao and Berger (1975)

presented any comparisons with experimental data. The thermal entrance region has been studied theoretically by Dravid et al. (1971) and by Tarbell and Samuels (1973). Both assumed the flow field at the start of the thermal entrance region to be fully-developed; and solved only the temperature equation, using finite-difference methods. Dravid et al. assumed the flow field to be that calculated by the analysis of Mori and Nakayama (1965) whereas Tarbell and Samuels obtained their velocity field from a numerical computation. Both theoretical solutions satisfactorily predicted the oscillatory development of the wall temperatures and Nusselt numbers observed in the experimental investigation of Dravid et al (1971) and of Seban and McLaughlin (1963).

Theoretical calculations taking into account the effects of viscosity, have not been yet made for the turbulent developing flow in curved pipes.

2.3 Turbulent flow in rectangular-sectioned curved ducts

2.3.1 Experimental studies

Measurements of the turbulent flow in bends of rectangular cross-section have been made by Joy (1950), Eichenberger (1953) and Squire and Winter (1951). In these investigations, the contours of stagnation pressure were measured at several axial positions along 90 and 180

degree bends. The conditions at the inlet were such that the stagnation pressure varied linearly from zero at the bottom wall to its maximum at the centre of the duct, the flow being nearly symmetrical about the central plane of curvature. The flow patterns observed have been similar to those observed in circular bends. A few experimental investigations have also been reported in which the primary interest has been to study the three-dimensional turbulent boundary-layer which developed on the top and bottom walls of the curved duct (Gruschwitz (1935), Francis (1965), Vermeulen (1971)). In these investigations, the measurements were confined to regions close to the bottom wall and the variations of flow variables normal to the bottom wall were measured at several locations in the flow field. Recently Young, Jerie and Howard (1972) and Young (1973) presented distributions of the overall flow-field in a curved rectangular duct whose outer wall was varied in an arbitrary manner so as to create a zero axial pressure-gradient along the centre line of the duct. They also made measurements of the velocities and flow angles in the region close to the bottom wall to study the three-dimensional boundary layer.

2.3.2 Theoretical studies

Calculations of the flow in rectangular curved ducts have been mostly restricted to the boundary-layer region close to the bottom wall of the duct. In these

calculations it is assumed that the properties of the boundary layer are the same at all the locations in the direction of the duct width; and thus the characteristics of the complete flow are inferred from studying the properties of the boundary layer at selected locations along the duct width. The calculation of this three-dimensional boundary-layer is made by one of the following two types of methods*.

(a) Integral methods in which the momentum-integral equations are solved to produce integrated properties of the boundary layer at various locations on the surface;

(b) Differential methods, in which the time-mean equations of motion are numerically solved to produce flow properties at discrete locations across the thickness of the boundary layer.

Calculations of flow in rectangular curved ducts have also been made using inviscid-flow analysis; (Squire and Winter (1951), Eichenberger (1952), Stuart and Hetherington (1968)); in these the viscous effects in the flow are neglected and thus no account is made of the effects of turbulence. The analyses of Squire

---

*A review of the calculation methods proposed for three-dimensional boundary layers is given in Patel and Nash (1972).

and Winter (1951) and Eichenberger (1952) are based on approximate solutions such as those discussed in Sec. (2.2.2), while Stuart and Hetherington (1968) propose a finite-difference solution to the inviscid equations.

2.4 Generalised calculation procedures

In the above two sections, the experimental and theoretical investigations in curved ducts were reviewed. The solution procedures proposed in these theoretical studies however have limited applicability in the sense that they are restricted only to the calculation of flows in curved ducts. In this section, a review is made of more-general calculation procedures for analysis of three-dimensional flow situations. Such calculation procedures comprise two distinct aspects: (a) the solution procedure for the governing equations; and (b) the mathematical modelling of the turbulence phenomena. These aspects are reviewed below separately.

Solution procedures

Generalised solution procedures for the equations governing two- and three-dimensional flows have been, because of the complexity of the equations, only of the finite-difference variety. One such calculation procedure for two-dimensional 'parabolic' flows was reported by

Patankar and Spalding (1967). Gosman et al (1969) later, reported a method applicable in two-dimensional elliptic flows (i.e. flows with recirculation). Among other calculation procedures for two- and three-dimensional steady and unsteady flows are those of Harlow and Welch (1965), Chorin (1968) and Amsden and Harlow (1970).

A procedure for calculation of three-dimensional 'parabolic' flows was reported by Gosman and Spalding (1971); subsequently a somewhat different calculation procedure for the same flow problem was reported by Caretto et al (1972). Later, Patankar and Spalding (1972) developed a calculation procedure for the same flow problem; but this procedure employed a more efficient numerical algorithm. The numerical scheme of Patankar and Spalding was also subsequently extended (Caretto et al (1972) to three-dimensional recirculating flows (also referred to as elliptic flows)). Several application studies of the latter two procedures have also been made e.g. (Sharma (1974); Tatchell (1975)). A calculation scheme for an intermediate class of flows, termed partially-parabolic, was proposed by Spalding (1971); it is this proposal which is developed further and applied in this thesis to predict the flow in strongly-curved ducts.

Two recent reviews of existing calculation procedures for steady, three-dimensional boundary layers are also available. They are due to Patankar (1971) and Nash and Patel (1972).

Turbulence models

Research on the nature of turbulence and on the calculation of the turbulent stresses is quite extensive. Methods proposed for calculation of the turbulence stresses date back to Prandtl's (1925) mixing-length hypothesis in which the Reynolds stresses are related to the velocity gradients through a prescribed length-scale distribution. Subsequent research in modelling the turbulence phenomena has led to the development of one, two- and multi-equation turbulence-models; each of these differ in their degree of complexity by the number of additional differential equations solved for the turbulence variables. The current status of such turbulence models has been reviewed by Launder and Spalding (1972), Harlow (1973), Mellor and Herring (1973) and Launder and Spalding (1973). In the latter, Launder and Spalding also discuss, in particular, the applicability and performance of a two-equation turbulence-model in which the additional equations solved are for the kinetic-energy of turbulence and for its dissipation-rate. They show, through comparison of predictions with experimental data, that such a turbulence model gives results which are satisfactory while also being economical from the

computational view-point. Based on the recommendation of Launder and Spalding (1973), the two-equation turbulence-model has also been applied in the present study.

2.5 Status of existing information

The status of existing information, both experimental and theoretical, on the flow and heat-transfer phenomena in curved ducts may be summarised as follows:

1) Studies of fully-developed laminar flow and heat-transfer phenomena in curved pipes have been made in sufficient detail to provide adequate information for the design of equipment involving such flow processes.

2) For turbulent flows, the experimental data on mean flow and heat transfer are adequate to test the prediction procedures and the turbulence models; but information on the structure of turbulence is lacking. Such information is needed to understand and to correctly represent the effects of curvature on the turbulence structure.

3) Measurements of the developing flow and temperature fields have been only few; it is therefore necessary to obtain additional data in order to test the calculation procedures over a wider range of flow parameters.

4) Calculations of the developing flow, with the viscous forces included in the equations, have only just begun. Calculations of turbulent flows with the effects of turbulence incorporated into the equations have not been reported.

5) The calculation of turbulent flow in rectangular-sectioned curved ducts has been attempted from a restricted view-point and needs to be extended to the prediction of the overall flow field; for this, further experimental information is needed of the overall distributions of the velocities and pressures over the flow field.

2.6 Concluding remarks

In the present chapter, a brief review has been made of the available experimental and theoretical information of the flow and heat-transfer phenomena in curved ducts; studies in ducts of circular and rectangular cross-section have been reviewed separately. The available experimental and theoretical information has been evaluated and the areas where further studies need to be undertaken are outlined.

CHAPTER 3

MATHEMATICAL DESCRIPTION OF THE FLOW SITUATIONS

3.1 Introduction

The present chapter and the next two describe the details of the theoretical calculations made in this thesis. These chapters are provided for the sake of completeness; and to some extent they review information already reported before, such as the calculation method and the turbulence model. First, in this chapter, the mathematical equations which govern the transport of mass, momentum, energy etc. in the various flow situations considered in this thesis are stated. These equations have been derived from the general form of the Navier-Stokes equations by the neglect of terms of small order of magnitude. The solution procedure for these equations is described in the next chapter; and the subsequent chapter is then devoted to the description of the turbulence model used in the present study.

The present chapter is arranged thus: first a classification system for steady-flow situations is introduced; in this, steady-flow situations are divided, from a computational view-point, into three distinct categories: elliptic, partially-parabolic and fully-parabolic. The distinctive features of each flow

category are pointed out and the differences in their mathematical nature are stated. The classification system is then applied to identify the flow phenomena in curved ducts, based on the curvature of the duct. The partial-differential equations solved in the present investigation are then stated for three different flow geometries considered in this thesis. The equations are stated in a form common to both laminar and turbulent flow situations. Finally, the auxiliary information necessary to complete the mathematical formulation of the problem is listed.

3.2 Classification of steady-flow situations

It has been useful (ref. Gosman et al (1969)) in numerical fluid dynamics to classify steady-flow phenomena into two main categories: elliptic and parabolic. Strictly speaking, all flows except wholly supersonic ones are elliptic; this means that perturbations of conditions at any point in the flow can influence conditions at any other point. The mechanisms of these interactions are usually:-

(i) convection (i.e. downstream transmission along stream lines);

(ii) conduction, diffusion and viscous action (i.e. dissemination in all directions by molecular inter-mixing);

(iii) pressure transmission (e.g. the tendency of a fluid in a subsonic flow to move out of the

way of a downstream obstacle before reacting it).

In parabolic flows, mechanisms (ii) and (iii) are weak enough to be ignored; and the flow configuration is free from "recirculation" so that mechanism (i) transmits effects only in one direction. Many boundary-layer, duct flow and jet phenomena are of this parabolic kind; for the Reynolds number is high enough to render the molecular actions to be insignificant in the streamwise direction; and the conditions of the flow provoke no sharp curvatures of the streamlines.

There is however, also another category of steady flows which lies in between the elliptic and parabolic categories. This category, studied extensively for the first time in this thesis, represents flows which are characterised by:

(a) absence of recirculation, so that mechanism (i) (convection) operates only in a single (downstream) direction;

(b) high Reynolds number, so that mechanism (ii) (molecular action) is significant only normal to the streamlines and

(c) significant curvature of the streamlines, rendering mechanism (iii) (pressure transmission) the dominant transmitter of influences in an upstream direction.

Examples of such flows include flow in strongly-curved ducts, flow in ducts with distributed resistances etc.

The consequences of the above classification are reflected through simplifications which are achieved in the governing differential equations for each flow category. These simplifications are explained below with reference to the differential equations governing a steady, three-dimensional, incompressible flow in the (x, y, z) coordinate system; the equations given below represent an elliptic flow situation; they will be later simplified to obtain those which describe parabolic and partially-parabolic situations.

Mass Conservation

$$\frac{\partial}{\partial x}(\rho u) + \frac{\partial}{\partial y}(\rho v) + \frac{\partial}{\partial z}(\rho w) = 0 \qquad (3.2.1)$$

Transport of:

x-momentum

$$\frac{\partial}{\partial x}(\rho uu) + \frac{\partial}{\partial y}(\rho uv) + \frac{\partial}{\partial z}(\rho wu) = -\frac{\partial p}{\partial x} + \frac{\partial \tau_{xx}}{\partial x} + \frac{\partial \tau_{xy}}{\partial y} + \frac{\partial \tau_{xz}}{\partial z} + S_u \qquad (3.2.2)$$

y-momentum

$$\frac{\partial}{\partial x}(\rho uv) + \frac{\partial}{\partial y}(\rho vv) + \frac{\partial}{\partial z}(\rho wv) = -\frac{\partial p}{\partial y} + \frac{\partial \tau_{yx}}{\partial x} + \frac{\partial \tau_{yy}}{\partial y} + \frac{\partial \tau_{yz}}{\partial z} + s_v \qquad (3.2.3)$$

z-momentum

$$\frac{\partial}{\partial x}(\rho uw) + \frac{\partial}{\partial y}(\rho vw) + \frac{\partial}{\partial z}(\rho ww) = -\frac{\partial p}{\partial z} + \frac{\partial \tau_{zx}}{\partial x} + \frac{\partial \tau_{zy}}{\partial y} + \frac{\partial \tau_{zz}}{\partial z} + s_w \qquad (3.2.4)$$

Scalar property, Φ

$$\frac{\partial}{\partial x}(\rho u\Phi) + \frac{\partial}{\partial y}(\rho v\Phi) + \frac{\partial}{\partial z}(\rho w\Phi) = \frac{\partial J_{\Phi,x}}{\partial x} + \frac{\partial J_{\Phi,y}}{\partial y} + \frac{\partial J_{\Phi,z}}{\partial z} + s_\Phi \qquad (3.2.5)$$

In the above equations, u, v and w respectively represent the components of the velocity along the x, y and z directions. ρ represents the density and p is the pressure field. The 'τ's represent the stresses in the fluid; and can be expressed in terms of a viscosity and the velocity gradients. The

'J's represent the fluxes of the entity Φ and can also be represented by gradient-type laws. The terms s_u, s_v, s_w and s_Φ stand for additional sources or sinks of the corresponding property which is being transported.

In the above equations, the terms on the left hand side represent the transport of flow properties by convection along the three coordinate directions. The mechanism of diffusion is represented by terms containing the shear stresses 'τ', and the 'J' fluxes. The mechanism of pressure transmission which exists only for the transport of momentum is represented by the pressure-gradient terms.

The equations for partially and fully-parabolic* flow situations can be now obtained from those given above by omitting the terms representing the mechanisms that are weak enough to be ignored. For partially-parabolic flows, the simplification consists of neglecting the diffusion fluxes along the predominant flow-direction. For a flow which is predominant along the z-direction, we can therefore write that

$$\tau_{xz} = \tau_{yz} = \tau_{zz} = J_{\Phi,z} = 0 \qquad (3.2.6)$$

---

*The term 'fully-parabolic' is synonymous with the term 'parabolic'; it is introduced in this thesis, wherever necessary, for more clear distinction from the term 'partially-parabolic'.

Equations for a partially-parabolic flow situation are obtained by substituting (3.2.6) into equations (3.2.2) to (3.2.5).

The governing differential equations for a fully-parabolic flow are the same as those for a partially-parabolic situation but for additional simplification in the treatment of the pressure field. For fully-parabolic flows, the absence of pressure transmission implies that there are no sharp curvatures of the streamlines and thus the streamwise pressure-gradient, $\frac{\partial p}{\partial z}$ is nearly uniform over the cross-stream; therefore $\frac{\partial p}{\partial z}$ can be calculated without reference to the momentum balances in the x- and y-directions. The independence of $\frac{\partial p}{\partial z}$ from $\frac{\partial p}{\partial x}$ and $\frac{\partial p}{\partial y}$ results in the decoupling of the z-direction momentum equation from the other two momentum-equations; and equation (3.2.4) can be recast in the following form:

$$\frac{\partial}{\partial x}(\rho uw) + \frac{\partial}{\partial y}(\rho vw) + \frac{\partial}{\partial z}(\rho ww) = -\frac{\partial \bar{p}}{\partial z} + \frac{\partial \tau_{zx}}{\partial x} + \frac{\partial \tau_{zy}}{\partial y} + S_w \qquad (3.2.7)$$

The quantity $\bar{p}$ may be interpreted as an average pressure over the x-y plane; $\bar{p}$ is constant in the x-y plane but

varies along the z-direction depending on the flow situation considered. The above-mentioned decoupling of the momentum equations presents a simpler solution task, as shall be seen in Chapter 4.

3.2.1 Classification of flows in curved ducts

Flows in curved ducts may also be classified as elliptic, partially-parabolic and parabolic. The factor that influences this classification most is the curvature of the duct. If the curvature of the duct is so large as to cause flow recirculation, the flow situation is necessarily elliptic. Flows in 90^{o} elbow bends are one example of flows in this category. In ducts with curvature too small not to cause recirculation, the flow may be a combination of both partially-parabolic and fully-parabolic flow-regions. The partially-parabolic regions for flows in curved ducts are usually only at the entrance and at the exit. The influence of these regions on the rest of the flow depends on (a) the curvature of the duct; (b) the cross-sectional shape of the duct; and (c) the state of the flow, laminar or turbulent. Although it is difficult to define a precise value of the curvature ratio distinguishing parabolic and partially-parabolic flows, as an approximate criterion, it may be stated that the flow in ducts with a radius ratio (R/a) greater than 15 is parabolic to a large

extent; and thus it can be accurately calculated by using a calculation procedure designed to handle parabolic flows.

3.3 Governing partial-differential equations

For later convenience, in this section the partial-differential equations governing the flow and heat-transfer phenomena in the various flow situations computed in this thesis are stated. The flow situations and the coordinate systems in which they have been mathematically described are shown in Figure (3.3.1). The flow geometries have been (a) a curved circular pipe; (b) a curved rectangular-sectioned duct and (c) a curved rectangular-sectioned diffuser; the coordinate systems in which these flow situations have been presented are respectively (a) the (r, θ, ϕ); (b) the (x, y, ϕ); and (c) a quasi-orthogonal system represented by the coordinates (η, ζ, ξ). The three sets of equations described below have been derived from the generalised form of the Navier-Stokes equations assuming the flow to be incompressible and predominant along the ϕ direction. The equations stated below are thus partially-parabolic; their parabolic form can be easily derived by rewriting the longitudinal momentum equation using a $\bar{p}$ pressure field. Since the equations for the three momenta and for other

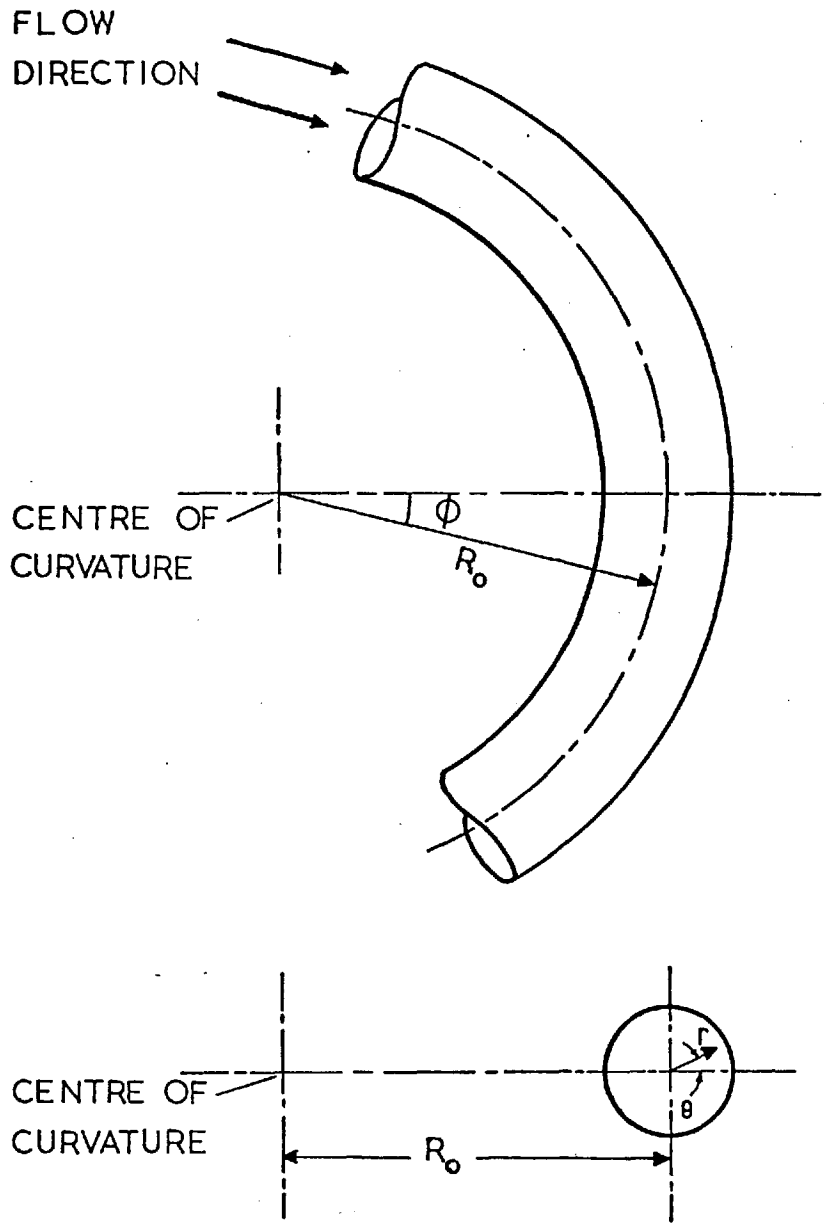

Fig. (3.3.1(a)): Coordinate system for a curved, circular pipe.

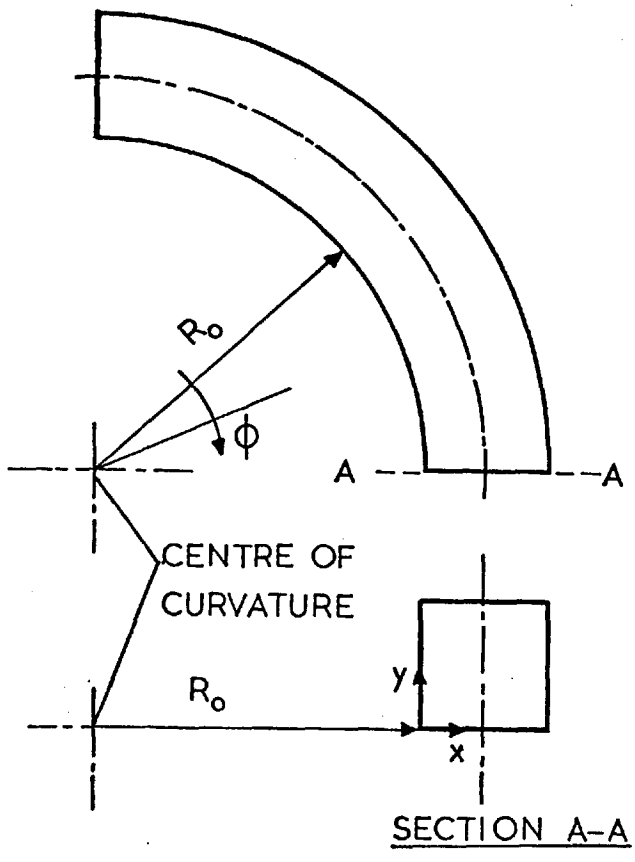

Fig. (3.3.1(b)): Coordinate system for a curved, rectangular duct.

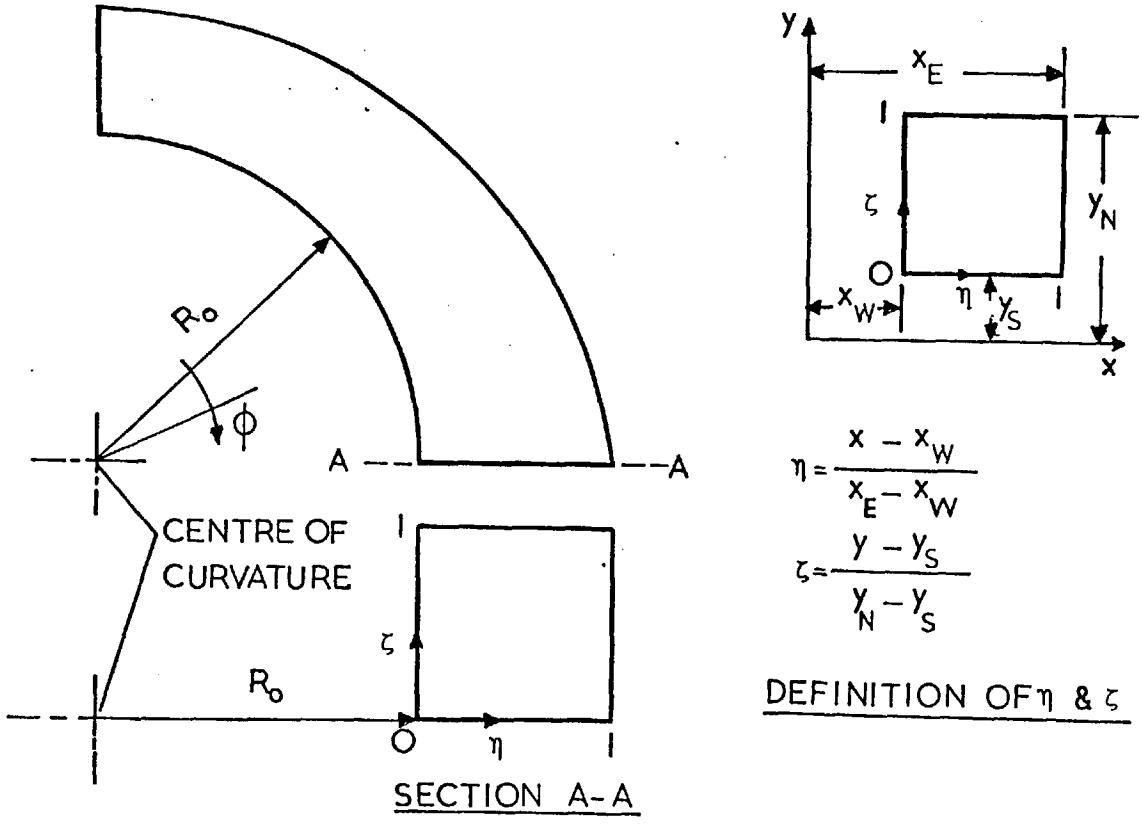

Fig. (3.3.1(c)): Coordinate system for a curved diffuser.

scalar flow-properties have similar structure, they have all been represented below by a single equation for a general variable Φ; the individual equations can easily be obtained and are given in Appendix A1.

(a) Curved circular pipe: (r, θ, ϕ)

Continuity:

$$\frac{\partial u}{\partial r} + \frac{1}{r}\frac{\partial v}{\partial \theta} + \frac{u}{r} + \frac{\partial w}{R\partial \phi} + \frac{1}{R} u \cos\theta - \frac{1}{R} v \sin\theta = 0 \qquad (3.3.1)$$

Transport of a general flow-property, Φ

$$\rho\left(u\frac{\partial \Phi}{\partial r} + \frac{v\partial \Phi}{r\partial \theta} + \frac{w\partial \Phi}{R\partial \phi}\right) = S_\Phi + \frac{1}{r}\frac{\partial}{\partial r}\left(\Gamma_\Phi \frac{r\partial \Phi}{\partial r}\right) + \frac{\Gamma_\Phi}{R}\left(\frac{\partial \Phi}{\partial r}\cos\theta - \frac{\partial \Phi}{r\partial \theta}\sin\theta\right) + \frac{\partial}{r\partial \theta}\left(\Gamma_\Phi \frac{\partial \Phi}{r\partial \theta}\right) \qquad (3.3.2)$$

(b) Curved rectangular-sectioned duct: (x, y, ϕ)

Continuity

$$\frac{\partial u}{\partial x} + \frac{\partial v}{\partial y} + \frac{w}{R} + \frac{\partial w}{R\partial \phi} = 0 \qquad (3.3.3)$$

Transport of Φ

$$\rho\left(\frac{u\partial\Phi}{\partial x} + v\frac{\partial\Phi}{\partial y} + w\frac{\partial\Phi}{R\partial\phi}\right) = S_\Phi + \frac{\partial}{\partial x}\left(\Gamma_\Phi\frac{\partial\Phi}{\partial x}\right) + \frac{\Gamma_\Phi}{R}\frac{\partial\Phi}{\partial x} + \frac{\partial}{\partial y}\left(\Gamma_\Phi\frac{\partial\Phi}{\partial y}\right) \qquad (3.3.4)$$

(c) Curved, rectangular-sectioned diffuser: (η, ζ, ξ)

Continuity:

$$\frac{1}{(x_E-x_W)}\left\{\frac{\partial u}{\partial\eta} - \frac{\partial w}{\partial\eta}\left(\frac{\partial x_E}{R\partial\xi} + \eta\frac{\partial}{R\partial\xi}(x_E-x_W)\right)\right\} +$$

$$\frac{1}{(y_N-y_S)}\left\{\frac{\partial v}{\partial\zeta} - \frac{\partial w}{\partial\zeta}\left(\frac{\partial y_S}{R\partial\xi} + \zeta\frac{\partial}{R\partial\xi}(y_N-y_S)\right)\right\} +$$

$$\frac{1}{R}\frac{\partial w}{\partial\xi} + \frac{u}{R} = 0 \qquad (3.3.5)$$

Transport of Φ:

$$\rho\left[\frac{1}{(x_E-x_W)}\frac{\partial\Phi}{\partial\eta}\left\{u - w\left(\frac{\partial x_E}{R\partial\xi} + \eta\frac{\partial}{R\partial\xi}(x_E-x_W)\right)\right\} + \frac{1}{(y_N-y_S)}\frac{\partial\Phi}{\partial\zeta}\left\{v - w\left(\frac{\partial y_S}{R\partial\xi} + \zeta\frac{\partial}{R\partial\xi}(y_N-y_S)\right)\right\} + \frac{w}{R}\frac{\partial\Phi}{\partial\xi}\right] = S_\Phi + \frac{1}{(x_E-x_W)^2}\frac{\partial}{\partial\eta}\left(\Gamma_\Phi\frac{\partial\Phi}{\partial\eta}\right) + \frac{1}{(y_N-y_S)^2}\frac{\partial}{\partial\zeta}\left(\Gamma_\Phi\frac{\partial\Phi}{\partial\zeta}\right) + \frac{1}{(x_E-x_W)}\frac{\Gamma_\Phi}{R}\frac{\partial\Phi}{\partial\eta} \qquad (3.3.6)$$

The nomenclature used in the above sets of equations is the same as that used earlier, for equations (3.2.2) to (3.2.5). u, v and w represent the three velocity-components along the three coordinate-directions; Φ is a general flow-variable which represents all scalar flow properties and also the three velocity components, u, v and w; S_Φ contains all the additional terms representing the source or sink of Φ ; it includes pressure gradients, body forces, heat fluxes etc. Γ_Φ is an exchange coefficient which relates the diffusion fluxes to the velocity or temperature gradients; for turbulent flows it represents the combined laminar and turbulent exchange coefficient and is calculated from the turbulence model. The expressions for the source terms and the exchange coefficients appearing in these equations can be obtained from the equations given in Appendix A1.

In the above coordinate systems, the one represented by (η, ζ, ξ) is only quasi-orthogonal; and the equations presented for this coordinate system imply a few more approximations, in addition to those because of the predominant flow direction. It is postulated that the errors introduced by these approximations are small for the diffuser angle (2.5^o) studied in the present thesis.

3.4 Auxiliary information

In addition to the set of equations described above, the mathematical specification of the flow situation also requires the following information.

(a) Initial conditions, i.e. initial values of dependent variables corresponding to the position along the predominant flow direction (i.e. ϕ) at which solutions to the set of equations are begun.

(b) Exit conditions, i.e. conditions at the outlet of the duct, either as a specified pressure-distribution or as a specified distribution of axial-velocity; these conditions are necessary only for the calculation of partially-parabolic flow situations.

(c) Boundary conditions, i.e. conditions of all the dependent variables at the four boundaries of the cross-sectional plane, as a function of ϕ.

(d) Auxiliary relationships, which allow the density, diffusion coefficients, sources and sinks in each of the equations to be computed in terms of the dependent variables of these equations, over the entire flow field.

The manner in which the auxiliary information is incorporated in the solution procedure will be described in Chapter 4.

3.5 Summary

The contributions of the present chapter may be summarised as follows:

1) Three categories of flow situations have been defined which are distinct from a computational view point; they are: elliptic, partially-parabolic and parabolic. The physical nature of the flow in each of the above categories has been discussed and the differences in the governing equations have been pointed out.

2) The nature of the flow phenomena in curved ducts has been examined from the view point of the above classification.

3) The partial-differential equations governing the transport of mass, momentum and energy etc. have been stated for three different flow geometries.

4) The auxiliary information necessary to complete the mathematical specification is listed.

The calculation procedures for solving the above sets of parabolic and partially-parabolic equations will be described in the following chapter.

CHAPTER 4

SOLUTION PROCEDURE

4.1 Introduction

The purpose of this chapter is to provide the details of the solution procedures for the equations governing three-dimensional parabolic and partially-parabolic flows. The calculation procedure described here for parabolic flows is that reported earlier by Patankar and Spalding (1972); the details of this procedure are thus given here only for the sake of completeness and for the reader's convenience. The partially-parabolic procedure, however has been a development of the present investigation; and is described here for the first time.

The two calculation procedures are quite similar in their approach; they share several important features but differ in the manner in which they calculate the pressure field. The partially-parabolic procedure employs a single pressure field common to all the three momentum-equations whereas the parabolic procedure employs two separate pressure fields - one for the solution of the lateral momentum-equations and the other for the longitudinal-momentum equation. Since the calculation steps in the two procedures are similar, only one procedure is described here in detail.

From the view-point of ease in understanding, the partially-parabolic procedure is presented in detail; the parabolic procedure is later explained only briefly, by outlining its distinctive features.

Both calculation procedures comprise the following main steps.

(a) Subdivision of the flow domain into smaller regions by a finite-difference grid;

(b) integration of the differential equations over the finite-difference 'cells'; and

(c) solution of the algebraic equations obtained from the integration of step (b).

The details of these steps are described below.

4.2 Calculation procedure for partially-parabolic flows

The present section describes the calculation procedure to solve the differential equations governing a partially-parabolic flow situation. This calculation procedure has been a development over the parabolic calculation procedure of Patankar and Spalding (1972); thus a number of important details described below have already been reported earlier; and are reproduced here for sake of completeness of the description. The main features of the partially-parabolic calculation procedure are as follows.

4.2.1 The finite-difference grid

The finite-difference grid consists of orthogonal, intersecting grid lines, disposed over the flow domain along directions parallel to the three coordinate-axes. The intersections of these grid lines, usually called 'grid nodes', form reference locations for identifying the discrete values of the flow variables. The spacing between the grid lines is not stipulated to be uniform but can be varied to locate more grid nodes in regions of steep variations of the flow variables. The finite-difference grid is chosen after experimentation with finer and coarser grids so as to make the results of the computations substantially independent of grid-fineness.

4.2.2 Location of flow variables

Figure (4.2.1) shows the manner in which the flow variables are arrayed in the finite-difference grid. The pressure and the scalar properties such as enthalpy, concentration etc. are stored at the grid nodes while the velocity-components are placed midway between adjacent grid nodes. The 'staggered-grid' system adopted here has the following advantages:

(a) the velocity components are conveniently located for calculating the convective fluxes of flow properties stored at the grid nodes;

(b) the calculation of mass balance over a region surrounding a grid node is made easy because

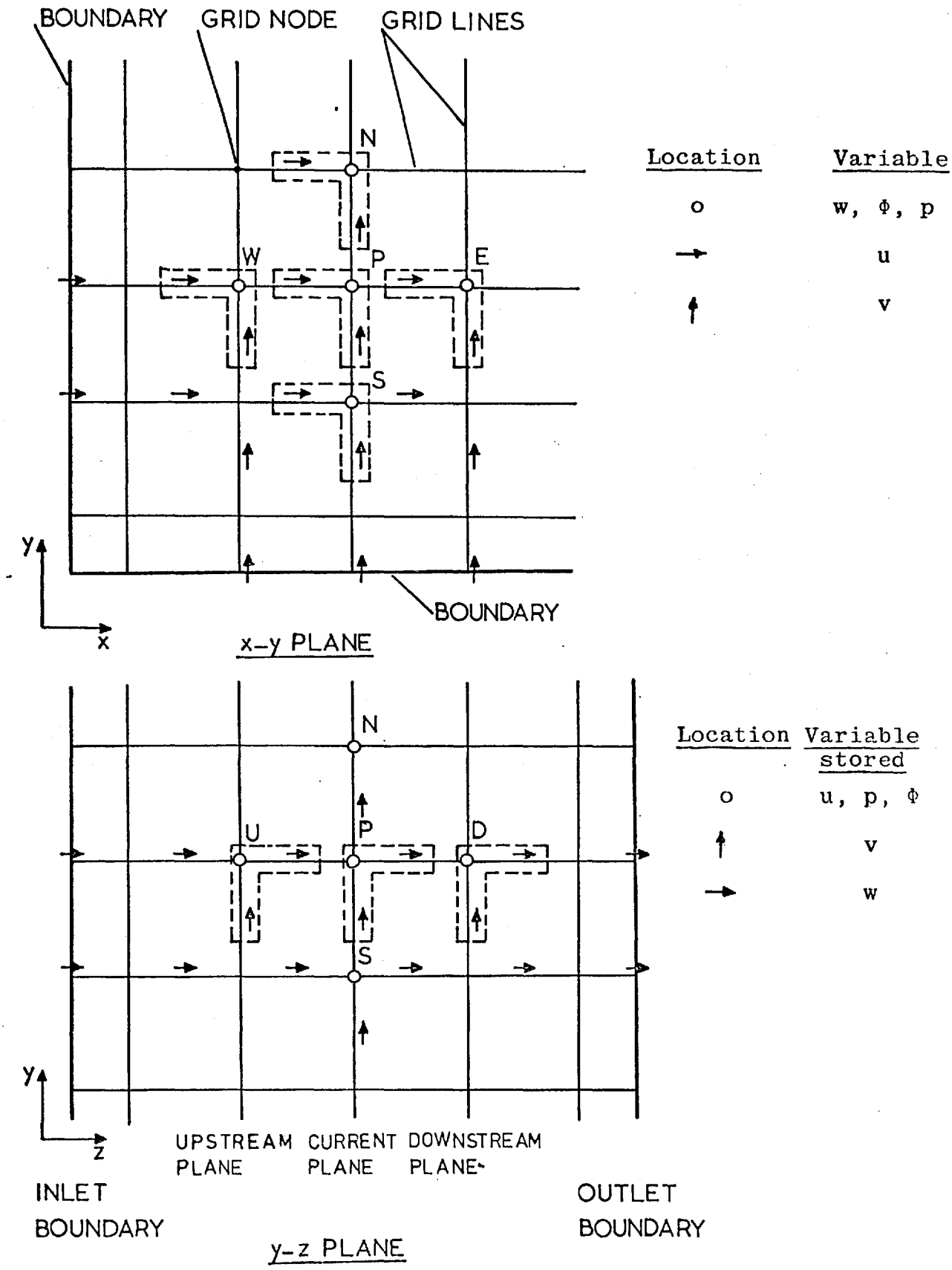

Fig. (4.2.1): Location of variables on the finite-difference grid.

the velocities normal to the boundaries of this region are located directly on the boundaries;

(c) the pressures are stored so as to make it easy to calculate the pressure gradients that affect the velocity components.

The dotted enclosures shown in the figure describe the manner in which the variables have been grouped for the purpose of identification; the variables enclosed by these dotted lines are denoted by the same subscript. (It is necessary to note here the slight difference in the practices for grouping the velocities in the x-y plane and in the y-z plane.)

4.2.3 Control volumes for integration

The 'control volumes' represent regions, over which the partial-differential equations are integrated to obtain their finite-difference form. These control volumes are different for each flow variable. Figure (4.2.2) shows the control volumes for the velocity components and for a general variable, Φ. The boundaries of these control volumes are defined as follows. For variables located at the grid nodes, the boundaries of the control volumes, in all the three directions, lie half-way between two grid nodes; thus

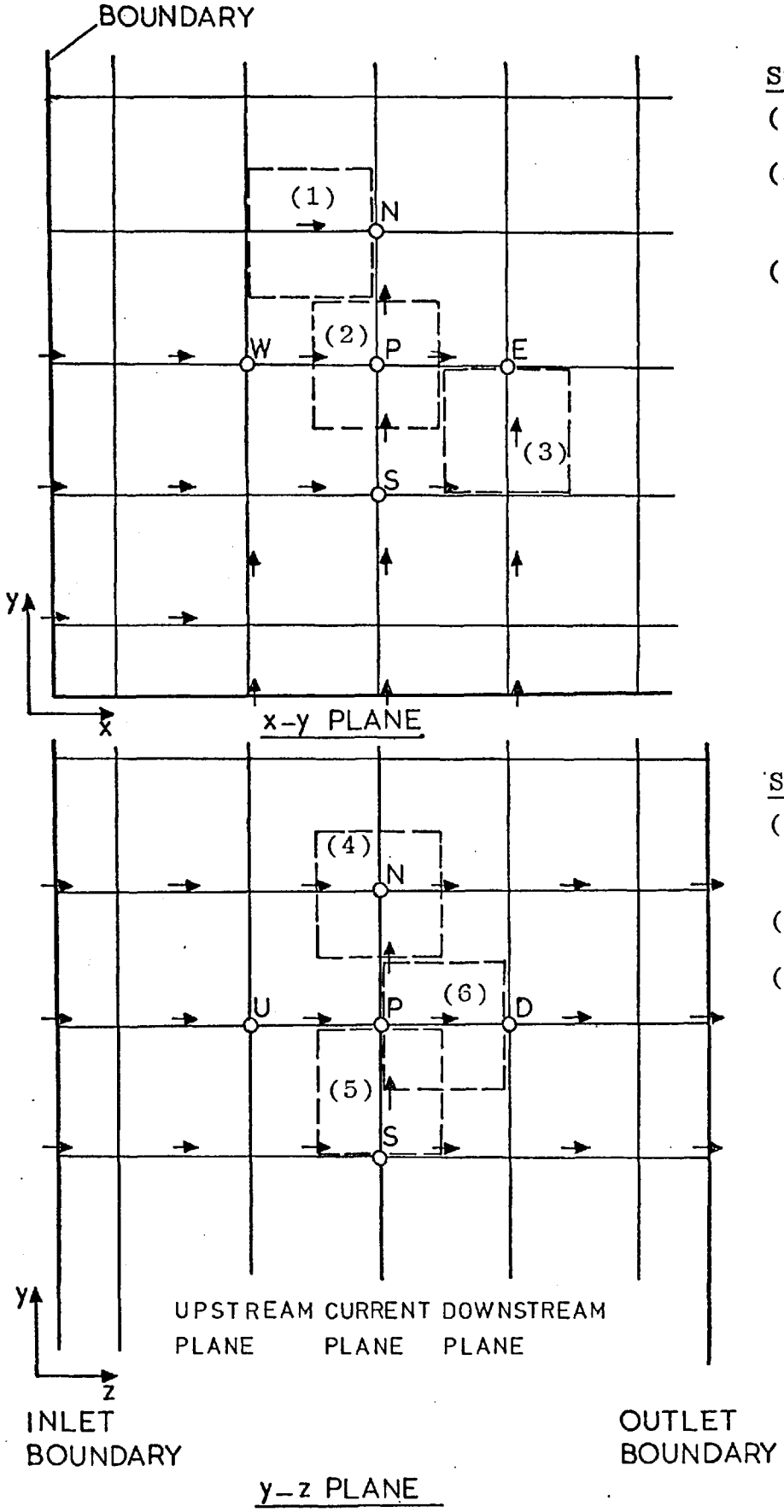

Symbol	Control volume for
(1)	u_N
(2)	w_P, Φ_P and continuity
(3)	v_E

Symbol	Control volume for
(4)	Φ_N, u_N and continuity
(5)	v_P
(6)	w_P

Fig. (4.2.2): Definition of control volumes.

the interfaces of the control volumes always pass through locations at which the normal-velocities are stored. The control volumes for velocity components are defined in a similar way, but the above practice is adopted only along those directions which are perpendicular to the velocity; for the direction along the velocity, the edges of the control volume pass through the grid nodes which lie on either side of the velocity.

4.2.4 Location of flow variables near the boundaries

The staggered grid system explained above for locating the velocity-components presents a few difficulties in calculating the flow variables situated adjacent to the boundaries of the flow domain. To overcome these difficulties, slightly different practices are adopted for locating the near-boundary velocities. Figure (4.2.1) illustrates the location of the velocities near the boundaries. The new practice consists of altering the locations of the velocities normal to the boundaries from their staggered positions to locations directly on the boundary. The new locations of the near-boundary velocities also modify the control volumes for the variables situated near the boundary; these changes are shown in Figure (4.2.3).

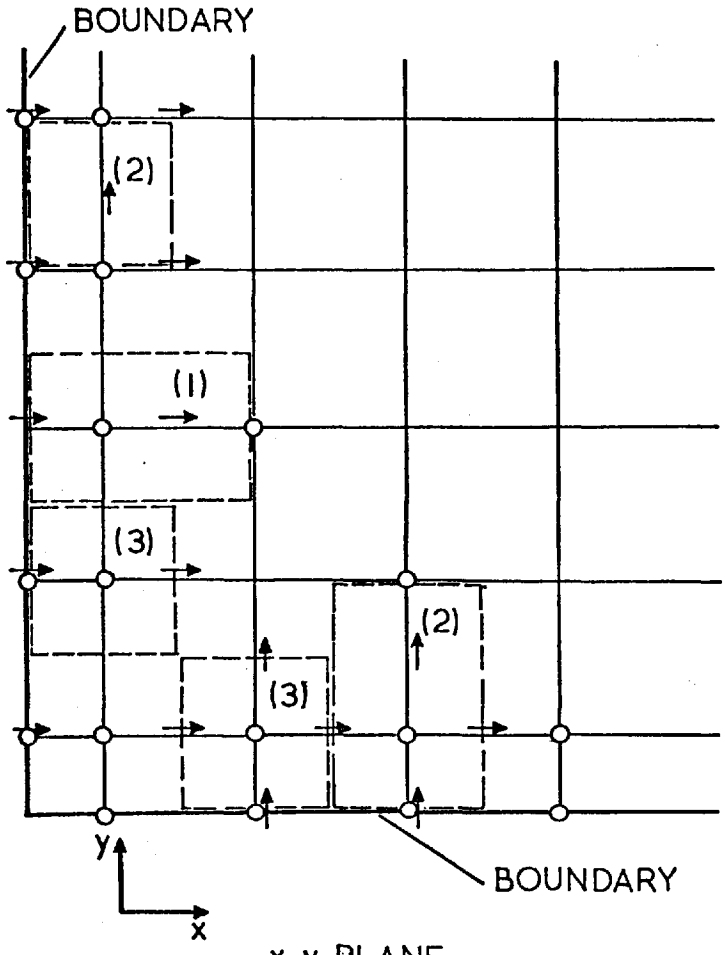

Symbol	Control volume for
(1)	u
(2)	v
(3)	w, Φ, p'

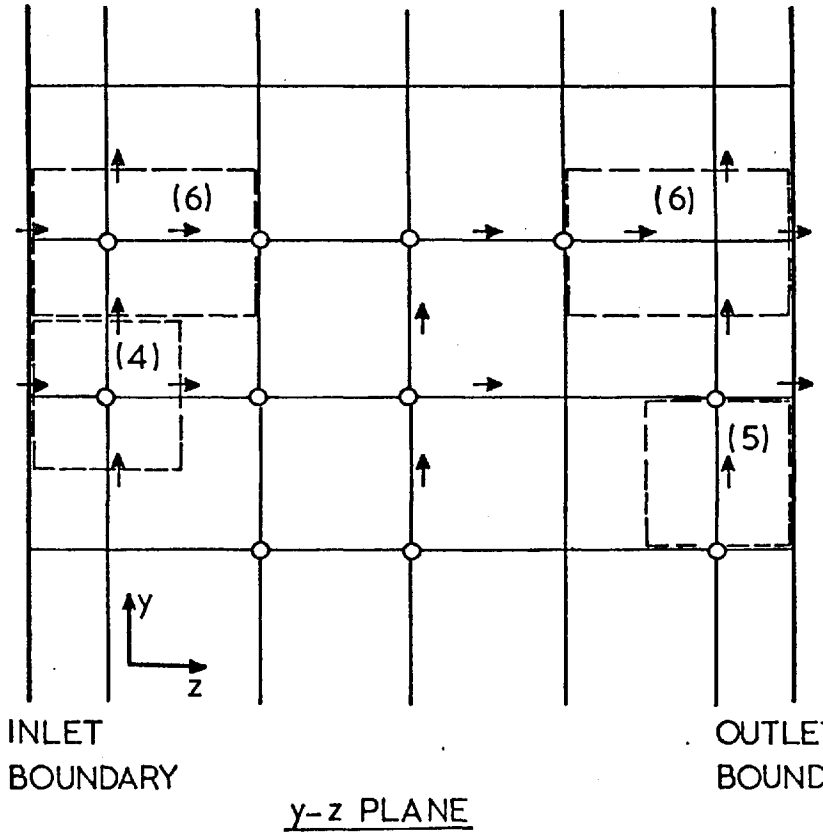

Symbol	Control volume for
(4)	u, Φ, p'
(5)	v
(6)	w

Fig. (4.2.3): Near-boundary control volumes.

4.2.5 Discretisation of the differential equations

The discretisation procedure described below is the same as that described in Patankar and Spalding (1972) except that it is now recast in a slightly different manner to suit the partially-parabolic equations. Since the transport equations have a generalised form (ref. Chapter 3), the procedures for their discretisation are identical; thus the steps in the discretisation procedure are explained below with reference to the differential equation for a general variable Φ. The equation considered is the partially-parabolic form of (3.2.5), written as

$$\underset{(1)}{\frac{\partial}{\partial x}(\rho u \Phi)} + \underset{(2)}{\frac{\partial}{\partial y}(\rho v \Phi)} + \underset{(3)}{\frac{\partial}{\partial z}(\rho w \Phi)} = \underset{(4)}{\frac{\partial}{\partial x}\left(\Gamma_\Phi \frac{\partial \Phi}{\partial x}\right)} + \underset{(5)}{\frac{\partial}{\partial y}\left(\Gamma_\Phi \frac{\partial \Phi}{\partial y}\right)} + \underset{(6)}{S_\Phi} \qquad (4.2.1)$$

The symbols in the above equation have the same meanings as in equation (3.2.5).

Assumptions.

To discretise the various terms of (4.2.1) a few assumptions are first made regarding the variation of Φ over the grid spacings. These assumptions have been earlier validated in the various application-studies of the parabolic procedure and are thus also adopted here. The assumptions are:

(a) For terms representing convection along the x and y-directions (i.e. terms (1) and (2)), the value of Φ is assumed to vary linearly between grid nodes. This implies that for an interface which is midway between two grid nodes, the value of Φ that is convected across the interface is the arithmetic mean of the Φ values at the grid nodes. However, this value of Φ is later modified in circumstances when the convective flux is much larger compared to the diffusive flux in the same direction. This modification, called the "high-lateral-flux modification" removes certain difficulties associated with the central-difference scheme (for details of this modification, refer Spalding (1971); or Patankar and Spalding (1972)).

(b) For convection in the z-direction (represented by term (3)), it is assumed that the value of Φ which is convected is equal to its upstream value, Φ_U. The variation of Φ_U in the x-y plane is assumed to be step wise, i.e. Φ_U is constant over the dotted region shown in Figure (4.2.2) but changes suddenly at its edges, to the values at the neighbouring nodes.

(c) For diffusion in the x-y plane, the variation of Φ is assumed to be linear; but is also altered later, by the high-lateral-flux modification.

The integrated equation

Equation (4.2.1) is now integrated over the control volume for the Φ variable; and in the integrated form it may be expressed as follows.

$$L_e^x \Phi_e - L_w^x \Phi_w + L_n^y \Phi_n - L_s^y \Phi_s + F_P \Phi_P - F_U \Phi_U$$

(1) (2) (3)

$$= T_e^x (\Phi_E - \Phi_P) - T_w^x (\Phi_P - \Phi_W)$$

(4)

$$+ T_n^y (\Phi_N - \Phi_P) - T_s^y (\Phi_P - \Phi_S)$$

(5)

$$+ s_{\Phi,U} \Delta x \, \Delta y \, \Delta z + s_{\Phi,P} \Phi_P \Delta x \, \Delta y \, \Delta z$$

(6) (4.2.2)

In the above equation, the symbols L, T and F stand for the following expressions:

$$L_e^x = (\Delta y\ \Delta z)\ (\rho u)_e$$

$$L_w^x = (\Delta y\ \Delta z)\ (\rho u)_w$$

$$L_n^y = (\Delta x\ \Delta z)\ (\rho v)_n$$

$$L_s^y = (\Delta x\ \Delta z)\ (\rho v)_s$$

$$T_e^x = \Gamma_e \left(\frac{\Delta y \Delta z}{\delta x} \right)_e \qquad (4.2.3)$$

$$T_w^x = \Gamma_w \left(\frac{\Delta y \Delta z}{\delta x} \right)_w$$

$$T_n^y = \Gamma_n \left(\frac{\Delta x \Delta z}{\delta y} \right)_n$$

$$T_s^y = \Gamma_s \left(\frac{\Delta x \Delta z}{\delta y} \right)_s$$

$$F_U = (\rho w)_U\ \Delta x\ \Delta y \quad ; \quad F_P = (\rho w)_P\ \Delta x\ \Delta y$$

where the subscripts E, W, N, S, P and U refer to the grid nodes E, W, N, S, P and U; the subscripts e, n, s, w refer to the corresponding locations, shown in Figure (4.2.4); and the dimensions Δx, Δy, Δz, δx and δy are as defined in Figure (4.2.4). The values of Φ_e, Φ_w, Φ_n, Φ_s represent the flow properties convected from the interfaces normal to the x and y directions; they are expressed as a linear combination of the values on either side of the interface, thus;

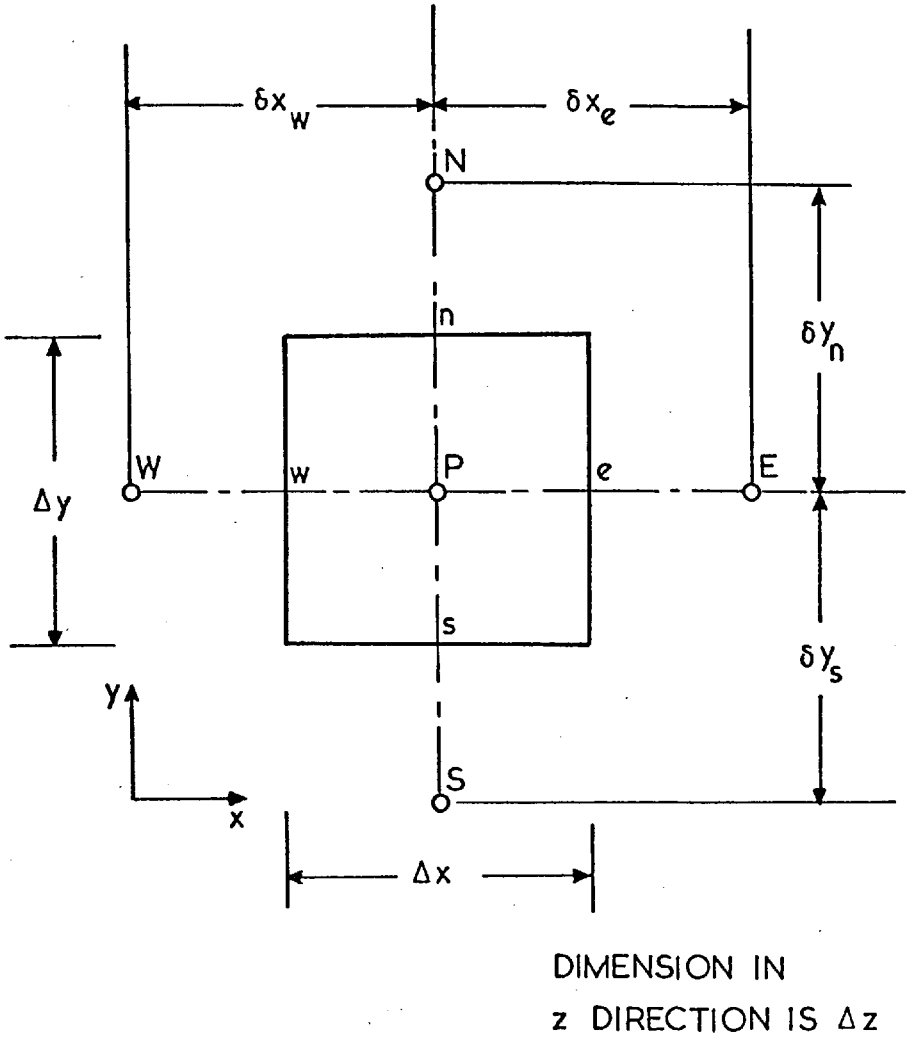

Fig. (4.2.4): Grid nomenclature for discretisation procedure.

$$\Phi_e = f_e^x \Phi_E + (1 - f_e^x) \Phi_P$$

$$\Phi_w = f_w^x \Phi_P + (1 - f_w^x) \Phi_W$$

$$\Phi_n = f_n^y \Phi_N + (1 - f_n^y) \Phi_P \qquad (4.2.4)$$

$$\Phi_s = f_s^y \Phi_P + (1 - f_s^y) \Phi_S$$

With the interpolation factors f_e^x, f_w^x, f_n^y, f_s^y having the following meaning:

$$f_e^x = \frac{(\delta x)_e}{2\Delta x}$$

$$f_w^x = \frac{(\delta x)_w}{2\Delta x} \qquad (4.2.5)$$

$$f_n^y = \frac{(\delta y)_n}{2\Delta y}$$

$$f_s^y = \frac{(\delta y)_s}{2\Delta y}$$

The expression for F_P may be obtained by integrating the continuity equation; and is as follows:

$$F_P = F_U - L_e^x + L_w^x - L_n^y + L_s^y \qquad (4.2.6)$$

The last two terms in (4.2.2) represent the contribution due to the source terms; they have been obtained by expressing s_Φ of (4.2.1) in a linearised form so that

$$S_\Phi = S_{\Phi,U} + S_{\Phi,P}\,\Phi_P \qquad (4.2.7)$$

where the subscripts U and P refer to the upstream and the 'current' values. $S_{\Phi,U}$ and $S_{\Phi,P}$ are volume-averaged values of the source terms and are prescribed after integrating the corresponding expressions over the Φ control-volume.

The expressions (4.2.4) to (4.2.7) when substituted into (4.2.2) give the following expression for Φ_P:

$$\Phi_P = A_E^{\Phi}\,\Phi_E + A_W^{\Phi}\,\Phi_W + A_N^{\Phi}\,\Phi_N + A_S^{\Phi}\,\Phi_S + B^{\Phi} \qquad (4.2.8)$$

where,

$$A_E = A'_E/A'_P$$

$$A_W = A'_W/A'_P$$

$$A_N = A'_N/A'_P$$

$$A_S = A'_S/A'_P$$

$$B = B'/A'_P$$

and,

$$A'_E = T_e^x - f_e^x L_e^x$$

$$A'_W = T_w^x + (1 - f_w^x) L_w^x$$

$$A'_N = T_n^y - f_n^y L_n^y$$

$$A'_S = T_s^y + (1 - f_s^y) L_s^y$$

$$B' = s_{\Phi,U} \Delta x \Delta y \Delta z + F_U \Phi_U$$

$$A'_P = A'_E + A'_W + A'_N + A'_S - s_{\Phi,P} \Delta x \Delta y \Delta z \qquad (4.2.9)$$

Equation (4.2.8) represents the final form of the finite-difference equation for the differential equation (4.2.1) and describes the general structure of the finite-difference equations solved by the solution scheme, to be described in Sec. (4.2.6).

Equations for the velocity components

The finite-difference equations for the velocity components are obtained in a manner similar to that of (4.2.8), by integrating each momentum-equation over the control volume for the appropriate velocity-component (shown in Figure (4.2.2)). The finite-difference equations so obtained for the

velocity components are:

$$u_P = A_E^u\, u_E + A_W^u\, u_W + A_N^u\, u_N + A_S^u\, u_S + B^u + D^u\,(p_P - p_W) \qquad (4.2.10)$$

$$v_P = A_E^v\, v_E + A_W^v\, v_W + A_N^v\, v_N + A_S^v\, v_S + B^v + D^v\,(p_P - p_S) \qquad (4.2.11)$$

$$w_P = A_E^w\, w_E + A_W^w\, w_W + A_N^w\, w_N + A_S^w\, w_S + B^w + D^w\,(p_D - p_P) \qquad (4.2.12)$$

The A and B coefficients in the above equations have similar meanings to those in (4.2.9); the subscript D (eqn. (4.2.12)) refers to the value at the downstream location. The new symbols D^u, D^v, D^w are defined as follows.

$$D^u = -\Delta y\, \Delta z / A'^u_P$$

$$D^v = -\Delta x\, \Delta z / A'^v_P \qquad (4.2.13)$$

$$D^w = -\Delta x\, \Delta y / A'^w_P$$

where the A's have the same meaning as in (4.2.9).

The continuity equation

The discretised form of the continuity equation is derived by making a mass balance over the control volume shown in Figure (4.2.2); and is expressed as follows:

$$C^u \{(\rho u)_E - (\rho u)_P\} + C^v \{(\rho v)_N - (\rho v)_P\}$$

$$+ C^w \{(\rho w)_P - (\rho w)_U\} = 0 \qquad (4.2.14)$$

where the quantities C^u, C^v and C^w represent the areas of the cell faces normal to the corresponding velocity-components. It may be interesting to note that equation (4.2.14) can also be obtained by substituting a value of Φ equal to unity in equation (4.2.2).

4.2.6 The solution procedure

Main features

The aim of the solution procedure described here is to seek a simultaneous solution of the finite-difference equations expressed by equations (4.2.8), (4.2.10) to (4.2.12) and (4.2.14). The unknowns in these equations are the three velocity-components u, v and w, the pressure and the scalar flow-properties. Since the three momentum equations are coupled through the unknown pressure field it has

been necessary to employ an iterative procedure for their solution in which the pressure field is guessed, and is corrected so as to bring the velocities in conformity with the continuity equation. The equations being nonlinear, this correction procedure necessitates more than one iteration. The main features of the present solution procedure are as follows:

1) The solution procedure employs a guess and correct procedure for the calculation of the correct pressure-field. Several 'sweeps' are made through the flow domain and the pressure field is corrected each time.

2) The flow variables are calculated by 'marching' through the flow domain, along the predominant flow direction; in this marching, the flow variables at any longitudinal station are calculated solely from values at an upstream location.

3) The finite-difference equations are solved by a tridiagonal matrix algorithm (TDMA), along lines in the x and y directions; in this, when the equations are solved along lines of constant-x, the values of the variables at adjacent y-locations are kept fixed; and vice versa.

4) The pressure field is stored as a <u>three-dimensional</u> array and is 'updated' in each

marching of the flow domain. All other variables and the coefficients are stored at any time as two-dimensional arrays along cross-sectional planes.

Sequence of calculation steps

The sequence in which the calculation steps are executed is as follows.

1) The pressure field which is stored in a three-dimensional array is assigned guessed values at the start of the integration.

2) Using the guessed values of the pressure field, the momentum equations in the x, y and z directions at a downstream station are solved; the coefficients in the equations are evaluated on the basis of flow properties at the upstream longitudinal-station. The sequence of the calculations has been to solve first for the u and v velocities and then for the w-velocity which is situated ahead of the cross-stream plane containing the u and v velocities.

3) The pressure field is corrected to bring the velocities in conformity with the continuity equation. These corrections are applied for one cross-stream plane at a time, and are calculated as follows:

(a) The pressure and velocity fields are first expressed as

$$\begin{aligned} p &= p^* + p' \\ u &= u^* + u' \\ v &= v^* + v' \\ w &= w^* + w' \end{aligned} \qquad (4.2.15)$$

where the primed quantities represent the corrections to the approximate (starred) values.

(b) The corrections to the velocities are related to the pressure corrections by substituting (4.2.15) in the momentum equations. The expressions for the velocity components are written in a simplified form as

$$\begin{aligned} u_E &= u_E^* + D_E^u (p'_E - p'_P) \\ u_P &= u_P^* + D_P^u (p'_P - p'_W) \text{ †} \\ v_N &= v_N^* + D_N^v (p'_N - p'_P) \end{aligned} \qquad (4.2.16)$$

---

†See footnote on next page.

$$v_P = v_P^* + D_P^v \, (p'_P - p'_S)$$

$$w_P = w_P^* - D_P^w \, (p'_P) \quad ^{\dagger\dagger} \qquad (4.2.16)$$

$$w_U = w_U^* + D_U^w \, p'_P \quad ^{\dagger\dagger\dagger}$$

(c) The relations expressed above are then substituted in the finite-difference form of the continuity equation (4.2.14); the coefficients for p'_P are collected and rearranged to obtain the following expression for p'_P.

$$A_P^p \, p'_P = A_E^p \, p'_E + A_W^p \, p'_W + A_N^p \, p'_N + A_S^p \, p'_S + \dot{m}_P \qquad (4.2.17)$$

---

† The complete expressions for these velocities are of the following form:

$$u_P = u_P^* + D_P^u \, (p'_P - p'_W) + A_E^u \, (u_E - u_E^*) + A_W^u \, (u_W - u_W^*) + A_N^u \, (u_N - u_N^*) + A_S^u \, (u_S - u_S^*);$$

by dropping the last four terms we get the expressions described by (4.2.16).

†† In deriving this expression and the one following it, it has been assumed that $p'_D = p'_U = 0$.

††† Although w_U is not calculated along with u_P, v_P and w_P, it <u>is</u> affected by a change in the pressure at P; hence the expression for w'_U.

where, p'_E , p'_W , p'_N , p'_S are corrections to the pressures at the nodes N, S, E and W; and the 'A's represent the products of the 'D' coefficients and the cell areas C^u, C^v and C^w. The quantity $\dot{m}_P$ expresses the mass imbalance over the region surrounding the grid node P and is given by

$$\dot{m}_P = C^u \{(\rho u^*)_E - (\rho u^*)_P\} + C^v \{(\rho v^*)_N - (\rho v^*)_S\} - C^w \{(\rho w^*)_P - (\rho w^*)_U\} \qquad (4.2.18)$$

and

$$A_P{}^p = A_E{}^p + A_W{}^p + A_N{}^p + A_S{}^p + A_U{}^p + A_D{}^p \qquad (4.2.19)$$

(d) Equation (4.2.19) which has the same form as (4.2.8) is solved in the same manner as the momentum equations are solved; and the pressure and velocities are thereafter corrected accordingly. However, while correcting the pressures it has been found beneficial to under-relax the corrections so that

$$p = p^* + \alpha p'$$

where p' is the correction calculated from the equation and α is a value between 0 and 1; α usually has a value around 0.5.

4) The equations for variables such as enthalpy, kinetic-energy of turbulence etc. are solved so as to provide distributions appropriate to the downstream station.

5) Steps 2, 3 and 4 are repeated at all the downstream locations in the flow domain.

6) Such sweeps through the flow domain, consisting of steps 2, 3, 4 and 5 are repeated several times, each time using a more-correct guess for the pressure-field; the procedure is terminated when the corrections to the pressure field have become smaller than a preassigned value. On the last sweep, the distributions of the velocities, shear stresses as are required are printed out.

Details of the TDMA sweeps

The TDMA sweeps by which the finite-difference equations are solved are described below in somewhat more detail. These sweeps are performed as follows. First, for the x-direction sweep, equation (4.2.8) is written as

$$\Phi'_P = A_E \Phi'_E + A_W \Phi'_N + (A_N \Phi_{N,U} + A_S \Phi_{S,U} + B) \qquad (4.2.20)$$

The expression in the parenthesis is calculated from the upstream values; and equation (4.2.20) is solved by an elimination procedure. The superscript I denotes the values obtained from this first phase of solution. In the second phase, the y-direction sweep is made in a similar manner; the equation now solved is

$$\Phi_P^{II} = A_N \Phi_N^{II} + A_S \Phi_S^{II} + (A_E \Phi_E^{I} + A_S \Phi_S^{I} + B) \qquad (4.2.21)$$

where, the quantities in the parenthesis represent those obtained from the x-direction sweep.

In order to reduce the errors in the solution of the equations, the TDMA sweeps are usually repeated a number of times, depending on the equation under consideration. For the momentum equation, it has been found sufficient, from the viewpoint of accuracy, to perform only one TDMA sweep in each direction. For the pressure-correction equation however, it has been advantageous to make at least three such sweeps along the x and y directions. The sequence in which these x and y direction sweeps are made is however, arbitrary; nevertheless, it is advantageous from accuracy view point to alternate this sequence, as the flow domain is swept through.

4.2.7 Incorporation of the auxiliary information

Boundary conditions

The boundary conditions for the equations described by (4.2.8) are normally of two types. They are such that either the value of the variable is specified at the boundary or a prescription is made, indirectly, of the gradient of the variable normal to the boundary. For example, at stationary, impervious walls, the velocities are zero; but at planes of symmetry, their gradients normal to the boundary are zero. The incorporation of either type of boundary condition, into the calculation procedure is easy; and is achieved by modifying either the source terms or the exchange coefficients in the finite-difference equations for the near-boundary variables. The boundary conditions for the pressure-correction equation are also prescribed in a similar manner. Thus, at boundaries where the velocities are fixed, the gradients of the pressure-corrections normal to that boundary are made zero; and when the values of the pressure themselves are prescribed, such as that at a free-stream boundary, the corrections to the pressure at that boundary are put to zero. As for other variables, the incorporation of either condition is straightforward .

Other auxiliary information

Other auxiliary information to be specified consists of: (a) the exchange coefficients (Γ's) and (b) the source terms in the individual equations.

These are prescribed as follows. The exchange coefficients are calculated from the physical conditions of the flow. For laminar flows, the Γ's are made equal to the molecular diffusion coefficients and are prescribed as a function of the fluid temperature; for turbulent flows, the exchange coefficients are calculated in conjunction with the turbulence model employed. The turbulence model employed for the present computations is described in Chapter 5. The source terms which usually represent the effects of body forces, chemical reaction, turbulence etc. are prescribed to the calculation procedure as values averaged over the appropriate control volumes; and are evaluated partly from the values of variables at the upstream. This partial use of upstream values of the source terms has been, in several earlier instances (see Sharma (1974), p. 208) beneficial in promoting stability of the numerical scheme; and is therefore adopted also in the present procedure.

4.2.8 Summary of the entire calculation procedure

The main steps in the partially-parabolic calculation procedure may now be summarised as follows:

1) The flow domain in which the distributions of velocity, temperature are to be calculated is divided into smaller flow regions, by a finite-difference grid.

2) The partial-differential equations governing the transport of various flow variables are integrated over finite-difference 'cells' and are expressed as algebraic equations. The auxiliary information consisting of boundary conditions, source terms and the exchange coefficients is incorporated into the algebraic equations.

3) The finite-difference equations are then solved by making repeated sweeps through the flow domain; at any longitudinal station in the flow domain, the variables are calculated solely from the values of the variables at the upstream station. In each sweep, the guessed three-dimensional pressure field is corrected for the simultaneous satisfaction of the momentum and continuity equations.

4) The procedure is terminated when the corrections to the pressure field have become smaller than a certain preassigned value.

4.3 Calculation procedure for parabolic flows

4.3.1 Introduction

This section describes the calculation procedure for parabolic flows. This procedure has been earlier reported by Patankar and Spalding (1972); and is

described here only for the sake of completeness. The partial-differential equations solved by this procedure are those expressed by equations (3.2.1) to (3.2.7). The distinctive features of the parabolic procedure in comparison with the partially-parabolic procedure are

(a) the pressure field, like all other variables, is stored in a two-dimensional array; and

(b) all variables are calculated in one single sweep through the flow domain; and no iterations are made.

In the following sub-sections, the details of the parabolic procedure are explained in the same manner as those for the partially-parabolic procedure. However, only the differences between the two procedures are described in detail; and the common features are only briefly mentioned.

4.3.2 A reminder of the parabolic concept

Parabolic flows, which have been defined in Chapter 3, are fundamentally one-way processes; i.e. influences travel only from upstream to downstream and not vice versa. Thus in these situations, diffusion and also pressure transmission are negligible along the predominant flow direction; and convection exerts influence only along the flow direction. The difference between the governing equations for parabolic and partially-parabolic flows is that for parabolic flows, the pressure field in the longitudinal momentum equation is simplified and is represented by a value $\bar{p}$

which is constant over a cross-sectional plane. The longitudinal momentum equation for parabolic flows is given by:

$$\frac{\partial}{\partial x}(\rho uw) + \frac{\partial}{\partial y}(\rho vw) + \frac{\partial}{\partial z}(\rho ww) = -\frac{\partial \bar{p}}{\partial z} + \frac{\partial \tau_{zx}}{\partial x} + \frac{\partial \tau_{zy}}{\partial y} + S_w \qquad (3.2.7)$$

The use of such a $\bar{p}$ pressure field prohibits any down-stream events to be transmitted upstream. It is economical to be employed because it permits a 'once-through' marching procedure through the flow domain. The use of a $\bar{p}$ field does not introduce large errors in the solution when there are no sharp curvatures in the stream lines.

4.3.3 The finite-difference grid

The finite-difference grid, the location of the flow variables and the definition of the control volumes in the parabolic calculation procedure are the same as those explained earlier except for one difference which is that the w-velocity in the parabolic procedure is no longer staggered between two grid nodes but instead is placed directly at the grid nodes where also the pressures are stored† Because of this new location of the w-velocity, the control volumes are defined in a

†Lately, Spalding (1975) has suggested that the w-velocity in parabolic procedure can also be considered as staggered, the above difference is based on the method as reported in (1972).

slightly different manner. The differences which are only in the y-z plane are shown in Fig. (4.3.1). The two cross-stream planes at the sides of the control volume are labelled as upstream and current, and are separated by the step size in the z-direction.

4.3.4 The finite-difference equations

The finite-difference equations for the parabolic procedure are derived in the same manner as explained in Sec. (4.2.6); they are:

$$u_P = A_E^u u_E + A_W^u u_W + A_N^u u_N + A_S^u u_S + D_P^u (p_P - p_W) + B^u \qquad (4.3.1)$$

$$v_P = A_E^v v_E + A_W^v v_W + A_N^v v_N + A_S^v v_S + D_P^v (p_P - p_S) + B^v \qquad (4.3.2)$$

$$w_P = A_E^w w_E + A_W^w w_N + A_N^w w_N + A_S^w w_S + \underline{D_P^w (\bar{p}_P - \bar{p}_U)} + B^w \qquad (4.3.3)$$

$$\Phi_P = A_E^\Phi \Phi_E + A_W^\Phi \Phi_W + A_N^\Phi \Phi_N + A_S^\Phi \Phi_S + B^\Phi \qquad (4.3.4)$$

The above equations are identical to those derived in Sec. (4.2.6) except for equation (4.3.3) which differs from its counterpart because of the underlined term.

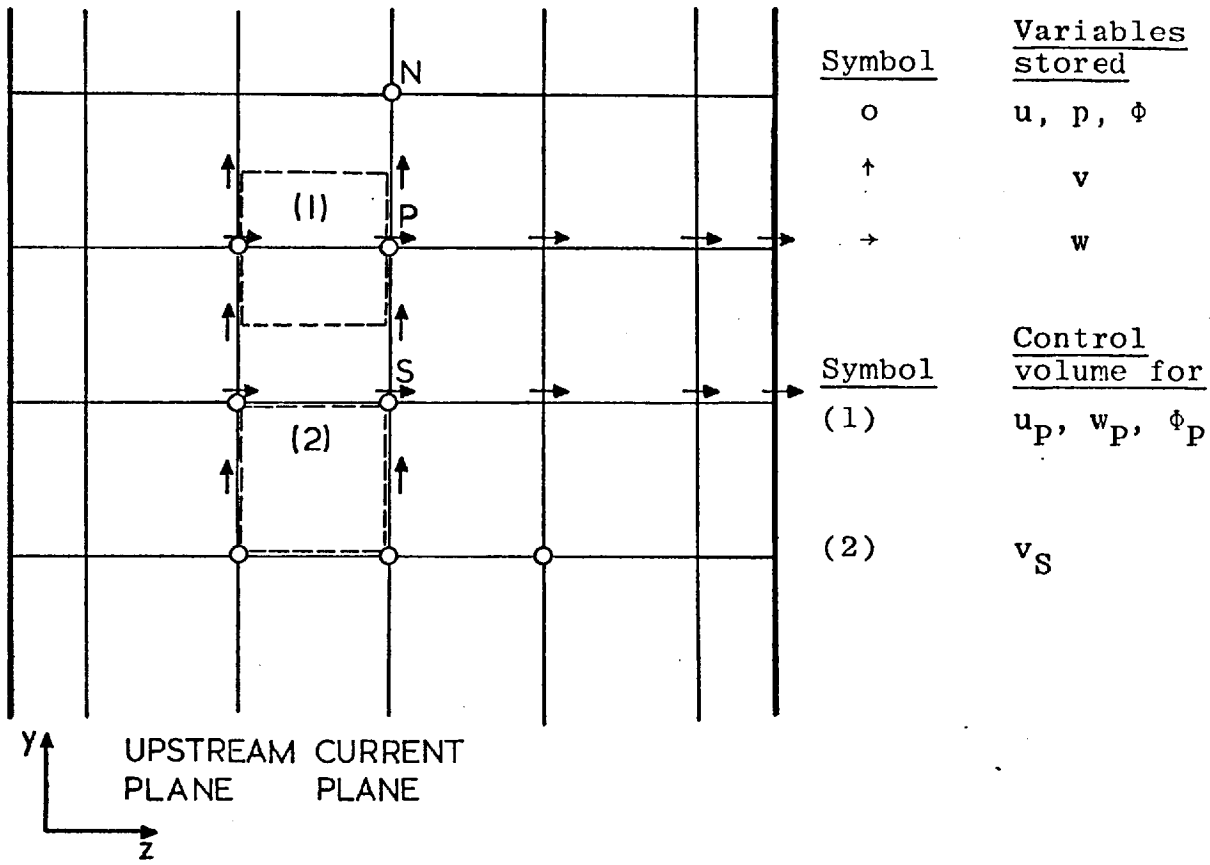

Fig. (4.3.1): Location of flow variables for the parabolic calculation-procedure.

4.3.5 Solution procedure

The finite-difference equations for a parabolic flow present a simpler task for their solution. Since the longitudinal momentum equation is not coupled with the other two momentum equations, it can now be solved independently, provided the coefficients and the pressure gradient term are correctly prescribed. Thus iteration is restricted to the cross-stream planes, so that all variables can be calculated by a single 'sweep' through the flow domain; in this sweep several forward steps are taken along the longitudinal direction, and at each forward step the flow variables are calculated for the cross-sectional plane at that location; the pressure fields p and $\bar{p}$ are first guessed and later corrected for the satisfaction of the continuity equation. The present procedure, which incorporates the above features, is comprised of the following calculation steps.

1) The pressure field 'p' at any longitudinal station and the value $\bar{p}$ at an adjacent downstream location are assigned values.

2) The three momentum equations expressed by (4.3.1) to (4.3.3) are solved to get a first approximation to the velocity field at the longitudinal station; the 'A' coefficients in the equations are calculated from upstream values of the flow variables.

3) The mean pressure $\bar{p}$, and the axial velocities, are thereupon corrected by reference to

continuity and the linearised longitudinal momentum equation, so as to ensure that the mass flow rate through the cross-sectional plane is the same as the true flow rate through the duct, $\bar{m}$, computed from inlet and boundary conditions. The expression for this pressure-correction is deduced as follows: we first write

$$\bar{p} = \bar{p}^* + \bar{p}' \qquad (4.3.5)$$

$$\text{and } w_p = w_p^* + D^w \bar{p}_p' \qquad (4.3.6)$$

Since it is desired that

$$\Sigma \Sigma \rho w_p \Delta x \Delta y = \bar{m} \qquad (4.3.7)$$

where Δx, Δy are the cell areas normal to the w-velocities and the summation is carried over all cells in the cross-stream plane, we get, by substitution of (4.3.6) into (4.3.7)

$$\bar{p}_p' = \bar{m} - \frac{\Sigma\Sigma \rho w_p^* \Delta x \Delta y}{\Sigma\Sigma \rho D^w \Delta x \Delta y} \qquad (4.3.8)$$

$\bar{p}_p'$ is assumed to be uniform over the cross-section.

The w-velocity field and the $\bar{p}$ pressure-field are thereafter corrected accordingly.

4) The cross-stream velocities are corrected for the local satisfaction of the mass-continuity. A pressure-correction equation is derived in a way similar to that of (4.2.17) but now the w-velocity field is kept fixed at the value calculated in step 3. This pressure correction equation which has the same form as (4.2.17) is also written as

$$A_P^p p_P' = A_E^p p_E' + A_W^p p_W' + A_N^p p_N' + A_S^p p_S' + \dot{m}_P \qquad (4.3.9)$$

However, the present value of A_P^p is different from that defined by (4.2.19); in the present case, it is given by the expression

$$A_P^p = A_E^p + A_W^p + A_N^p + A_S^p \qquad (4.3.10)$$

The difference between (4.2.19) and (4.3.10) is the absence of terms A_U^p and A_D^p in equation (4.3.10). These terms connect the downstream regions with the upstream ones and are absent in (4.3.10) as a consequence of the fully-parabolic nature of the flow.

Another important aspect to note is that the pressure field calculated in this step

corresponds to an upstream station whereas the $\bar{p}$ field calculated in step 3 is at the current longitudinal station; this difference is conceptually important but as such has no specific bearing on the calculation scheme.

5) The pressure field p and the velocity fields u and v are accordingly corrected.

6) The equations for the general flow variables such as enthalpy etc. are solved as to provide new distributions appropriate to the current longitudinal station.

7) A forward step is taken and calculation steps 1 to 6 are repeated at the new longitudinal station. The process of taking forward steps and calculating the flow variables is repeated till the end plane of the flow domain is reached.

4.4 Some improvements to the partially-parabolic calculation procedure

In this section, three modifications are suggested to the partially-parabolic calculation procedure described in Sec. (4.2). The objective of making these modifications is to procure faster rates of diminution of the pressure-corrections. These modifications have been successfully tested for the calculation of flow in curved ducts; but need further testing before being recommended for a permanent inclusion into the calculation procedure.

The first two modifications described below are the author's contributions, while the third was originally suggested by Spalding (1974).

1) Under-relaxation of the variables

While describing the calculation steps for the partially-parabolic procedure, it was mentioned that the pressure-corrections were under-relaxed before they were applied to the pressure field. A similar under-relaxation procedure has also been adopted for the calculation of flow variables themselves. The procedure consists of under-relaxing the variables calculated at any longitudinal station with their values at the upstream location. Thus, Φ_P is calculated by the relation

$$\Phi_P = \alpha \, \Phi_{P,0} + (1 - \alpha) \, \Phi_{P,U} \qquad (4.4.1)$$

where the '0' refers to the value calculated with no under relaxation (α=1) and the subscript U refers to the value at the upstream. α is the under-relaxation factor, usually of a value close to 0.5. It is however important to note here that the above under-relaxation, although will promote convergence, will give incorrect solutions when convergence is obtained. This is because of the 'weighting' done by the values at the upstream location. It is therefore necessary to remove this modification before final solutions are obtained, by making α=1.

2) Bulk-correction to the pressure field

This improvement consists in making an additional correction to the pressure field by reference to the integral mass-balance over the cross-sectional plane. The correction which is analogous to the correction of the $\bar{p}$ pressure field in the parabolic procedure, is also derived in a similar manner. This correction is applied to the pressure (p_D) at the downstream plane and is calculated from an expression similar to (4.3.8), thus:

$$p_D' = \bar{m} - \frac{\Sigma\Sigma\ \rho\ w_p\ \Delta x\ \Delta y}{\Sigma\Sigma\ \rho\ D^W\ \Delta x\ \Delta y} \qquad (4.4.2)$$

where the symbols have the same meaning as in (4.3.8). The pressures and velocities are also corrected accordingly. It is necessary to mention that this correction, as in the parabolic procedure, is applicable only for the calculation of confined flows.

3) Upstream shifting of pressure corrections

In the calculation procedure described earlier in Sec. (4.2), the downstream influences travel upstream at a rate which is only one cross-stream plane per iteration of the flow domain. This rate of transmission of downstream events is slow; and it necessitates a large number of marching sweeps through the

flow domain before the downstream events are made to influence the upstream flow. The present modification is designed to overcome this disadvantage. The procedure is to apply parts of the pressure corrections calculated at any longitudinal station also to the pressures at the upstream locations. Thus,

$$(p_U)_{new} = (p_U)_{old} + \beta\ p'_P \qquad (4.4.3)$$

where p_U is the pressure at a typical upstream plane and p'_P is the pressure correction calculated at the 'current' longitudinal station. β is a 'reduction factor' which depends on the dimensions Δx, Δy and the proximity of the upstream plane; β diminishes in a somewhat geometric way with distance between the upstream plane and the plane where the pressure-correction is calculated. The formula for β is derived in Appendix A2.

The experiences of using the present modification have been encouraging; savings in computer time to the extent of 25 percent have been observed using this modification.

4.5 Summary

In the present chapter, two calculation procedures have been described for the calculation of parabolic and partially-parabolic flow situations. The

procedures are based on finite-difference methods and share several important features. The calculation procedures are general and are flexible to be applied to calculate various physical flow situations, governed by different boundary-conditions.

The results of the computations made using the above calculation procedures will be presented in Chapters 7 and 8.

CHAPTER 5

MATHEMATICAL MODELLING OF TURBULENCE

5.1 Introduction

This chapter outlines the mathematical problem of turbulent flows and describes the way in which the effects of turbulent motion have been mathematically represented in the present study. First, the equations governing turbulent flows are stated; these equations are derived by time-averaging the equations governing the instantaneous transport of the flow variables. The additional terms which arise because of the turbulent motion are mathematically represented using a two-equation turbulence-model. In this turbulence model, the additional terms are related to the gradients of the corresponding flow property through an eddy viscosity; this viscosity is allowed to vary from one location in the flow domain to the other; but, at any point, it is assumed to be isotropic. The distribution of the eddy viscosity is calculated from the value of two turbulence variables, for which a pair of partial-differential transport equations is solved. The two variables in the present turbulence model are the kinetic energy of turbulence k, and its rate of

dissipation, ε.

The $k\sim\varepsilon$ turbulence model was first put forward by Harlow and Nakayama (1968) and has been subsequently used by many authors (e.g. Jones and Launder (1972), Launder et al (1972), Sharma (1974) and Tatchell (1975)). A full account of the model is given by Launder and Spalding (1973). The following description reproduces some of that account for completeness and draws special attention to a few novelties that have been introduced.

5.2 The mathematical problem

The present approach to calculate turbulent flows is to solve the equations which govern the transport of mean-flow variables; these equations are obtained by time-averaging the transport equations for the instantaneous values of the flow variables. Mathematically, this means expressing a general variable Φ as

$$\Phi = \bar{\Phi} + \Phi' \qquad (5.2.1)$$

where Φ is the time-averaged value and Φ' is the fluctuating component; and time-averaging the

resulting equations after substitution of the above relation. The time-averaged equation governing the property Φ in a steady, uniform density flow may be expressed as follows.

$$\rho \frac{\partial}{\partial x_i} (\bar{u}_i \bar{\Phi}) = \overline{s_\Phi} - \frac{\partial}{\partial x_i} (J_\Phi)_i - \rho \frac{\partial}{\partial x_i} (\overline{u_i' \Phi'}) \qquad (5.2.2)$$

where the bars denote the average values and the primes denote the fluctuating components. u_i is the velocity in the i^{th} coordinate direction; and the repetition of the subscript 'i' implies summation over all values of i[†]. $\overline{s_\Phi}$ denotes the source of Φ; and $(J_\Phi)_i$ is the molecular-diffusion flux in the i^{th} coordinate direction; ρ represents the fluid density.

The mathematical problem of turbulence lies in evaluating the 'turbulent fluxes', expressed by $\rho \frac{\partial}{\partial x_i} (\overline{u_i' \Phi'})$ in terms of the known variables of the equations. A relation of the following form is

---

[†]The summation convention is introduced here for sake of brevity. In the next sections, the nomenclature used earlier in Chapter 3 will be reintroduced.

therefore sought:

$$\overline{u_i' \Phi'} = f(\bar{u}_i, \bar{\Phi}) \qquad (5.2.3)$$

The manner in which the above functional relationship is expressed in the present study is explained below.

5.3 The k∿ε turbulence model

In this turbulence model, the turbulent fluxes are related to the gradients of the flow properties through a viscosity which, at any location in the flow, is assumed to be isotropic. The distribution of this viscosity over the flow domain is calculated from two turbulence variables; for which a pair of partial-differential equations is solved. The two variables in the present turbulence-model are the kinetic-energy of turbulence k, and its rate of dissipation, ε. The quantity k is defined as follows

$$k = \frac{1}{2} \left(\overline{u'^2} + \overline{v'^2} + \overline{w'^2} \right) \qquad (5.3.1)$$

where u', v' and w' are the fluctuating components of the three velocity-components u, v and w. The turbulent viscosity is calculated from the values of k and ε through the following formula

$$\mu_t = \rho C_\mu \frac{k^2}{\varepsilon} \qquad (5.3.2)$$

where μ_t is the scalar eddy viscosity; ρ is the density of the fluid and C_μ is a constant.

The partial-differential equations governing the transport of the k and ε, after making simplifications for the predominant nature of the flow, are represented, as follows†:

$$\rho \left(u \frac{\partial k}{\partial x} + v \frac{\partial k}{\partial y} + w \frac{\partial k}{\partial z}\right) = \frac{\partial}{\partial x}\left(\Gamma_k \frac{\partial k}{\partial x}\right) + \frac{\partial}{\partial y}\left(\Gamma_k \frac{\partial k}{\partial y}\right) + G - \rho\varepsilon \qquad (5.3.3)$$

$$\rho \left(u \frac{\partial \varepsilon}{\partial x} + v \frac{\partial \varepsilon}{\partial y} + w \frac{\partial \varepsilon}{\partial z}\right) = \frac{\partial}{\partial x}\left(\Gamma_k \frac{\partial \varepsilon}{\partial x}\right) + \frac{\partial}{\partial y}\left(\Gamma_k \frac{\partial \varepsilon}{\partial y}\right) + C_1 \frac{\varepsilon}{k} \cdot G - C_2 \rho \frac{\varepsilon^2}{k} \qquad (5.3.4)$$

---

†These equations have been obtained through a straightforward extension of their two-dimensional form, as described in Launder and Spalding (1972).

Equations described here are for the (x,y,z) system; equations for the coordinate systems (r,θ,ϕ), (x,y,ϕ) and (η,ζ,ξ) are given in Appendix A1.

where G represents the generation of turbulence energy; Γ_k and Γ_ε represent the diffusion coefficients for k and ε respectively; and C_1, C_2 are constants in the turbulence model.

The three constants in the turbulence model have been assigned the following values*

C_1	C_2	C_μ
1.47	1.92	0.09

(5.3.5)

The 'effective' exchange coefficient

It is now easy to obtain the value of the effective exchange coefficient which relates the combined molecular and turbulent fluxes to the gradients of the flow variables; it may be expressed by the following relation:

$$\Gamma_{eff,\Phi} = \frac{\mu_\ell}{\sigma_{\ell,\Phi}} + \frac{\mu_t}{\sigma_{t,\Phi}} \qquad (5.3.6)$$

where the subscript Φ denotes the values for the variable Φ; μ_ℓ and μ_t are the laminar and turbulent viscosities; and σ_ℓ and σ_t represent the laminar and turbulent

---

*based on Launder and Spalding (1973).

Prandtl/Schmidt numbers.

The value of σ_ℓ is dependent on the molecular properties of the fluid; and is equal to unity for the velocities and for k and ε. The value of σ_t on the other hand, is a property of the turbulence phenomena; and is assigned the following values:

$$\sigma_{t,u} = \sigma_{t,v} = \sigma_{t,w} = \sigma_{t,k} = 1.0;$$

$$\sigma_{t,\varepsilon} = 1.3; \quad \sigma_{t,T} = 1.0 \qquad (5.3.7)$$

where the subscript T denotes the value for the transport of temperature.

5.4 Treatment of near-wall regions

Special practices are needed to compute the near-wall region, for the following reasons. In the central region of the flow, the gradients of flow properties are usually not very steep; a moderately fine finite-difference grid yields accurate solutions. However, close to solid walls the variations of flow properties are much steeper, thus necessitating an extremely fine grid for their accurate computation. Also, the present form of the turbulence model is valid only for fully-turbulent flows; modifications are required to make it apply to regions where the

Reynolds number of turbulence ($\equiv \rho k^{\frac{1}{2}} \ell / \mu_\ell$ where $\ell \equiv k^{\frac{3}{2}}/\varepsilon$) is low (or alternatively when $y^+ \equiv \frac{y\sqrt{\tau_W \rho}}{\mu_\ell}$ is less than 11.5, where y = the distance from the wall; τ_W = wall shear stress).

There are two methods for accounting the near-wall regions in numerical methods for computing turbulent flows; the wall-function method, and the method of modelling the low-Reynolds-number phenomena. In the present study the wall-function approach is adopted chiefly because of its economy from the view points of both computer storage and computer time.

Wall functions have been proposed and used earlier by several authors including Wolfshtein (1969), Runchal (1969) and Ng and Spalding (1972). In a recent review Launder and Spalding (1973) described the wall functions which have been proved to be satisfactory in two-dimensional situations. It is these wall functions, with their appropriate extension to three dimensions, that have been employed in the present study. The practices adopted are as follows.

The first feature of the method is to locate all the finite-difference grid nodes (except for those representing the wall values) in the fully-turbulent

region. Thus the point P adjacent to a wall is located sufficiently far from the wall for the local turbulent Reynolds number $(\rho k^{\frac{1}{2}} \ell/\mu_\ell)_P$ to be much greater than unity. It is then assumed that a logarithmic velocity-profile prevails in the region between the wall and the node P, the expression being

$$\frac{q_P}{(\tau/\rho)_W^{\frac{1}{2}}} = \frac{1}{\kappa} \ln \left(\frac{E\, y_P\, (\tau\rho)_W^{\frac{1}{2}}}{\mu_\ell} \right) \qquad (5.4.1)$$

where the subscript P indicates that the values are those at grid node P; and the subscript W indicates the values at the wall. y_P is the distance of P from the wall and κ and E are the log-law constants (κ = 0.4187 and E = 9.8 from Patel (1965)); q_P is the resultant velocity at P and is assumed to be parallel to the wall shear-stress (this latter assumption is made in the present extension to three dimensions).

The shear stress in the fluid layer between P and W is then related to the kinetic-energy of turbulence by considering that, in the uniform-shear-stress layer, the generation and dissipation of k are nearly in balance; this leads to the relation

$$\tau_P = \tau_W = \rho\, C_\mu^{\frac{1}{2}}\, k_P \qquad (5.4.2)$$

where C_μ is the constant (= 0.09) in the turbulence

model. By the use of (5.4.2) in conjunction with (5.4.1), the shear stress is expressed by the relation

$$\tau_p = \frac{\rho \kappa C_\mu^{\frac{1}{4}} k_p^{\frac{1}{2}} q_p}{\ln \{ \frac{E\, y_p C_\mu^{\frac{1}{4}} \rho k_p^{\frac{1}{2}}}{\mu_\ell} \}} \qquad (5.4.3)$$

The rate of dissipation of kinetic energy, ε_p near the wall is fixed by reference to the requirement that the length scale varies linearly with distance from the wall; the corresponding expression for ε_p is then given by

$$\varepsilon_p = C_\mu^{\frac{3}{4}} k_p^{\frac{3}{2}} / (\kappa y_p) \qquad (5.4.4)$$

k_p being the near-wall kinetic energy of turbulence. The quantity k_p is calculated from the regular balance equation but with following changes. First, diffusion of energy is set equal to zero; the generation term in the kinetic-energy equation is then modified to account for the value of wall shear-stress calculated from (5.4.3). The dissipation term is also modified in the light of (5.4.4) and is assigned an average value over the control volume for the near-wall node; thus

$$\rho\bar{\varepsilon} = \rho \int_{o}^{y_N} \varepsilon \, dy = C_\mu^{\frac{3}{4}} k_P^{\frac{3}{2}} \int_{o}^{y_N} \frac{1}{\kappa y} \, dy \qquad (5.4.5)$$

The wall functions for the transport of temperature (or enthalpy) are derived in a manner similar to (5.4.3). The near-wall variation of temperature is also assumed to be logarithmic, the expression being,

$$\frac{c_P (T - T_W) \tau_W}{J_h} = \frac{1}{\kappa} \ln \left(\frac{E \, y \sqrt{\tau_W \rho}}{\mu_\ell} \right) + P_T \qquad (5.4.6)$$

where, τ_w is given by (5.4.2); and J_h represents the heat flux from the wall. c_P stands for the specific heat of the fluid; and the symbol T represents temperature. The term P_T (absent in equation (5.4.1)) represents the additional resistance caused by the laminar sublayer to the transport of heat and is of the following functional form (from Patankar and Spalding (1970)).

$$P_T = 9.24 \left(\frac{\sigma_{\ell,T}}{\sigma_{t,T}} - 1 \right) \left(\frac{\sigma_{\ell,T}}{\sigma_{t,T}} \right)^{-0.25} \qquad (5.4.7)$$

5.5 Summary and concluding remarks

In the present chapter, the details of the turbulence model employed in the present calculations of turbulent flows have been described. In this turbulence model two additional equations are solved for the transport of the kinetic-energy of turbulence, k and its dissipation rate, ε. The turbulent fluxes are related to the gradients of the time-averaged flow properties through an exchange-coefficient. This exchange coefficient is assumed to be isotropic and is calculated from the distributions of k and ε. Special practices are adopted for the treatment of near-wall regions. The fluxes of momentum and heat for grid nodes adjacent to a wall are not calculated from usual gradient laws but are empirically prescribed based on a simplified analysis.

The results of the computations employing the calculation procedures described in Chapter 4 and the present turbulence model will be presented in Chapters 7 and 8.

CHAPTER 6

THE EXPERIMENTAL PROGRAM

6.1 Introduction

An experimental investigation of the turbulent flow in curved ducts was undertaken to collect data suitable for validation of the partially-parabolic procedure. The distributions of mean velocity and static pressure in the developing flow field of a strongly-curved duct have been measured. The height and the width of the duct were respectively 0.304 m and 1.22 m; and the duct curved through 90 degrees with a centre-line radius equal to 2.52 metres. Two different configurations of the duct shape have been studied. In the first configuration, the cross-sectional dimensions of the duct were kept constant throughout the flow domain; in the second, the outer wall of the duct was made to diffuse outwards by 2.5 degrees. The measurements in the central region of the duct were made using a three-hole pitot static probe whereas in the region close to the bottom wall, a single hole total-head tube was employed. The flow Reynolds number based on the average velocity and hydraulic diameter of the duct (4 x area/perimeter) was about 7×10^5.

The measurements described in this chapter have been made in an existing experimental set-up at the University of Waterloo, Canada. In the following sections, first a brief description is given about the experimental apparatus and the measuring devices; the details concerning the design and fabrication of the apparatus however, have been omitted from the present description as they can be obtained from Jerie (1971). The experimental procedure is outlined and the scope of the present measurements is stated. Later the experimental data are presented and analysed; in this chapter, only a selected amount of data are presented; the complete set of experimental data will be described in Chapter 8 where they will be compared with the predictions.

6.2 Description of the experimental apparatus

6.2.1 General layout

A schematic layout of the experimental apparatus employed in the present investigation is shown in Figure (6.2.1). Figure (6.2.2) shows the overall view of the apparatus. It consisted of a blower, settling chamber, a 6 m. long straight duct and a 90^{o} curved duct, all connected in series in the above sequence. The blower was driven by a 20 h.p. A.C. motor and was connected to the settling chamber through flexible rubber bellows which prevented the

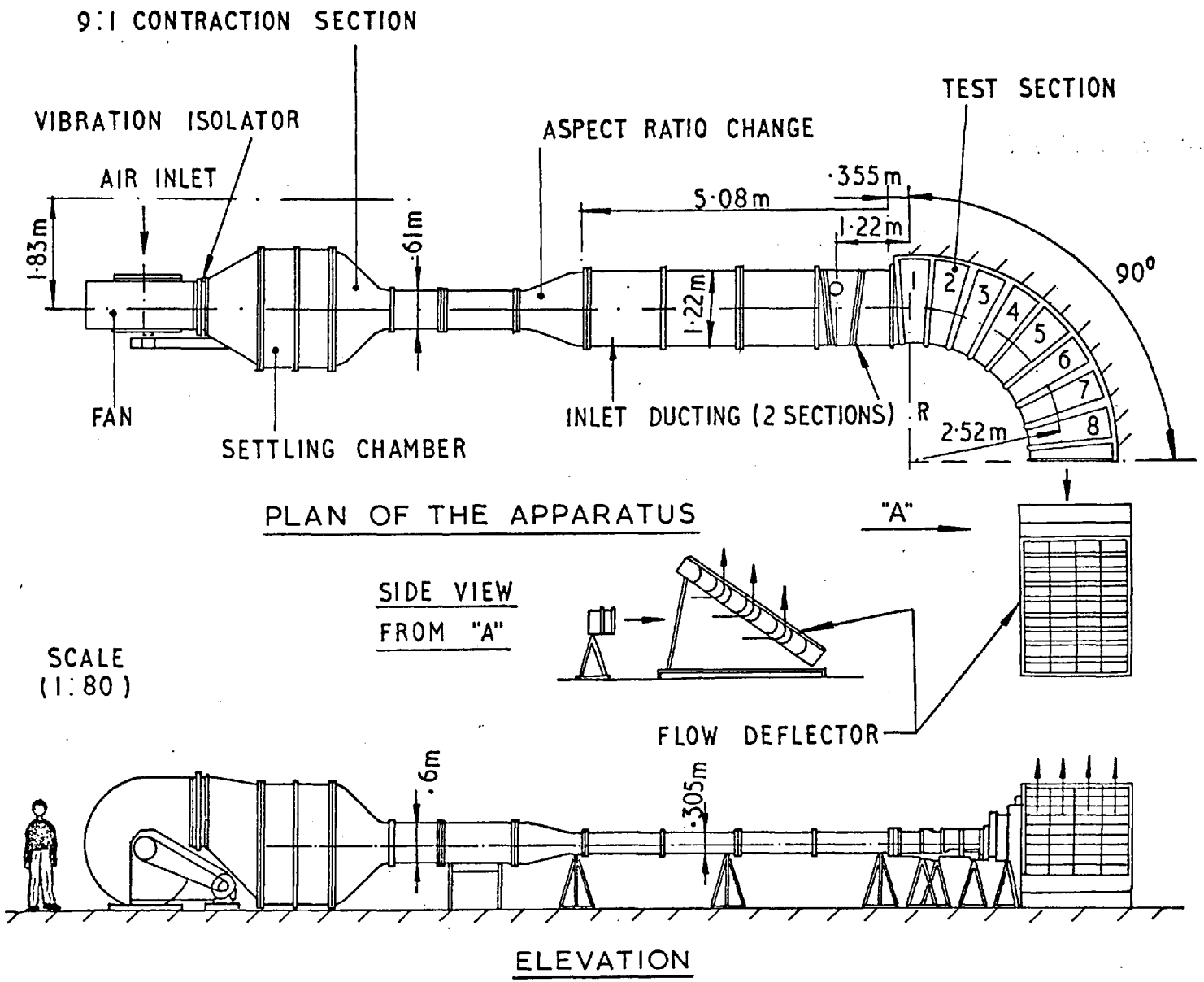

Fig. (6.2.1): Schematic layout of the experimental apparatus.

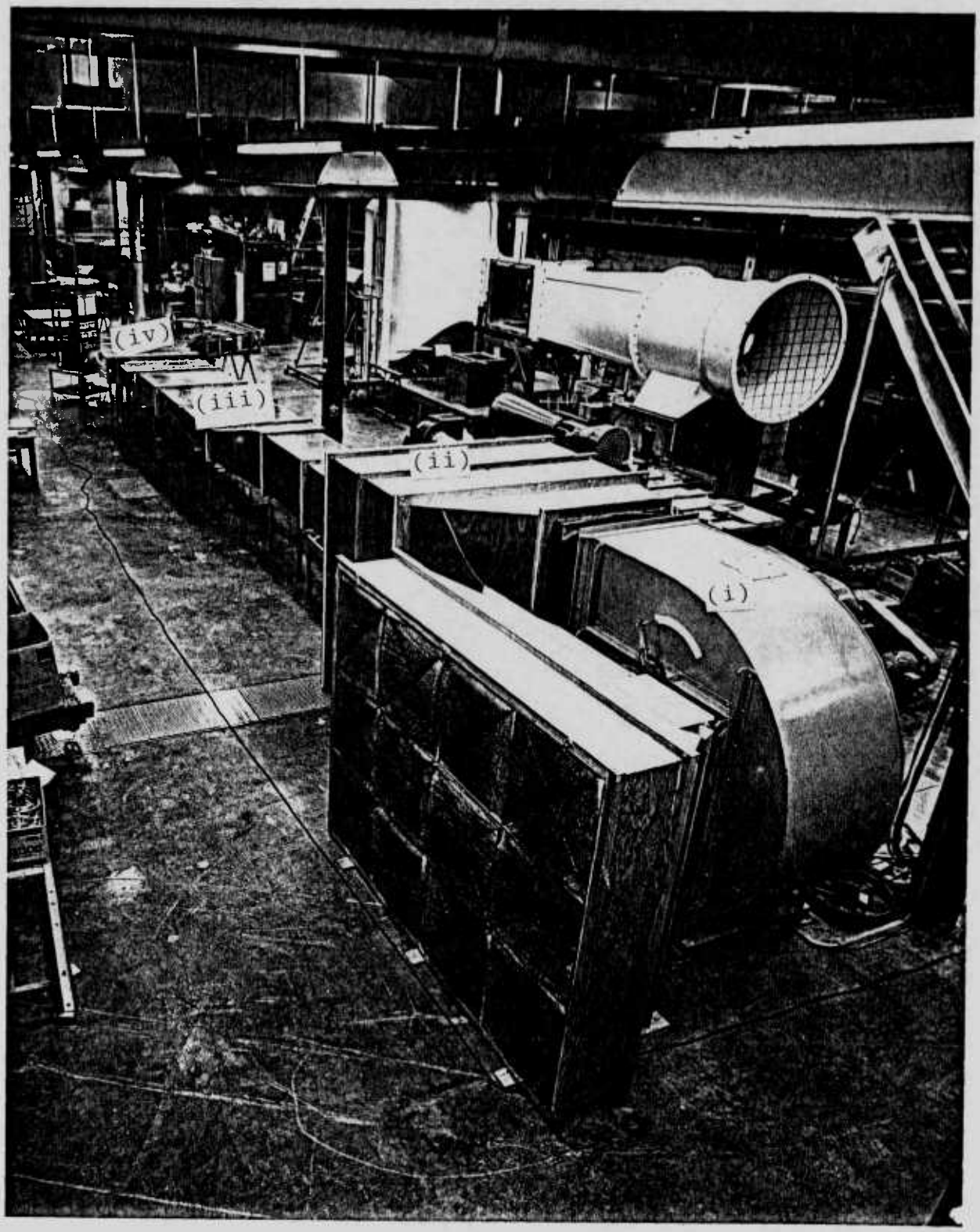

Fig. (6.2.2): Overall-view of the apparatus.
(i) Blower, (ii) Plenum chamber,
(iii) Straight section, (iv) Curved duct.

vibrations of the motor from being transmitted to the test section. The settling chamber was 1.22 m. long and 1.83 m. square in cross-section and contained honey-combs and wire screens to smoothen the non-uniformities in the flow from the blower. The exit of this settling chamber was 0.61 m. square in cross-section and provided an area reduction of 9:1. The complete set-up was supported on angle-iron frameworks which contained provisions for levelling. The amount of air supply to the test section was controlled either by varying the opening of the inlet vanes; or by using different combinations of pulley drives connecting the motor and the blower. The present apparatus was capable of producing a maximum average-velocity of 22.5 m/sec in the test section; the corresponding Reynolds number, based on this velocity and the hydraulic diameter (4 x area/perimeter) of the test section, is 7.05×10^5.

6.2.2 The test section

The test section in which measurements were made is shown in Figure (6.2.3). The test section was rectangular in cross-section with a width and height respectively equal to 1.22 m and 0.304 m. It was curved in the horizontal plane, with a centre-line radius of 2.52 metres. The top and bottom walls and the inner side wall of this test section were firmly

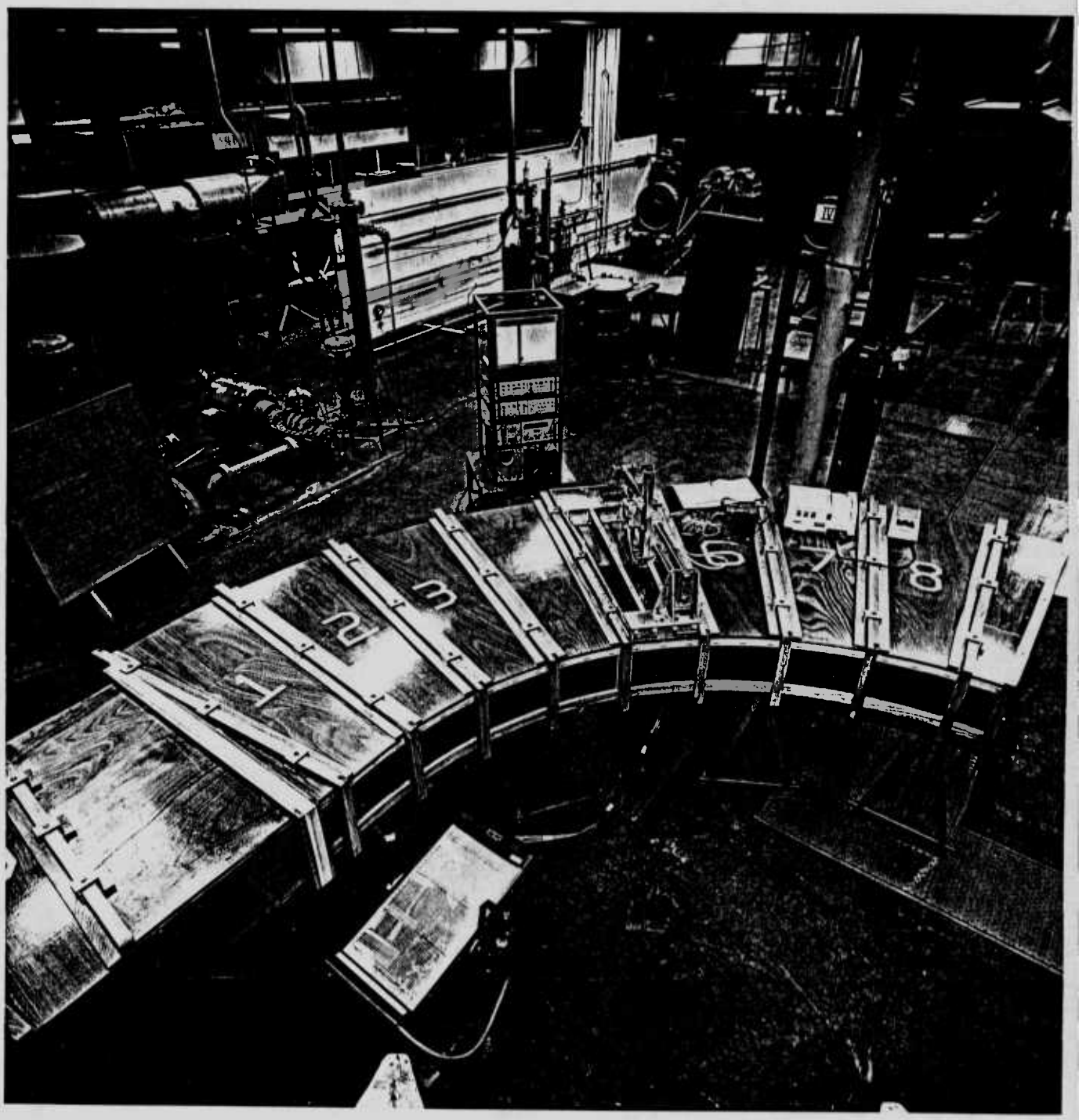

Fig. (6.2.3): View of the test section.

connected to each other but the outer wall was allowed to be freely positioned. The inner side wall was made of a transparent material so as to permit flow-visualisation and to ease the task of positioning the probes. The bottom wall was made of 6 mm. thick plywood and was supported by a wooden framework. On this bottom wall static-pressure taps were provided at 24 equally-spaced axial positions; each axial position contained nine taps which were placed at 5 cm intervals on either side of the duct centre-line. The top wall was constructed of eight wedges of equal size and was clamped to a wooden framework on the top of the duct. During the measurements the top wall wedge corresponding to the location of measurements was unclamped and replaced by the traversing gear to which the measuring devices were fixed. The outer wall of the test section was made of plastic and was manoeuvred by long metallic-screws; the desired variation in the duct width was achieved by advancing or retracting these metallic screws. The maximum permissible width in the present test section was limited to 1.42 m, the nominal width being 1.22 m.

6.2.3 The traversing mechanism

The mechanism employed to traverse the pitot probes to the desired location in the flow field is shown in Figure (6.2.4). The main component in this

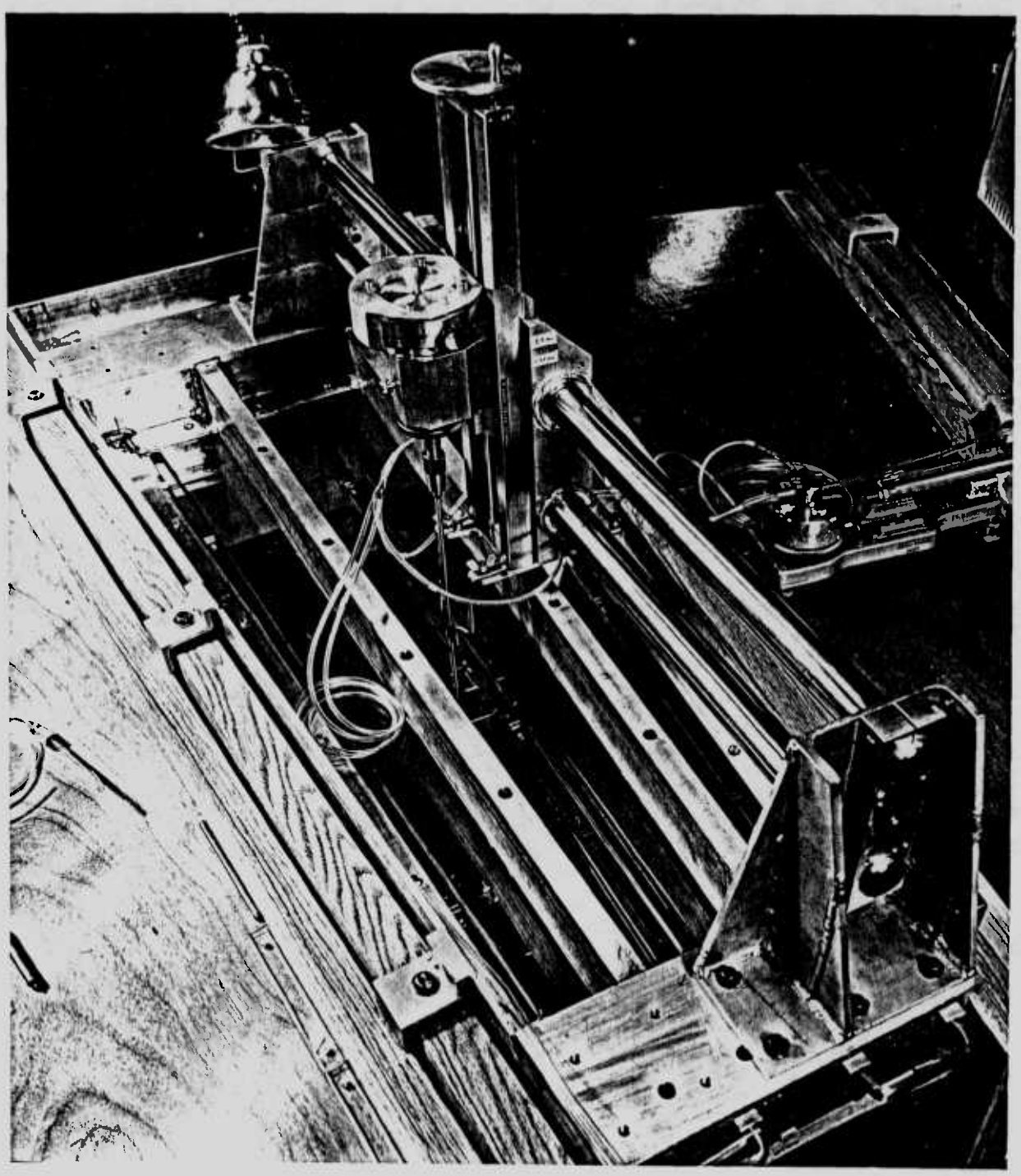

Fig. (6.2.4): The traversing mechanism.

mechanism is the traversing gear to which the probes were attached through a miniature chuck. This traversing gear was supported on two horizontal steel shafts which in turn, were fixed to an aluminium platform. The aluminium platform was made of the same dimensions as the top-wall wedges; and could be conveniently positioned on the top wall by replacing the corresponding top-wall wedge.

The above-mentioned arrangement permitted movement of the probe along the three coordinate directions (x,y,ϕ) shown in Figure (6.2.5). The movement normal to the bottom wall (i.e. the y-direction) was achieved by a lead screw mechanism which formed an integral part of the traversing gear. The total vertical traverse permitted by this mechanism was 33 cm. The vertical position of the probe was measured on a vernier scale to an accuracy of 0.05 mm. The movement in the horizontal direction (i.e. along the x-coordinate) was obtained by sliding the traversing gear on the steel shafts. The horizontal position of the probe was measured by a simple tape-scale device to an accuracy of 2.5 mm. For movement in the direction along the bend the aluminium platform itself was unclamped from one position and was placed at the other. This aluminium platform also contained three traversing slots, where the traversing gear could be fixed. The

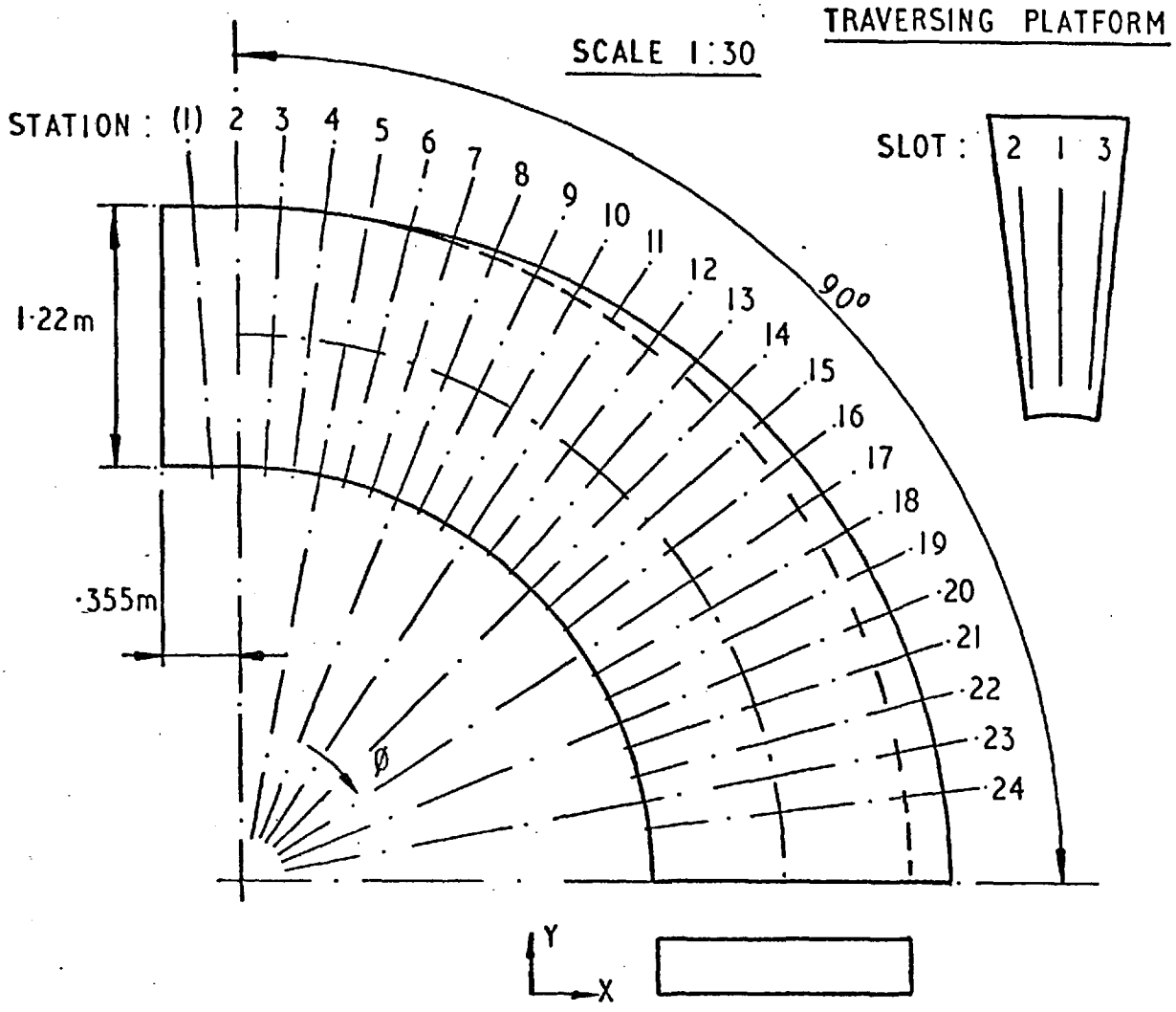

MEASURING STATION	1	2	3	4	5	6	7	8	9	10	11	12
SLOT IN THE TRAVERSING PLATFORM	2	1	3	2	1	3	2	1	3	2	1	3
ANGULAR (DEG.) POSITION OF THE STATION	-3·75	0	3·75	7·50	11·25	15·0	18·75	22·50	26·25	30·0	33·75	37·50

MEASURING STATION	13	14	15	16	17	18	19	20	21	22	23	24
SLOT IN THE TRAVERSING PLATFORM	2	1	3	2	1	3	2	1	3	2	1	3
ANGULAR (DEG.) POSITION OF THE STATION	41·25	45·0	48·75	52·50	56·25	60·0	63·75	67·50	71·25	75·0	78·75	82·50

Fig. (6.2.5): Coordinate system and positions for traversing along the ϕ-direction.

positions available for traversing are shown in Figure (6.2.5).

In addition to the vertical movement, the traversing gear also provided angular rotation to the probe about the vertical axis. The rotation of the probe which was employed to align the probe with the flow direction was read on a vernier scale to an accuracy of 0.1 degree.

6.2.4 Measuring devices

In the present investigation, the measurements were made using Pitot probes. Two different probes were employed and are shown in Figure (6.2.6). Probe (a) was a direction - sensitive probe and was employed for measurements in the central region of the duct. This probe contained four pressure-sensing holes; three of these were located on the nose while the fourth, which measured the static pressure, was displaced slightly away from the nose. Of the three holes located on the nose, the central one was employed in the measurement of the total pressure; the other two, called the directional holes, were used in aligning the probe with the flow direction. The directional holes were drilled at an angle of 40 degrees to the stagnation point. Probe (b) which is referred to as the 'total-head tube' was much smaller in size than

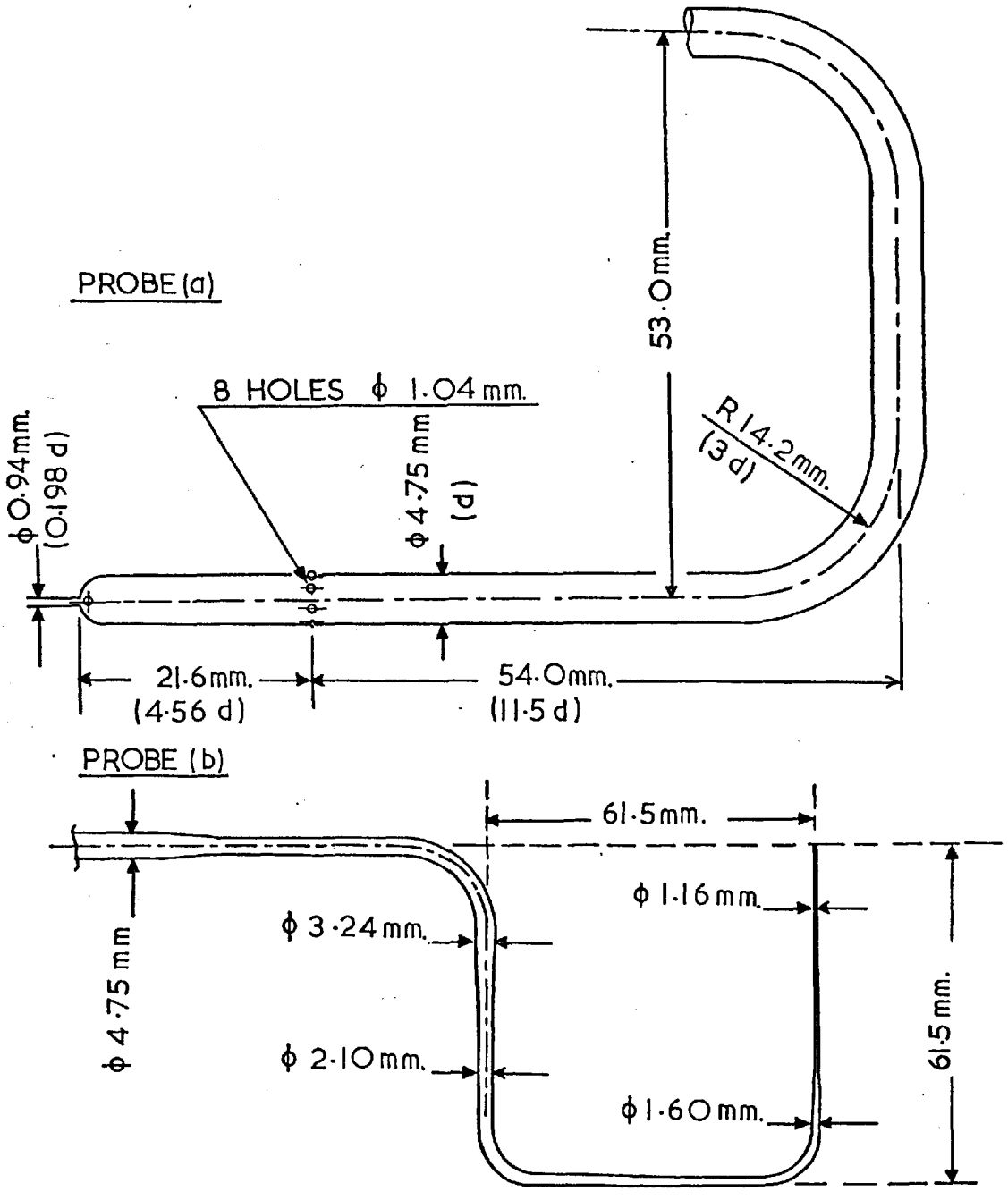

Fig. (6.2.6): Pitot-probes used for the present measurements.

Probe (a) and was used in measuring the flow variables in the region close to the bottom wall. Probe (b) comprised only one pressure-sensing hole; and for this reason, the flow angles with this probe were measured using the bisection method. Probe (b) did not have any provision for measuring the static pressure.

The pressure outputs from the pitot-probes were measured using a pressure transducer and an integrating digital-voltmeter. The transducer converted the pressure signal to a voltage which was then read on the voltmeter; the integration time on the voltmeter was set to 1 sec. The voltages were read to an accuracy of .001 volts in a nominal value of 3 volts for the present values of velocities. For measurements with probe (b) a time-delay circuit (time constant = 10 secs) was also used in addition to the integrating circuit of the digital voltmeter; this additional device was necessary because of the large turbulence-levels in the near-wall regions.

6.3 Calibration of measuring devices

The measuring devices used in the present experiments were already calibrated, for accuracy and consistency, in a recent investigation by Young (1972). For this reason, no calibration tests were made in the present investigation; but instead, the recommendations

of Young (1972) were followed. The recommended corrections to the measured values, in all instances, have been small; they are listed in Appendix A3 and have been applied to the experimental data during the data-conversion process.

6.4 Experimental procedure

The procedure for measurements was simple and straightforward. It involved systematic and patient traversing of the probes from one end of the flow domain to the other and recording the various pressure outputs in the form of voltages which were indicated on the digital voltmeter. The traversing and the data recording were done manually; and no automatic devices were employed. The following two preliminary checks were first made to ascertain the correctness of the experimental apparatus.

1) The experimental apparatus was ensured to be levelled along both its length and width; the heights of its supporting frameworks were accordingly adjusted wherever necessary.

2) Second, a few measurements were made to examine the symmetry of the flow about the central horizontal plane of the duct. These preliminary measurements indicated some asymmetry which could be partially removed by making all top-wall wedges to be in flush with each other.

For the measurements reported in this thesis, the maximum difference between flow angles measured at two symmetrically placed locations was 0.7 degrees in a nominal flow angle of 20 degrees; asymmetry in the mean velocity was about 2 percent.

The final measurements comprised two identical sets of measurements in the same test section but with differing positions of the outer wall. For the first set, the width of the duct was kept constant at a value equal to 1.22 m throughout the flow domain. In the second, the outer wall was displaced uniformly outwards to provide a diffuser angle of 2.5 degrees. For each of the above flow configurations 8 axial stations along the duct were chosen to represent the flow field. Of these the first one was placed in the straight section, at a location 1.22 m. upstream of the curved duct. The others were dispersed in the curved duct at intervals of 11.25 degrees, the first being at the 0 degrees position. At each axial station, first, measurements were made of the flow in the central region; the mean velocity, the flow angle and the static pressure were measured at a total of 108 locations which were disposed over the cross-sectional plane in a manner shown in Figure (6.3.1). The measurements were made using the Pitot directional probe; the shaded areas shown in Figure (6.3.1) were

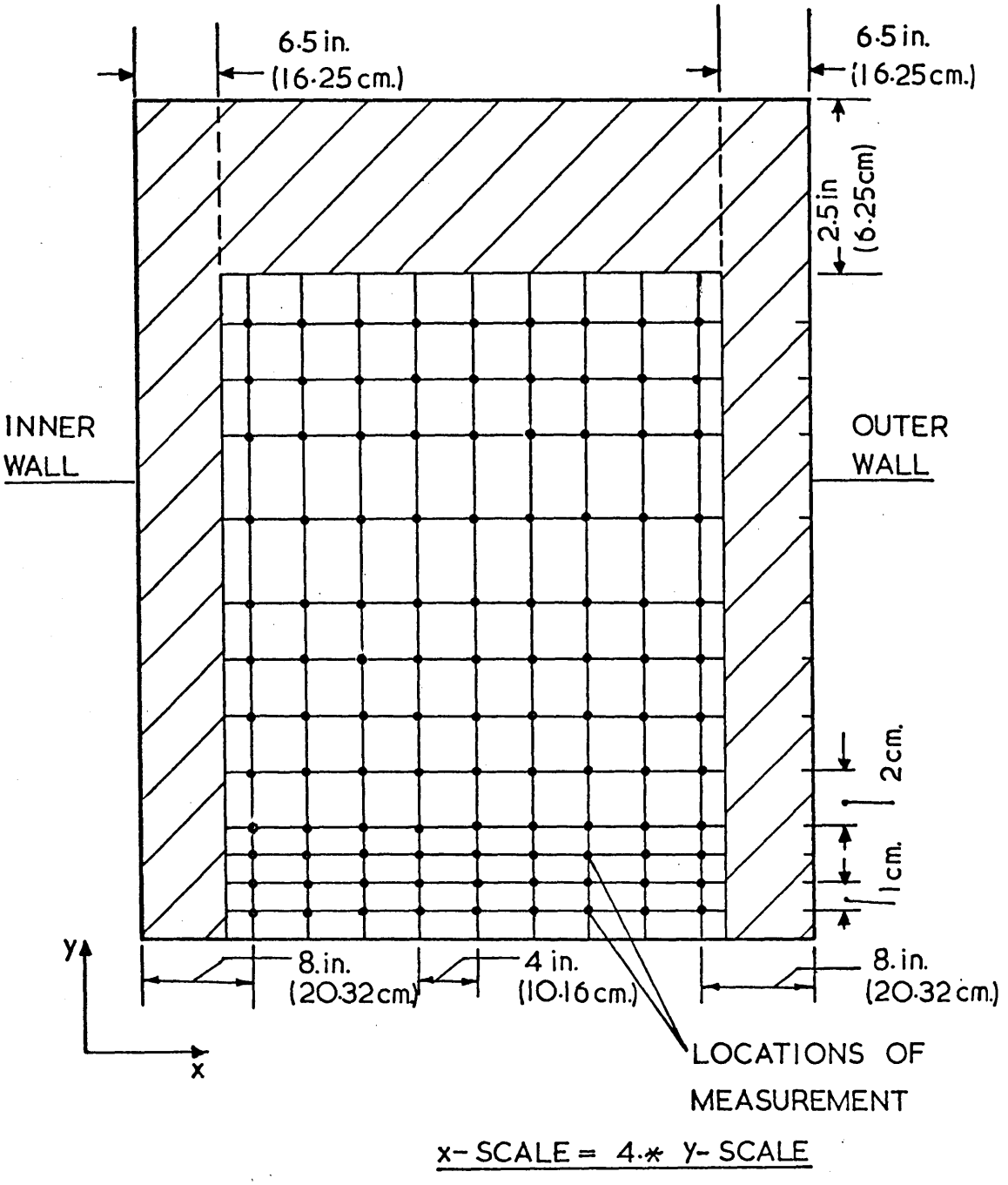

Fig. (6.3.1): Grid-arrangement for measurement of the central flow region.

not traversed due to obstructions caused by the side supports of the traversing mechanism. Later, attention was focussed on the flow region close to the bottom wall of the duct; and the distributions of mean velocity and flow angle normal to the bottom wall were measured at a distance of 61 cm from the inner side wall. A total of 12 readings were taken in a vertical distance of 15 mm, the first measurement being with the probe touching the bottom wall of the duct. These measurements were made using the total-head tube.

In addition to the above measurements of the mean flow, measurements were also made of the distributions of wall static-pressure; these measurements were made using the pressure taps situated on the bottom wall of the duct. The wall static pressures provided an estimate of the radial and axial pressure gradients; and in addition, also acted as a check on the corresponding values measured by the pitot directional probe. A few auxiliary variables such as the barometric pressure, the dry-bulb and wet-bulb temperatures of the room air were also measured, at frequent time-intervals during the experiment.

(Contd.)

6.5 Data conversion

The data-conversion procedure consisted of obtaining the distributions of velocities and static pressures from the 'raw' experimental data which were measured in the form of output voltages of the transducer. The first step in this procedure was to apply corrections to the data to account for the errors due to imperfections in the measuring devices. These errors which were determined from the calibration tests have in general been small; and are summarised in Appendix A3. In addition, corrections were also made to account for the effects of the displacement of the pressure centre of the pitot probe. These corrections consisted in increasing the heights of the measurement location by an amount equal to .15 times the diameter of the probe (as recommended by McMillan (1957)). For the measurements with the total-head tube this amounted to a correction of .16 mm to the heights of the measurement points; similar correction for the pitot directional probe was 1.35 mm.

The remaining data-conversion procedure consisted of converting the corrected output-voltages to the corresponding pressures and calculating the distributions of the desired flow variables. The velocities measured along the flow direction were resolved into two components, one along the longitudinal

direction and the other along the transverse direction (i.e. along x); and the velocities were non-dimensionalised with the vector velocity at the centre of the cross-section. The static pressures were similarly interpreted in terms of non-dimensional pressure coefficients, defined as

$$c_f = (p - p_o)/\tfrac{1}{2}\rho Q^2 \qquad (6.5.1)$$

where, p is the static pressure at any location and p_o is the value at the 0^o position; Q is the vector velocity at the centre of the cross-sectional plane and ρ is the density. The value of the skin friction was also calculated, from the total pressure measured with the total-head probe resting on the bottom wall (i.e. as a Preston tube). The procedure adopted for these calculations has been that recommended by Patel (1965).

All the calculations described above have been made on a IBM 370 computer at the University of Waterloo, Canada.

6.6 Presentation of experimental results

In this section, a few results are presented which describe the general flow-pattern observed in the present flow situation. The complete data obtained in the present investigation will be presented

in Chapter 8 where they will be compared with the predictions from the calculation procedures.

Figure (6.6.1) shows one typical plot for the variation of longitudinal-direction velocity (i.e. along the ϕ-direction) for various angular positions along the curved duct; these velocities have been measured in the constant-area duct at a height of 1 cm from the bottom wall. The velocities have been non-dimensionalised with the vector velocity at the centre of the cross-sectional plane. From this figure it can be seen that the velocity profiles are distorted with their maximum towards the inside of the curved duct; and the flow field is distorted even before it enters the curved duct. Figure (6.6.2) presents the development of the transverse velocities in the constant-area duct at a location 61 cm. from the inner side-wall; and Figure (6.6.3) shows the development of the radial pressure gradient in the same situation. It has been observed that, in the flow region presently investigated, the static pressure is nearly constant along lines normal to the bottom wall; the values plotted in Figure (6.6.3) are the average values normal to the bottom wall.

Figures (6.6.4) and (6.6.5) show the results of the measurements in the near-wall region. In these

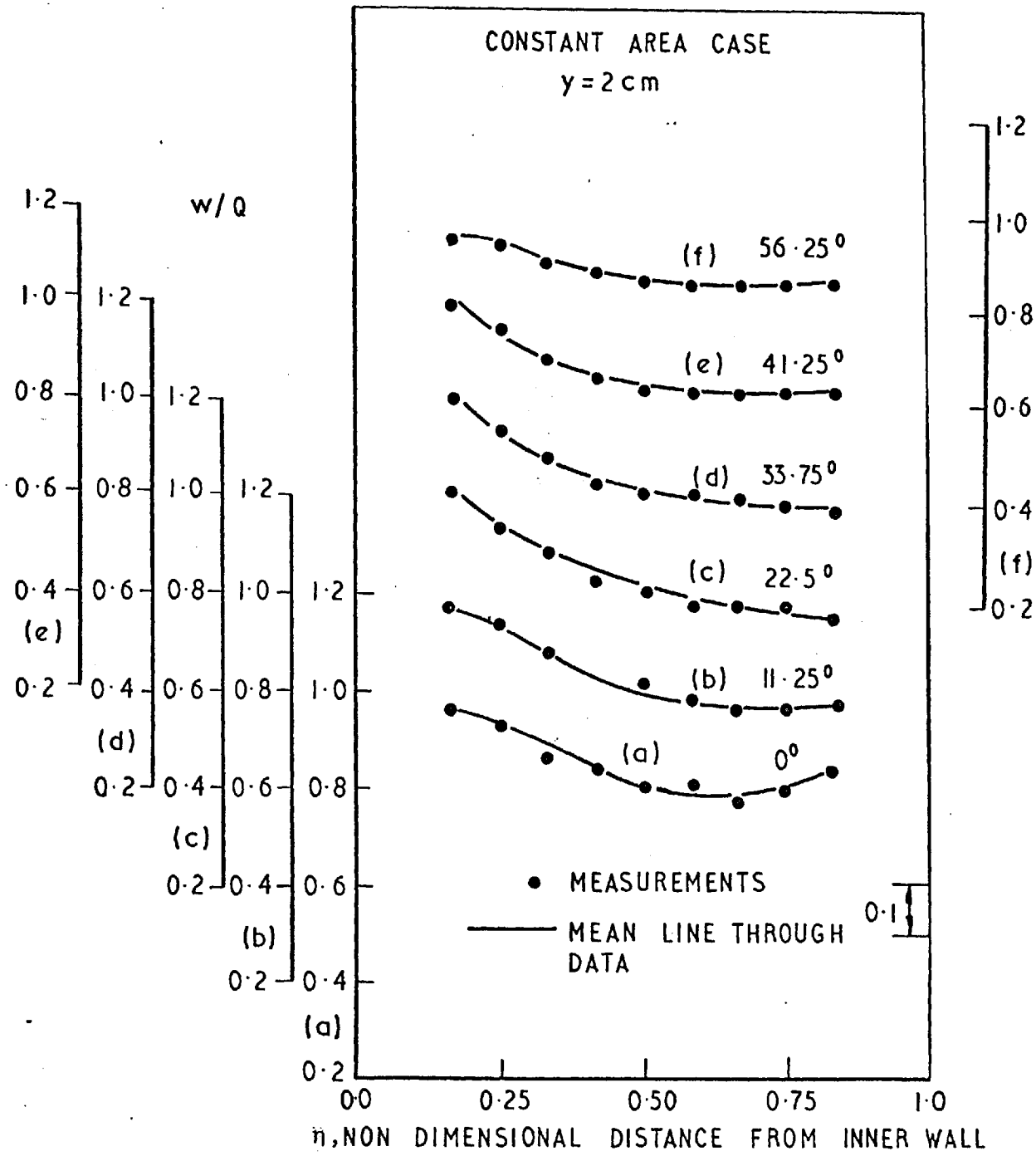

Fig. (6.6.1): Development of longitudinal velocity along the bend at plane y = 2 cm.

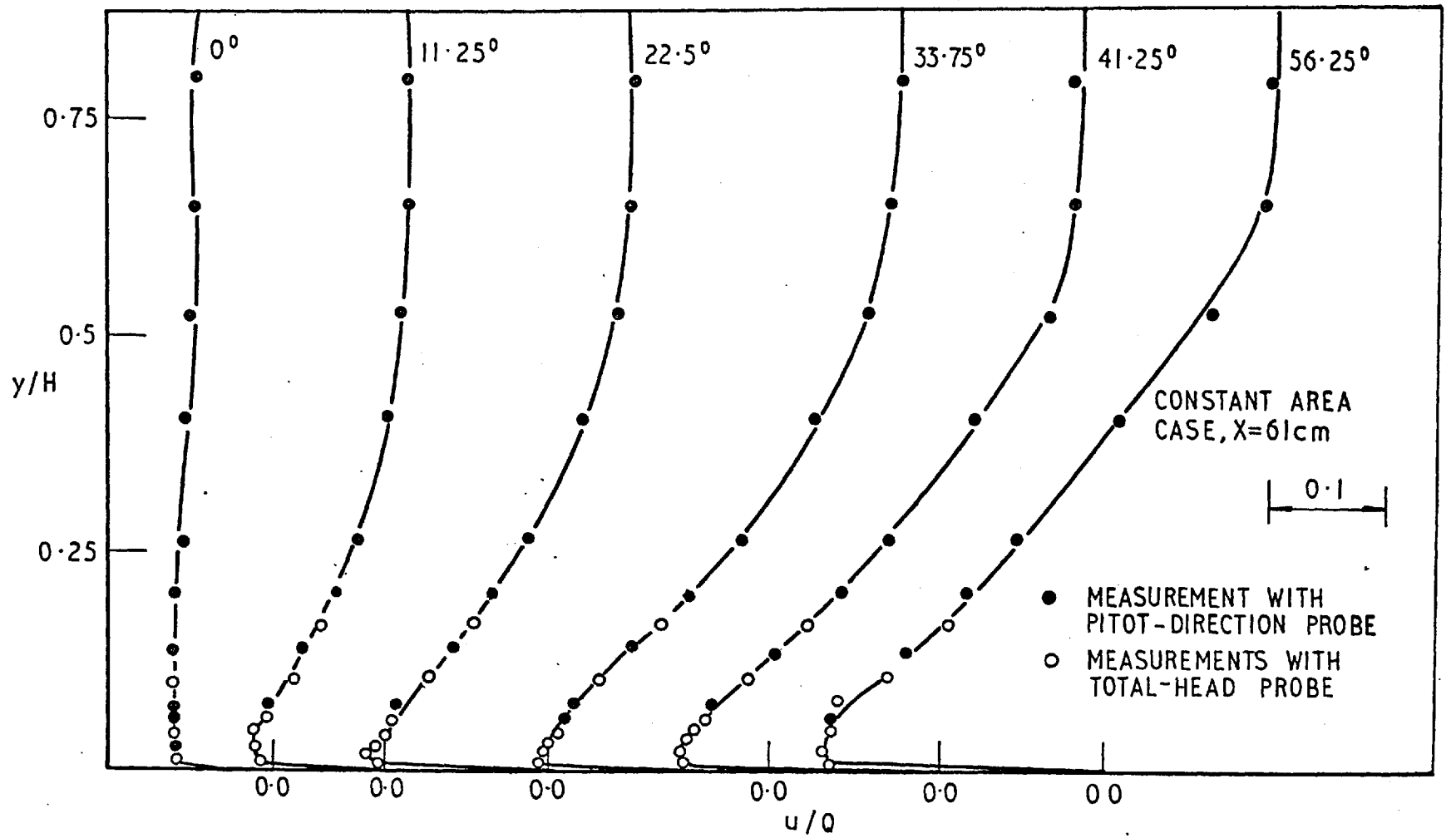

Fig. (6.6.2): Development of transverse velocity along the bend at x = 61 cm.

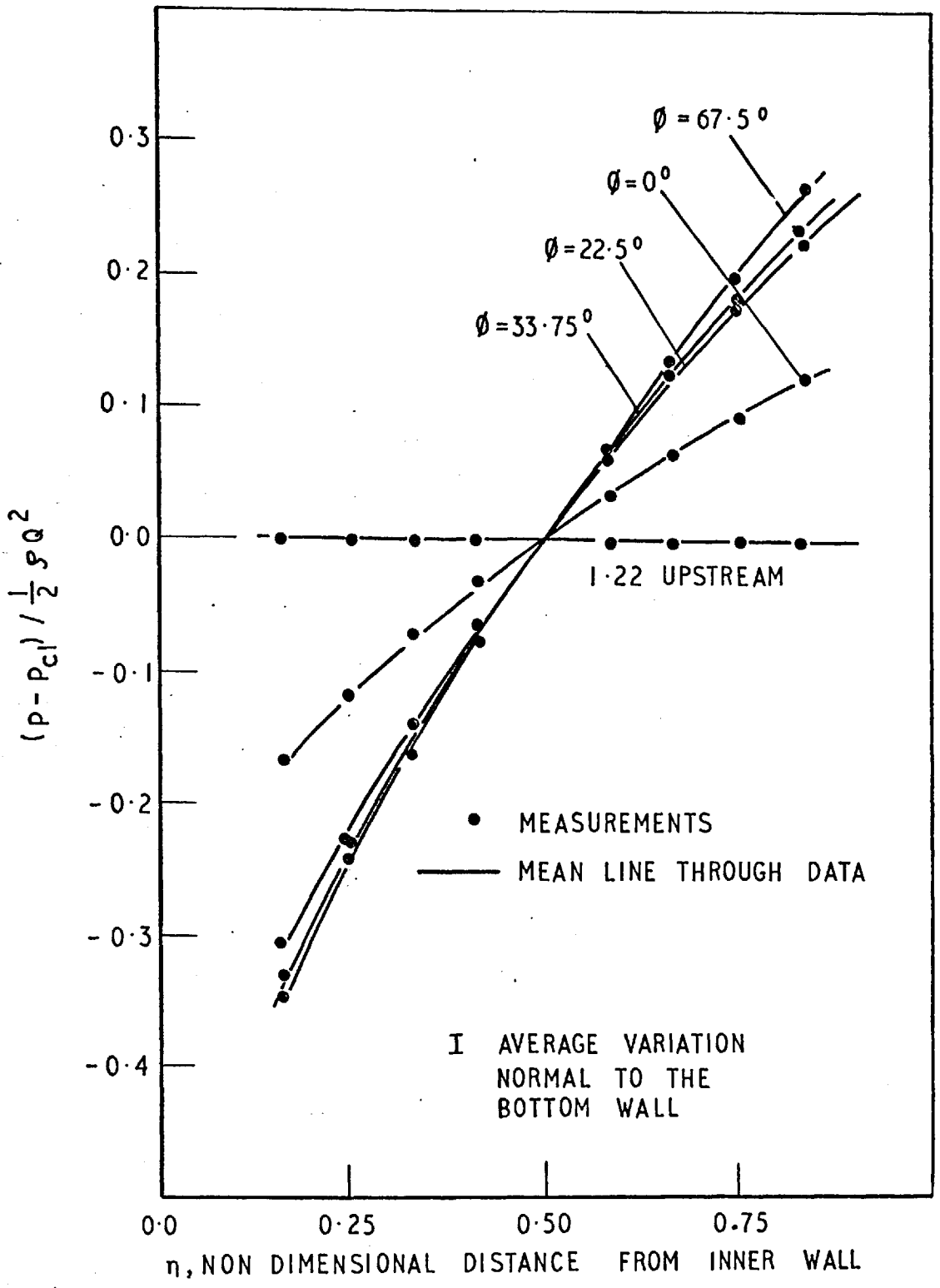

Fig. (6.6.3): Development of static-pressure distribution along the bend.

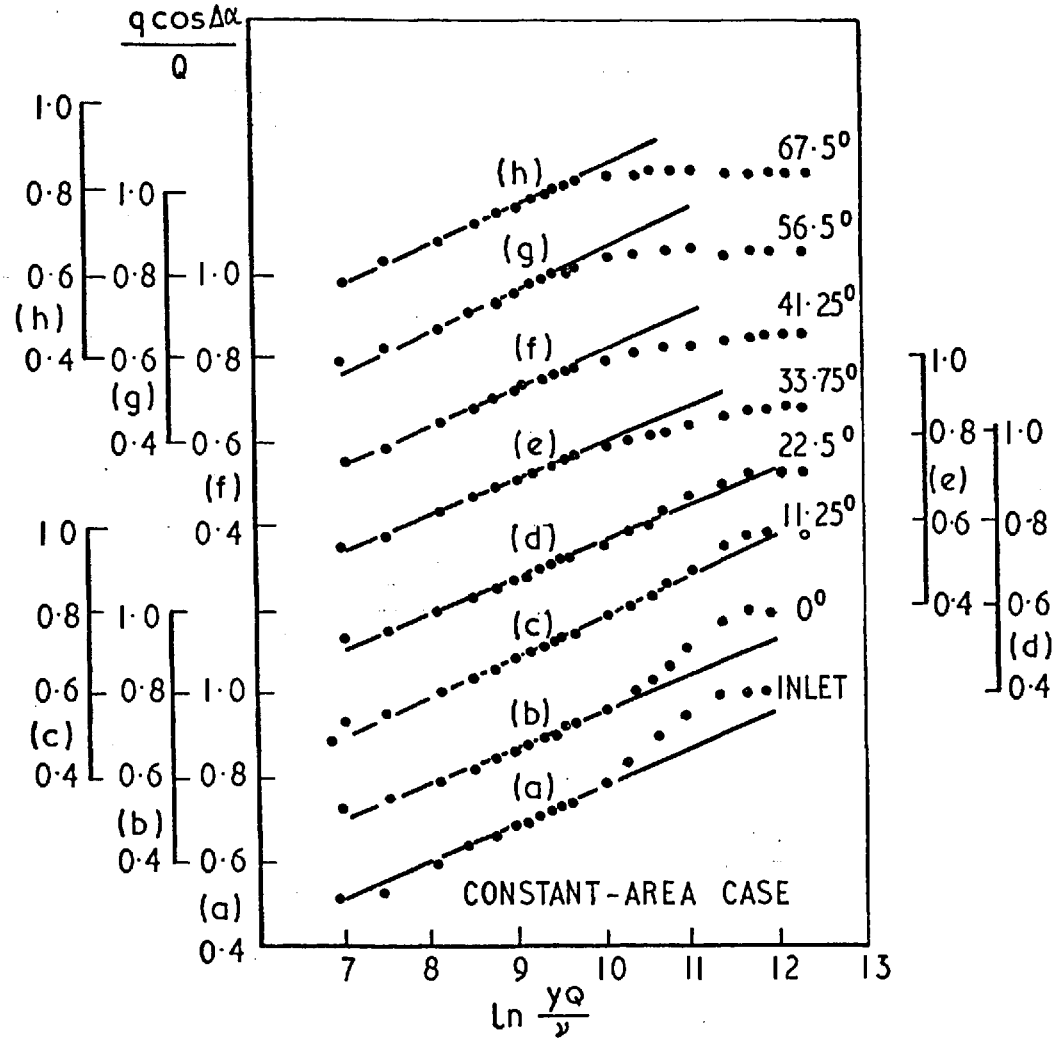

Fig. (6.6.4): Variation of velocity in the near-wall region measured at a distance of 61 cm from inner wall in the constant-area duct.

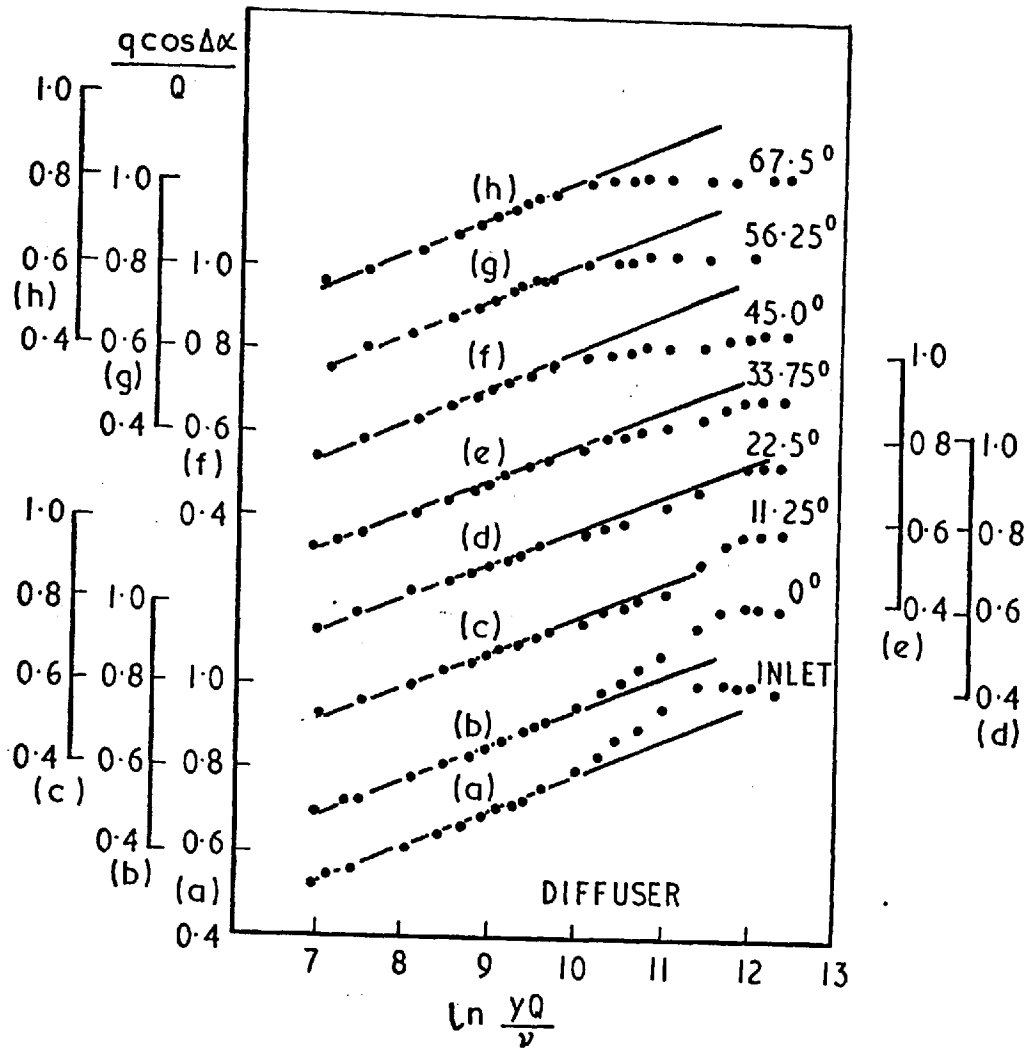

Fig. (6.6.5): Variation of velocity in the near-wall region in the diffuser, at a distance of 61 cm. from innerwall.

figures, the variation of velocity normal to the bottom wall is plotted for a location 61 cm. from the inner side wall. The coordinates are chosen to suit the verification of a logarithmic variation, of the following form:

$$\frac{w_f}{Q\sqrt{\frac{c_f}{2}}} = \frac{1}{\kappa} \log_e\left(\frac{E\ y\ Q\sqrt{c_{f/2}}}{\nu}\right) \qquad (6.6.1)$$

where w_f = the component of velocity in the direction of wall shear-stress,

c_f = skin-friction coefficient = $\frac{\tau_w}{\frac{1}{2}\rho Q^2}$,

Q = velocity at the centre of the cross-sectional plane,

ρ = the density,

y = the normal distance from the bottom wall,

ν = kinematic viscosity,

κ and E = constants in the logarithmic law.

The dots in the above figures represent the experimental results; and the straight lines represent the best logarithmic fit to the experimental points. The straight lines were obtained by chosing a value of the skin friction, c_f in (6.6.1), so that they contained the maximum number of experimental points. The values of skin friction calculated from Figures

(6.6.4) and (6.6.5) are shown in Figure (6.6.6).

The results presented above lead to two main conclusions. First, it is observed that the flow in a strongly-curved duct is partially-parabolic in nature. This is seen through the significant influence of the downstream events on the flow at the 0^{o} position. Second, it may be concluded that in the region close to the bottom wall, the variation of velocity is logarithmic with distance from the bottom wall; a large proportion of the experimental points have been observed to lie on the 'best-fit' straight lines.

6.7 Concluding remarks

In the present chapter, the details of the experimental program have been described. The test rig, the measuring devices have been briefly described and the sequence and scope of measurements were outlined. The experimental results show that the flow is partially-parabolic in nature and is considerably influenced by the transmission of downstream events through the pressure field. The present experimental results also provide proof to the existence of a logarithmic variation of the frictional component of velocity with distance from the bottom wall. This information adds support to the assumptions made in deriving the wall functions explained in Chapter 5.

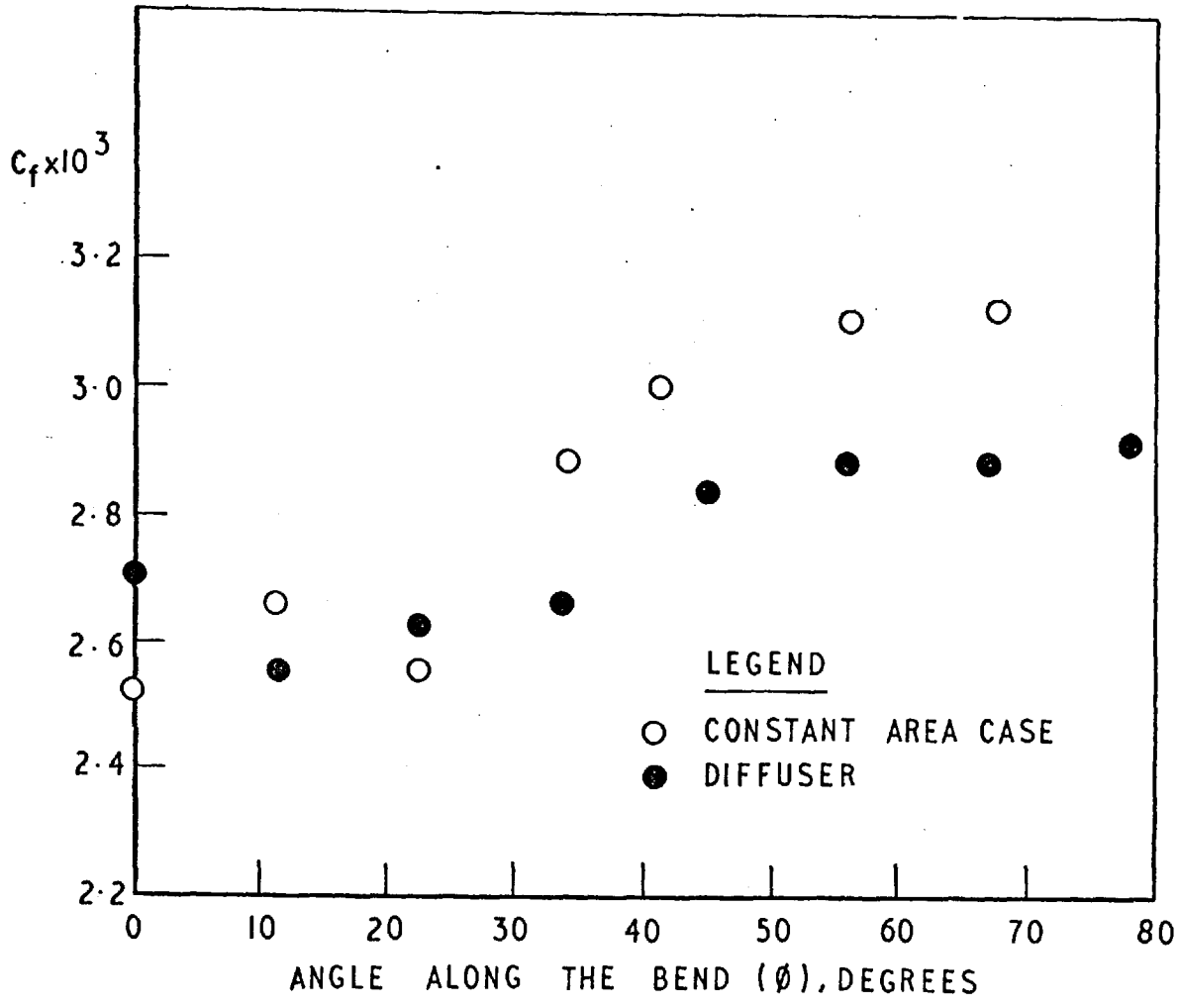

Fig. (6.6.6): Variation of skin friction (resultant) with bend angle, for a location 61 cm from inner side wall.

CHAPTER 7

PREDICTION OF FLOW IN MILDLY-CURVED DUCTS

7.1 Introduction

The flow and heat-transfer phenomena in mildly-curved ducts have been predicted using the parabolic calculation procedure described in Sec. (4.3). Computations have been made of the developing and fully-developed flow and temperature fields in curved pipes of circular cross-section. Both laminar and turbulent flow situations have been studied and the predictions have been compared with experimental data. For calculation of turbulent flows the Reynolds stresses have been modelled, using the two-equation turbulence-model, explained in Chapter 5. In this chapter, the results of these computations are presented, in two separate sections. In the first, the predictions of laminar flow and heat transfer are presented and their agreement with experimental data is examined. From these comparisons, the validity of the 'parabolic' assumptions and the accuracy of the calculation procedure are ascertained. Later, the results of the turbulent-flow calculations are presented and compared with experimental data. The results presented in this chapter have also been reported earlier by the author in Patankar, Pratap

and Spalding (1974 and 1975).

7.2 Prediction of laminar flows

7.2.1 Computational details

The physical situation considered for the present computations is illustrated in Figure (7.2.1). The flow situation has been mathematically represented in the (r,θ,ϕ) coordinate system by the equations described in Chapter 3. Because of the mild curvature of the duct, the flow was assumed to be parabolic. The fluid properties namely viscosity, density and specific heat have been assumed, in the present computations, to be uniform throughout the flow domain. The computations were started at the 0^{o} position of the bend with the inlet conditions prescribed to be those of a fully-developed pipe flow. Because the flow is symmetrical about the diameter in the plane of curvature (plane AA), the finite-difference grid in the present computations covered only a semi-circular sector of the cross-section, as shown in Figure (7.2.2). The boundaries of this flow domain comprised the two radial lines on the horizontal diameter, a semicircular region of small radius at the centre, and the pipe wall. The first three boundaries were considered as planes of symmetry; and the gradients of variables normal to the boundary were prescribed to be zero. The finite-difference

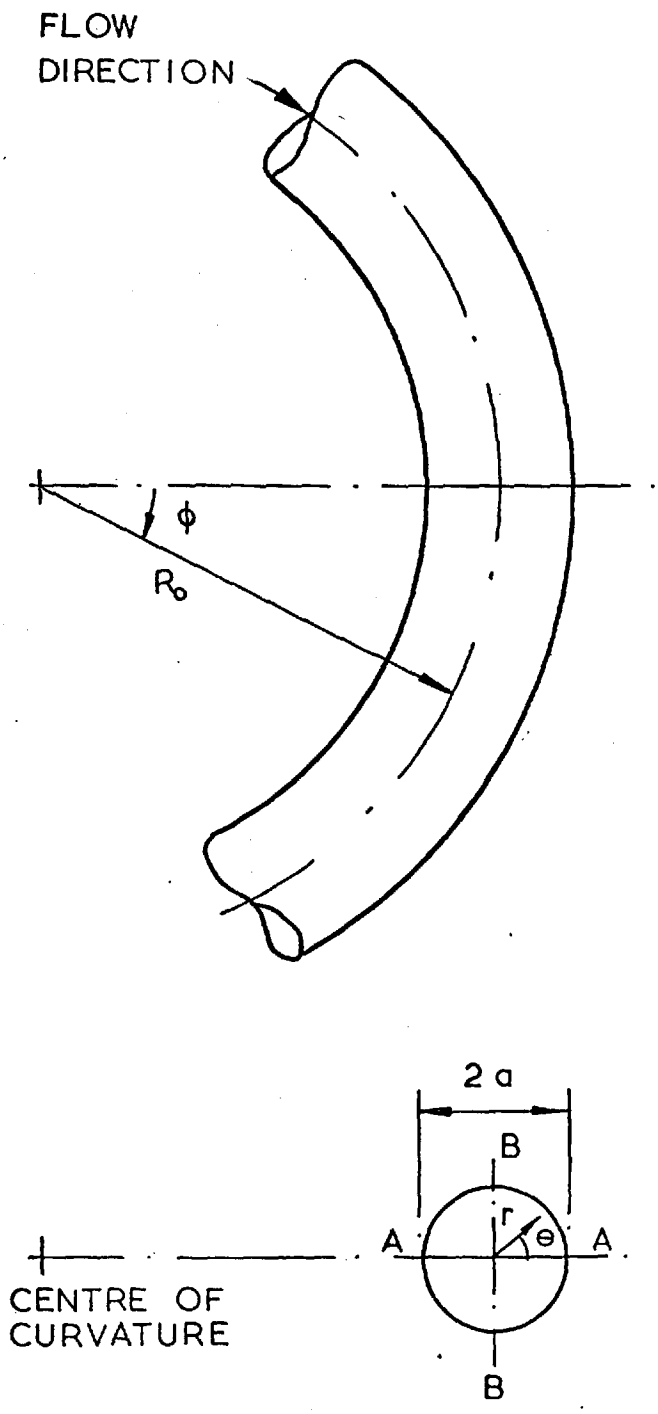

Fig. (7.2.1(a)) : The physical situation

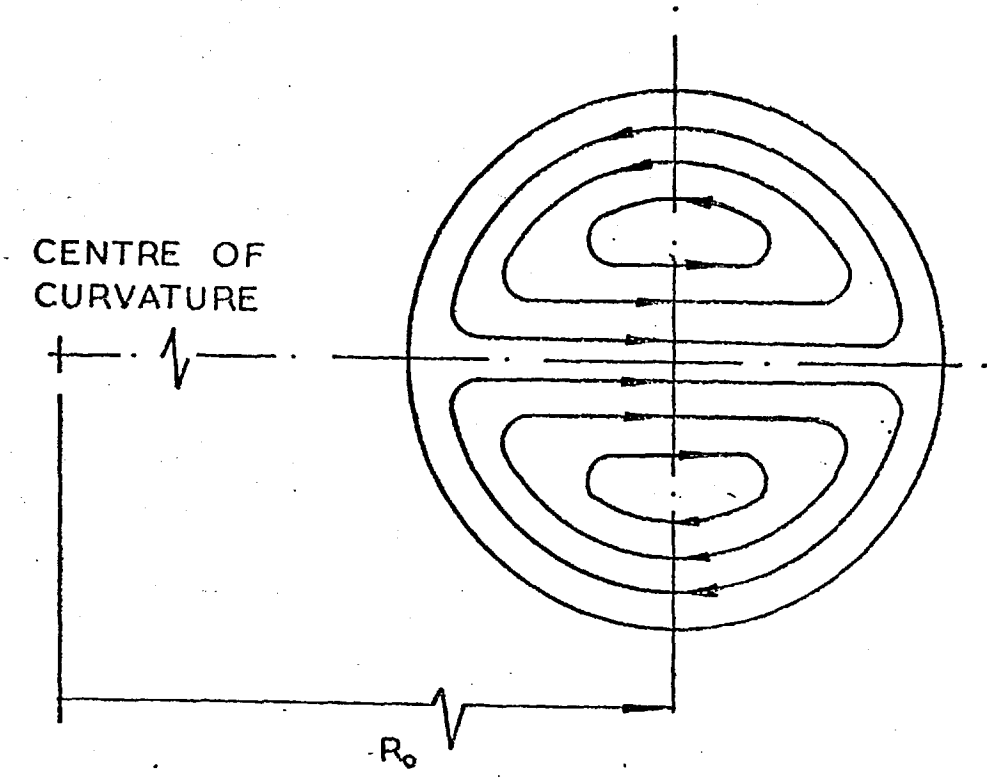

Fig. (7.2.1(b)): General flow pattern in the cross-sectional plane of a curved pipe.

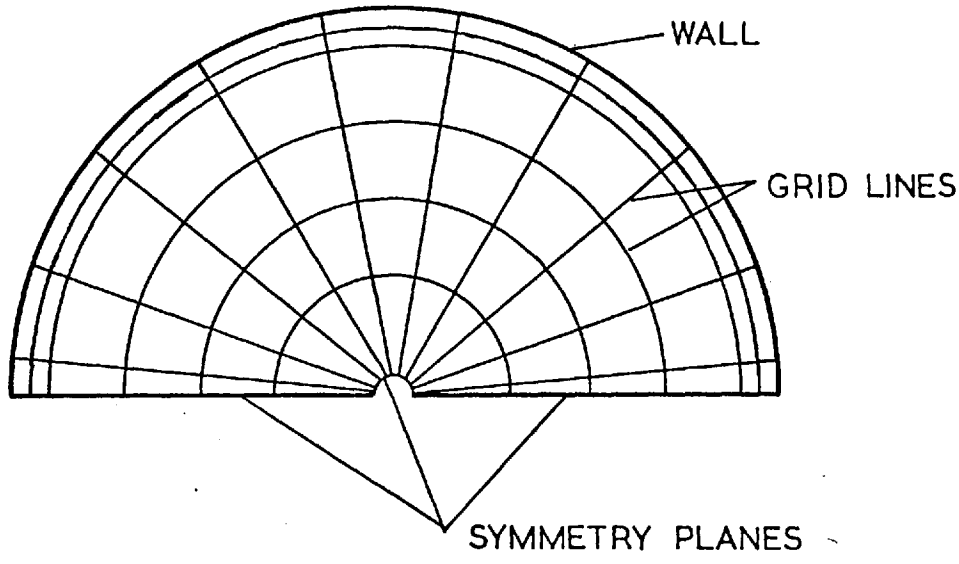

Fig. (7.2.2): Flow domain considered for computations.

grid in the cross-sectional plane possessed 15 intervals in the r-direction and 11 intervals in the θ-direction. That the 15x11 grid gave sufficient accuracy was confirmed by repeating the computations with finer and coarser grids; the results of one such 'grid-independency test' (along r-direction) are shown in Figure (7.2.3). The forward-step dependency was tested by repeating the computations with smaller and larger step sizes; a step size was then chosen which was small enough not to affect the solution.

The developing flow solutions were obtained by the marching procedure with small forward steps. However, when only the fully-developed flow was to be computed very large forward steps were taken and the velocities were under-relaxed at each step. The fully developed computations, starting with a uniform velocity profile, usually needed about 140 steps for convergence of the solution. The computer time needed for each forward step was of the order of 0.28 secs on a CDC 6600 computer.

7.2.2 The developing region

Figures (7.2.4) to (7.2.6) display the development of the axial-velocity field along the ϕ-direction and comparisons with experimental data of Austin (1971). The agreement is quite good considering

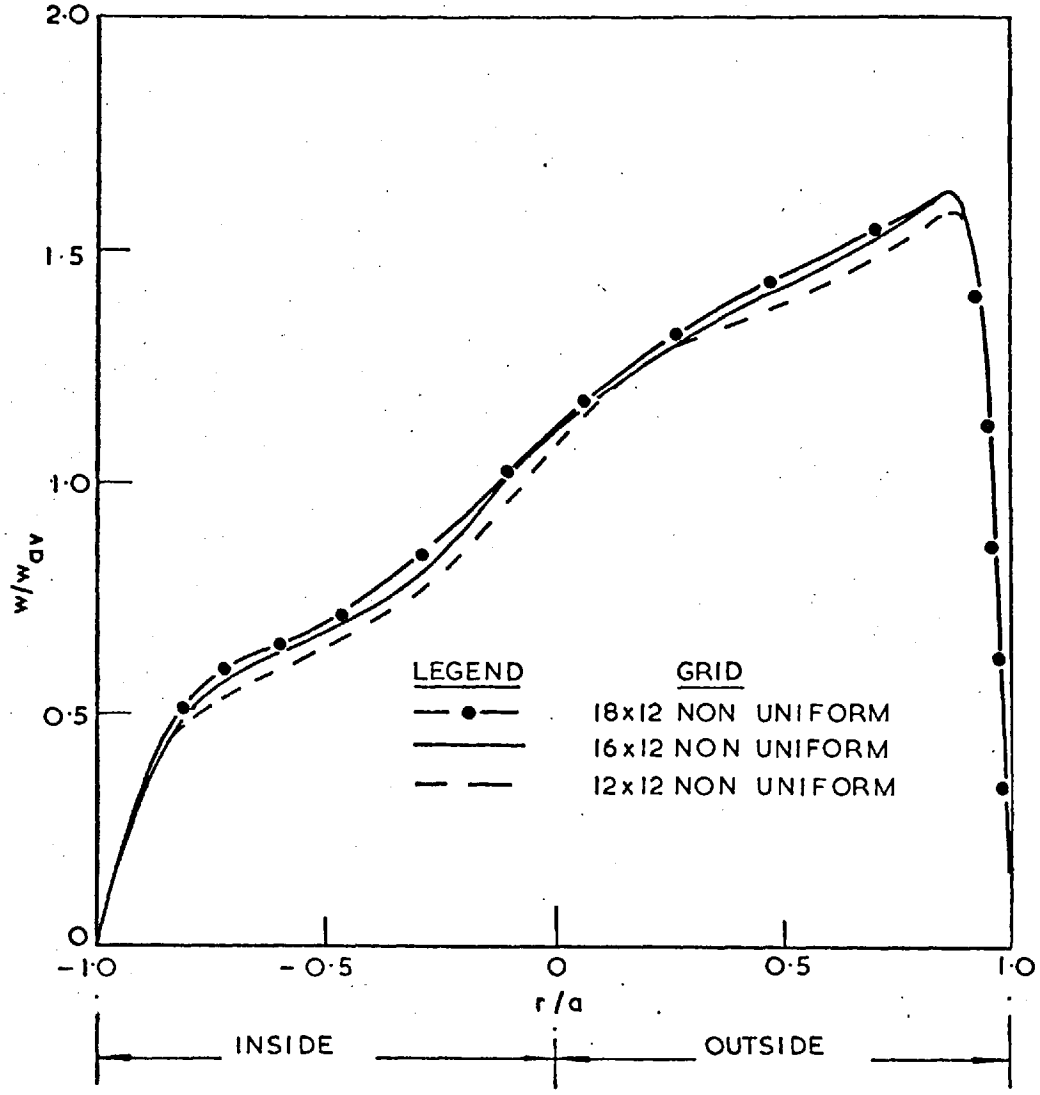

Fig. (7.2.3): Effect of grid size on the calculation of flow for a Dean number of 800 and radius ratio of 16.4. The velocity profiles are along plane AA.

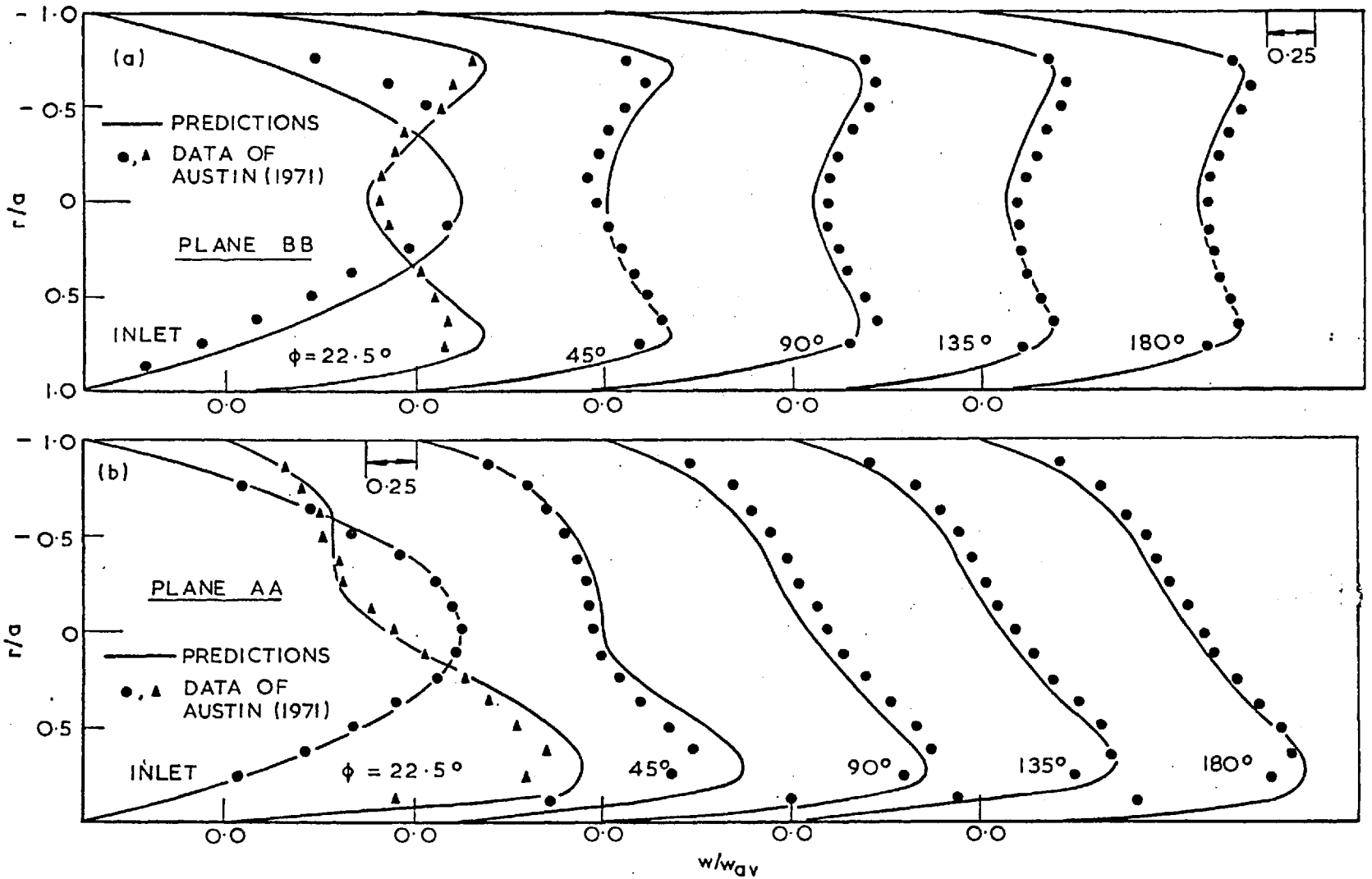

Fig. (7.2.4): Development of axial velocity at K=198.0 and R/a=29.1 in (a) the plane BB and (b) the plane AA.

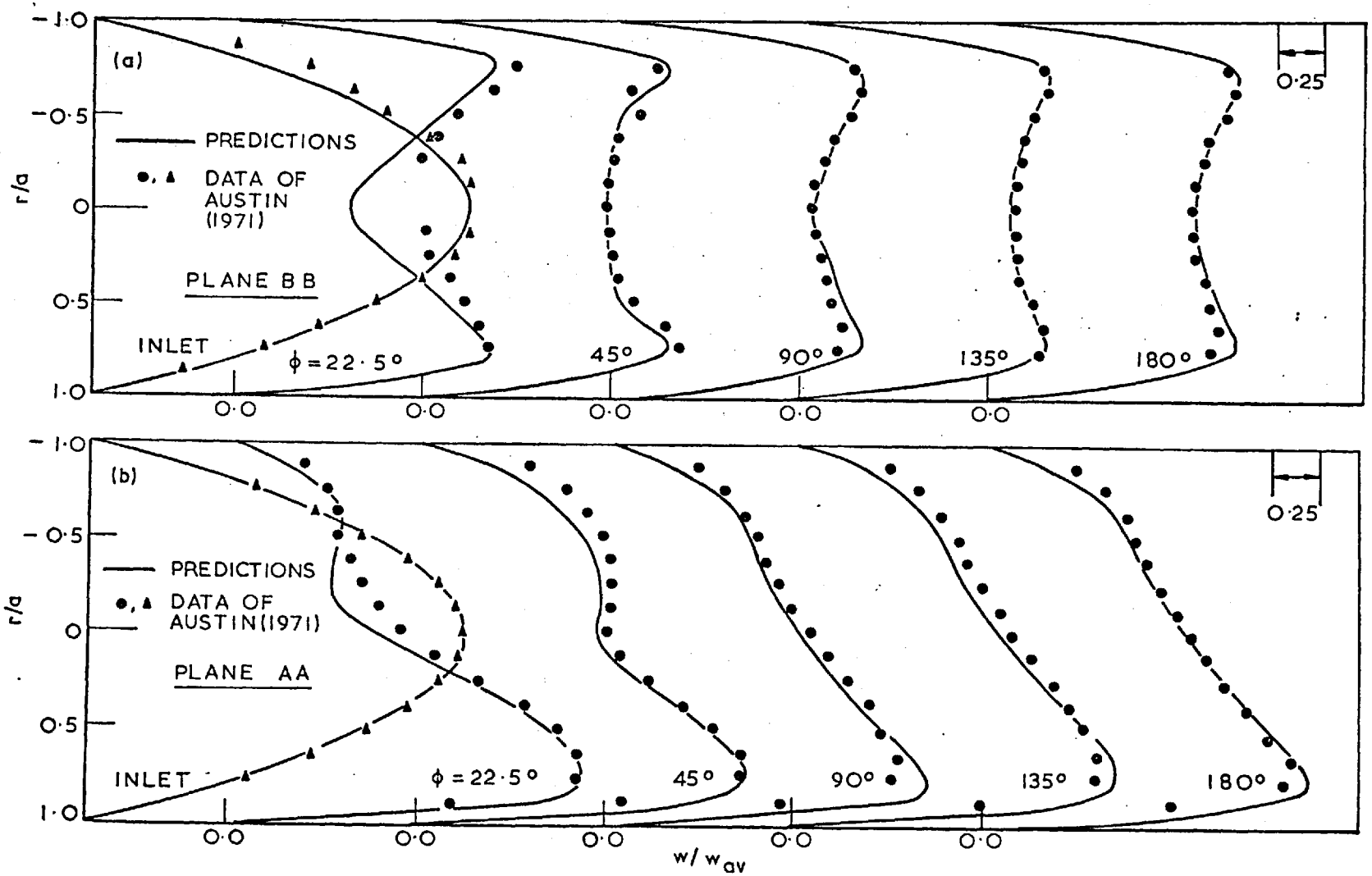

Fig. (7.2.5): Development of axial velocity at K=280.0 and R/a=29.1 in (a) the plane BB and (b) the plane AA.

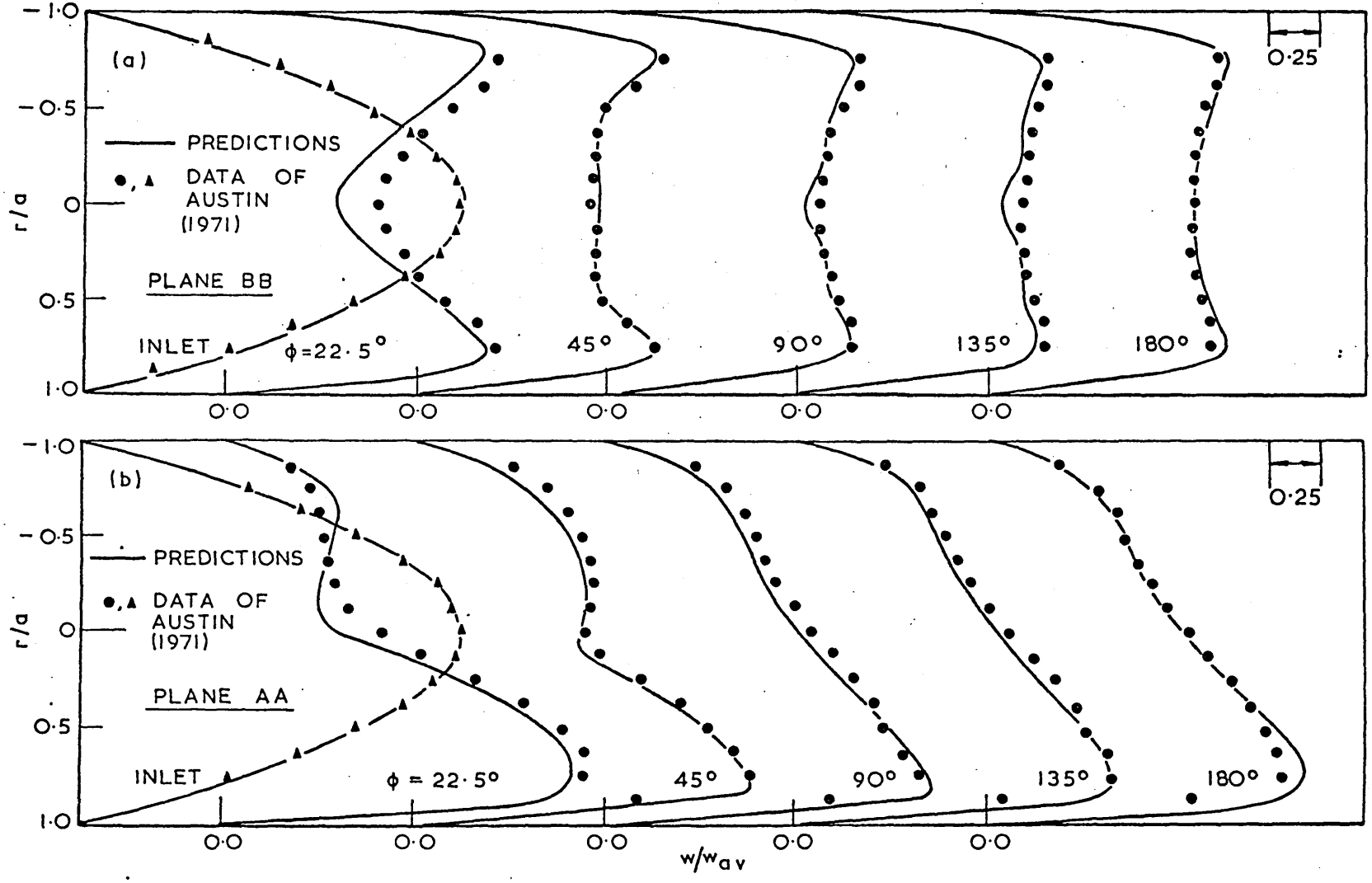

Fig. (7.2.6): Development of axial velocity at K=372.0 and R/a=29.1 in (a) the plane BB and (b) the plane AA.

the fact that the inlet velocity-profiles in the experiment were not exactly parabolic. Figure (7.2.7) shows the development of the secondary flow field along the ϕ-direction. The predictions indicate that the secondary velocities develop in a damped oscillatory manner in which the amplitude of the oscillations is greatly diminished after the first oscillation. Because of lack of experimental data, the present oscillatory behaviour could not be compared with results of Austin (1971); but it is qualitatively in conformity with some other measurements such as those of Hawthorne (1951) and Squire (1954) for turbulent flow in curved pipes. The secondary velocities (θ-components) plotted in Figure (7.2.7(b)) at two typical locations in the cross-section show that the period of first oscillation is about 75 degrees. Figure (7.2.8) shows the radial variation of static pressure plotted for various angular positions in the ϕ-direction. Close examination of this plot shows that the static-pressure distribution also develops in an oscillatory manner but attains a uniform value much quicker than the secondary velocities. Figure (7.2.9) shows the development of the friction factor ($f = \frac{2d\bar{p}}{dz} \cdot \frac{1}{\rho w_{av}^2}$) and comparison with the empirical relation of Kulegan and Beij (1936); the agreement is

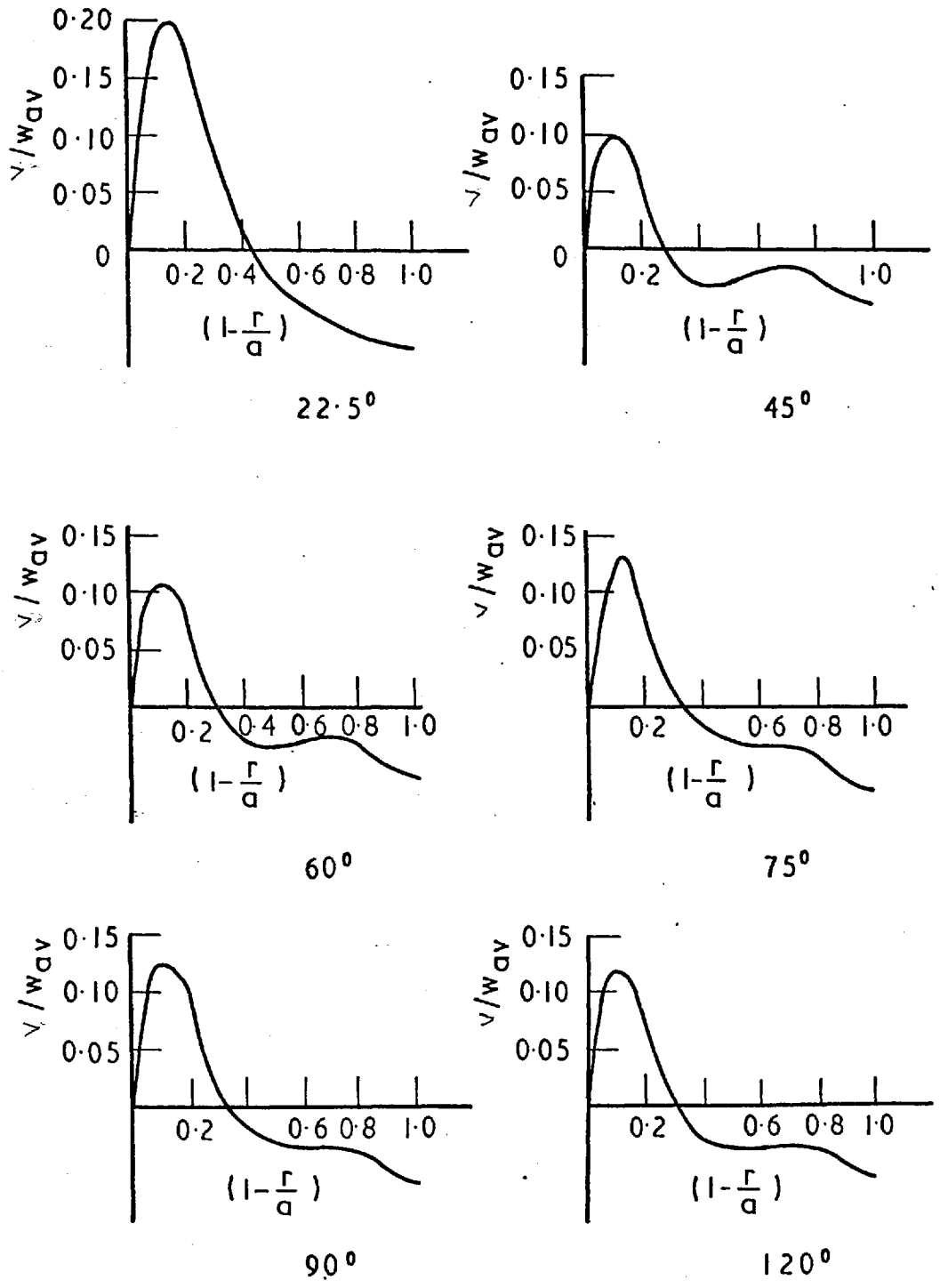

Fig. (7.2.7(a)): Development of secondary velocity along the diameter BB. K=198.0, R/a=29.1.

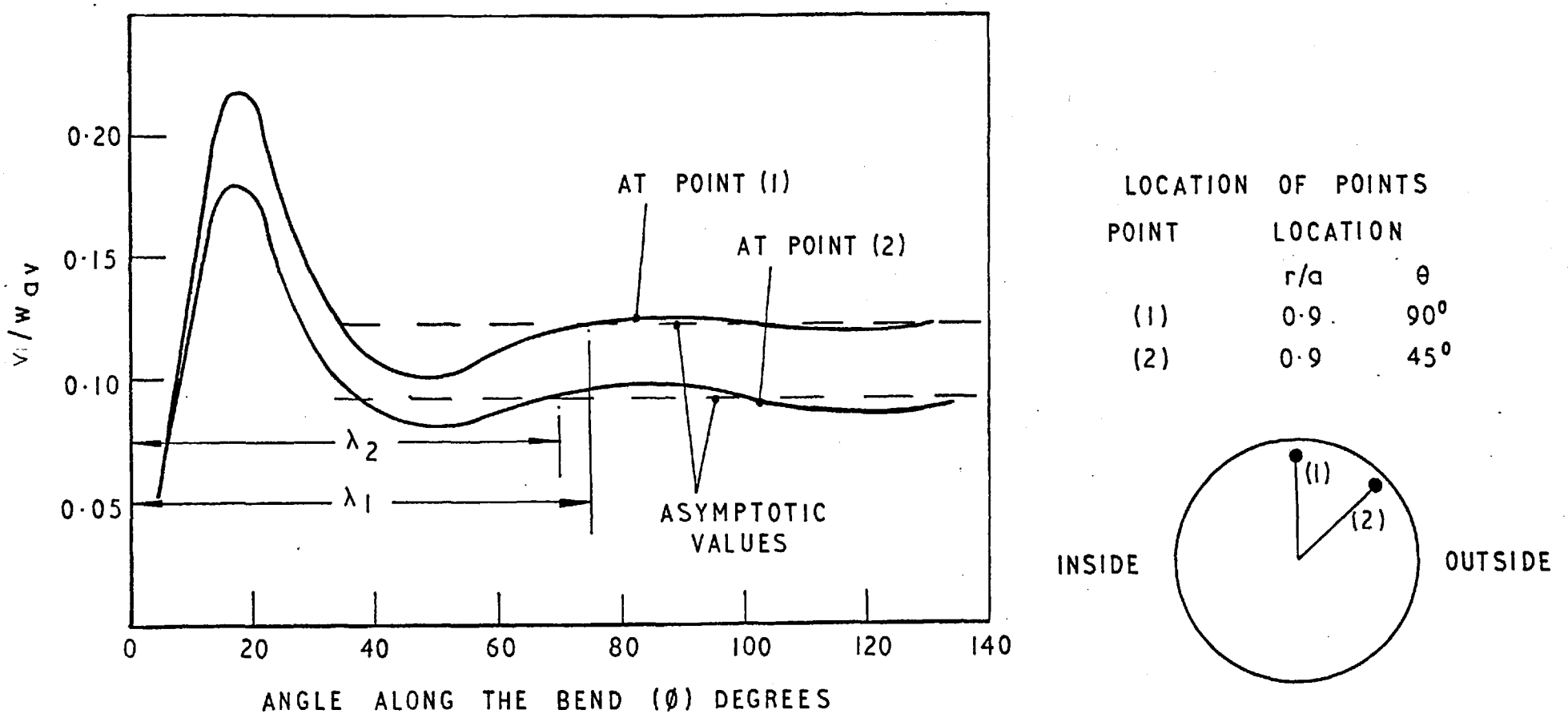

Fig. (7.2.7(b)): Variation of secondary velocity with bend angle, for two typical locations in the cross-sectional plane.

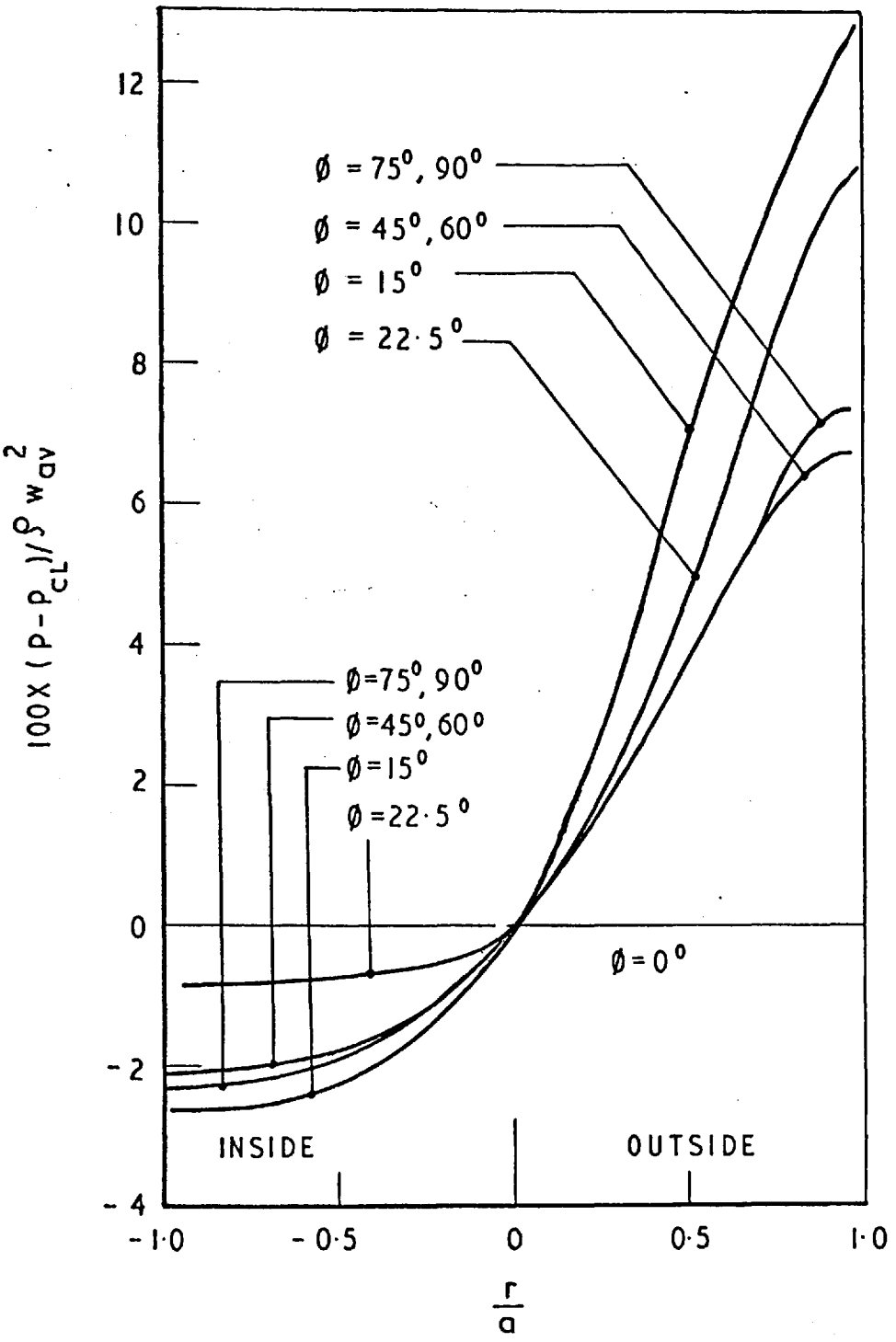

Fig. (7.2.8): Development of static-pressure variation in plane AA at K=198.0, R/a=29.1.

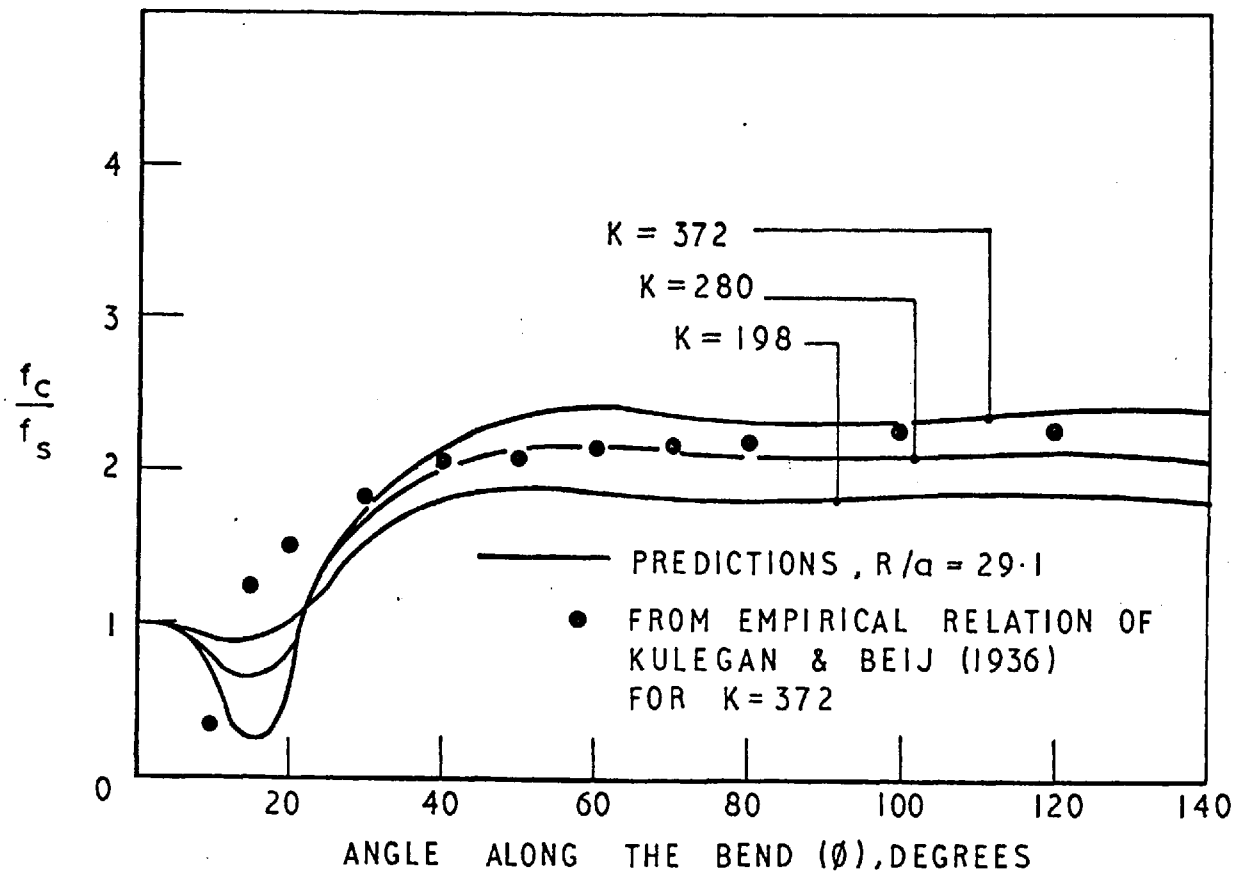

EMPIRICAL RELATION OF KULEGAN AND BEIJ (1936):

$$\frac{f_c}{f_s} = \left(\frac{f_c}{f_s}\right)_\infty - \frac{\frac{d}{x}\left(\left(\frac{f_c}{f_s}\right)_\infty - 1\right)}{\left(.0059 + 0.844\left(\frac{d}{D}\right)^{\frac{1}{2}}\right)}$$

where d = pipe diameter

D = coil diameter

$\frac{x}{d}$ = distance along bend

f_c = curved tube friction factor (peripheral average)

f_s = straight tube friction factor

Subscript ∞ = fully-developed value

Fig. (7.2.9): Development of friction factor along a bend, R/a=29.1.

seen to be satisfactory. Figure (7.2.10) shows the development of the temperature field for the condition of axially-constant heat flux with isothermal periphery. The flow field for these computations was prescribed to be fully-developed at the entrance of the temperature field in accordance with the experimental conditions reported by Dravid et al. (1971). The Prandtl number of the fluid was varied linearly from 6 at the inlet to 4 at location where $(R\phi/a)$ (ϕ in radians) equals 250. The calculations reproduce the oscillatory development of the temperature field which has been observed in the experiments; but the predictions show a quicker damping of the oscillations. Figures (7.2.11) and (7.2.12) show the effect of Prandtl number on the nature of these oscillations. It is seen that the oscillations are more pronounced at larger Prandtl numbers. A dimensionless wavelength λ of the first oscillation, defined as the distance $(R\phi/a)$ between the point at which a line parallel to the bulk temperature line is tangential to the first maximum and first minimum in the wall-temperature curve is compared with experimental results for various Prandtl and Dean numbers. The present computations confirm the experimental results of Dravid (1971) that the Prandtl number, in the range studied (0.7 - 15.0) has little effect on the wavelength λ. The values of the wavelength λ for a few Dean numbers are shown in Table (7.2.1).

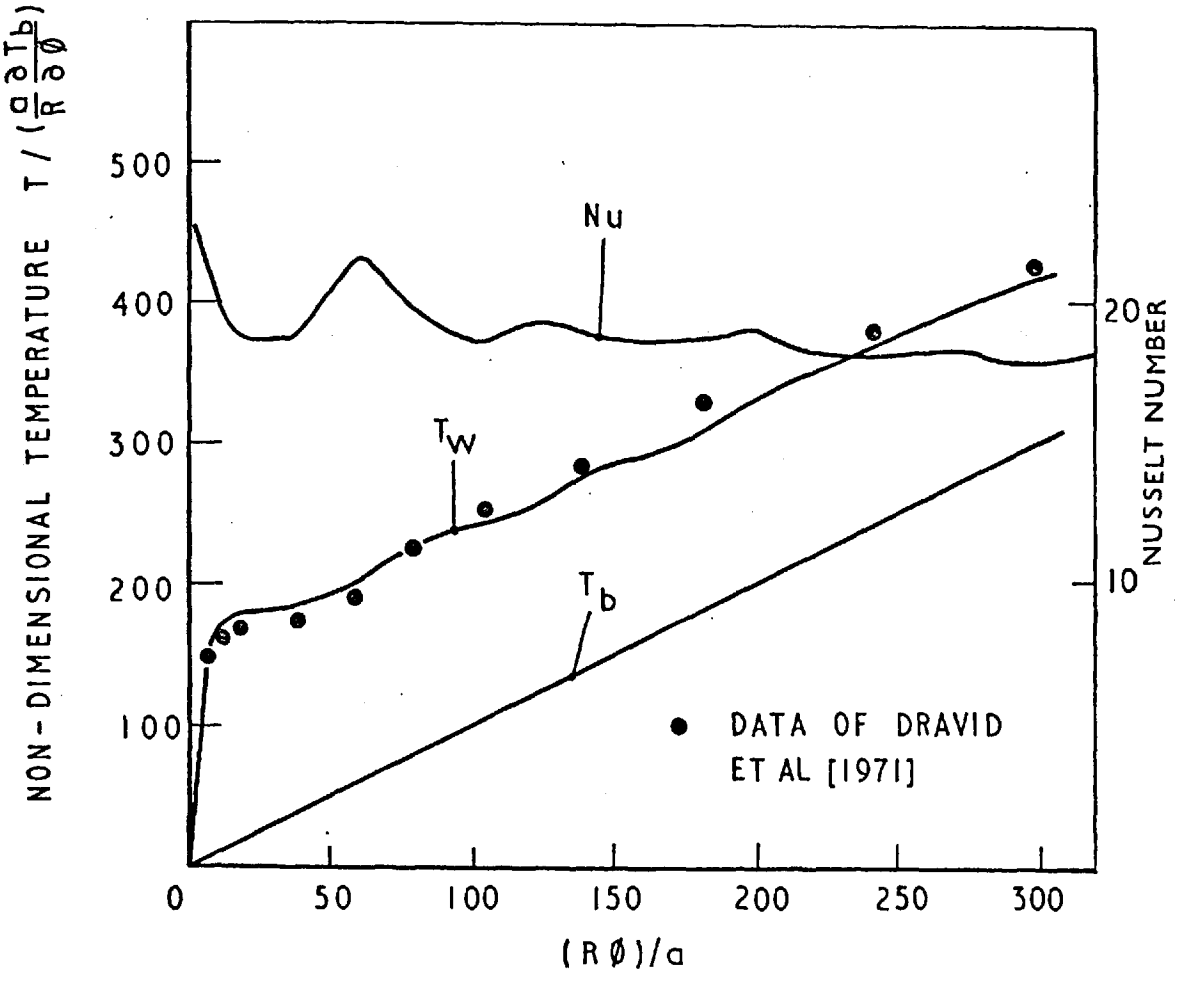

Fig. (7.2.10): Development of wall temperature and Nusselt number for the case of axially-constant heat flux at K=225.0 and R/a=20.0; Pr_{mean}=5.0.

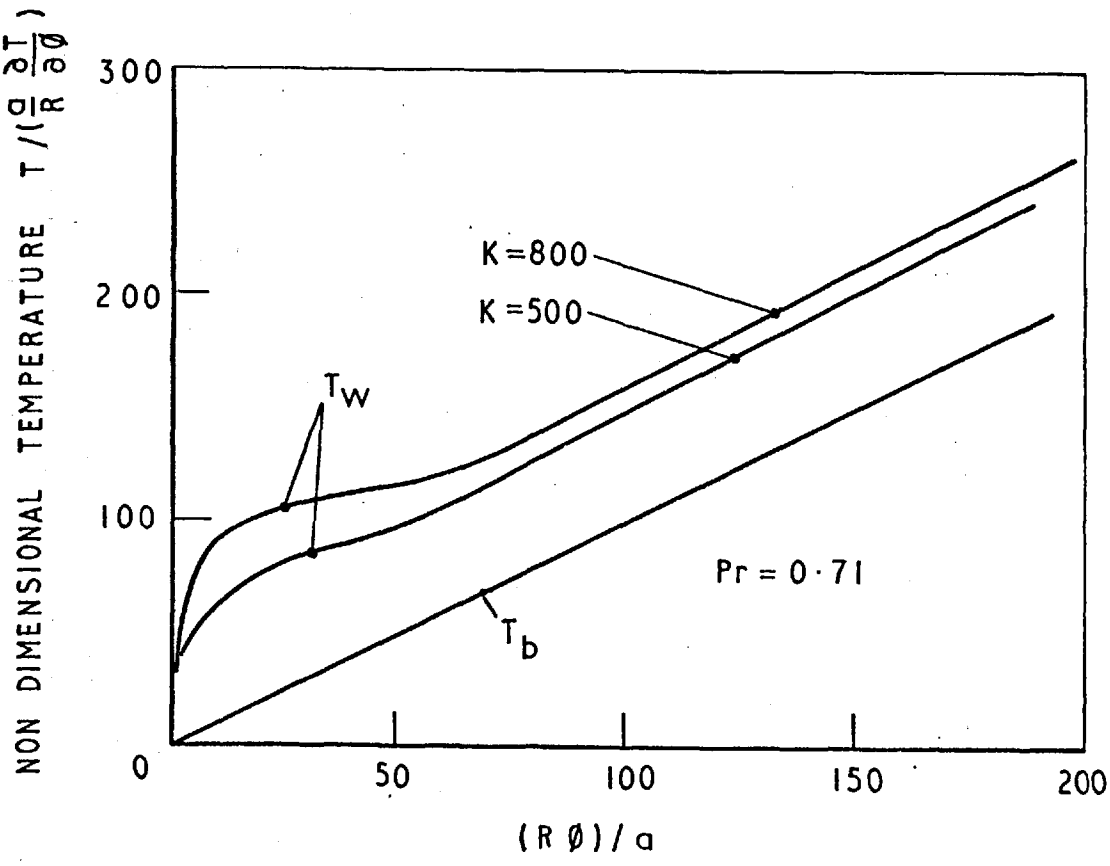

Fig. (7.2.11): Development of wall temperature and Nusselt number for the case of axially-constant heat flux at K=225.0 and R/a=20.0; Pr=0.71.

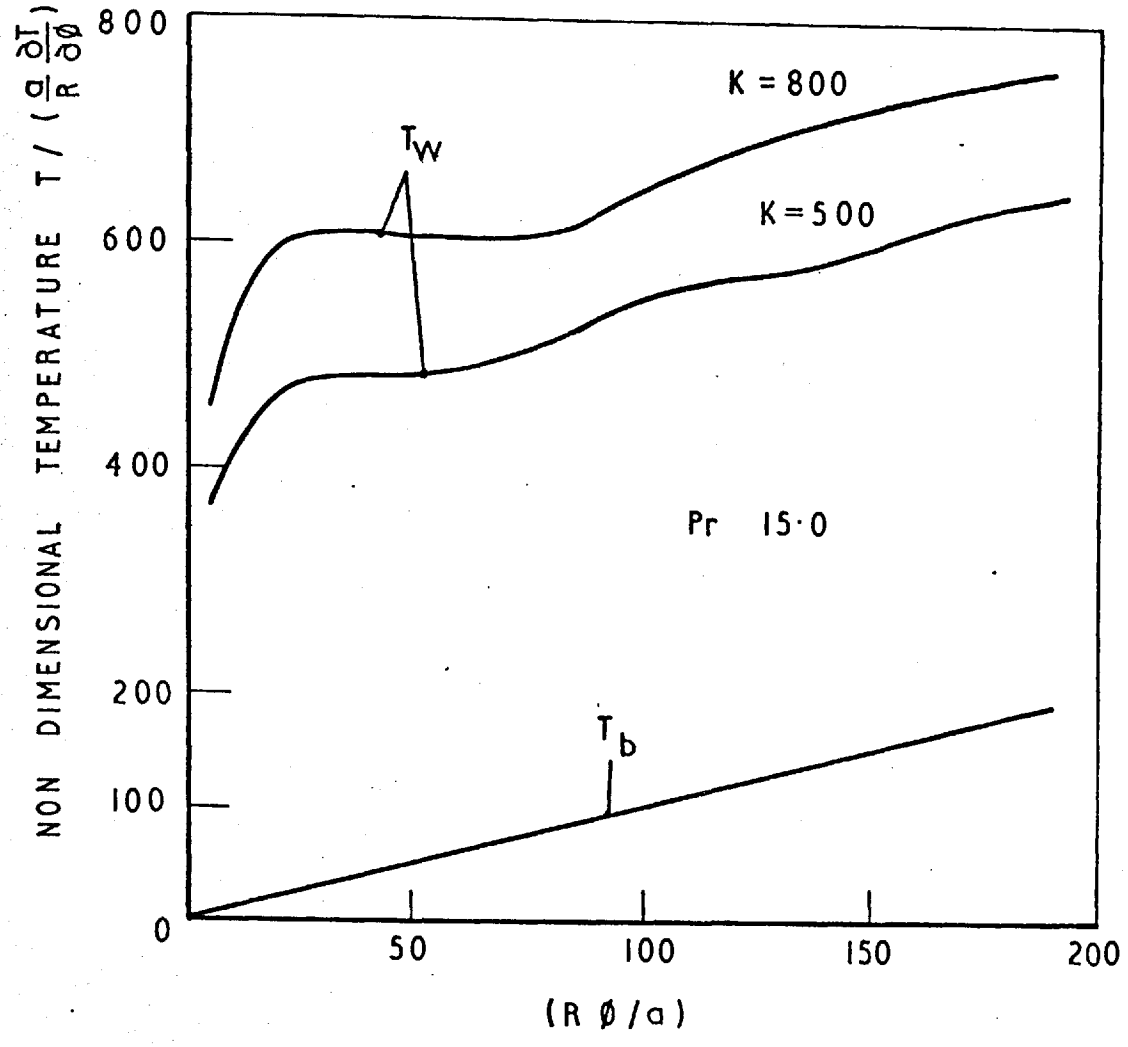

Fig. (7.2.12): Development of wall temperature and Nusselt number for the case of axially-constant heat flux at K=225.0 and R/a=20.0; Pr=15.0.

Table 7.2.1

Dean number (K=Re√a/R)	λ	
	Computed	Measured
225.0	51.0	52.5
447.0	71.0	75.0
800.0	73.0	100.0

7.2.3 The fully-developed region

The computations of flow and heat-transfer characteristics in fully-developed regions have also been compared with experimental data of various authors. Figure (7.2.13) compares the present predictions of the fully-developed velocity profiles with those of Adler (1934) and Mori and Nakayama (1965). Figure (7.2.14) compares the corresponding friction factors with data of various authors (from Ito (1969)). The agreement of the predicted velocity profiles and friction factors with experimental data is good. The computed axial-velocity profiles at various angular planes are shown in Figure (7.2.15), and Figure (7.2.16) displays the effect of Dean number on the axial-velocity profiles. It can be seen that the velocity peak is shifted towards the outside as the Dean number is increased. Consistent with the angular variation of the velocity profile is also the variation of the friction factor along the periphery of the cross-section, as shown in Figure (7.2.17);

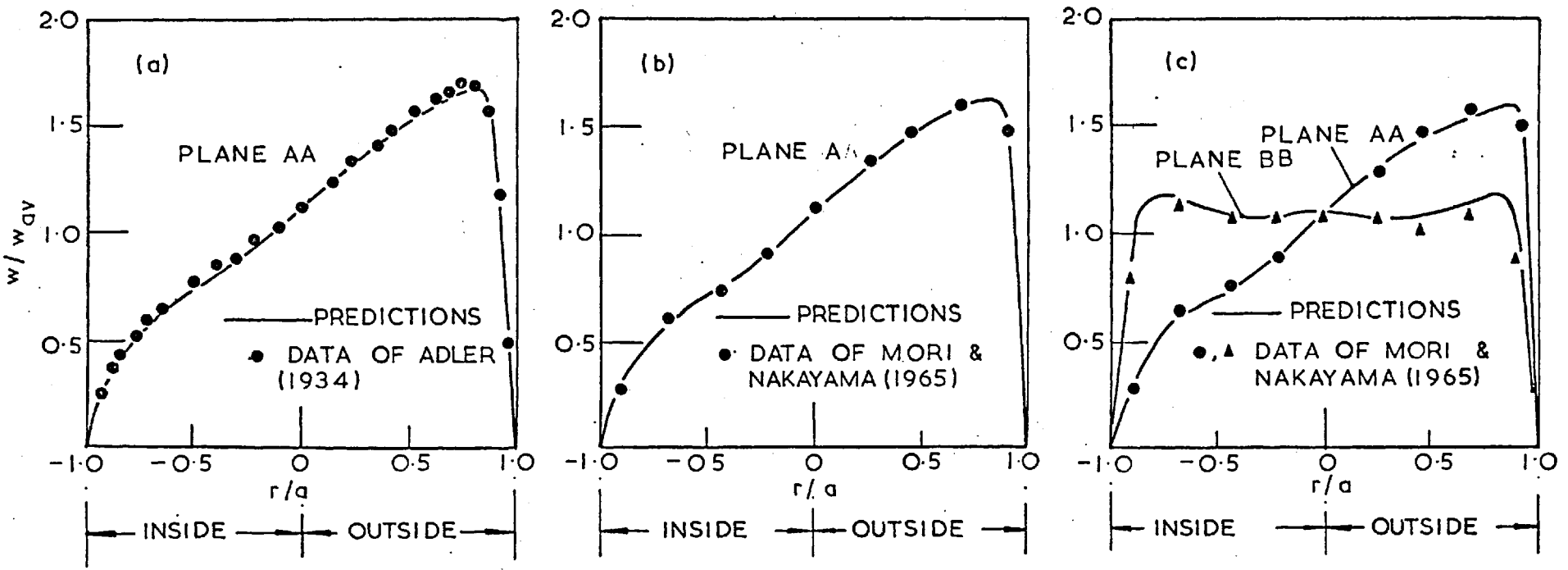

Fig. (7.2.13): Comparison of axial-velocity profiles with experimental data.
(a) K=372.0, R/a=100; (b) K=442.7, R/a=40.0; (c) K=632.4, R/a=40.0.

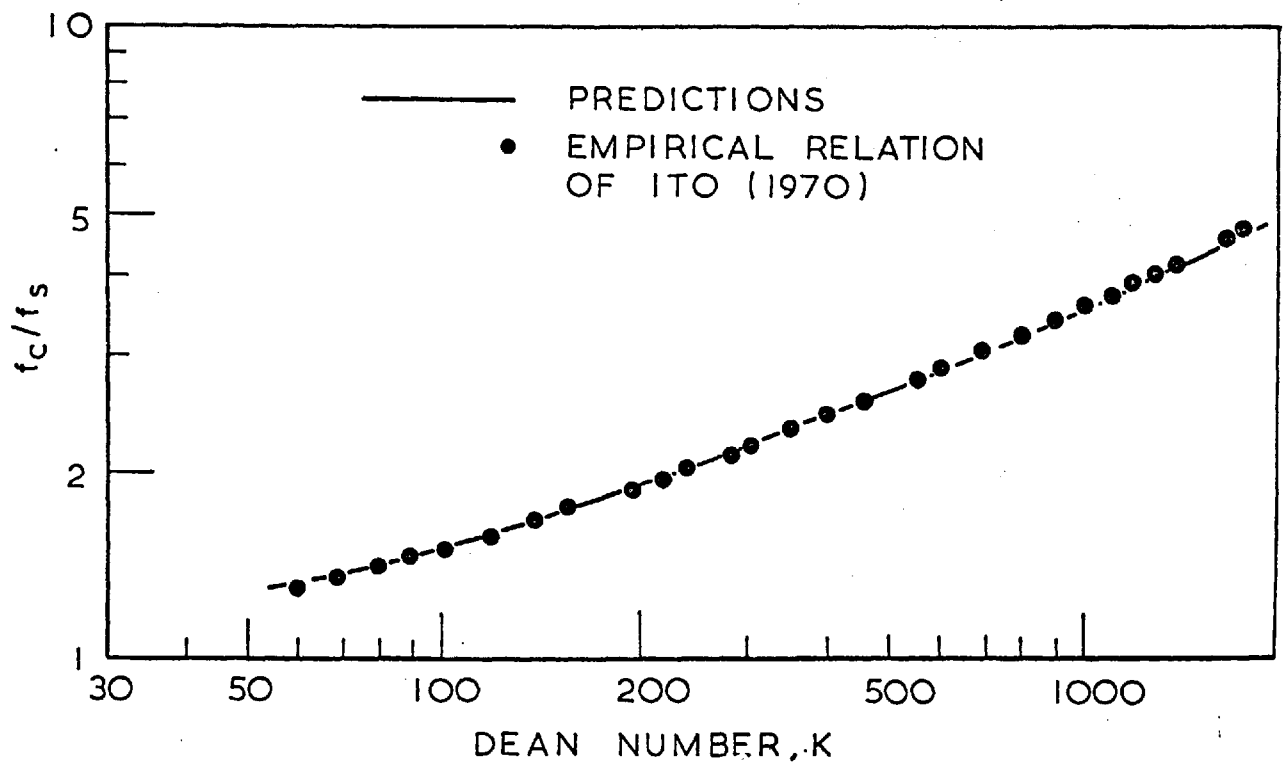

Fig. (7.2.14): Comparison of fully-developed friction factors with experimental data.

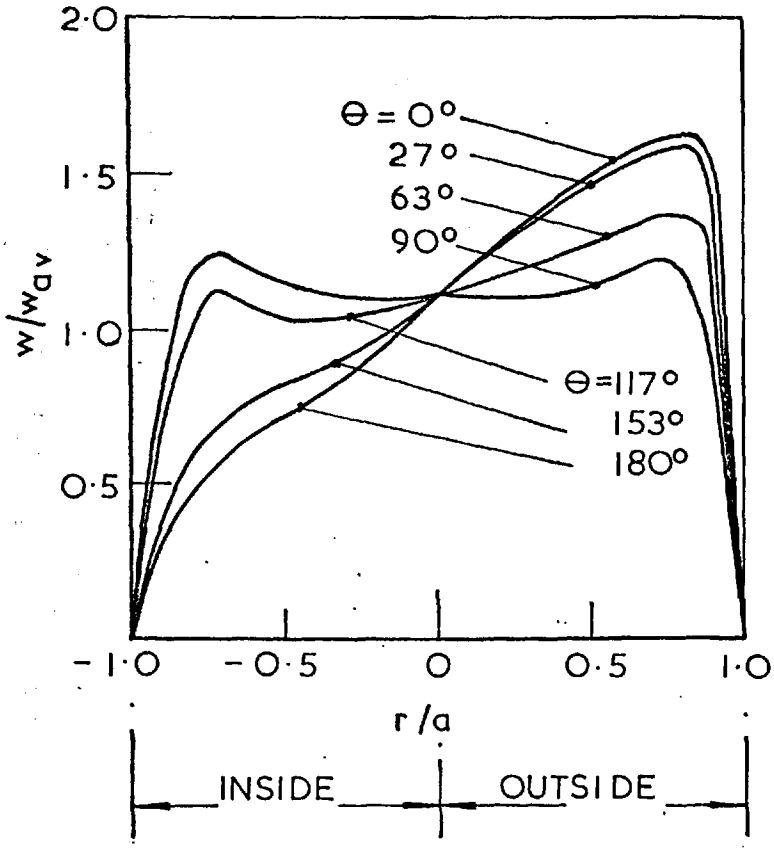

Fig. (7.2.15): Axial-velocity field represented along various planes at K=442.7; R/a=40.

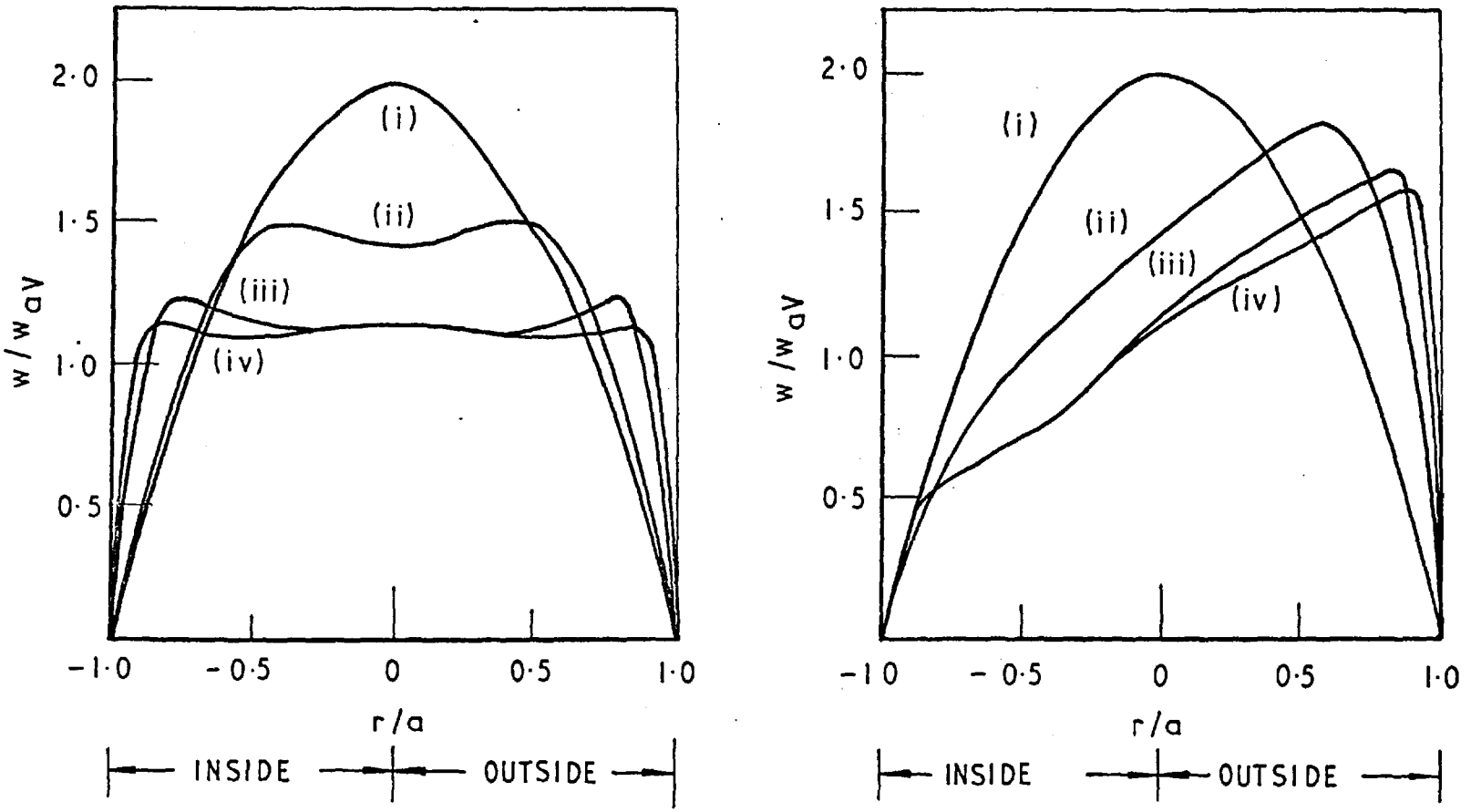

Fig. (7.2.16): Effect of Dean number on axial-velocity profiles in (a) the plane AA and (b) the plane BB. (i) Straight tube; (ii) K=60.0; (iii) K=500.0; (iv) K=1200.0; R/a=16.0.

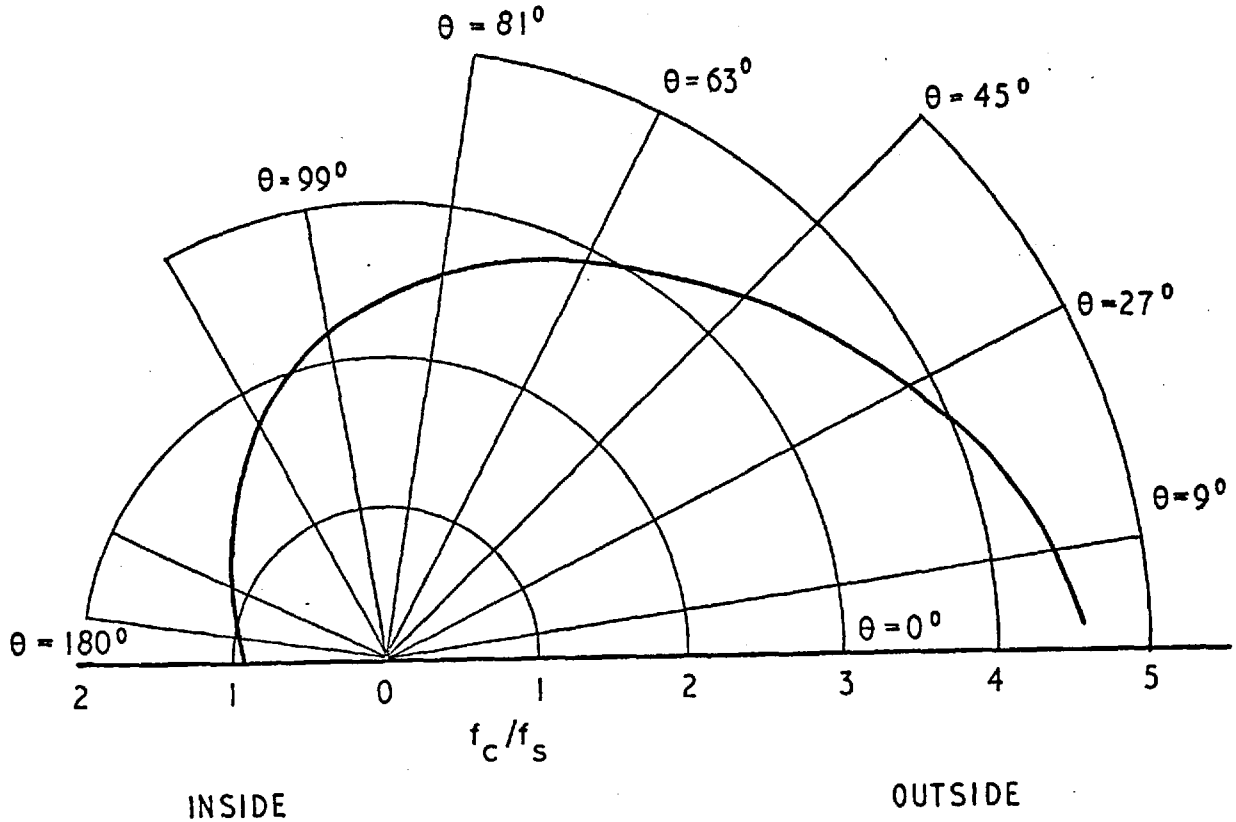

Fig. (7.2.17): Angular variation of fully-developed friction factor for K=442.7 and R/a=40.0.

the friction factors at the outside are considerably higher than those at the inside.

The fully-developed temperature field has been computed under the conditions of axially-uniform heat flux and is compared in Figure (7.2.18) with the experimental data of Mori and Nakayama (1965). The comparison shows good agreement in the outside half of the plane; but there are significant differences in the inside region. To investigate the reason for this discrepancy, further comparisons of the predictions have been made with the theoretical solutions of Akiyama and Cheng (1971); from (7.2.19) it is seen that the present calculations of peripheral variations in Nusselt number are in good agreement with Akiyama and Cheng's results for the Dean numbers they considered. It is also seen from Figure (7.2.20) that the inside heat-transfer coefficient approaches half the straight tube value at a Dean number of about 300 and then increases slowly to the straight tube value at a Dean number of 1200; these observations which are in agreement with the solutions of Akiyama and Cheng (1971) disagree with the experimental findings of Mori and Nakayama which show much steeper temperature-gradients on the inside. In view of the comparisons in Figures (7.2.19) and (7.2.20), it appears that the temperature profile of Mori and Nakayama (1965) may be in error,

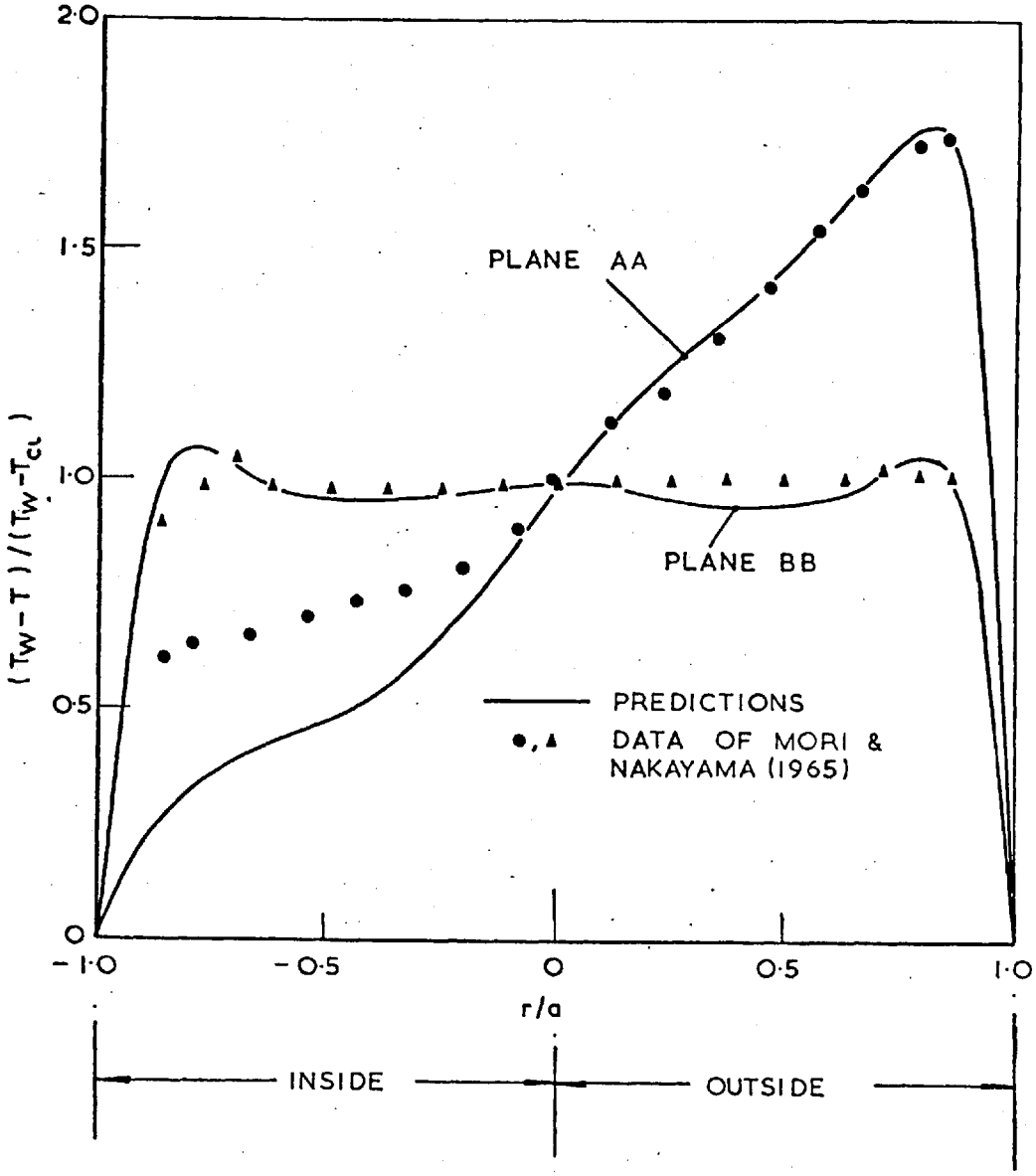

Fig. (7.2.18): Temperature profiles along planes AA and BB; K=632.4, R/a=40.0 and Pr=0.71.

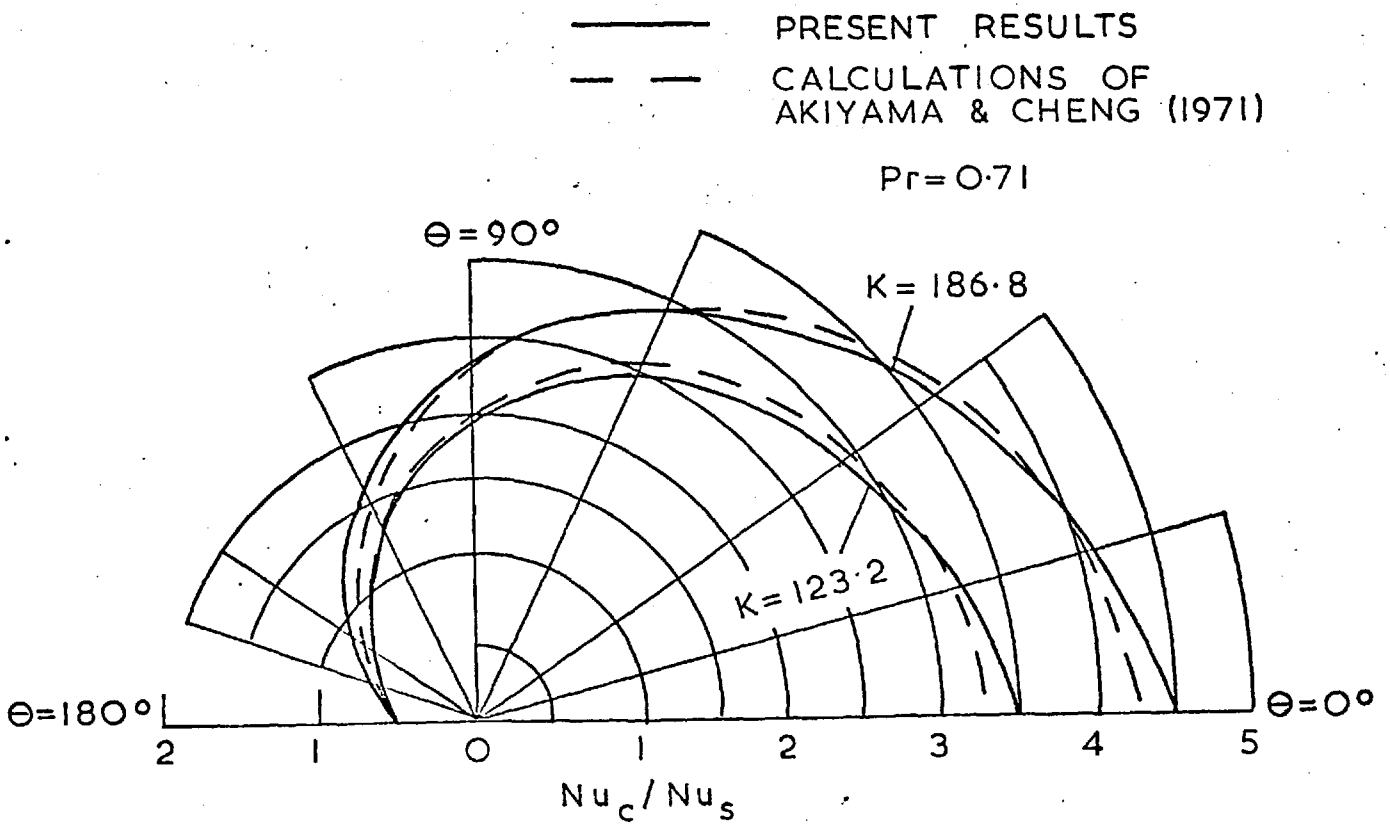

Fig. (7.2.19): Angular variation of Nusselt number with Dean number.

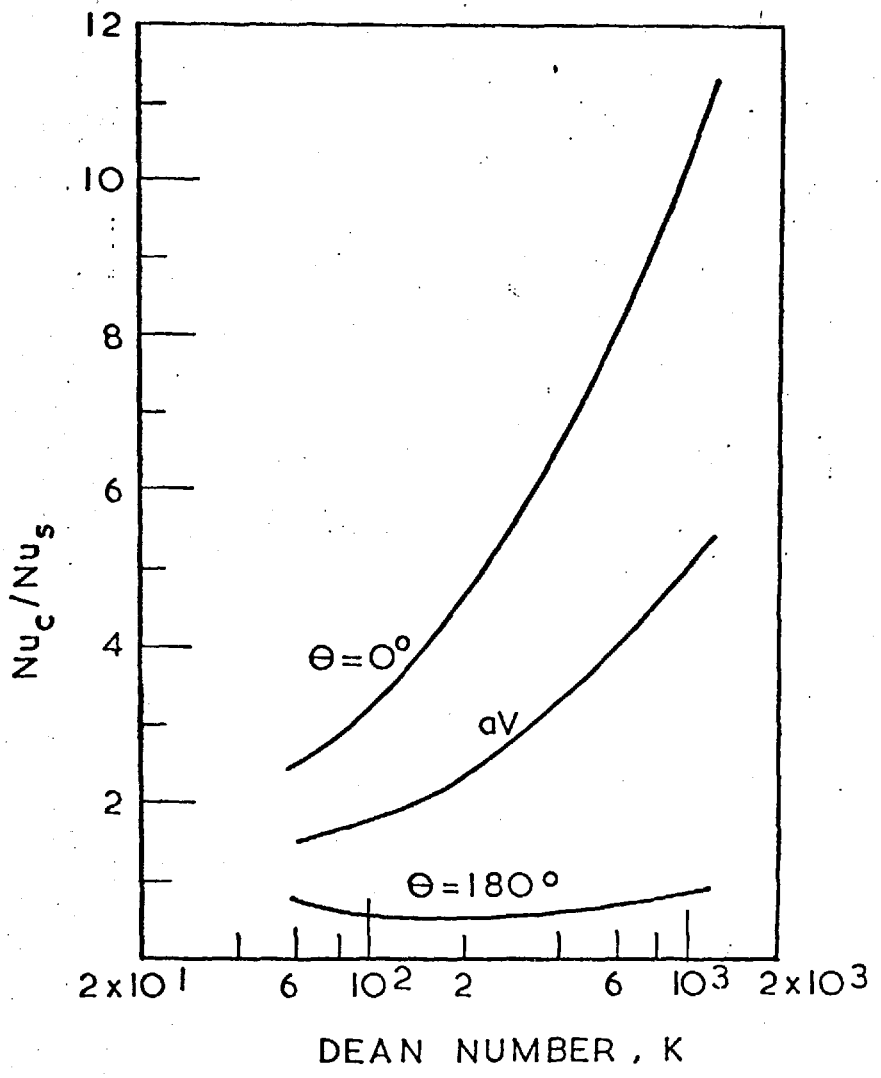

Fig. (7.2.20): Variation of Nusselt number with Dean number for R/a=40 and Pr=0.71.

either owing to inaccuracy in measurement or imperfection in setting up the stated temperature boundary-conditions. However, despite the discrepancy in temperature profile the agreement in the mean Nusselt numbers seems to be good, as can be seen from Figure (7.2.21(a)). Further comparisons of the predicted fully-developed Nusselt numbers have been made with the experimental results of Dravid et al. (1971) and are shown in (7.2.21(b)); the agreement is satisfactory. In Dravid's experiments the Prandtl number varied from 6 to 4 over the developing region. Since the comparison in Figure (7.2.21(b)) is for the fully-developed condition, the computations were based on a uniform Prandtl number of 4, which was appropriate to the outlet condition. Figure (7.2.22) illustrates the effect of Dean number on the temperature profiles along plane AA; the effect is observed to be the same as that on the velocity profiles. The effect of Prandtl number on the heat-transfer rates is shown in Figure (7.2.23). It is seen that the peripheral variation of the heat-transfer rates is larger for fluids with high Prandtl numbers.

7.2.4 Discussion

The predictions presented above show good agreement with experimental data and thus validate the accuracy of the calculation procedure. The good

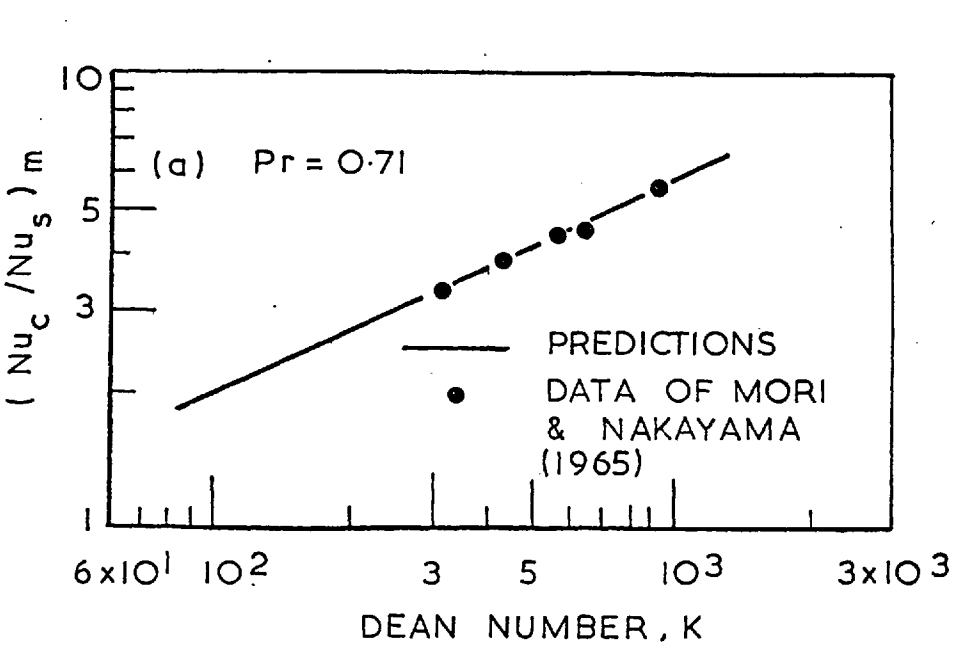

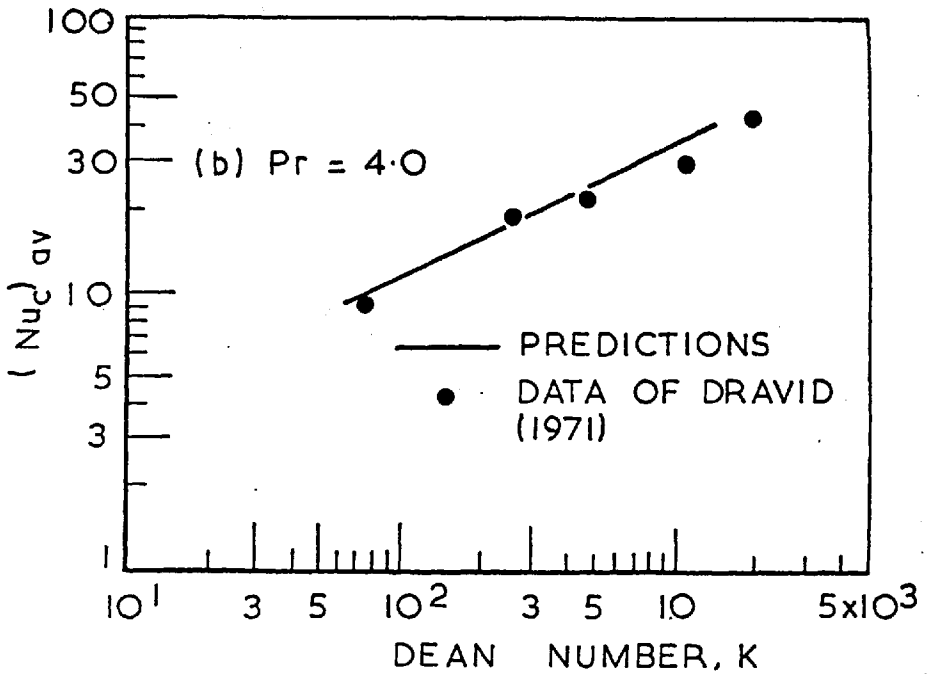

Fig. (7.2.21): Variation of Nusselt number with Dean number. (a) Pr=0.71. The subscript 'm' indicates the mean value of outside and inside. (b) Pr=4.0. The subscript 'av' indicates peripheral average.

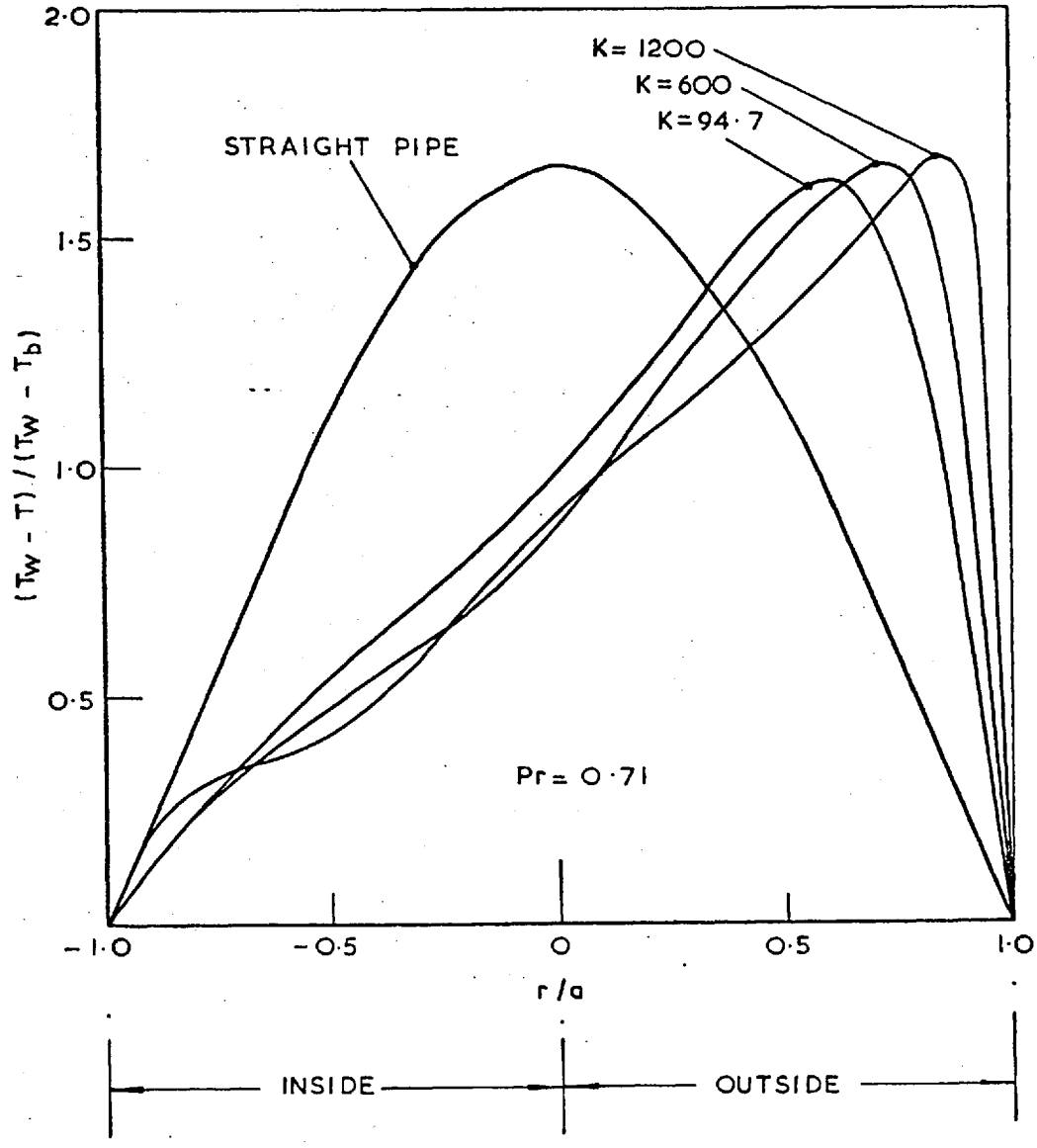

Fig. (7.2.22): Effect of Dean number on temperature profiles along plane AA.

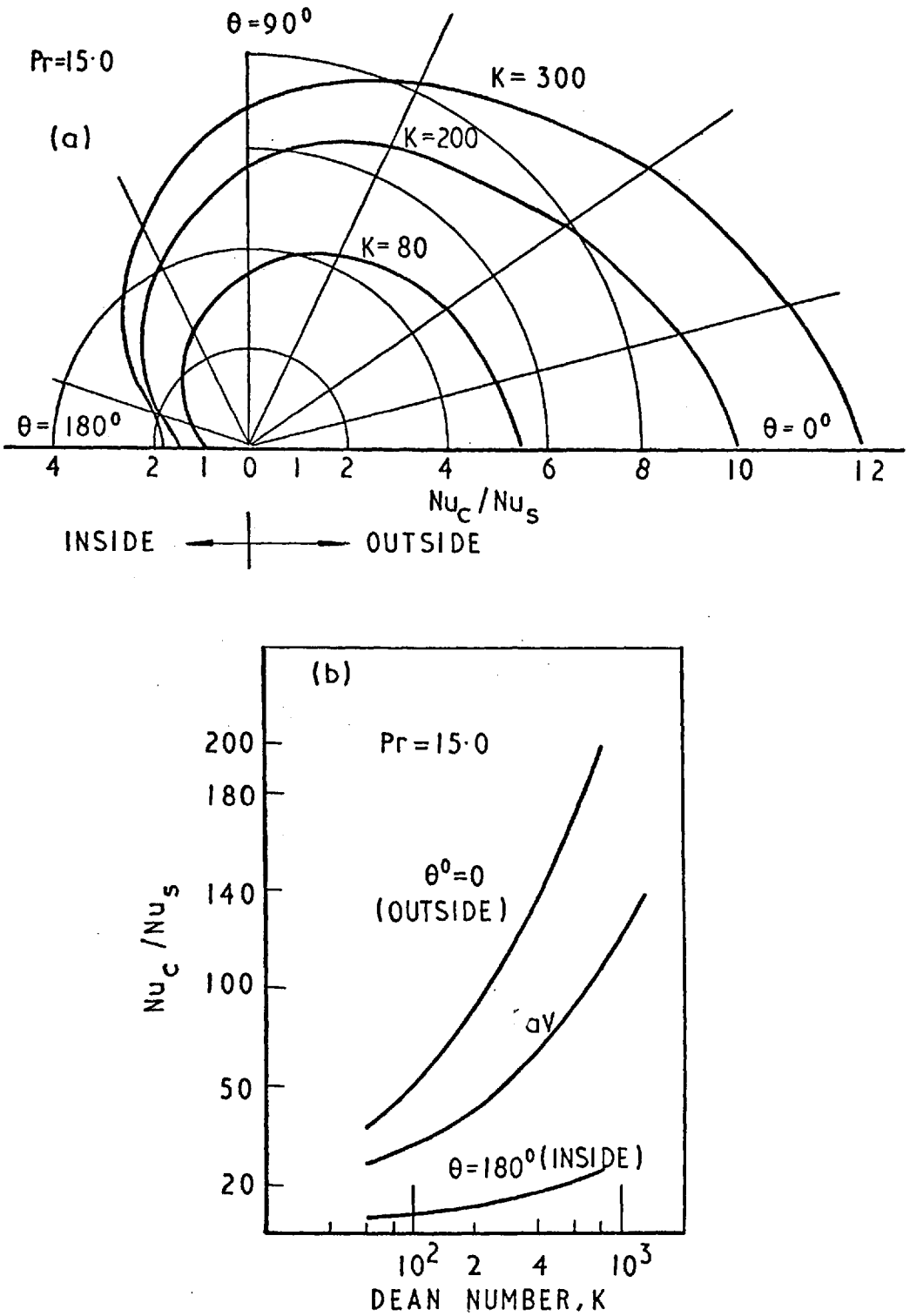

Fig. (7.2.23): Variations of Nusselt number for Pr=15.0. (a) Peripheral variation; (b) Variation with Dean number.

agreement observed in the predictions of the developing flow-field also proves that the flow in mildly-curved ducts is parabolic in nature. The flow phenomena observed in the present flow situation may be described as follows: The curvature of the duct gives rise to centrifugal forces which act at right angles to the main flow direction; in order to balance the centrifugal forces, pressure-gradients along the cross-stream directions are set up with the high-pressure zone at the outside of the curvature. As a consequence of these cross-stream variations in the pressure field, secondary velocities are generated, which distort the primary (axial) velocity field, the distortions increasing with the Dean number. The secondary flow pattern which consists of two symmetrical vortices in the cross-sectional plane is shown in Figure (7.2.1(b)). The secondary flows have two main consequences: Firstly, they cause an increased 'mixing' in the flow, thereby enhancing the friction factors and the rates of heat and mass transfer over their straight-tube values. Secondly, because of the distortions in the velocity field, the friction factors and heat transfer rates vary significantly over the periphery, the ratio of outside to inside values being as large as 4. Also, as a consequence of these secondary flows, the heat-transfer rates increase with Reynolds number compared with the case of the laminar flow in straight pipes where the

heat-transfer rates remain constant at a value depending on the thermal boundary condition. The secondary flow is thus the chief distinguishing feature of the flow phenomena in curved pipes.

The development of the flow and temperature fields in curved pipes has been observed, both experimentally and theoretically, to be oscillatory. Squire and Winter (1951) explain the oscillations in the flow field to be a result of the changes in the kind (sign) of streamwise vorticity which is produced as the flow passes around the bend. Hawthorne (1951), shows using an inviscid analysis that the period of first oscillation is approximately equal to $2.36\ \pi\ \sqrt{2a/R}$ which for the present radius ratio of $\frac{a}{R} = 29.1$ gives a value of 110 degrees. Compared with this value, the present computations, which include the effects of viscosity, give a period of first oscillation of about 75 degrees. However, the inlet conditions assumed in Hawthorne's theory have been somewhat different than those employed in the present computations and because of this fact, some difference may be expected between the two solutions. The oscillations in the development of the temperature field however, are not a result of the oscillations in the secondary flow; this is because, in the present computations, the flow field has been prescribed to be fully-developed at the start

of computations. Therefore these oscillations can be due to the secondary flow itself which provides the mechanism for convecting colder temperatures from the central core to the near-wall regions. A detailed explanation, of this kind, has been given earlier, by Dravid et al.(1971).

7.3 Prediction of turbulent flows

7.3.1 Computational details

The success achieved in the prediction of laminar flows in curved pipes encouraged the author to extend the application of the parabolic procedure to predict the turbulent flow and heat transfer characteristics in curved pipes. The computations have been made in a manner similar to the laminar flow computations; but for the turbulent flow calculations two additional differential equations have been solved for the transport of the turbulence kinetic-energy and the volumetric rate of its dissipation. The details of the practices adopted in representing the turbulence structure have already been described in Chapter 5.

The finite-difference grid, as in the case for laminar flows, covered only a semi-circular sector of the cross-section; and possessed 14 intervals in the r-direction and 11 intervals in the θ-direction. The forward-step size was fixed, after tests for grid

independency of the results to be 0.1 degrees. The computer time for the calculation of turbulent flow was of the order of 0.45 secs per forward step, on a CDC 6600 computer.

7.3.2 The developing region

Figure (7.3.1) provides a comparison of the predicted velocity-head contours with the experimental data of Rowe (1966) for a 180^{o} pipe bend. The Reynolds number of the flow was 2.36×10^{5} and the ratio of bend radius to pipe radius was 24. Comparisons are made for various angular positions along the bend, the inlet being a fully-developed turbulent pipe-flow. It is seen that,both for the predictions and the experiments, the velocity head is distorted with the velocity maximum shifted to the outside of the bend. The agreement with experimental data has been satisfactory although it is not as good as that observed for laminar flows. Figures (7.3.2) and (7.3.3) present the predicted development of the secondary flow field for the above flow situation. It is seen that, as in the laminar-flow case, the development of secondary flow-field is oscillatory; but the present period of oscillations is somewhat larger than that for laminar flows. For the present radius ratio of 24, the period of oscillations has been observed to be about 135 degrees which is in close agreement with the measured value of

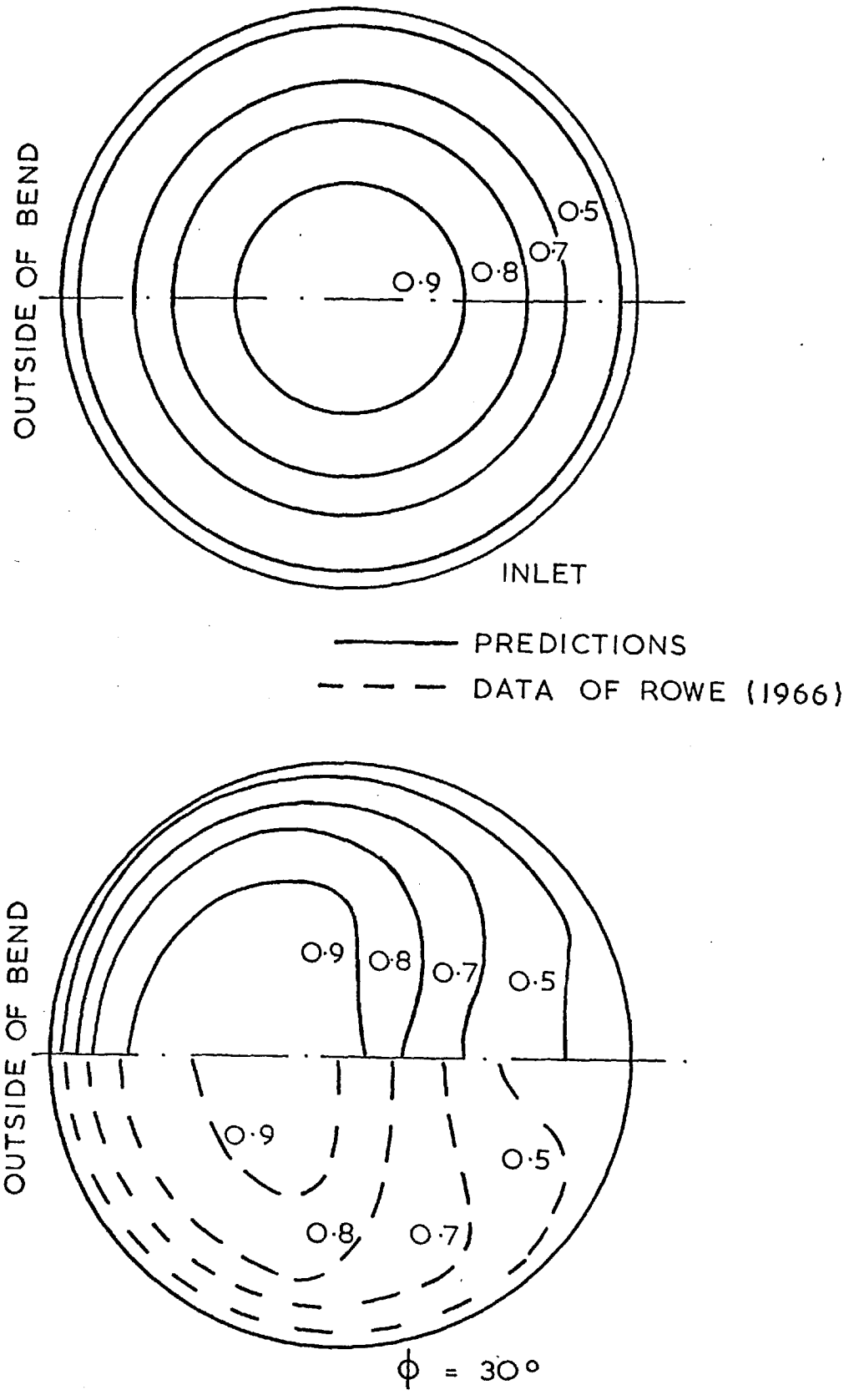

Fig. (7.3.1): Contours of velocity head in a curved pipe, nondimensionalised with $\frac{1}{2} \rho U_o^2$ for a Reynolds number of 2.36×10^5 and for R/a of 24.

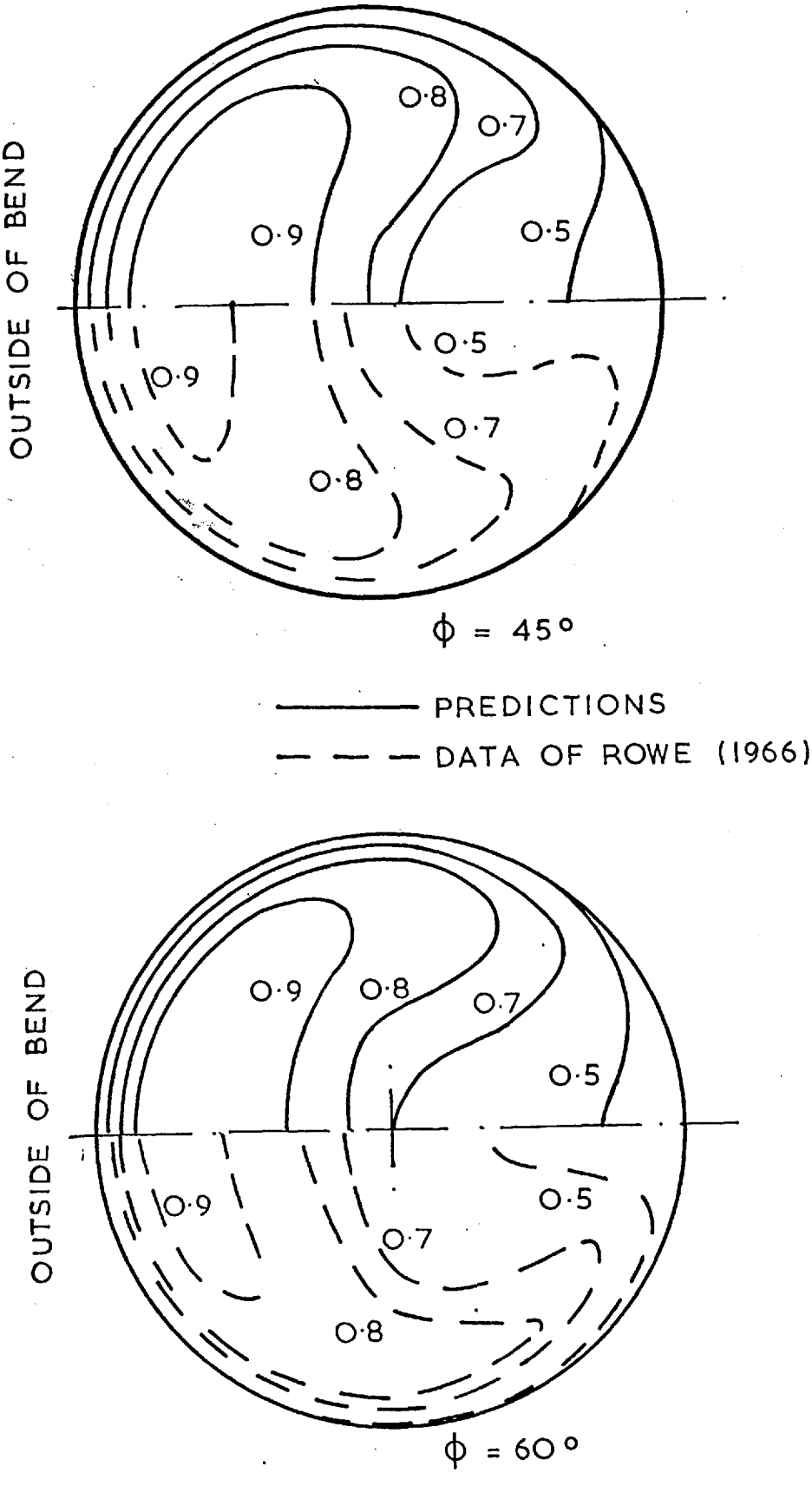

Fig. (7.3.1) Contd.

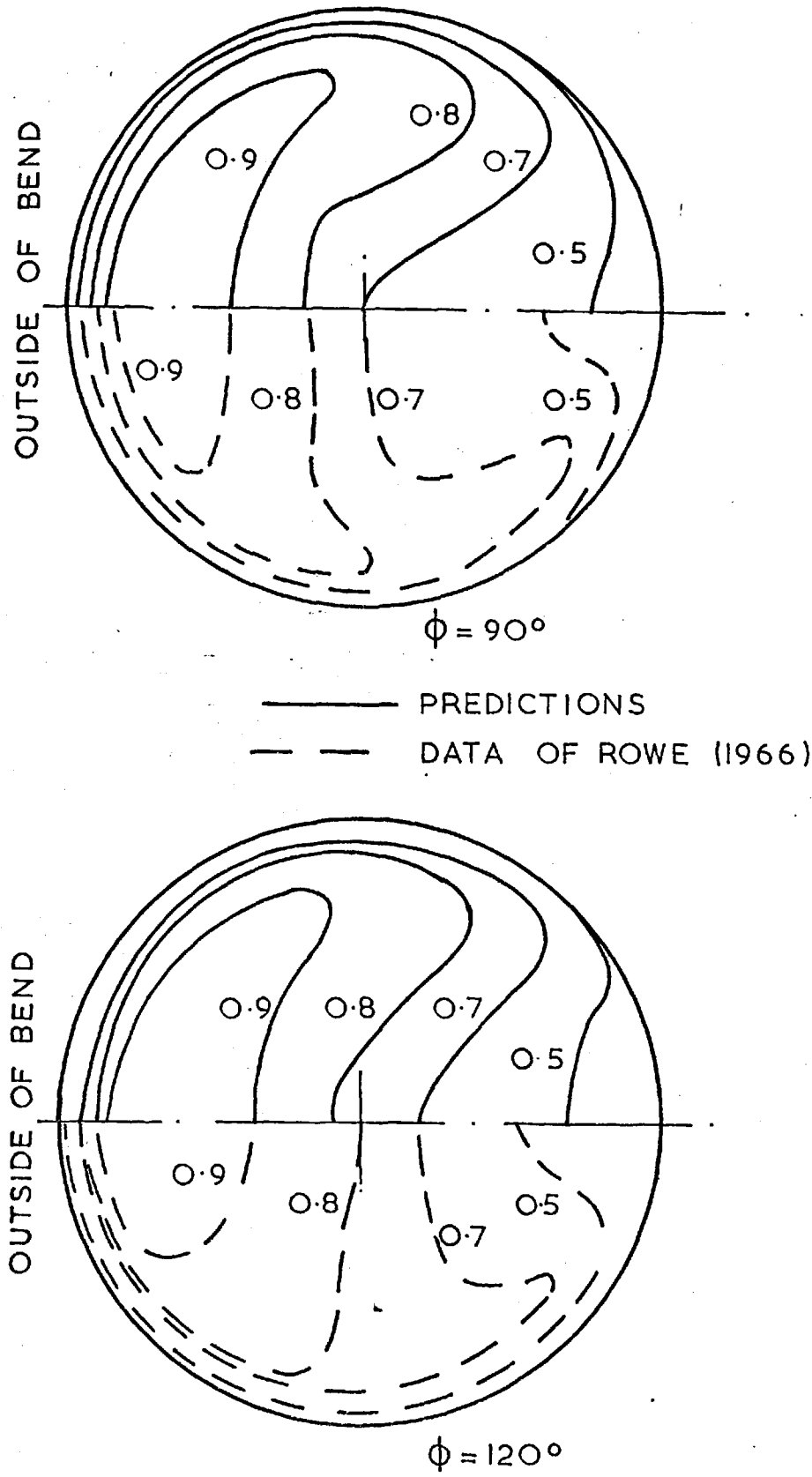

Fig. (7.3.1): Contd.

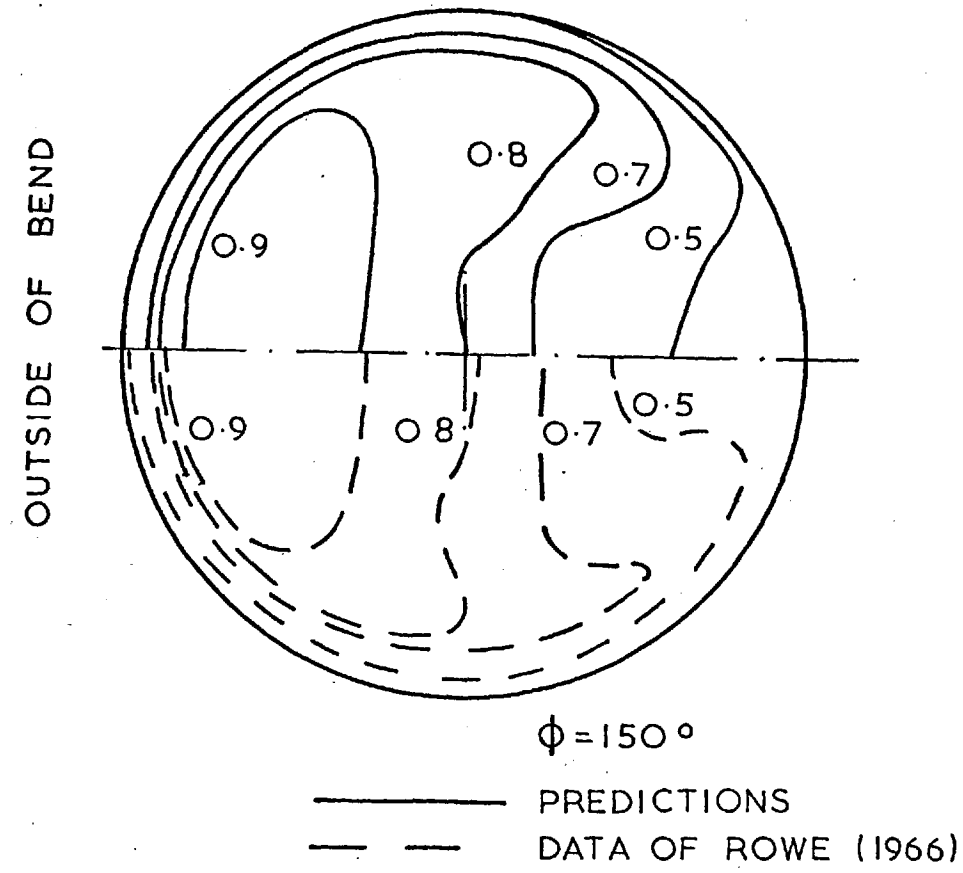

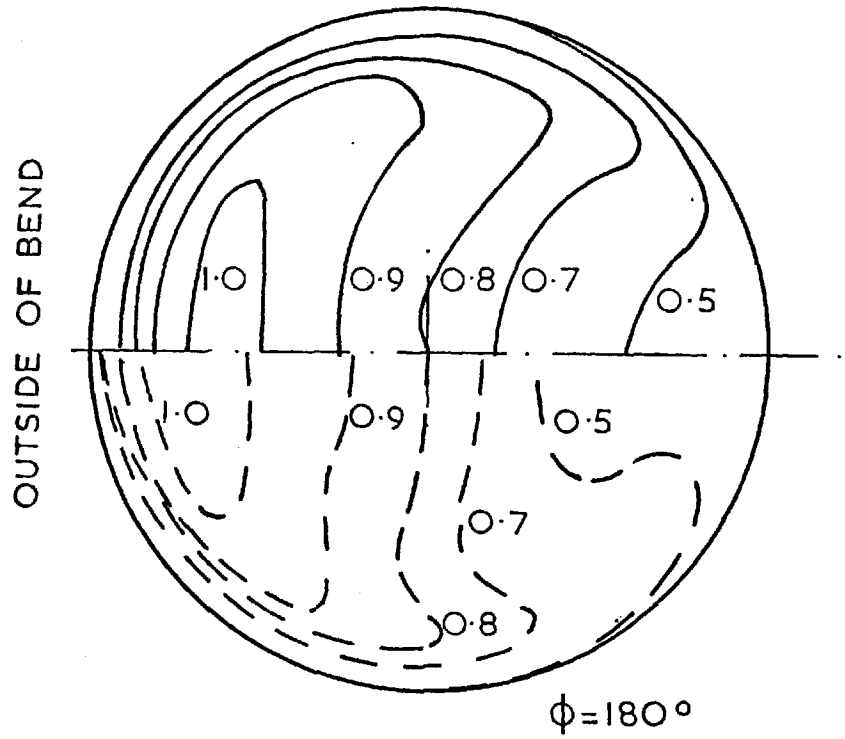

Fig. (7.3.1): Contd.

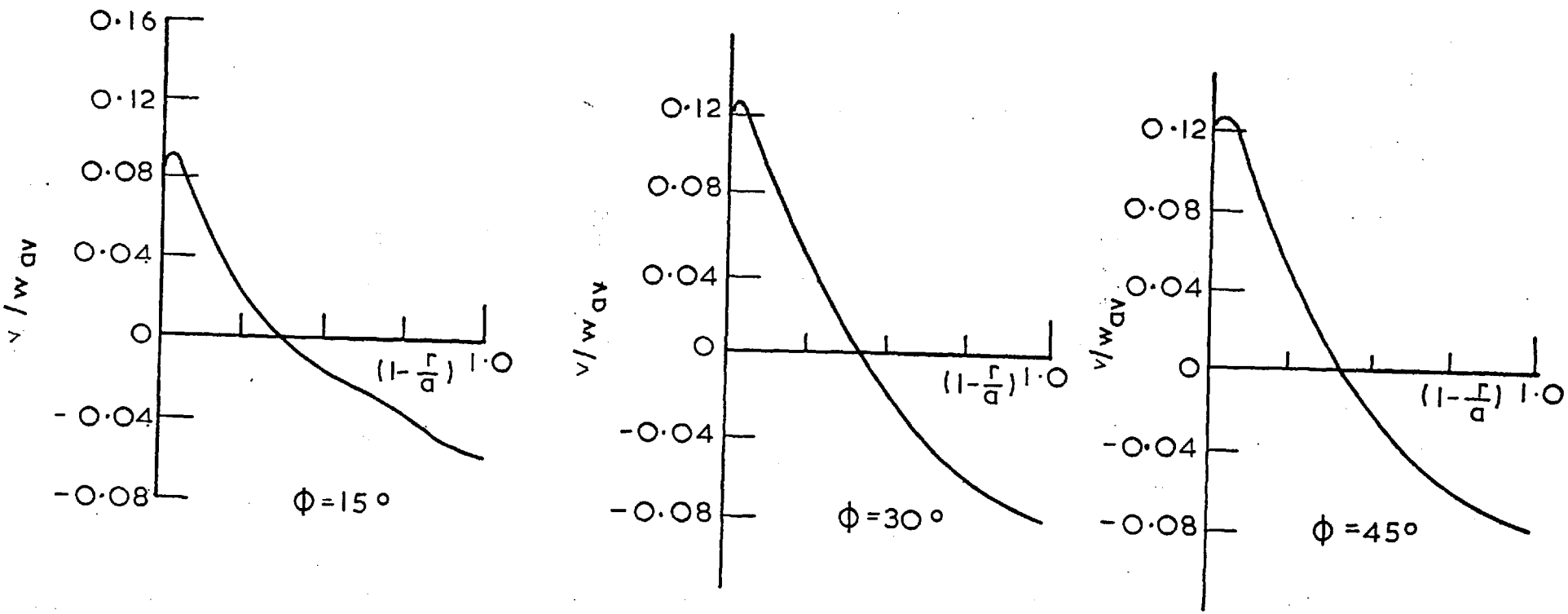

Fig. (7.3.2): Secondary-velocity profiles along a vertical radius in a 180 degree bend. Reynolds number equals 2.36 x 10^5 and R/a equals 24.

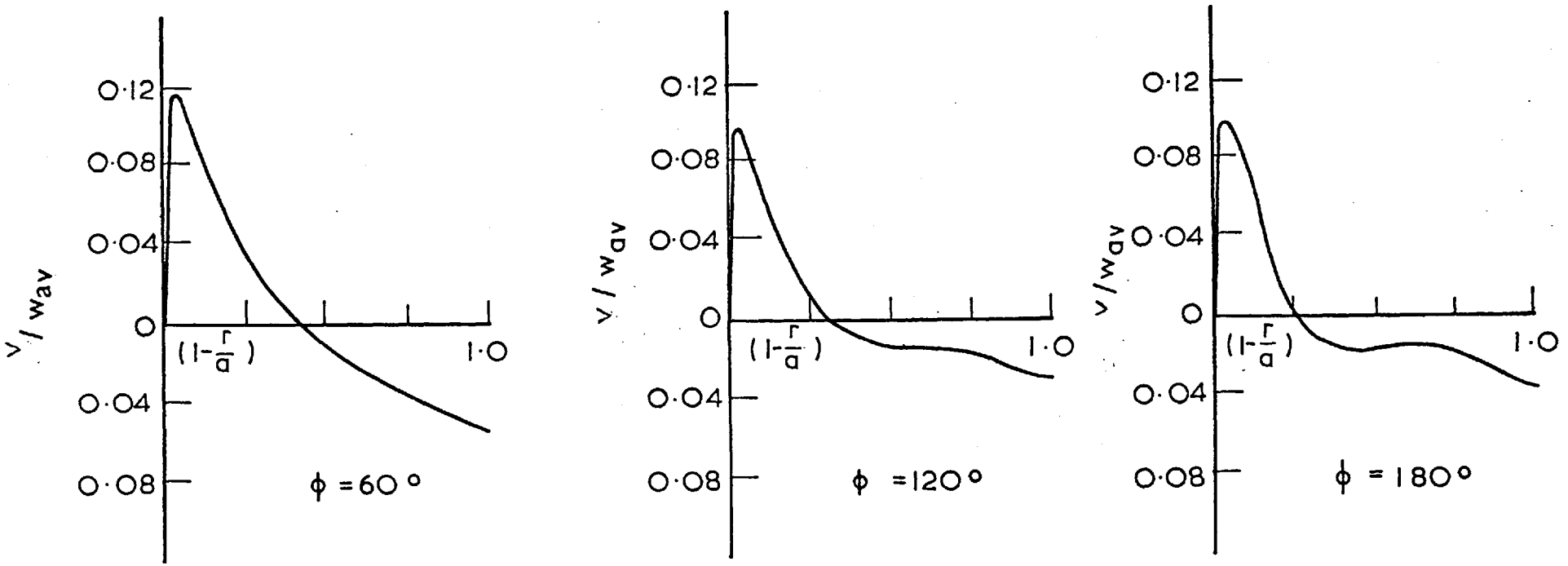

Fig. (7.3.2): Continued.

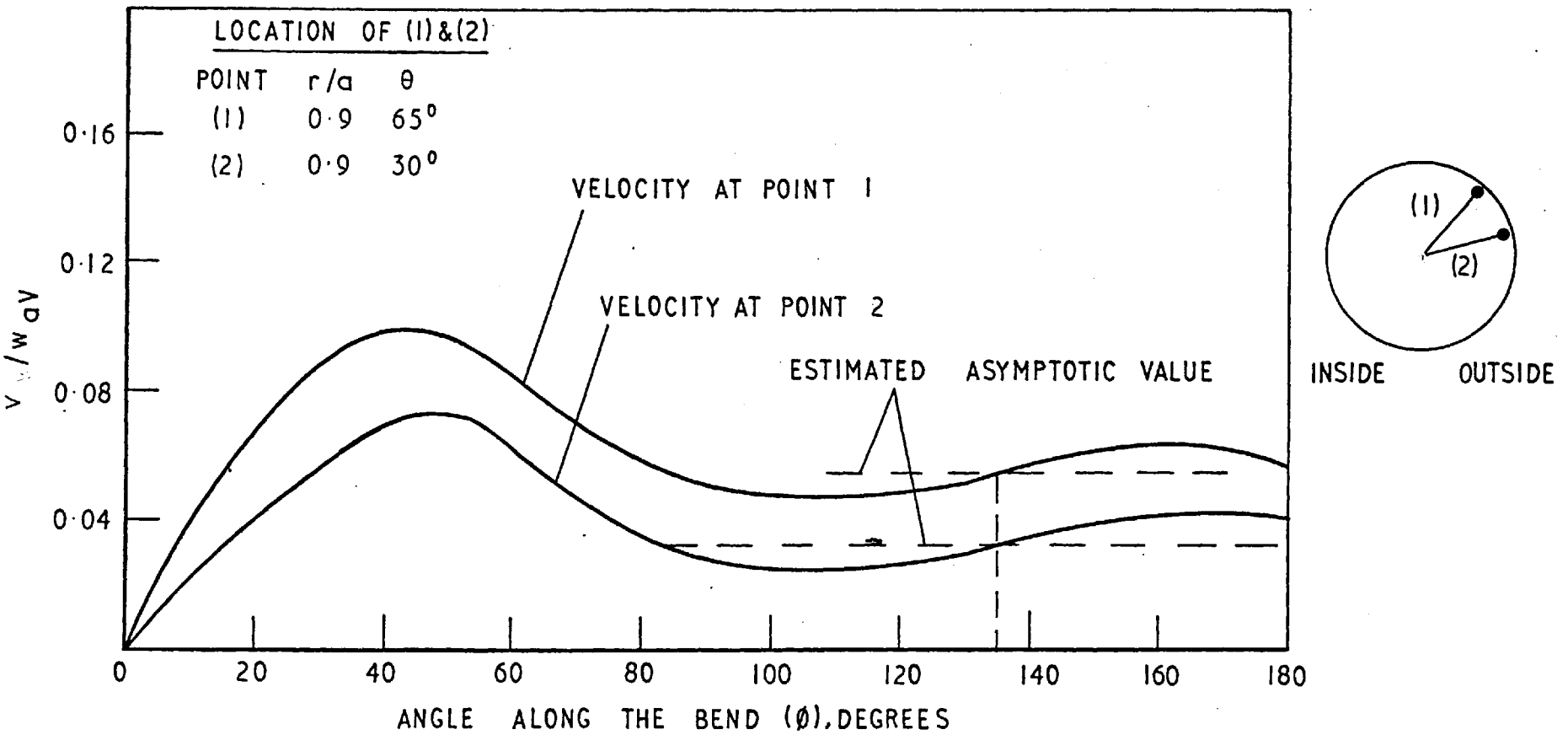

Fig. (7.3.3): Variation of secondary velocities with bend angle.

150 degrees by Squire (1954). The development of the temperature field in a 180^{o} bend has been calculated for the boundary condition of constant heat flux and the results are compared in Figure (7.3.4) with experimental data of Ede (1963). The flow field at the inlet was prescribed to be that of a fully-developed turbulent pipe-flow. The agreement with experimental data is satisfactory. The heat transfer rates and the wall temperatures in case of turbulent flows also display oscillations in their development but the amplitude of these oscillations is less than that observed in the laminar flow situation.

7.3.3 The fully-developed region

Figure (7.3.5) displays the comparison of fully-developed axial-velocity profiles along the diametrical planes AA and BB (ref. Fig. (7.2.1)) with experimental data of Hogg (1968) and Mori and Nakayama (1967). In Figure (7.3.5(c)), results are also presented for calculations using a form of the mixing-length hypothesis. It can be seen that the two-equation turbulence-model yields superior predictions. The fully-developed secondary velocities along plane BB are compared in Figure (7.3.6) with the experimental data of Hogg (1968); the agreement is good for both the Reynolds numbers. Figure (7.3.7) shows the fully-developed friction factors compared with the empirical relation

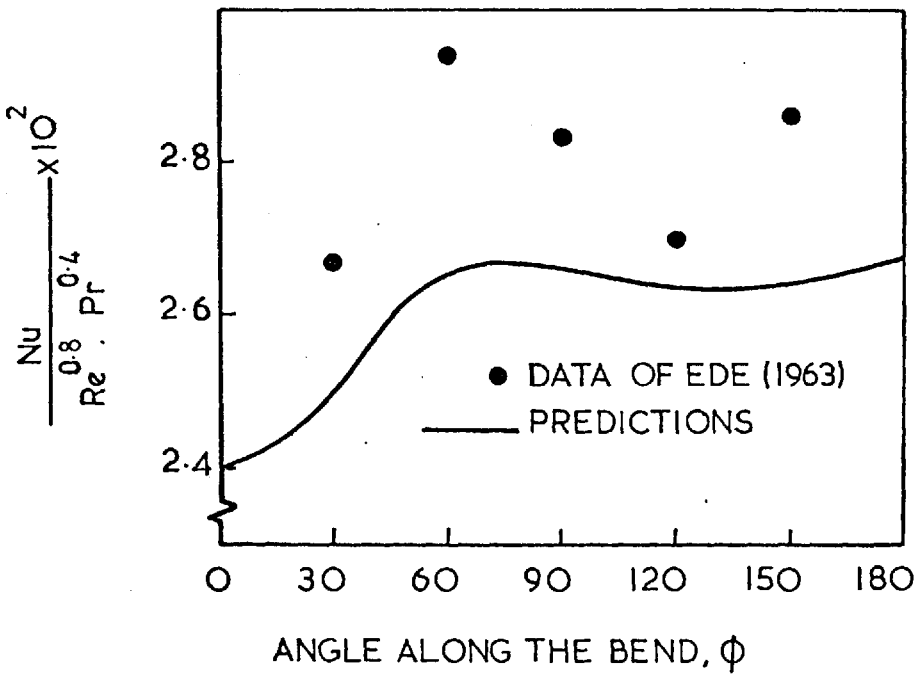

Fig. (7.3.4): Development of Nusselt number for flow in a 180 degree bend; R/a=22; Reynolds number = 3.99 x 10^4; and Pr=10.3.

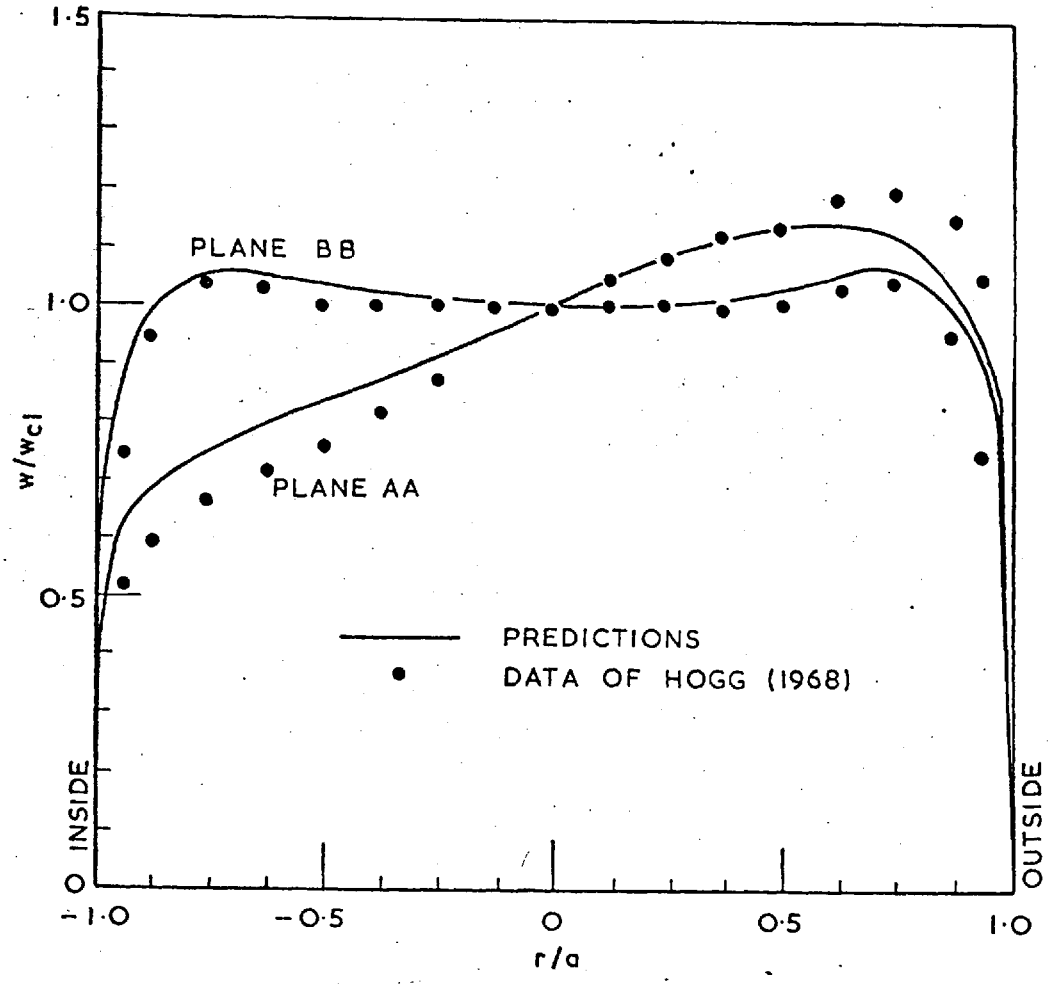

Fig. (7.3.5(a)): Comparison of fully-developed axial velocity profiles along plane AA and BB. Reynolds number = 6.8×10^4, R/a=25.9.

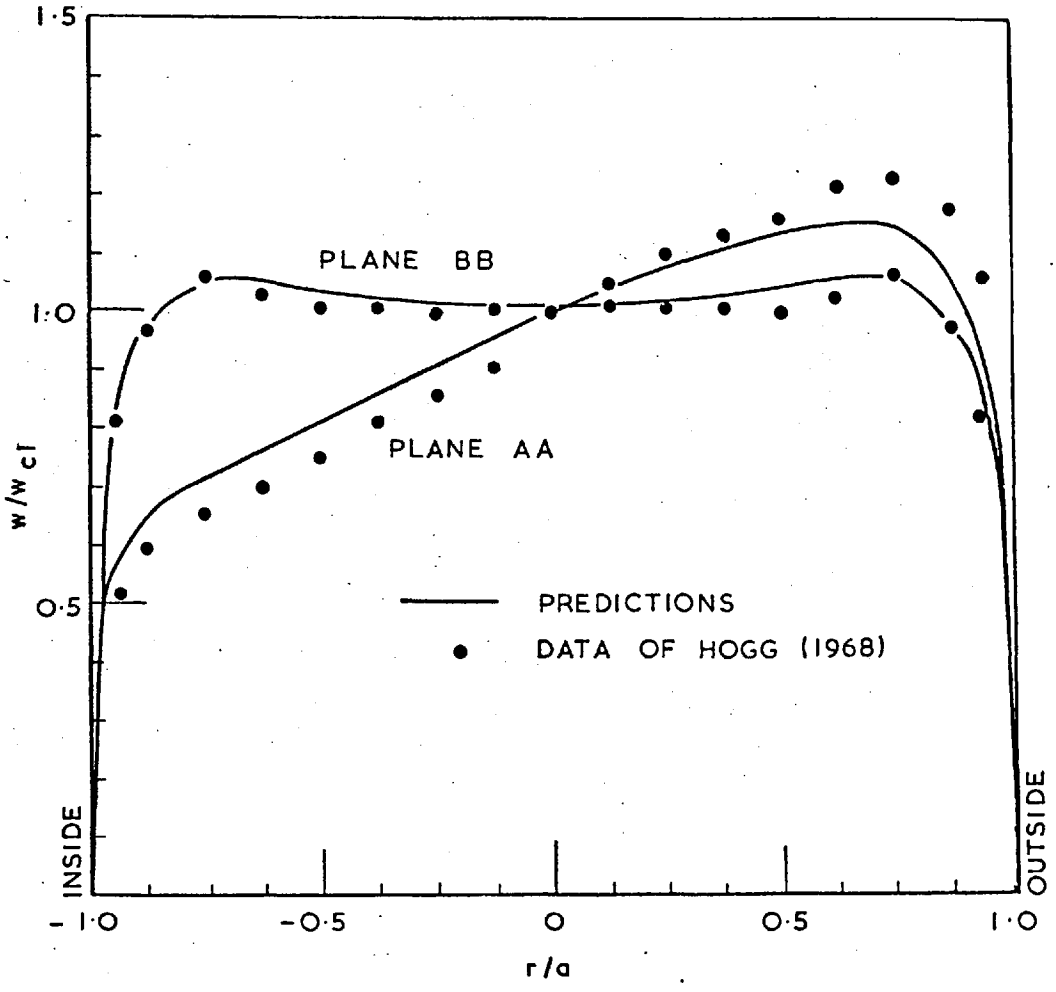

Fig. (7.3.5(b)): Comparison of fully-developed axial velocity profiles along plane AA and BB. Reynolds number = 8.9 x 10^4 and R/a=25.9.

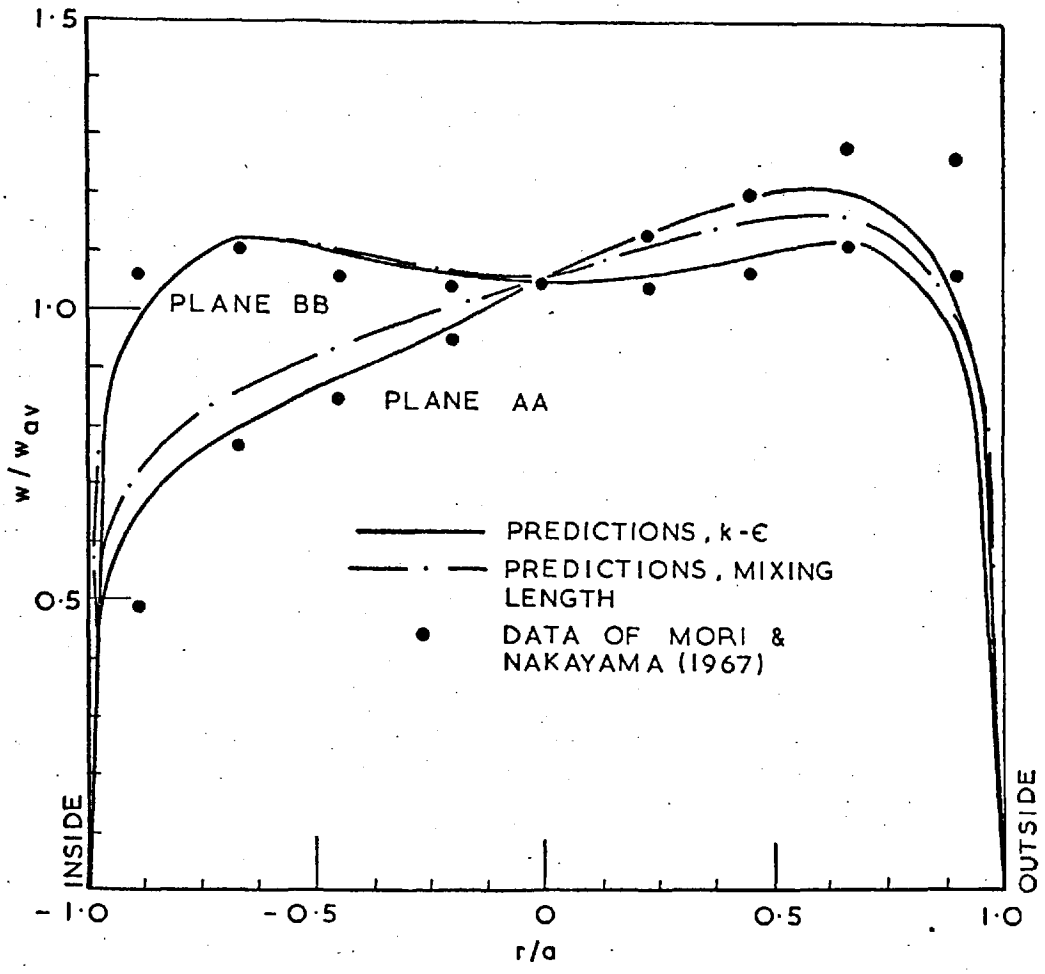

Fig. (7.3.5(c)): Comparison of fully-developed axial velocity profiles along plane AA and BB. Reynolds number = 2.5×10^4 and R/a=40.

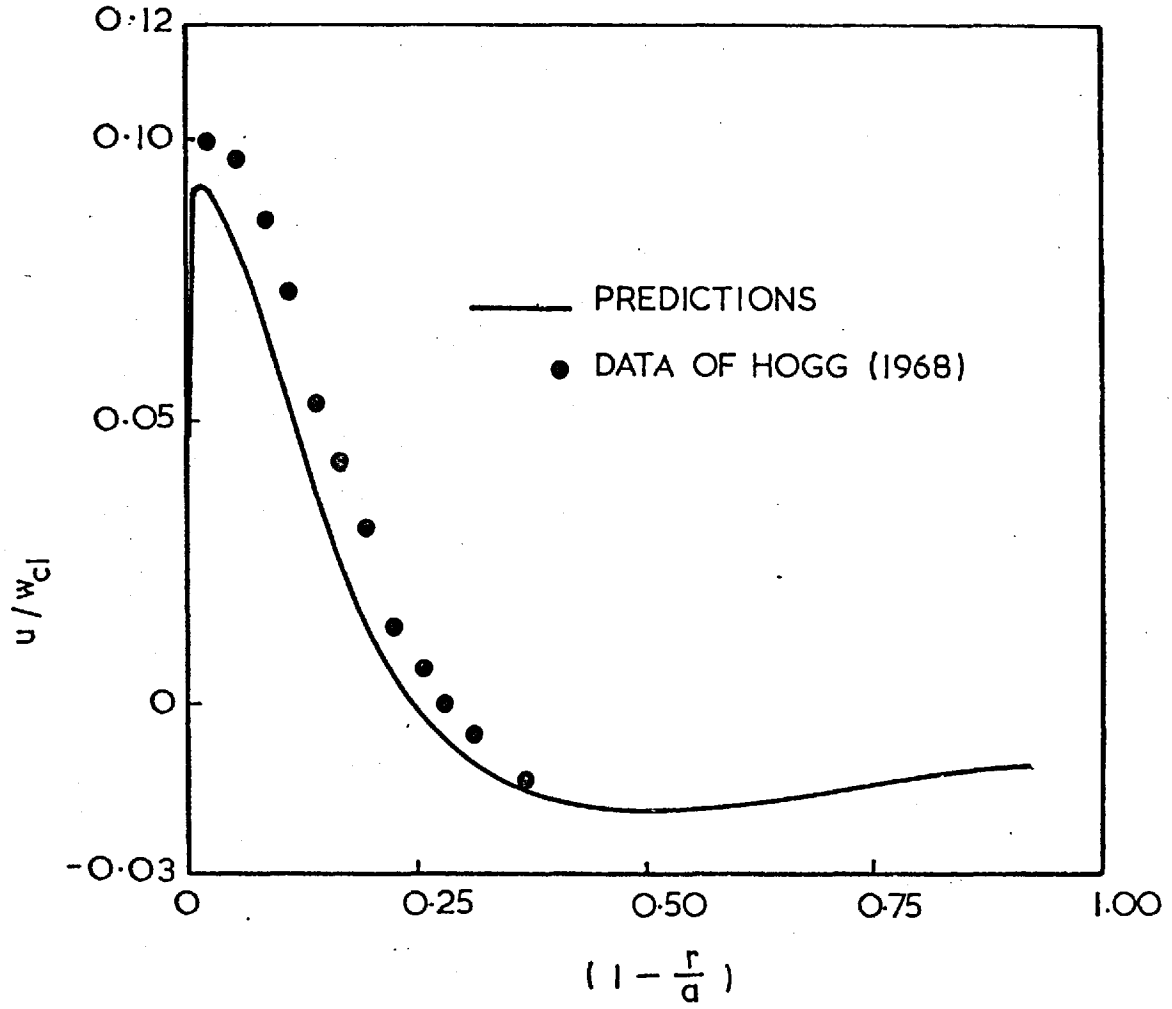

Fig. (7.3.6(a)): Comparison of fully-developed secondary-velocity profile along the vertical diameter. Reynolds number = 6.8×10^4 and R/a=25.9.

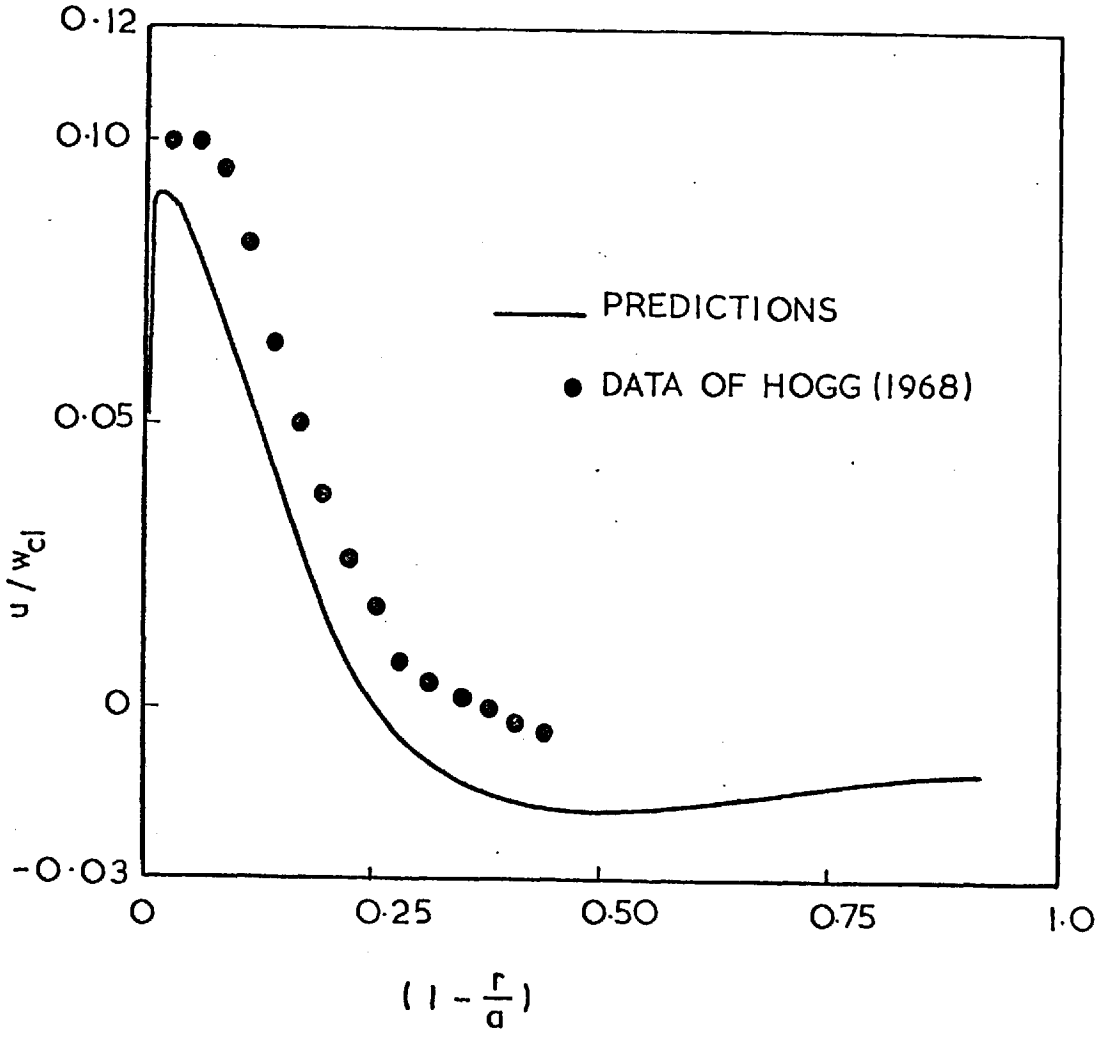

Fig. (7.3.6(b)): Comparison of fully-developed secondary-velocity profile along the vertical diameter. Reynolds number = 8.9×10^4 and R/a=25.9.

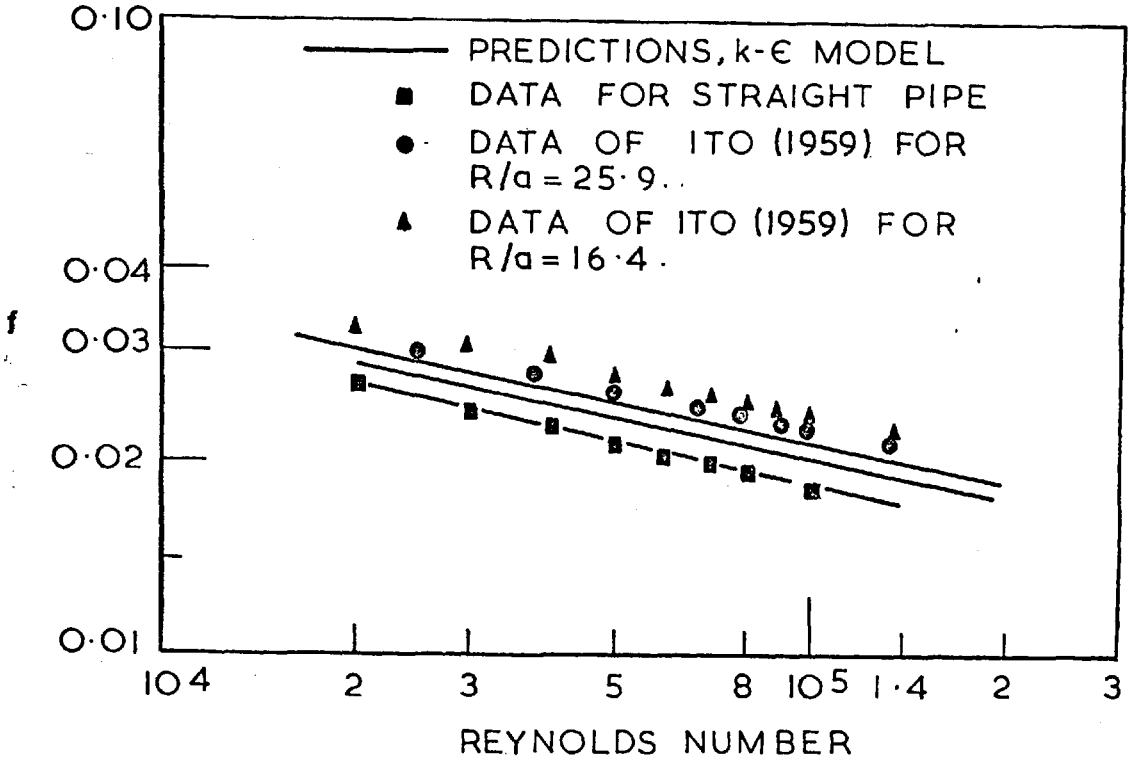

Fig. (7.3.7): Comparison of fully-developed friction factors with experimental data.

of Ito (1959); also shown in Figure (7.3.7) are the computed friction factors for turbulent flow in straight circular pipes. The agreement with experimental data is quite satisfactory in case of straight pipes but for the case of curved pipes, the magnitude of the friction factor is under-predicted, the maximum difference between the experimental and computed values being about 8 percent. Figure (7.3.8(a)) shows the fully-developed axial-velocity profiles at various angular positions along the bend; it is observed that the angular variation of the velocity, in case of turbulent flow, is smaller than that observed for laminar flows. The peripheral variation of the friction factor is also observed to be smaller, as shown in Figure (7.3.8(a)); the ratio of friction factors at outside to those at inside is about 2 whereas for laminar flows it was about 4.

Computations have also been made of the fully-developed temperature field for the boundary condition of constant heat flux around the periphery. Figure (7.3.9) and (7.3.10) show results of computations made in coils of radius ratio of 104 and comparison with experimental data of Seban and McLaughlin (1963). The agreement is observed to be good both in the peripheral variation of the Nusselt number and in its average value. However, some discrepancies have been observed when the

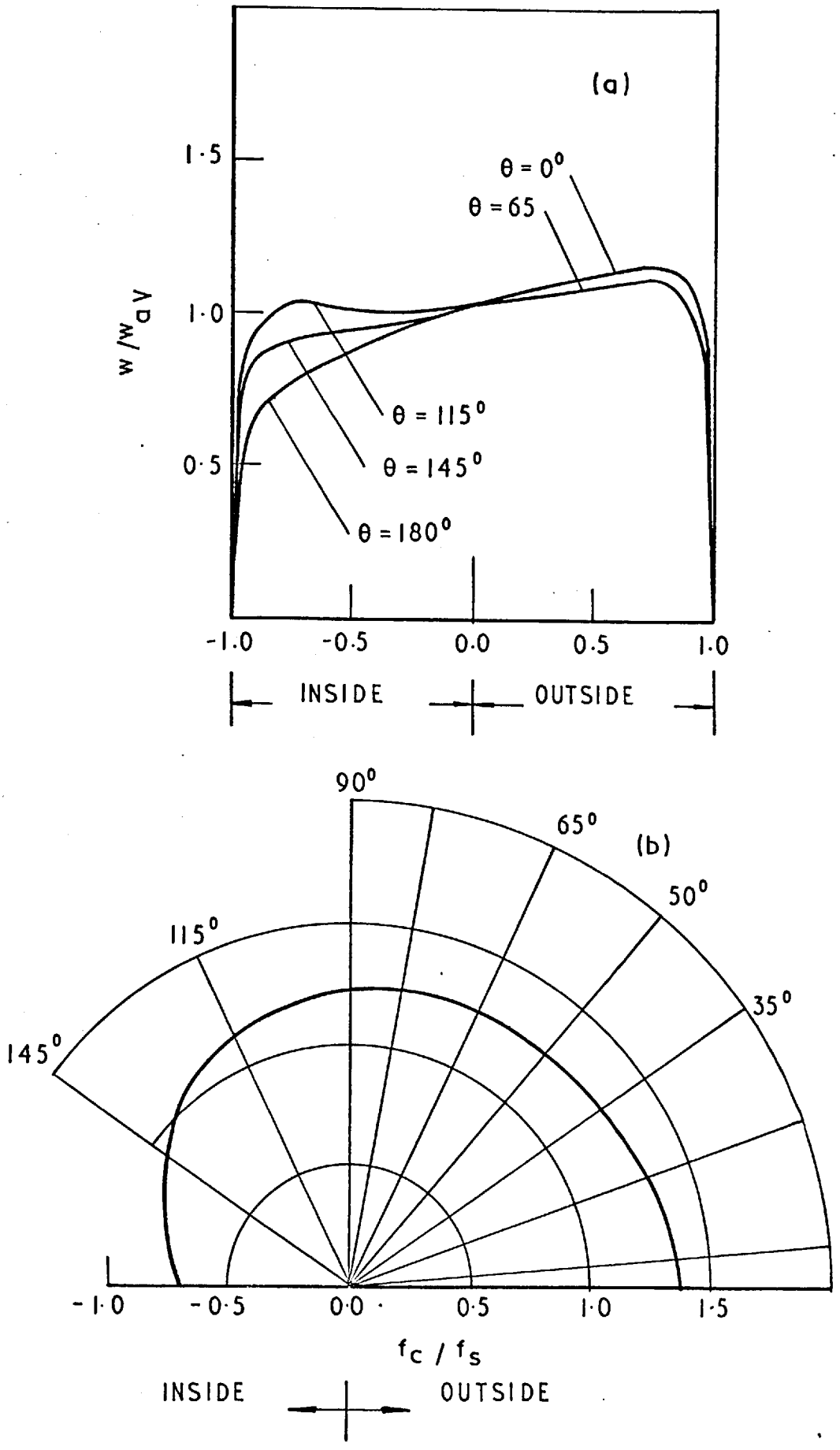

Fig. (7.3.8): Angular variation of (a) axial velocity, (b) friction factor for fully-developed turbulent flow in a curved pipe. R/a=25.9, Reynolds number = 8.9×10^4.

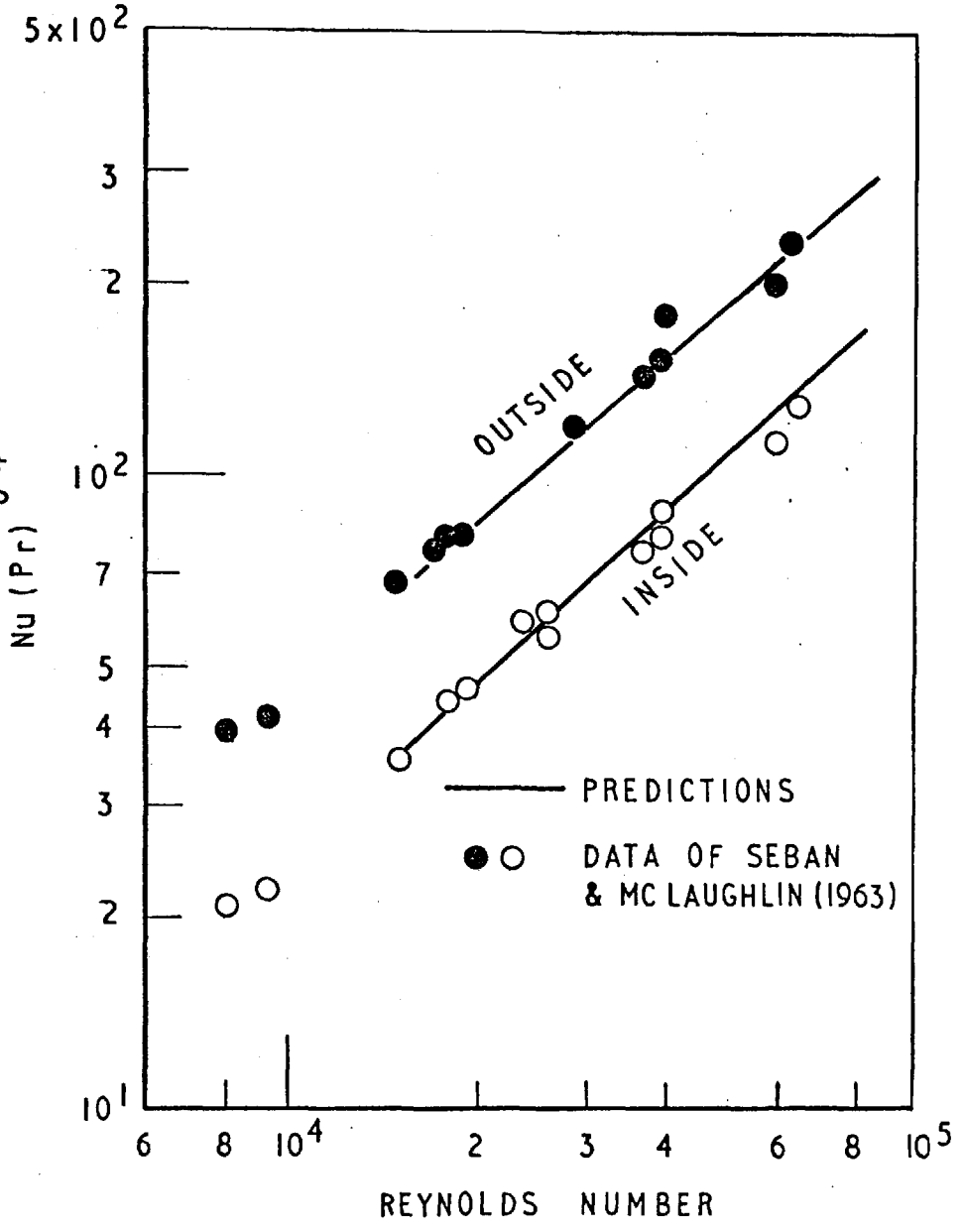

Fig. (7.3.9): Variation of fully-developed Nusselt number with Reynolds number. R/a=104 and Pr=5.7, 4.3, 2.9.

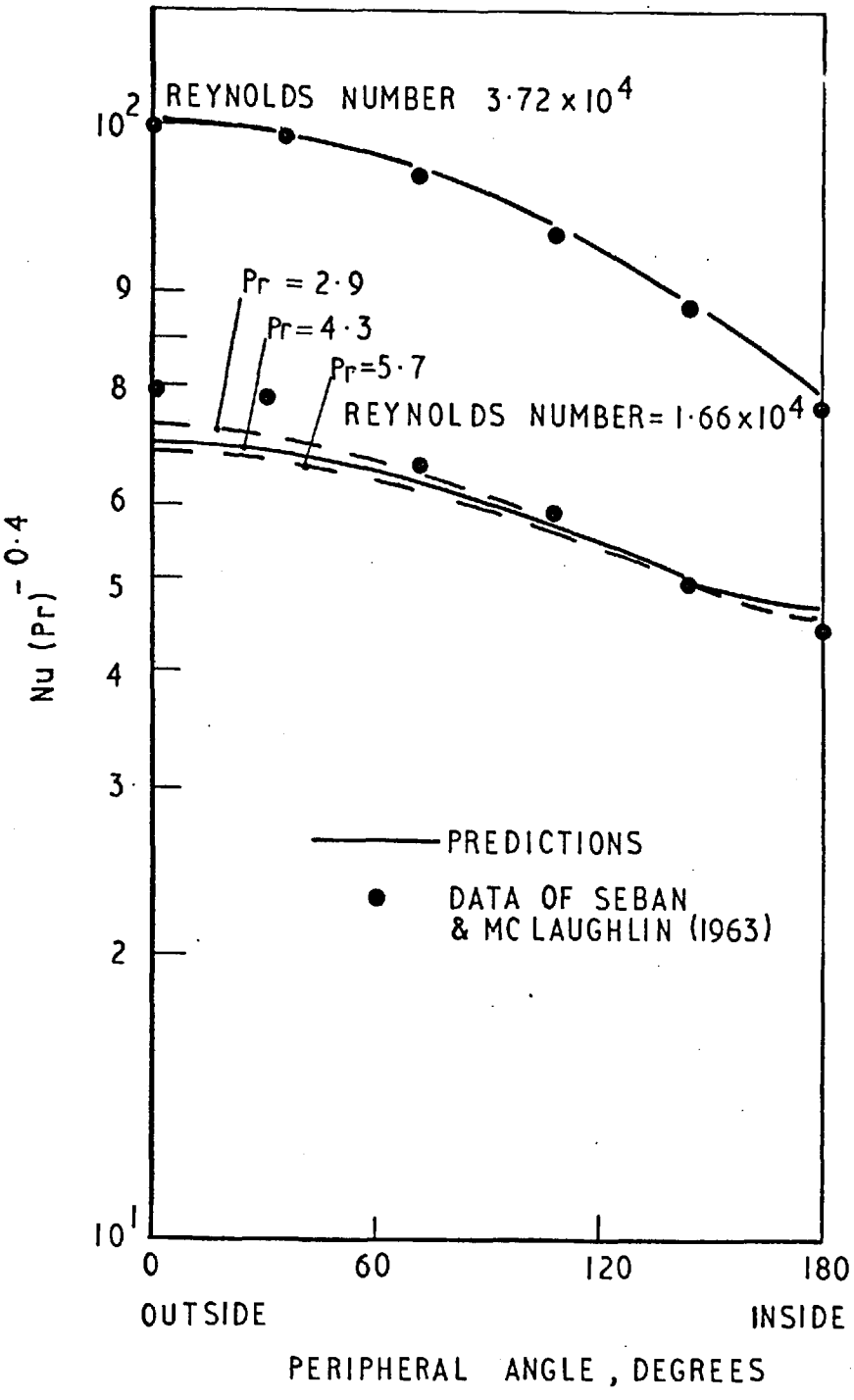

Fig. (7.3.10): Peripheral variation of Nusselt number compared with experimental data. R/a=104.

predictions at lower values of radius ratio have been compared with experimental data. Figures (7.3.11) shows the computed temperature profiles (non-dimensionalised with inside wall temperature) in coils with radius ratio of 25.9 and comparison with experimental data of Hogg (1968). The agreement is satisfactory in the inside region but discrepancies exist in the outside region. The Nusselt numbers, shown in Figure (7.3.12), also seem to be under-predicted in the outside region. The discrepancies in the computed heat transfer rates and the friction factors suggest that the turbulence model presently used needs further refinements to account for the effects of curvature on the turbulence structure.

7.3.4 Discussion

From the experimental and theoretical results presented above for turbulent flows, it is observed that the effects of curvature on turbulent flows are smaller than those observed for laminar flows. Thus, the distortion of the velocity-profile is less than that observed for laminar flows; and consequently the magnitudes of friction factors and heat-transfer rates vary less over the periphery. For example, the turbulent friction-factors (Figure (7.3.7)) vary only half as much as that observed in Figure (7.2.17) for the laminar flow case. The development of secondary flow-field

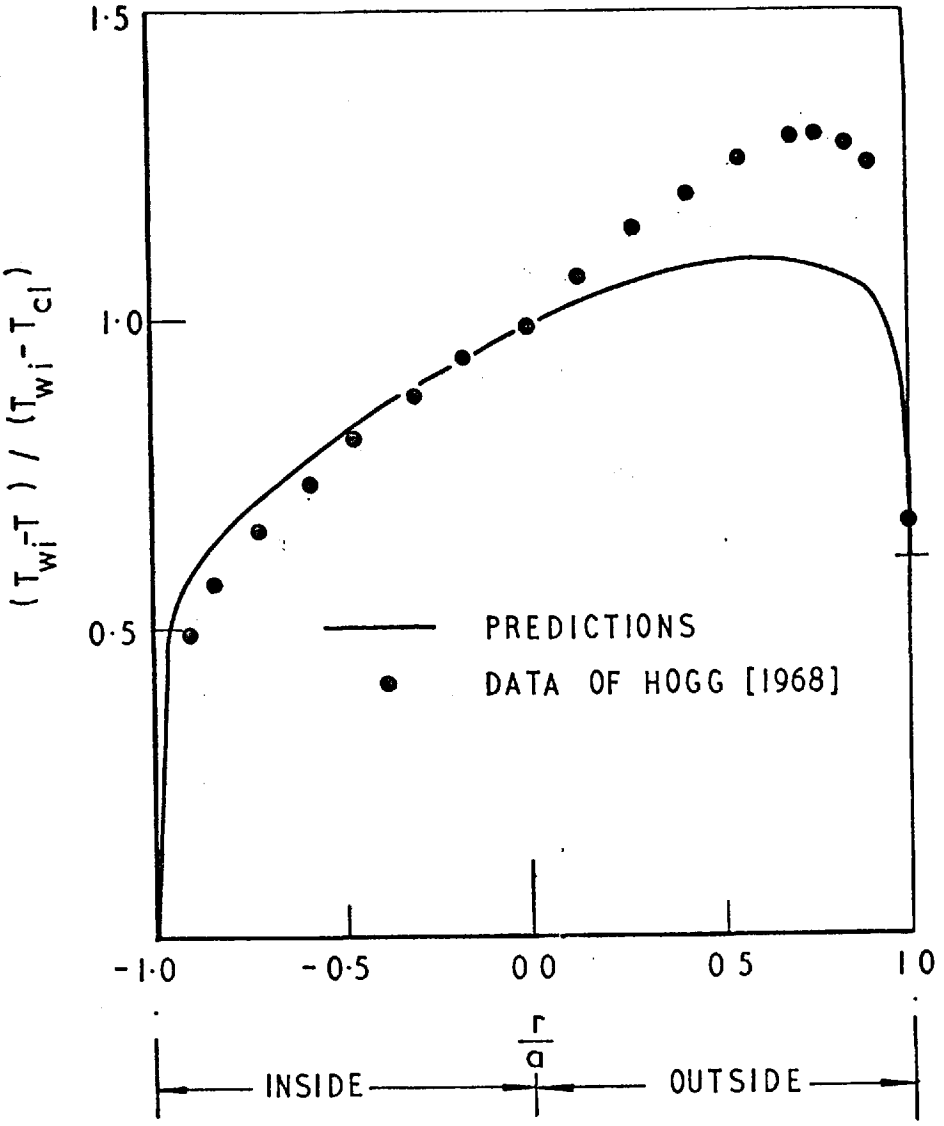

Fig. (7.3.11(a)): Comparison of predicted fully-developed temperature profiles with experimental data. Reynolds number = 1.35×10^5, R/a=25.9, Pr=0.71.

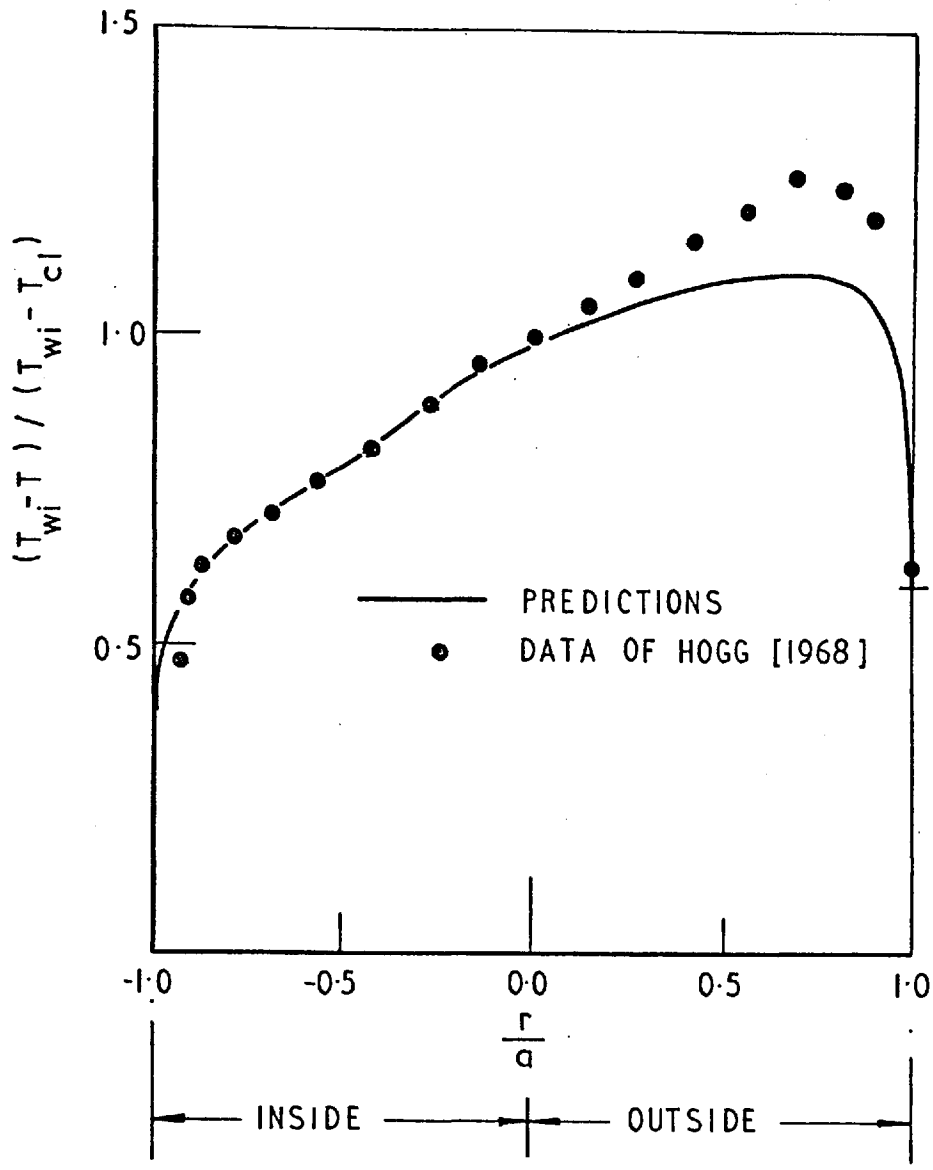

Fig. (7.3.11(b)): Comparison of predicted fully-developed temperature profiles with experimental data. Reynolds number = 6.8×10^4. R/a=25.9, Pr=0.71.

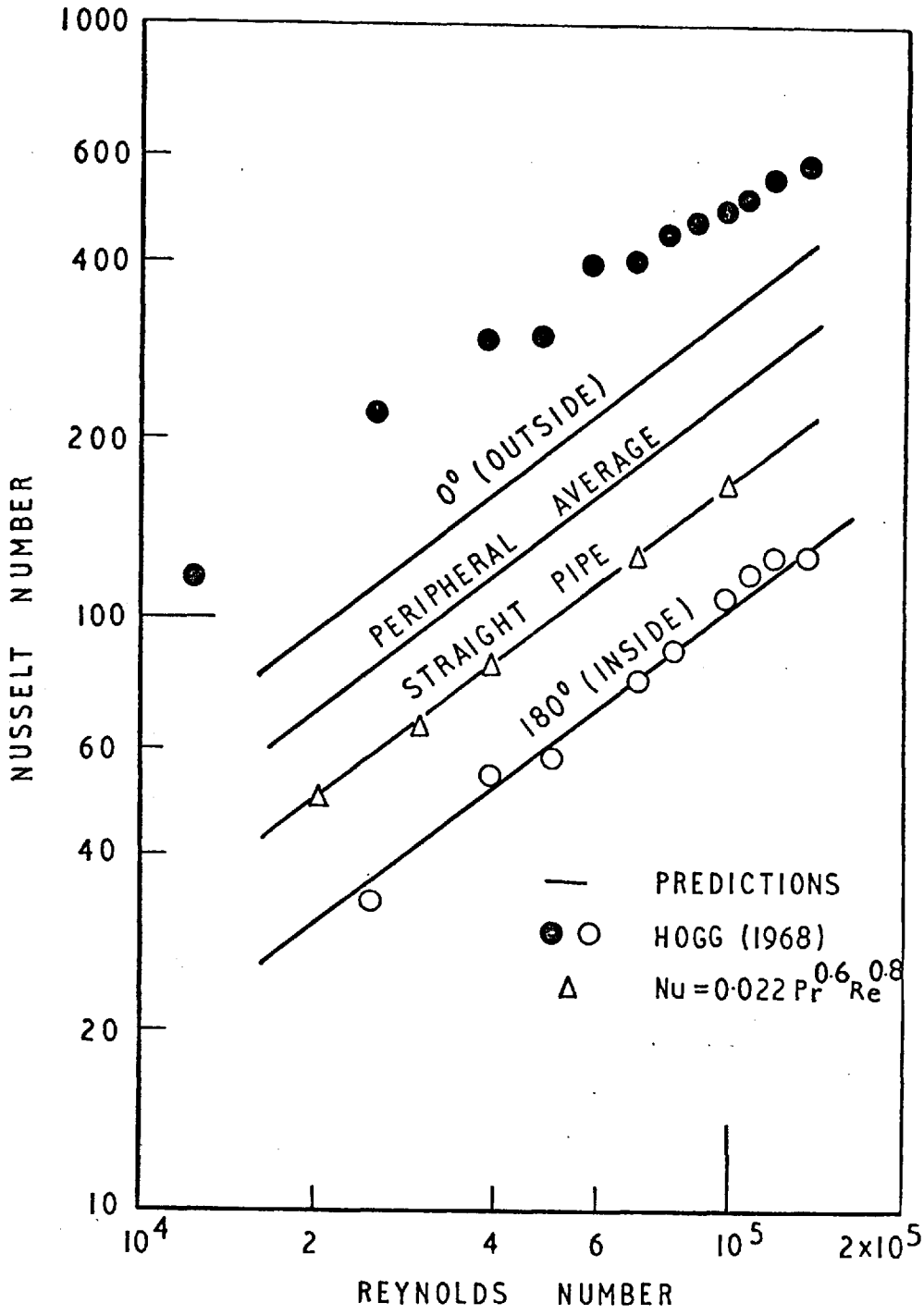

Fig. (7.3.12): Variation of fully-developed Nusselt number with Reynolds number for R/a=25.9 and Pr=0.71.

in turbulent flows is also oscillatory; the period of first oscillation is in good agreement with the experimentally observed value. The development of the temperature too is oscillatory but the oscillations are small; in the present computations, the inlet flow was prescribed to be the fully-developed straight-pipe flow; and thus the oscillations now observed are also partly due to the development of the flow field.

The agreement between the present computations and the experimental measurements is satisfactory; the velocity contours have been predicted to be distorted and the friction factors have been observed to be larger than the straight-pipe values. However, their quantitative agreement is not as good as that observed for laminar flows; hence it is probable that the turbulence model is the source of what discrepancies exist. Possible modifications to the turbulence model that may be considered in future studies are:

(i) to discard the effective-viscosity approach and to solve differential equations for each individual shear stress; or

(ii) to employ an intermediate approach, such as that proposed by Launder (1971) where the differential equations for turbulent shear-stresses are approximated by algebraic equations.

Of these, the second one is somewhat easy but the first possibility, namely the use of Reynolds-stress models will involve considerable development effort and validation over simpler three-dimensional flow situations before their being applied to predict the present flow situation.

7.4 Concluding remarks

The parabolic calculation procedure has been successfully applied to predict the three-dimensional flow and heat-transfer phenomena in mildly-curved circular pipes. For laminar flows, the agreement between predictions and the corresponding experimental data has been observed to be good. For turbulent flows however, the agreement is not as good as that observed in the predictions for laminar flow-situations. It is concluded that some modifications need to be made to the turbulence-model to account for the effects of secondary flow; possible approaches have been outlined.

CHAPTER 8

PREDICTION OF FLOW IN STRONGLY-CURVED DUCTS

8.1 Introduction

The flow phenomena in strongly-curved ducts are different from those in ducts with mild curvature because of their substantial elliptic effects in the pressure field. These elliptic effects make the flow partially-parabolic; and require for their computation a different numerical scheme. In the present chapter, the partially-parabolic procedure described in Sec. (4.2) is employed to compute the flow in the geometrical situation described in Chapter 6. A sketch of this geometry is provided in Figure (8.1.1). The flow was turbulent; and the turbulent stresses were modelled using a two-equation ($k\text{-}\varepsilon$) turbulence-model, the details of which have already been described in Chapter 5. The computations covered both the geometrical configurations experimentally studied, namely the constant-area duct and the diffuser. The computed distributions of static pressure and mean velocity are compared in this chapter, with experimental data and also with the calculations using the parabolic procedure.

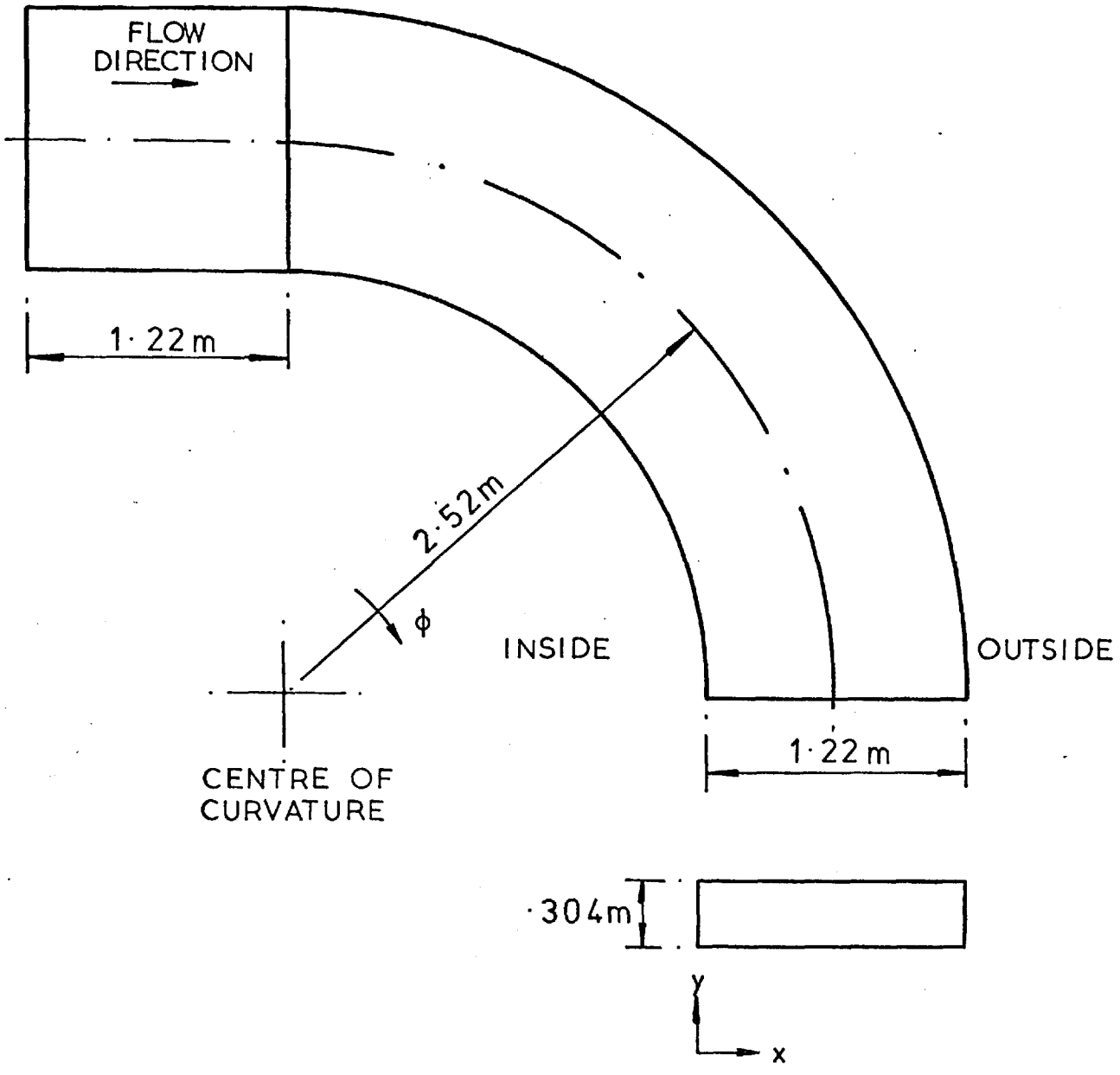

Fig. (8.1.1): Geometry considered.

8.2 Computational aspects

The flow domain in which computations have been made consisted of the 1.22 m. long straight section and the 90 degrees of the curved duct; because of the symmetry of the flow, only one half of the height has been considered. The finite-difference grid possessed 17 nodes in the x direction and 14 in the y direction; the grid was non-uniform with more nodes in the near-wall regions. In the longitudinal direction, 10 stations were placed in the straight section and 24 in the curved section, the latter with an approximate spacing of about 5 degrees. The computations were confirmed, by experimentation with finer and coarser grids to be substantially independent of grid fineness.

The partially-parabolic procedure converged in 50 sweeps of the flow domain; and the necessary computing time on a CDC 6600 computer was about 15 minutes. In the parabolic scheme only one sweep of the flow domain was necessary; but it was necessary to reduce significantly the forward step size (to $\sim$ 0.2 degrees) in order to make the computations numerically stable. The computing time in the parabolic case was about 5 minutes.

8.3 Prescription of inlet and exit conditions

The flow conditions at the inlet plane to the calculation domain were prescribed based on experimental measurements at the location 1.22 m. upstream of the curved duct. Figure (8.3.1(a)) shows the inlet profiles for the longitudinal-direction velocity (w) measured at the above location; the transverse velocities at the same location were observed to be negligibly small and the static pressure was uniform over the cross-sectional plane. The inlet-values of kinetic energy of turbulence were prescribed based on measurements of the intensity of turbulence (w'/w) along the axial-direction; Figure (8.3.1(b)) shows the variation of turbulence intensity with distance from bottom wall at one location in the inlet plane (from Young (1972)). The inlet values of dissipation of kinetic energy were calculated assuming a dissipation length-scale distribution similar to the ramp function for the mixing length in two-dimensional boundary layers (Patankar and Spalding (1972), p. 20). The sensitivity of the predictions to the prescription of the inlet values of turbulence kinetic-energy and its dissipation rate was however, observed to be only small. The boundary condition at the exit was prescribed to be that of the uniform pressure, corresponding to the physical condition of free discharge into the atmosphere. These inlet and exit conditions were the same for both the geometrical configurations.

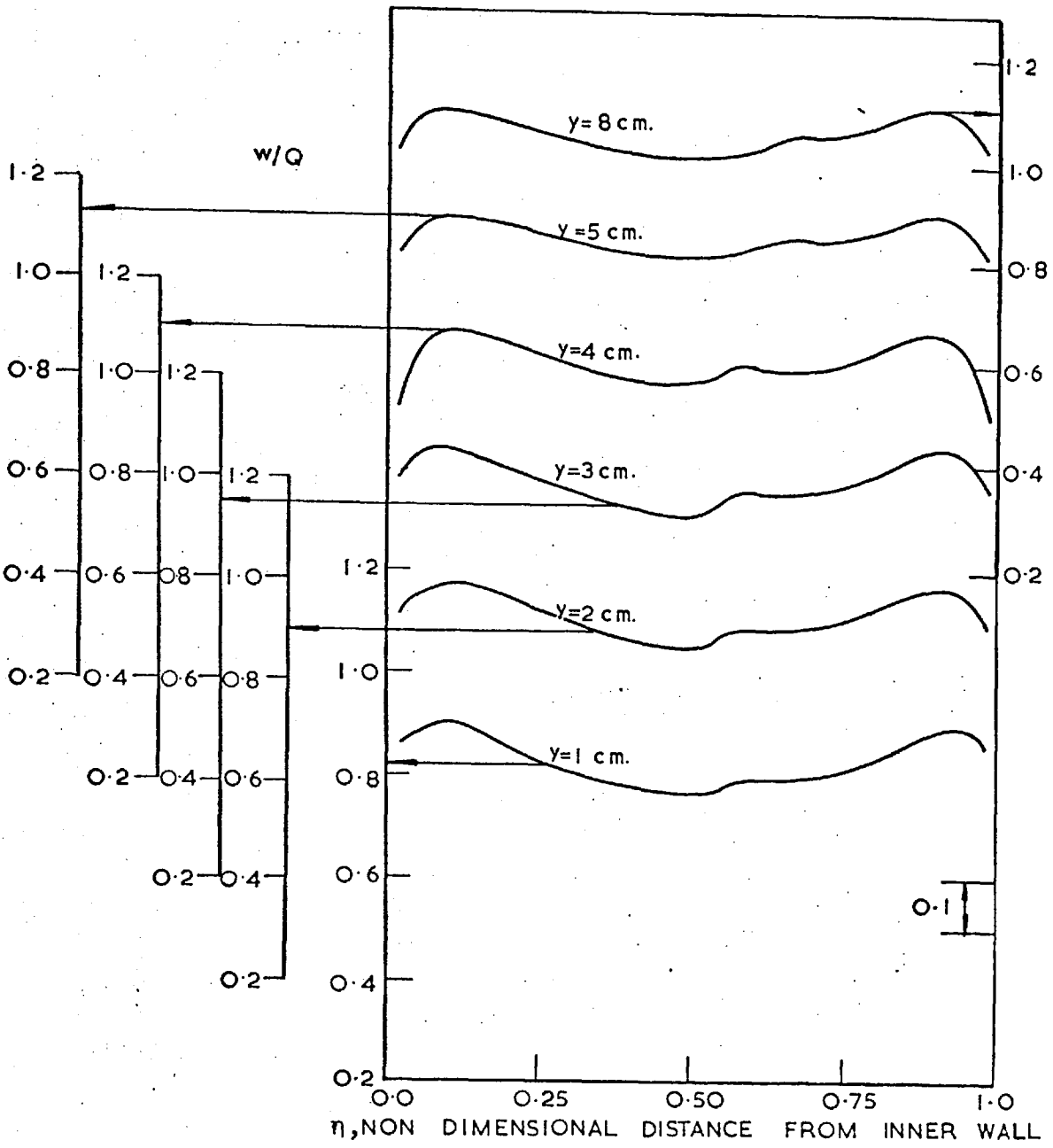

Fig. (8.3.1(a)): Profiles of longitudinal velocity at the location 1.22 m. upstream.

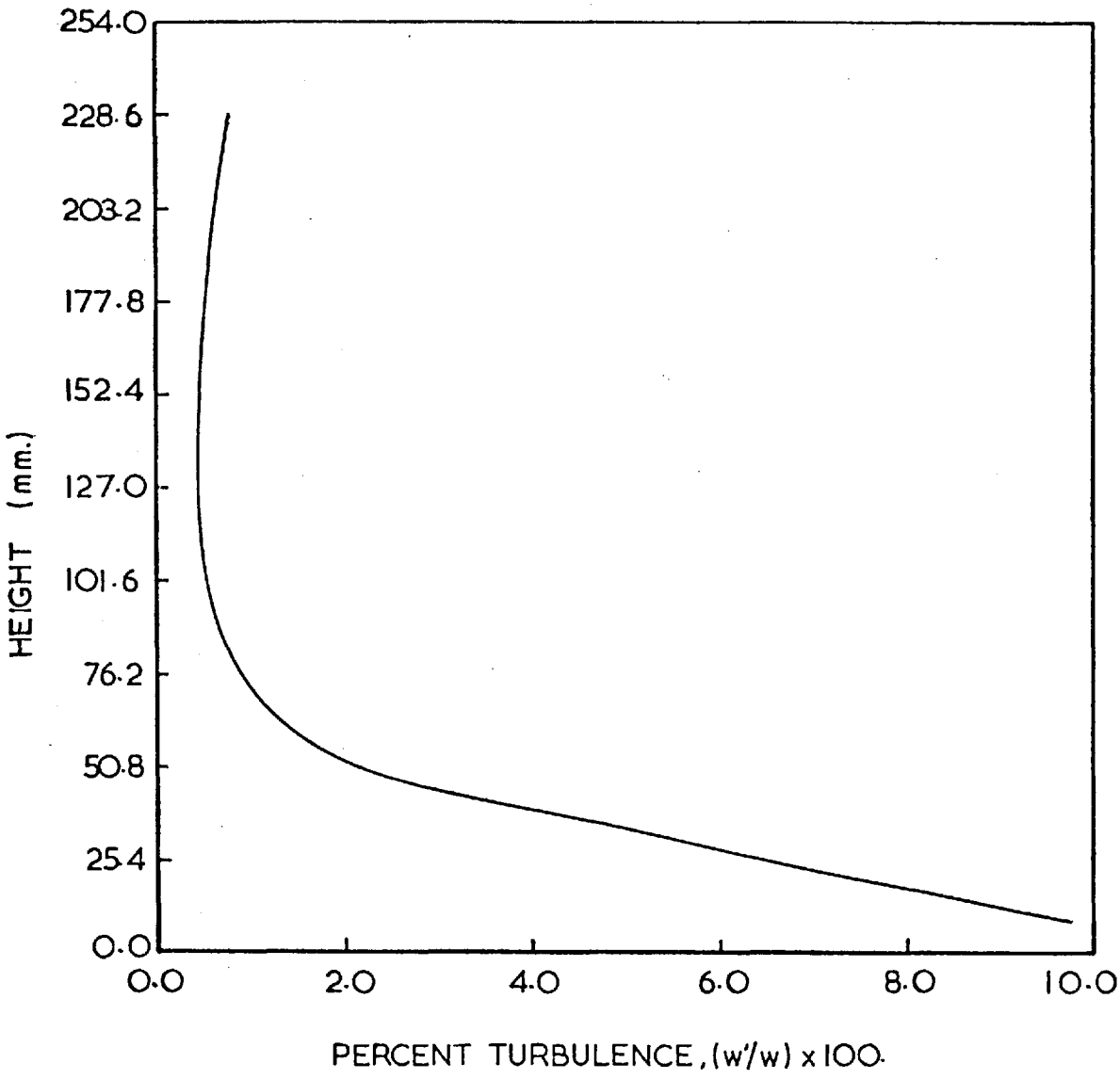

Fig. (8.3.1(b)): Variation of inlet turbulence intensity at the centre of the duct width(x=24 in.).

8.4 Results for constant-area case

Figures (8.4.1) to (8.4.4) show the predicted development of the longitudinal velocity and comparisons with experimental data. The comparisons have been made at different values of normal distance (y) measured from the bottom wall. The velocities have been non-dimensionalised with the total velocity at the centre of the cross-sectional plane. Figures (8.4.5) to (8.4.7) display the development of transverse-direction velocity, along the curved duct; the predictions using the parabolic and the partially-parabolic procedures are compared with measurements. Figure (8.4.8) illustrates the distribution of static pressure in the curved duct. It has been observed both from the experiments and the computations that for regions farther than 10 cm from the side walls, the static pressure is constant along the y-direction; the values plotted here are thus the mean values along the y-direction. The velocities and static pressures presented above are also represented in Figure (8.4.9) as contours of total pressure ($= p + \frac{\rho}{2} (u^2+v^2+w^2)$). In Figure (8.4.10), comparisons are presented for the longitudinal variation of the static pressure along the duct centre-line; it is referred to its value at the 0^o position and is non-dimensionalised with the velocity-head corresponding to the total velocity at the centre of the 0^o cross-sectional plane. Figure (8.4.11) presents the predicted variation of skin friction

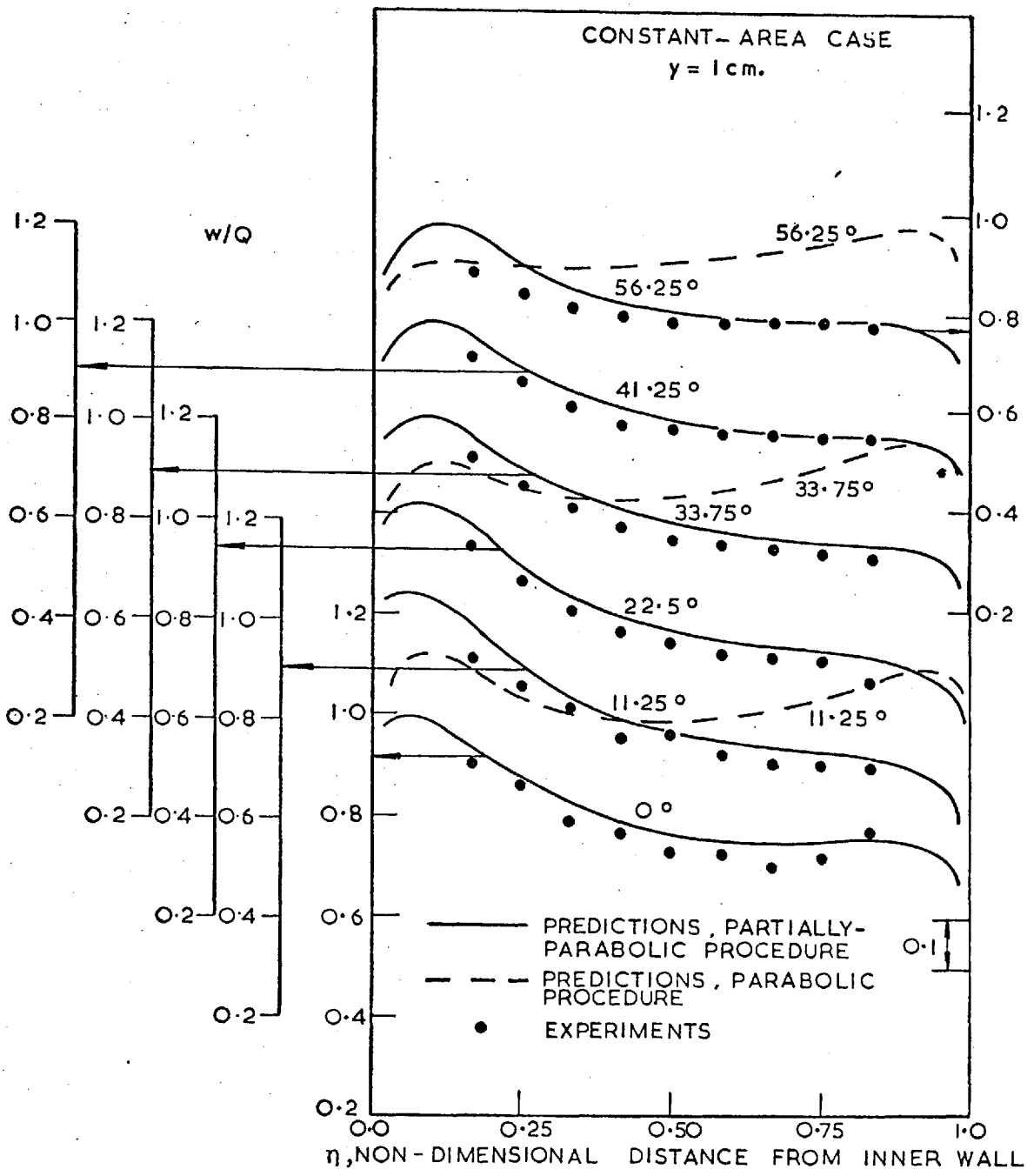

Fig. (8.4.1): Development of longitudinal velocity along the constant-area duct for y=1 cm from bottom wall.

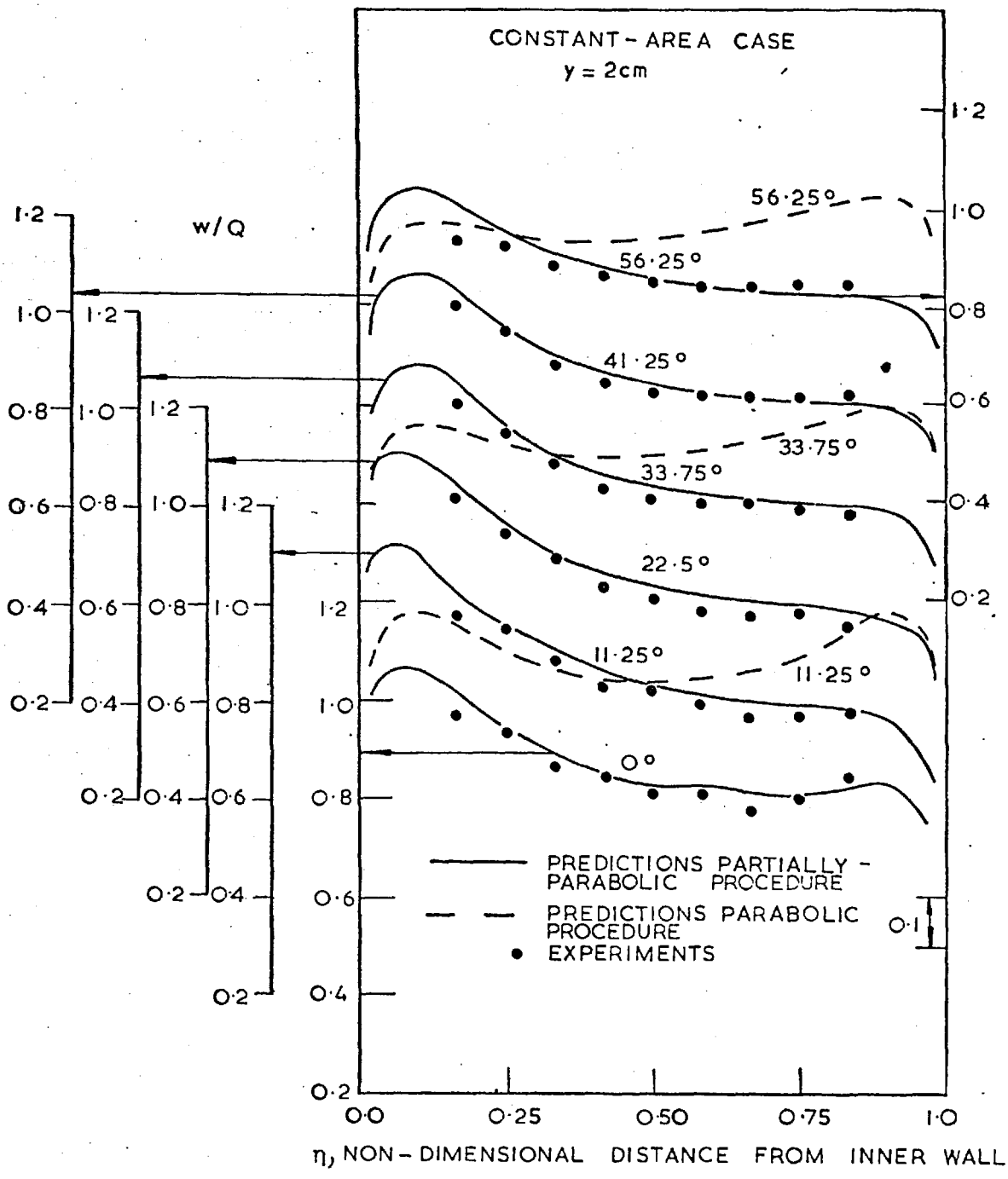

Fig. (8.4.2): Development of longitudinal velocity along the constant-area duct for y=2 cm from bottom wall.

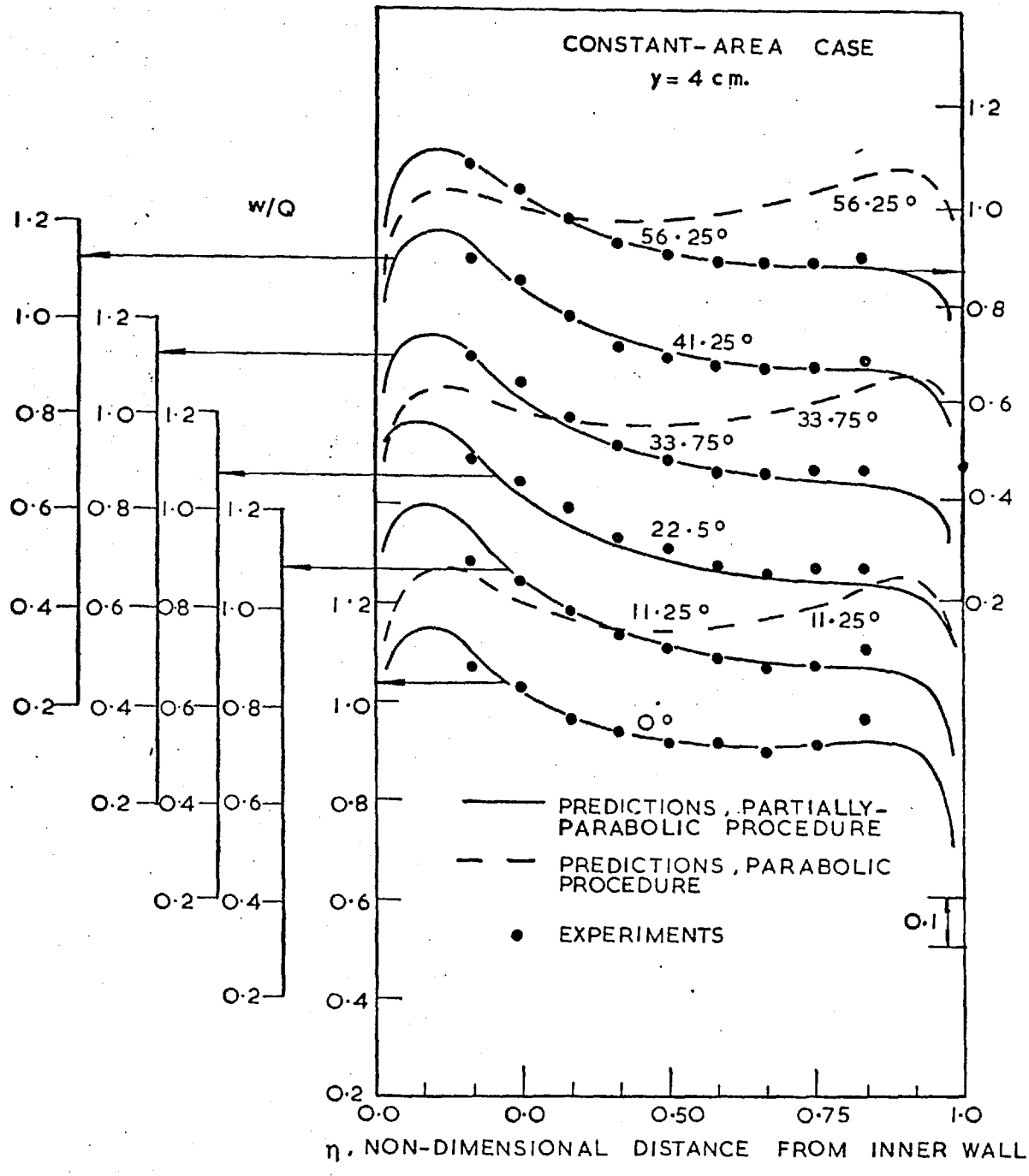

Fig. (8.4.3): Development of longitudinal velocity along the constant-area duct for y=4 cm from bottom wall.

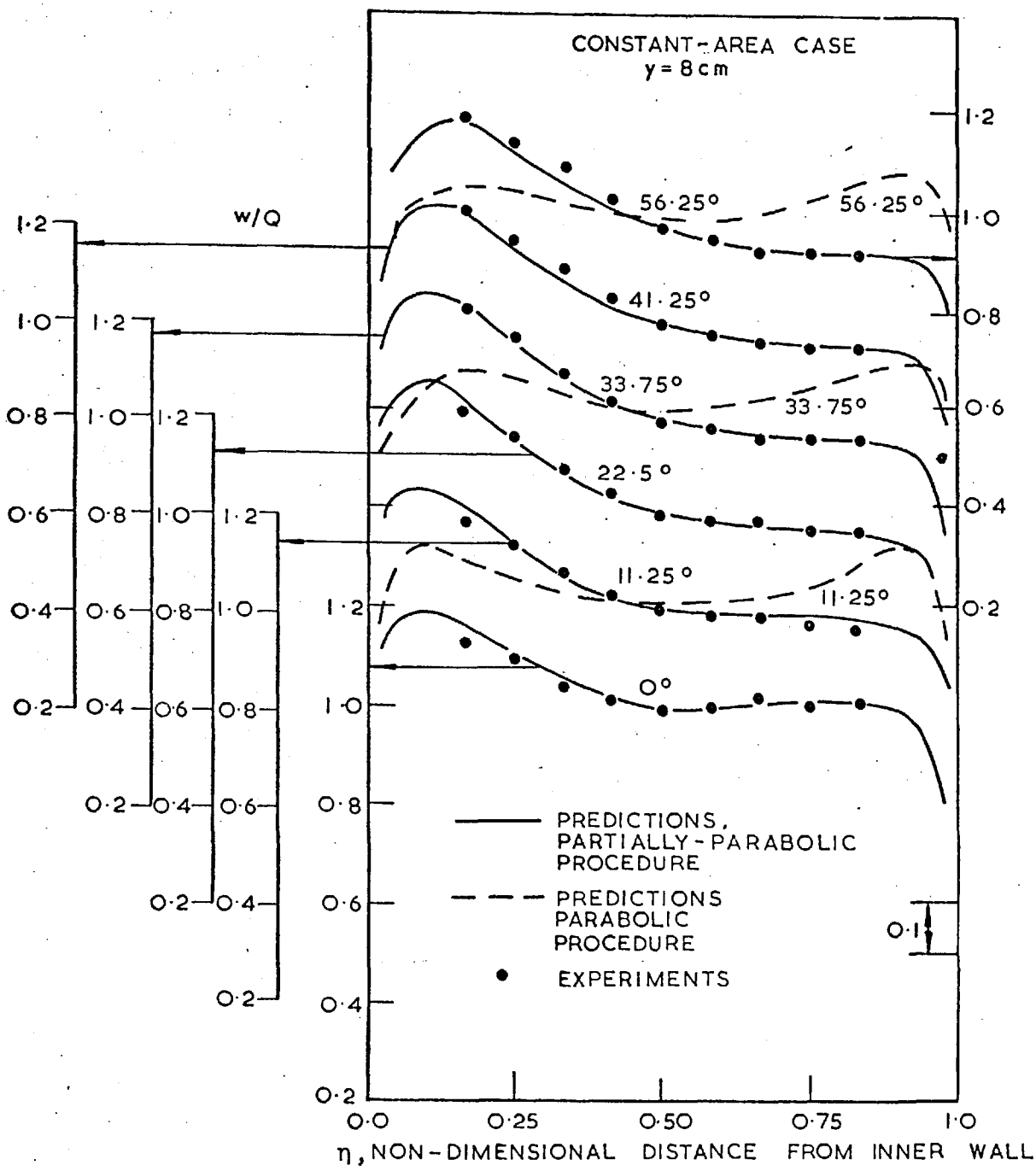

Fig. (8.4.4): Development of longitudinal velocity along the constant-area duct for y=8 cm from bottom wall.

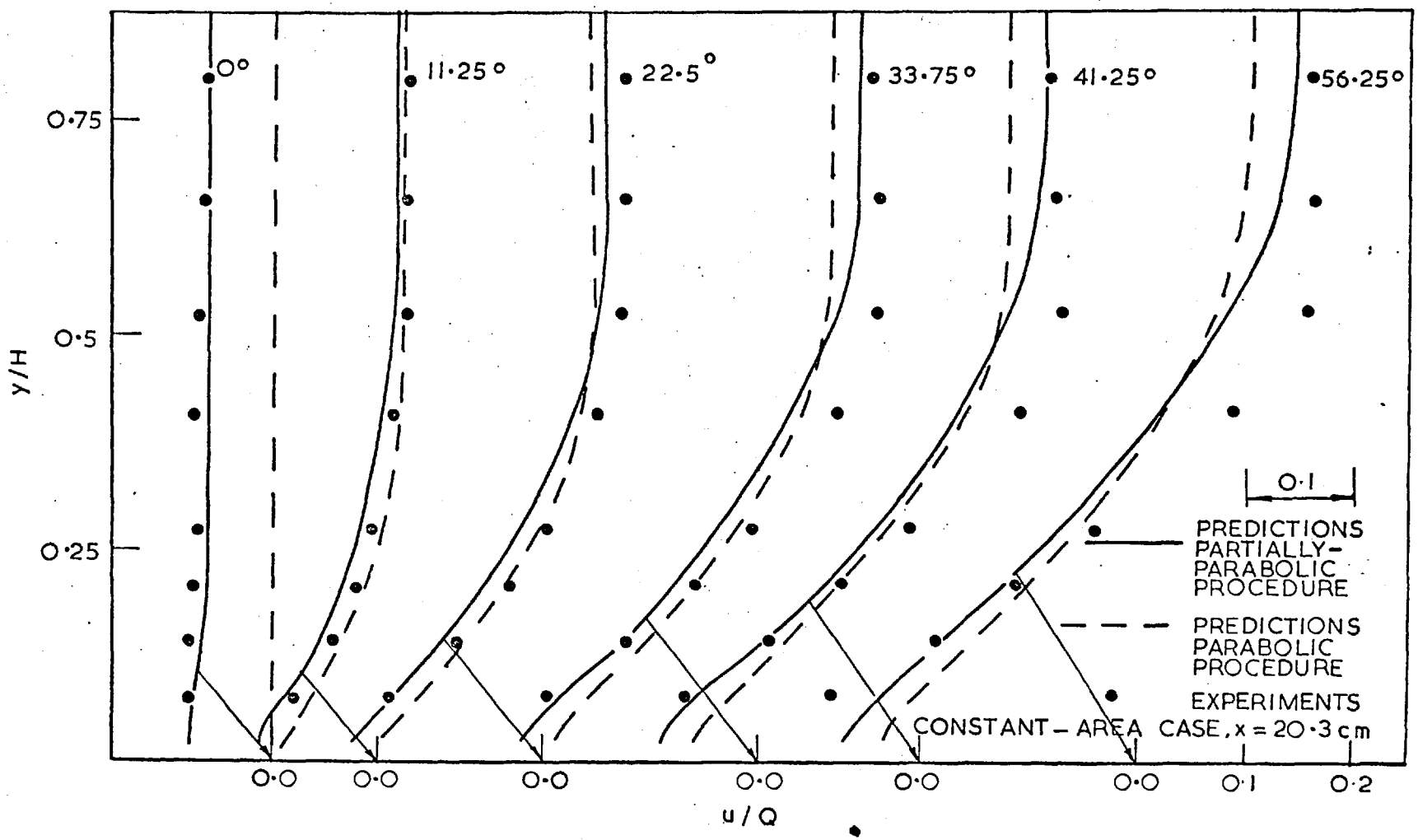

Fig. (8.4.5): Development of transverse velocity along the constant-area duct for x=20.3 cm from inner wall.

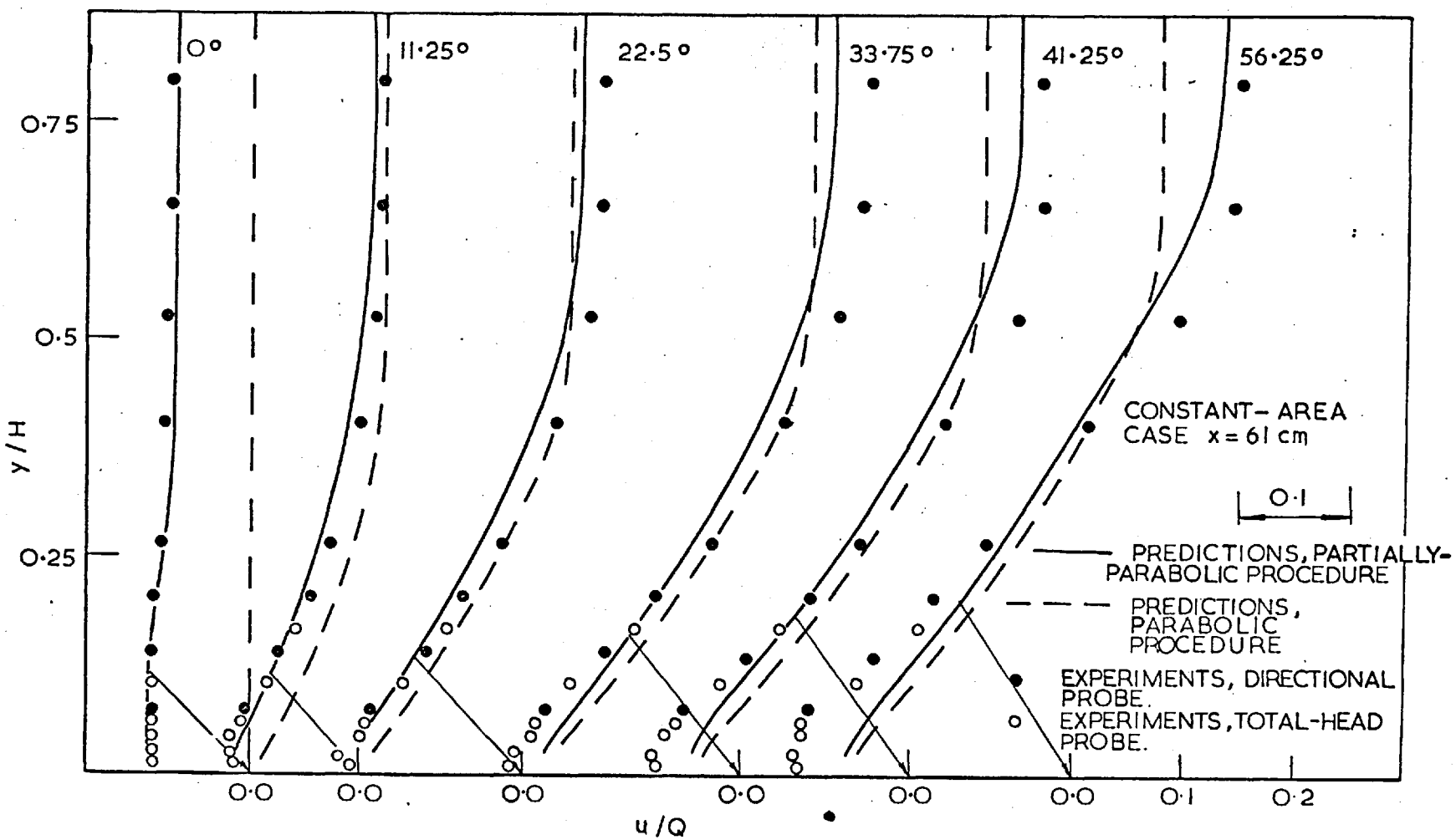

Fig. (8.4.6): Development of transverse velocity along the constant-area duct for x=61 cm. from inner wall.

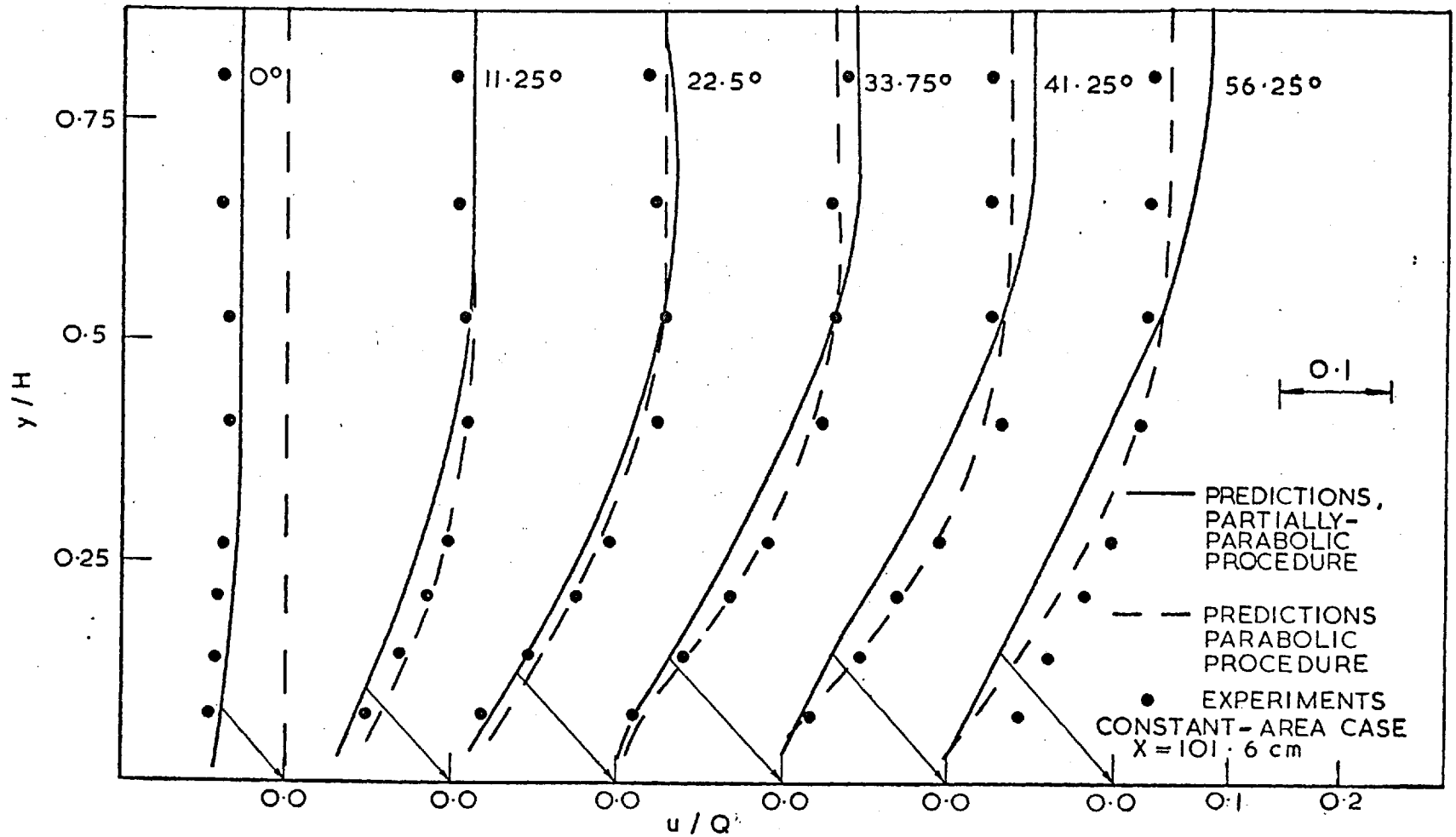

Fig. (8.4.7): Development of transverse velocity along the constant-area duct for x=101.6cm. from inner wall.

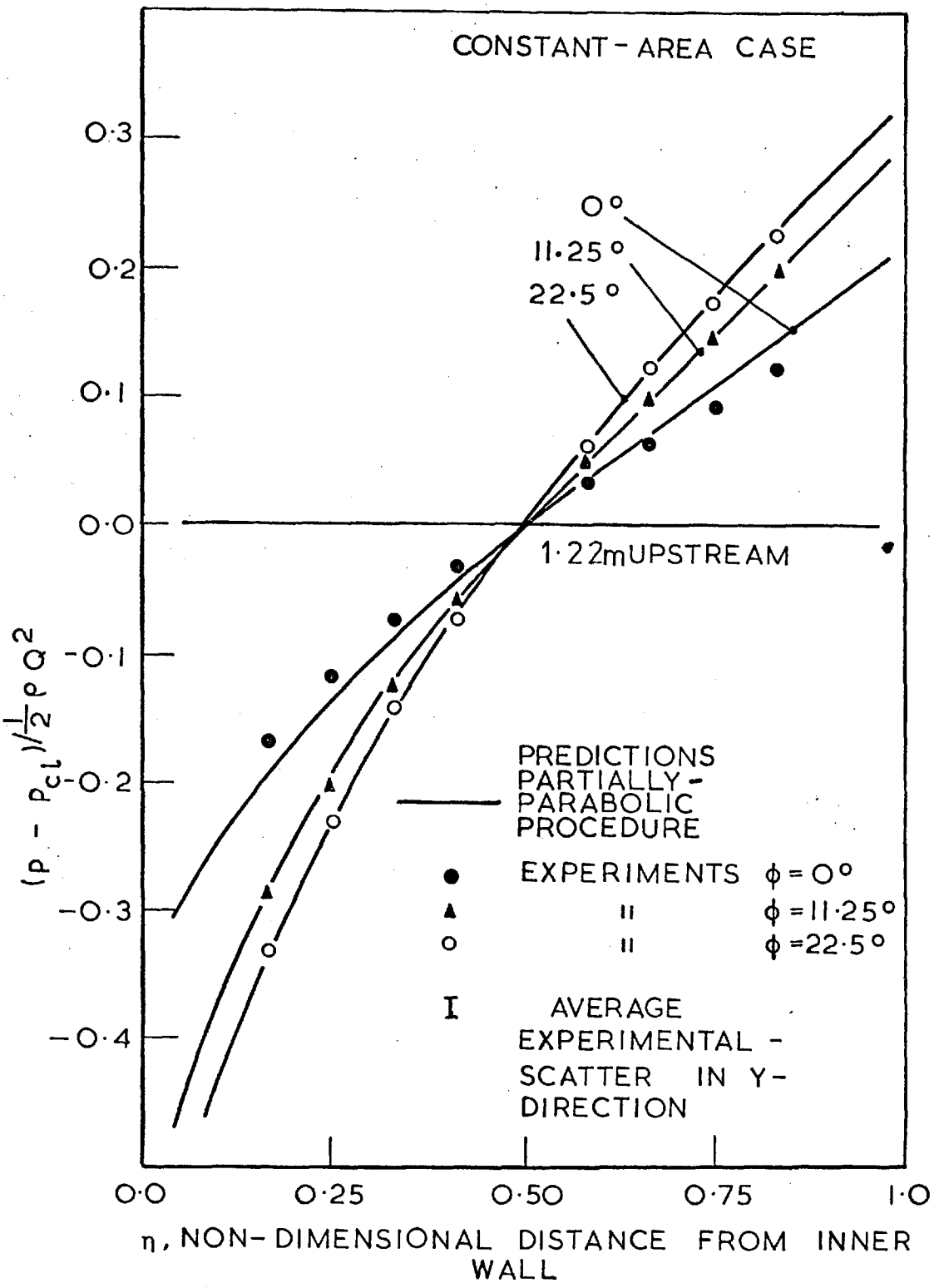

Fig. (8.4.8): Development of static-pressure distribution along the constant-area duct.

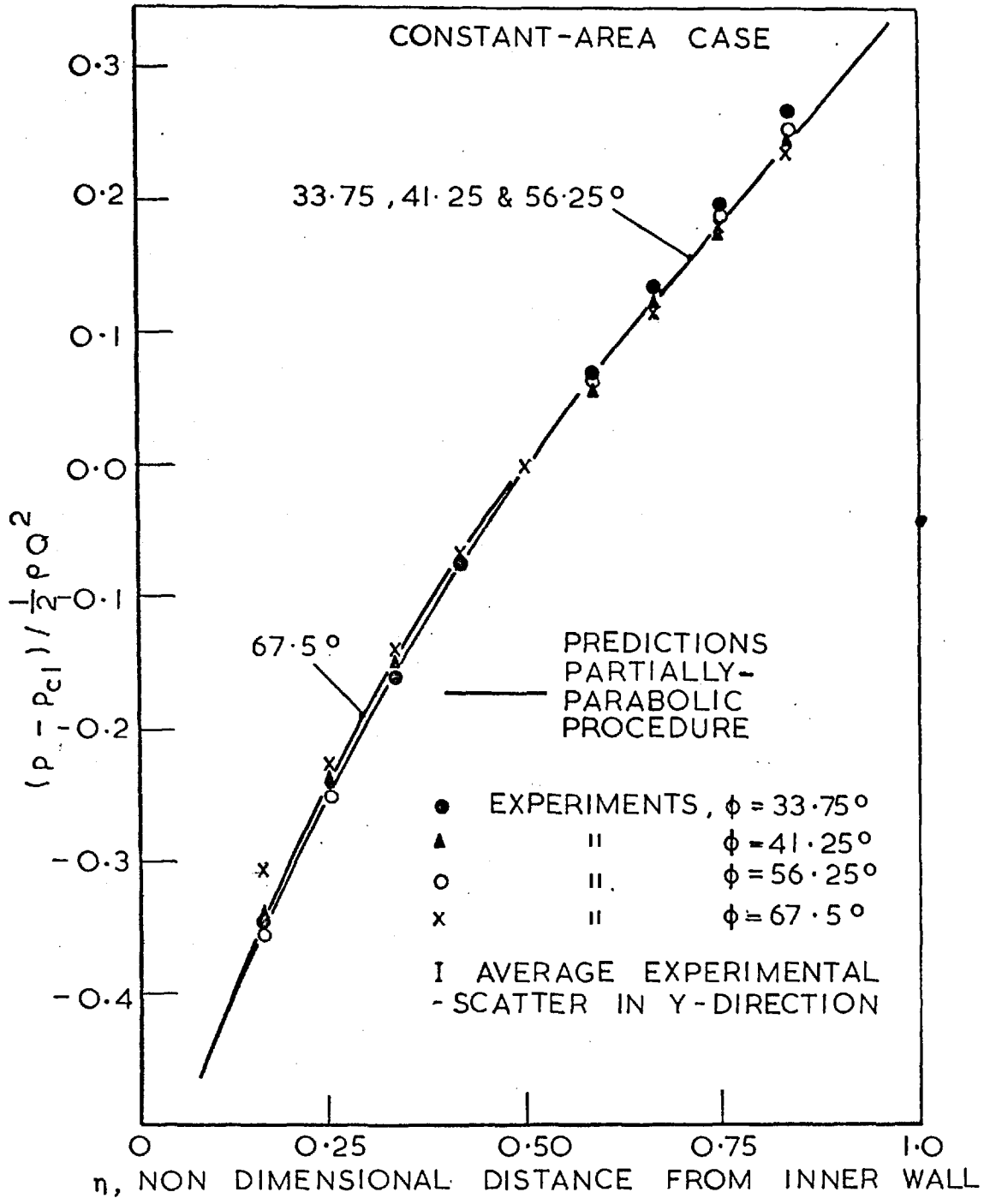

Fig. (8.4.8): Continued.

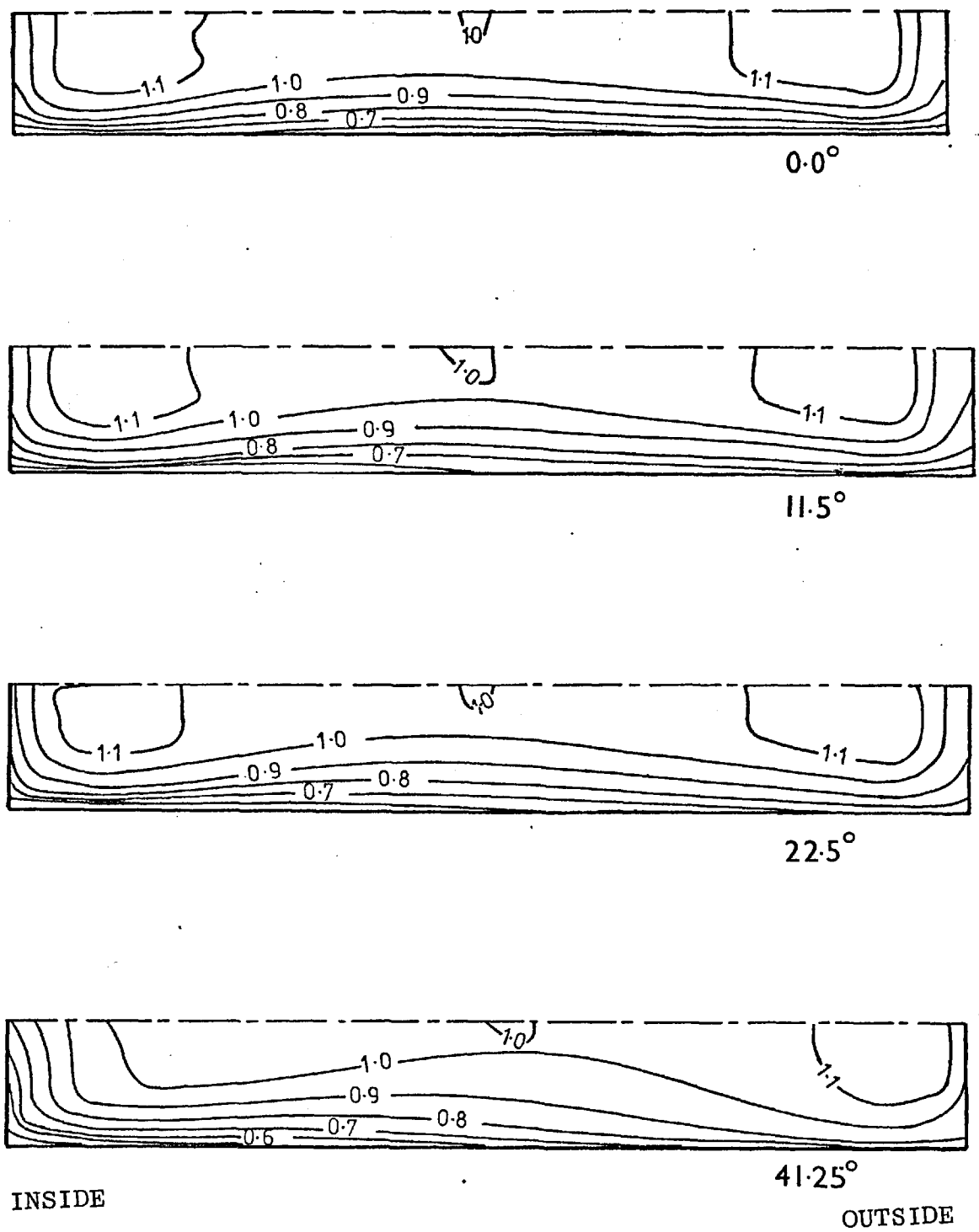

Fig. (8.4.9): Contours of total pressure along the constant-area duct, nondimensionalised with the total pressure at the centre of the cross-section.

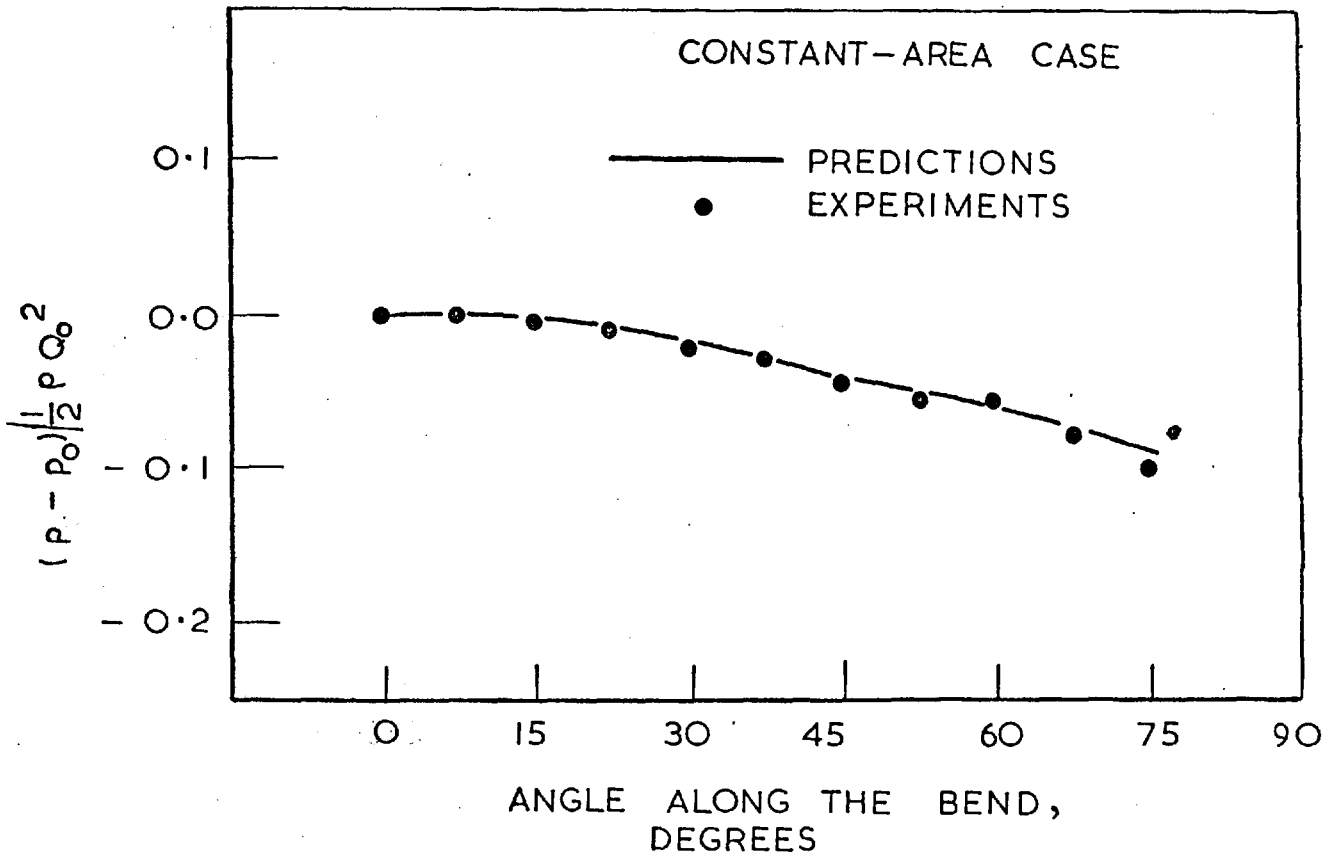

Fig. (8.4.10): Development of static pressure along the centreline of the constant-area duct.

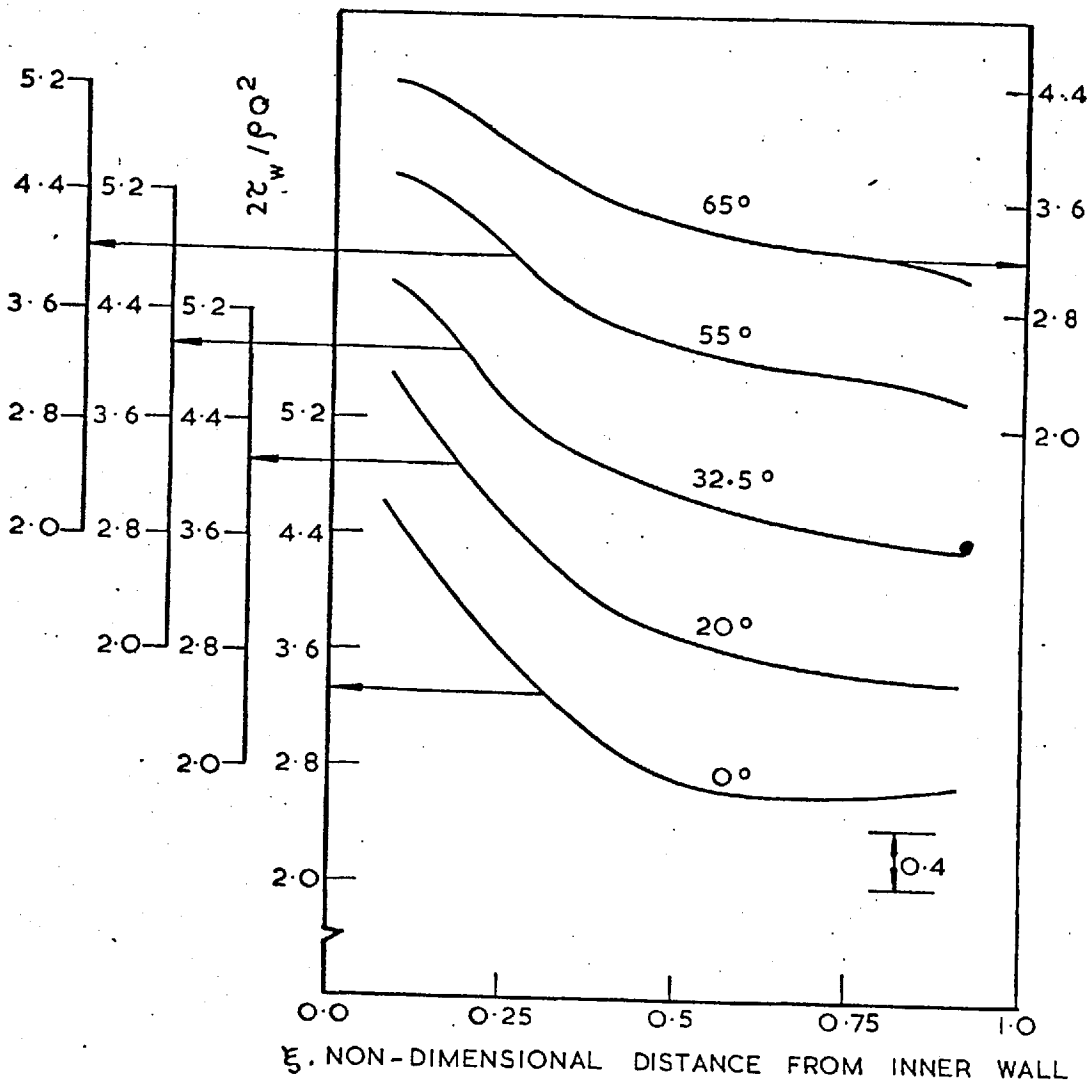

Fig. (8.4.11): Predicted distribution of skin friction coefficient in the cross-section for several axial stations along the constant-area duct.

coefficient ($2\tau_w/\rho Q^2$ where τ_w = wall shear stress; Q = total velocity at the centre of the cross-sectional plane and ρ is the fluid density) at several angular positions along the bend. It is observed that the skin-friction coefficient in the inside region is larger compared with its outside value. From the above results it is seen that the flow situation presently considered is partially-parabolic in nature; and the computations using a partially-parabolic calculation procedure display good agreement with experimental data; but when the flow is treated as fully-parabolic, the results are in disagreement. The origin of the elliptic effects in the pressure field will be discussed in a later section.

8.5 Results for the diffusing-area case

Computations of the flow in a curved diffuser were made in an identical manner; except that in these, the width of the duct was varied along the ϕ-direction; and a different coordinate system (η, ζ, ξ) was employed. The inlet and exit conditions for these computations were the same as those for the constant-area case, as presented in Sec. 8.3. The results of the computations for the diffuser are presented in Figures (8.5.1) to (8.5.9). It is observed that these results do not differ significantly from those for constant-area duct; this may be because of the small diffuser angle (2.5^o) considered in the present study.

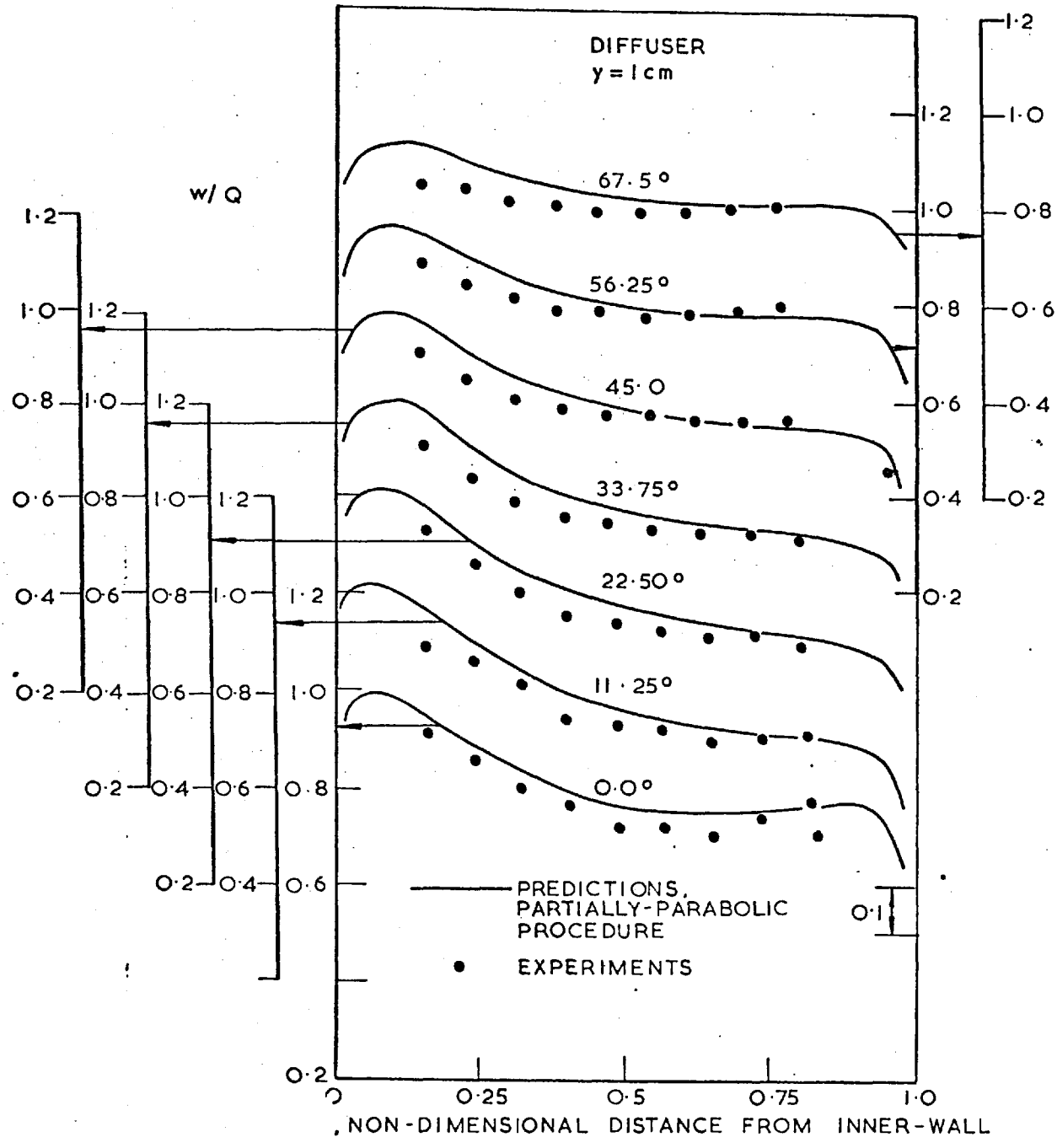

Fig. (8.5.1): Development of longitudinal velocity along the diffuser for y=1 cm from bottom wall.

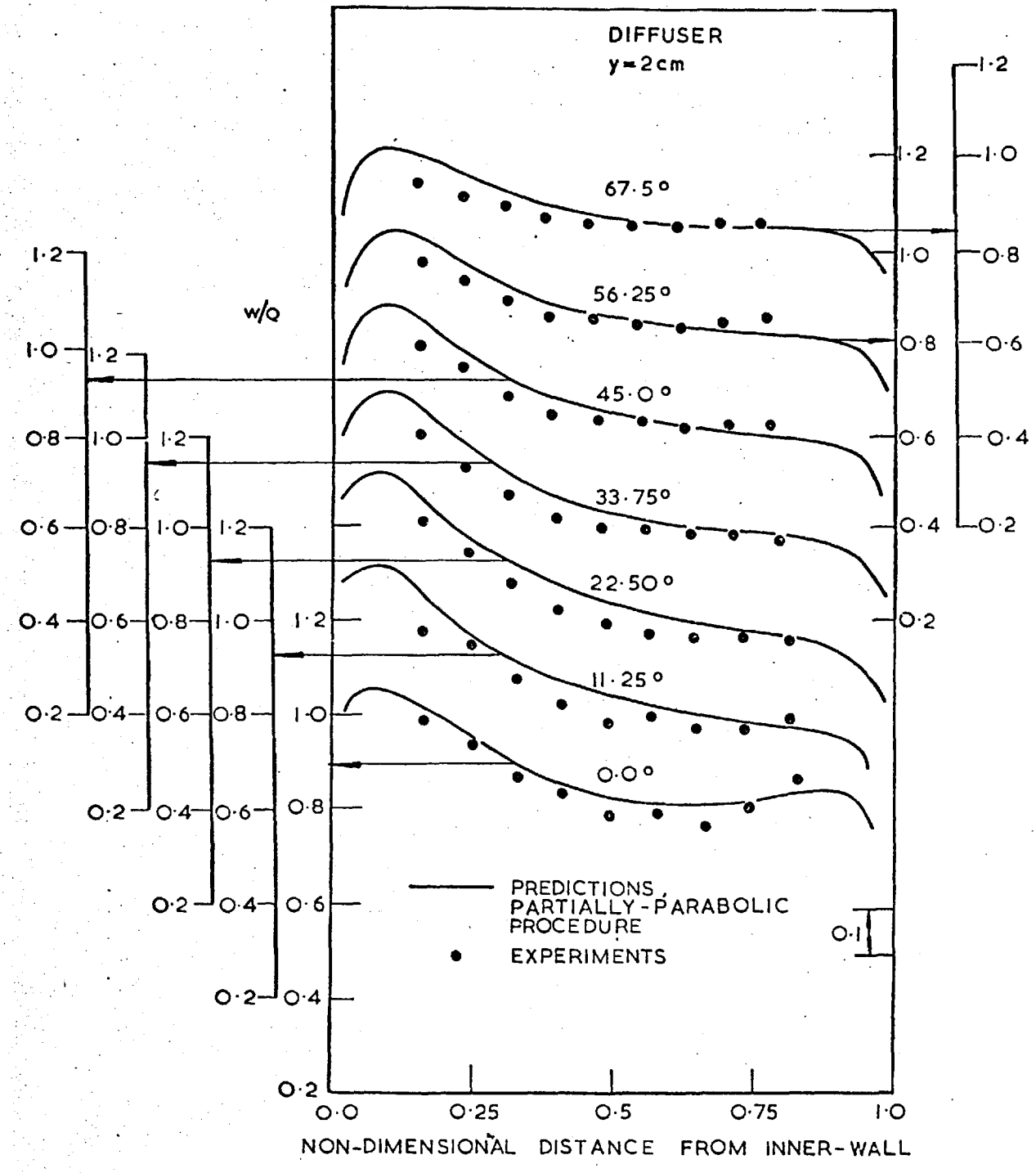

Fig. (8.5.2): Development of longitudinal velocity along the diffuser for y=2 cm from bottom wall.

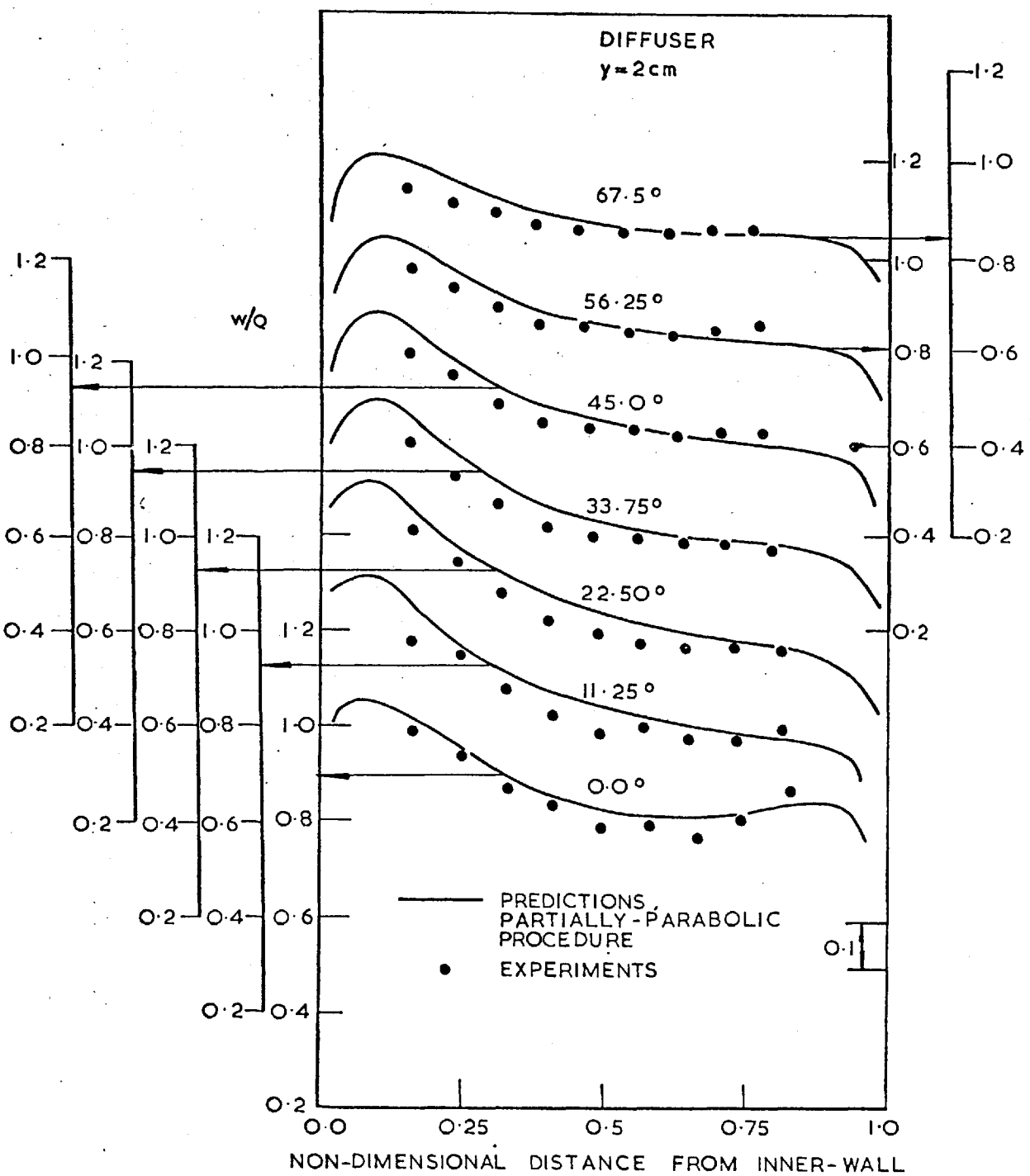

Fig. (8.5.2): Development of longitudinal velocity along the diffuser for y=2 cm from bottom wall.

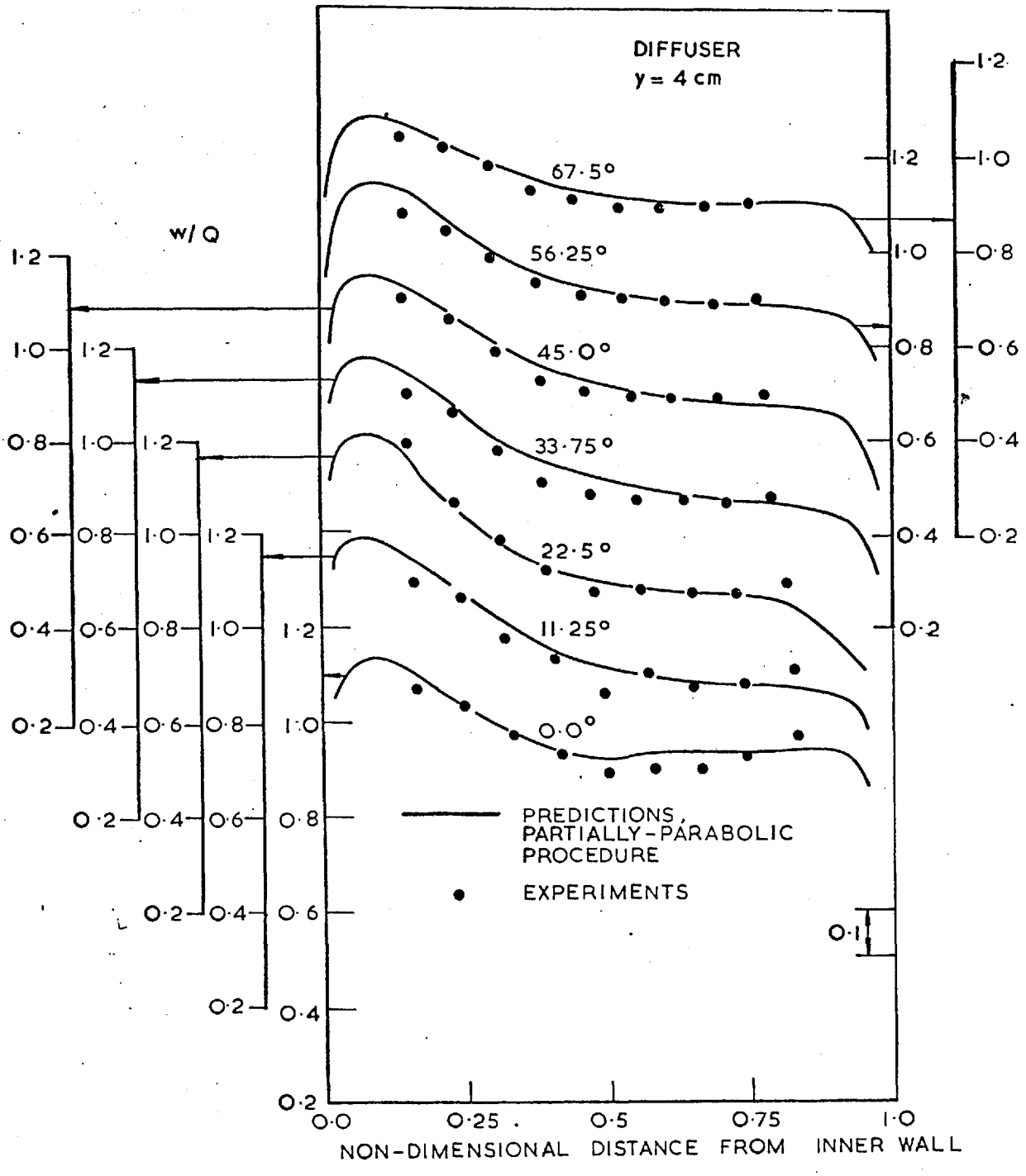

Fig. (8.5.3): Development of longitudinal velocity along the diffuser for y=4 cm from bottom wall.

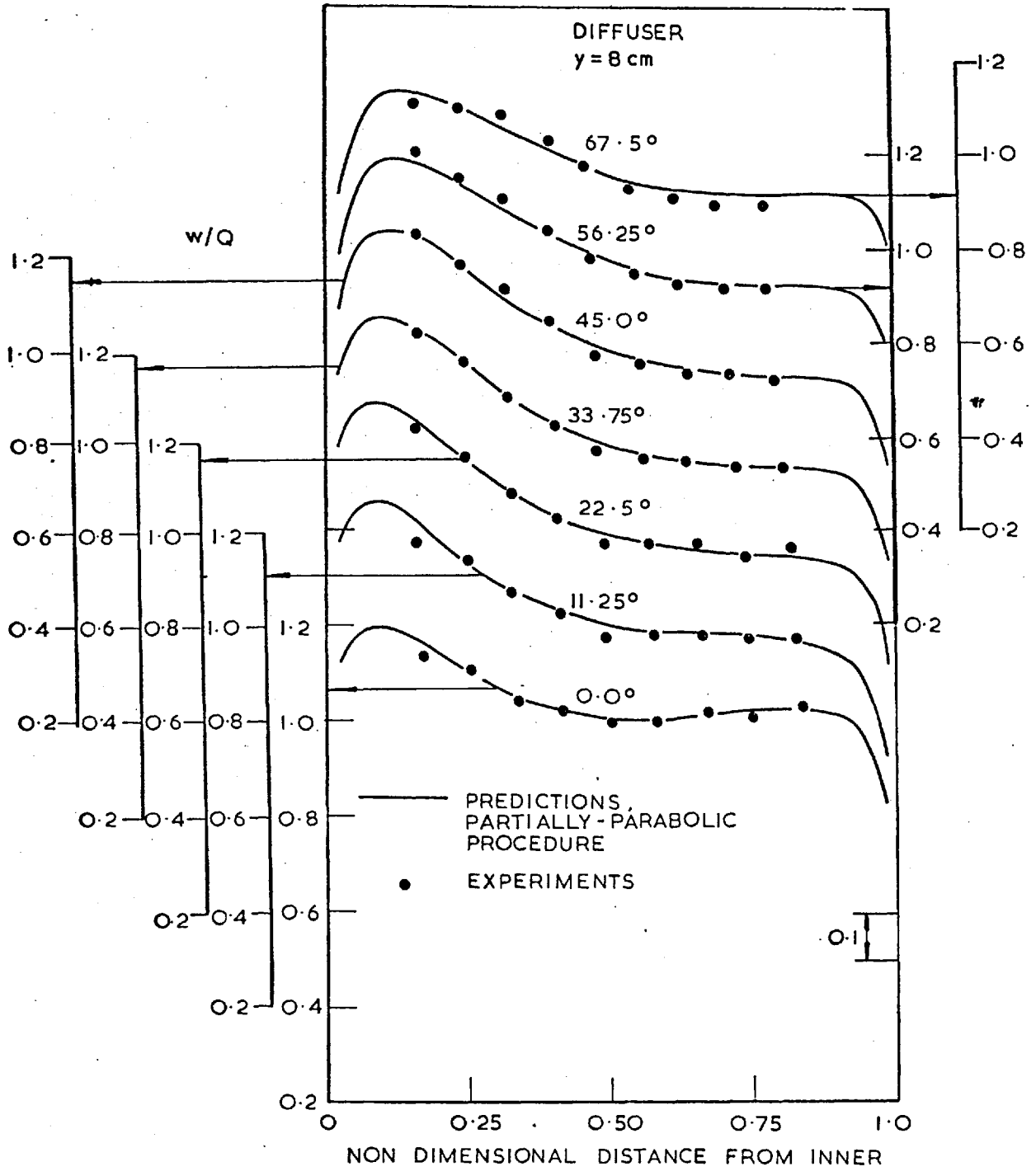

Fig. (8.5.4): Development of longitudinal velocity along the diffuser for y=8 cm from bottom wall.

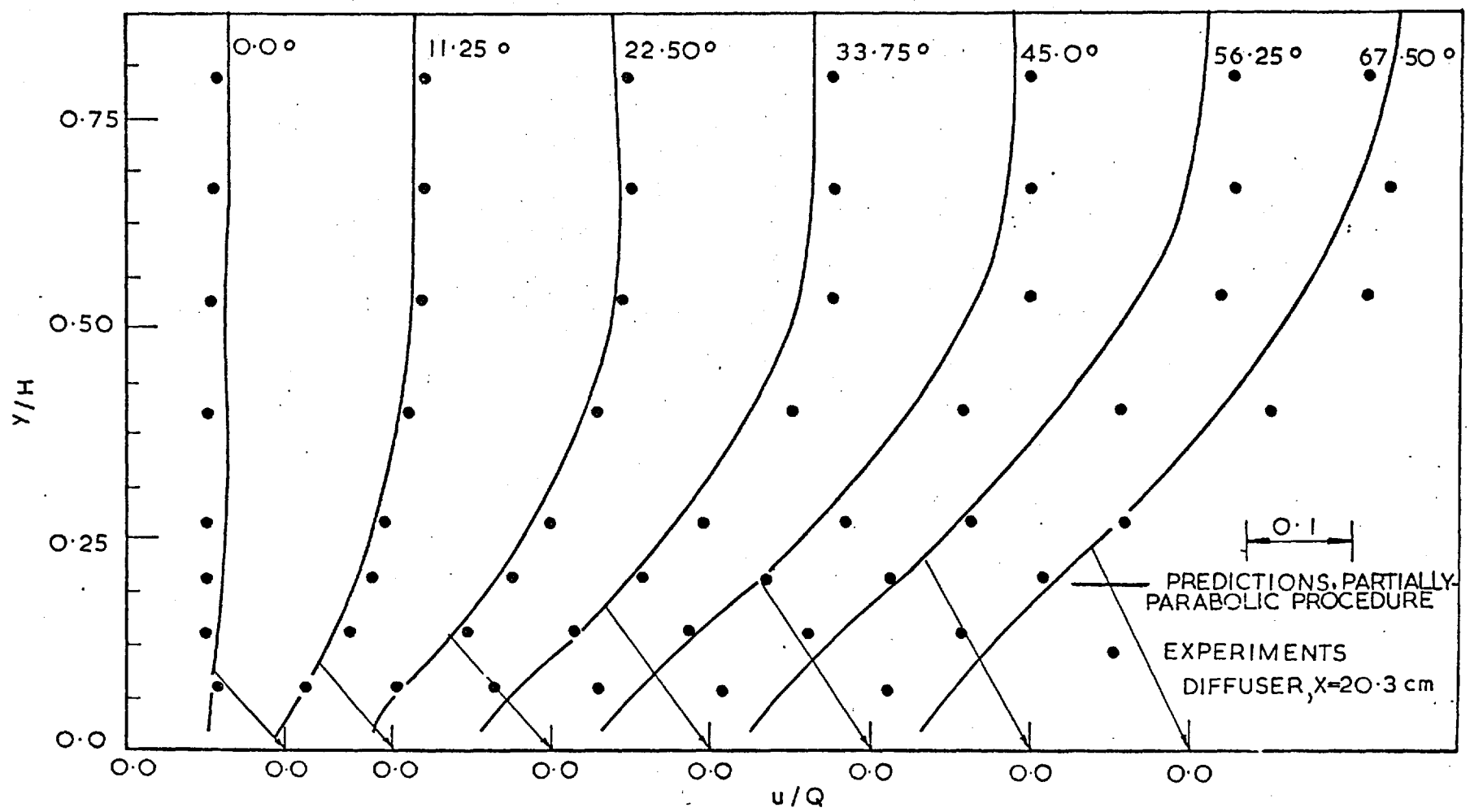

Fig. (8.5.5): Development of transverse velocity in the diffuser for x=20.3 cm from inner wall.

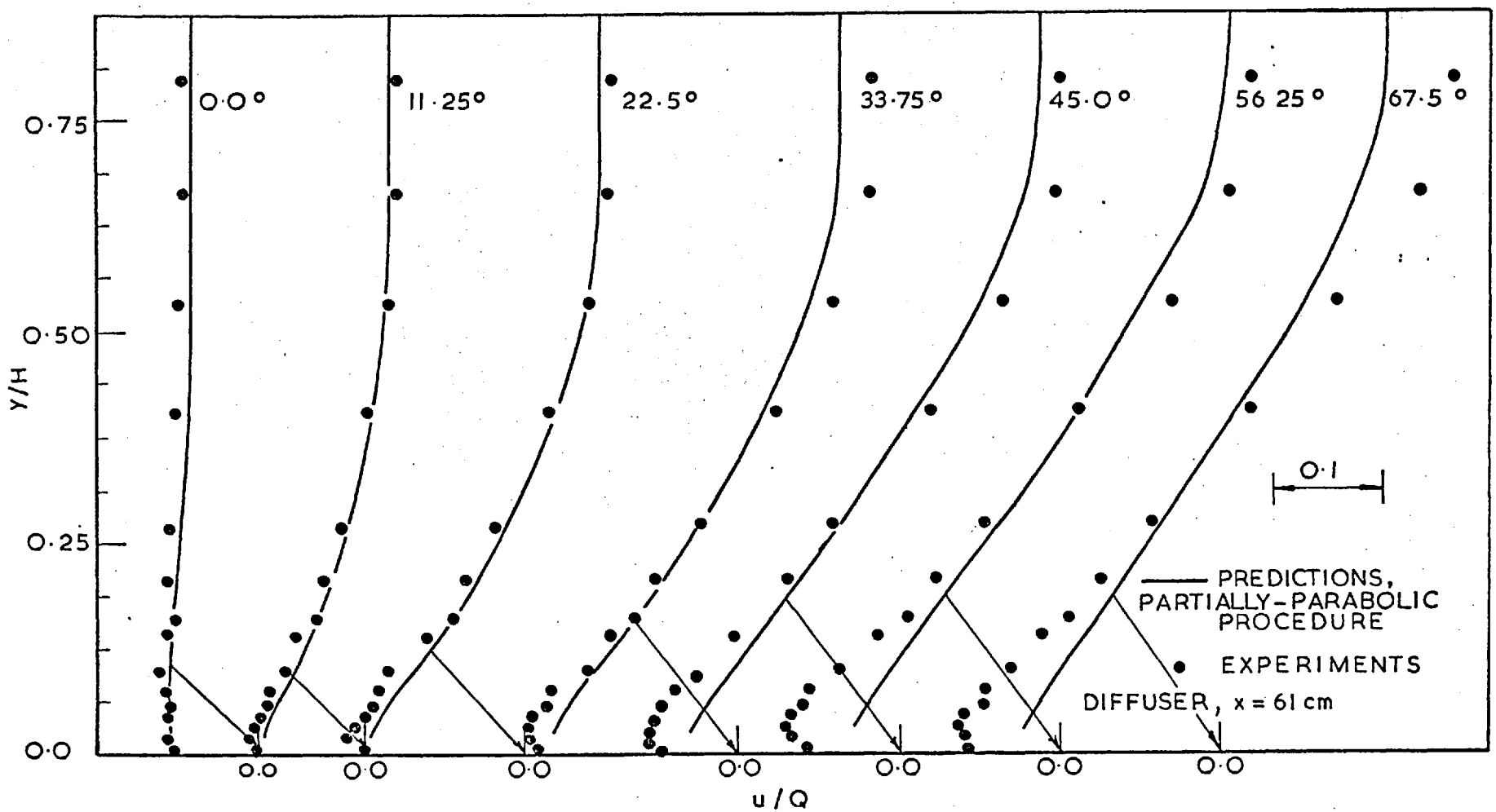

Fig. (8.5.6): Development of transverse velocity in the diffuser for x=61.0 cm from inner wall.

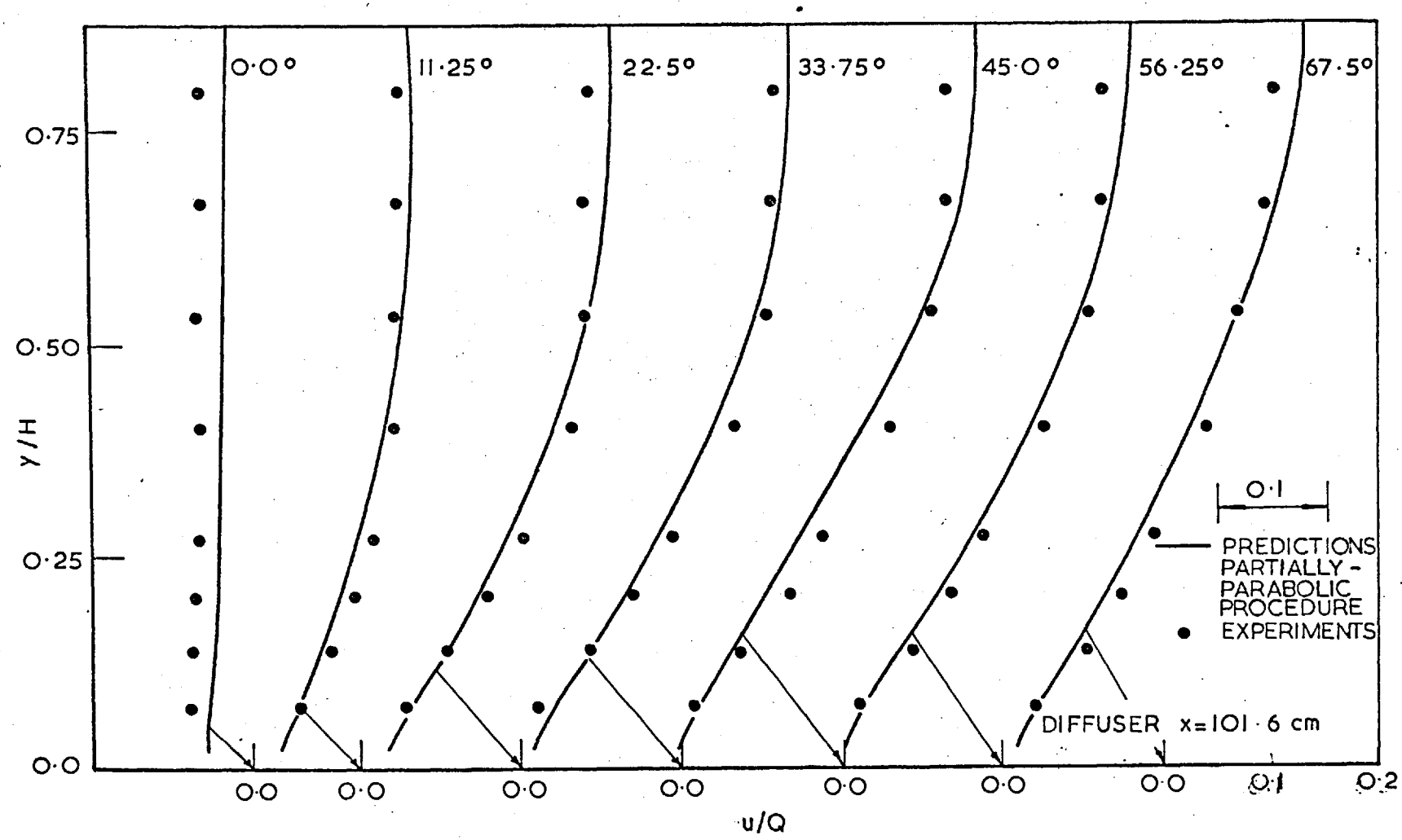

Fig. (8.5.7): Development of transverse velocity in the diffuser x=101.6 cm from inner wall.

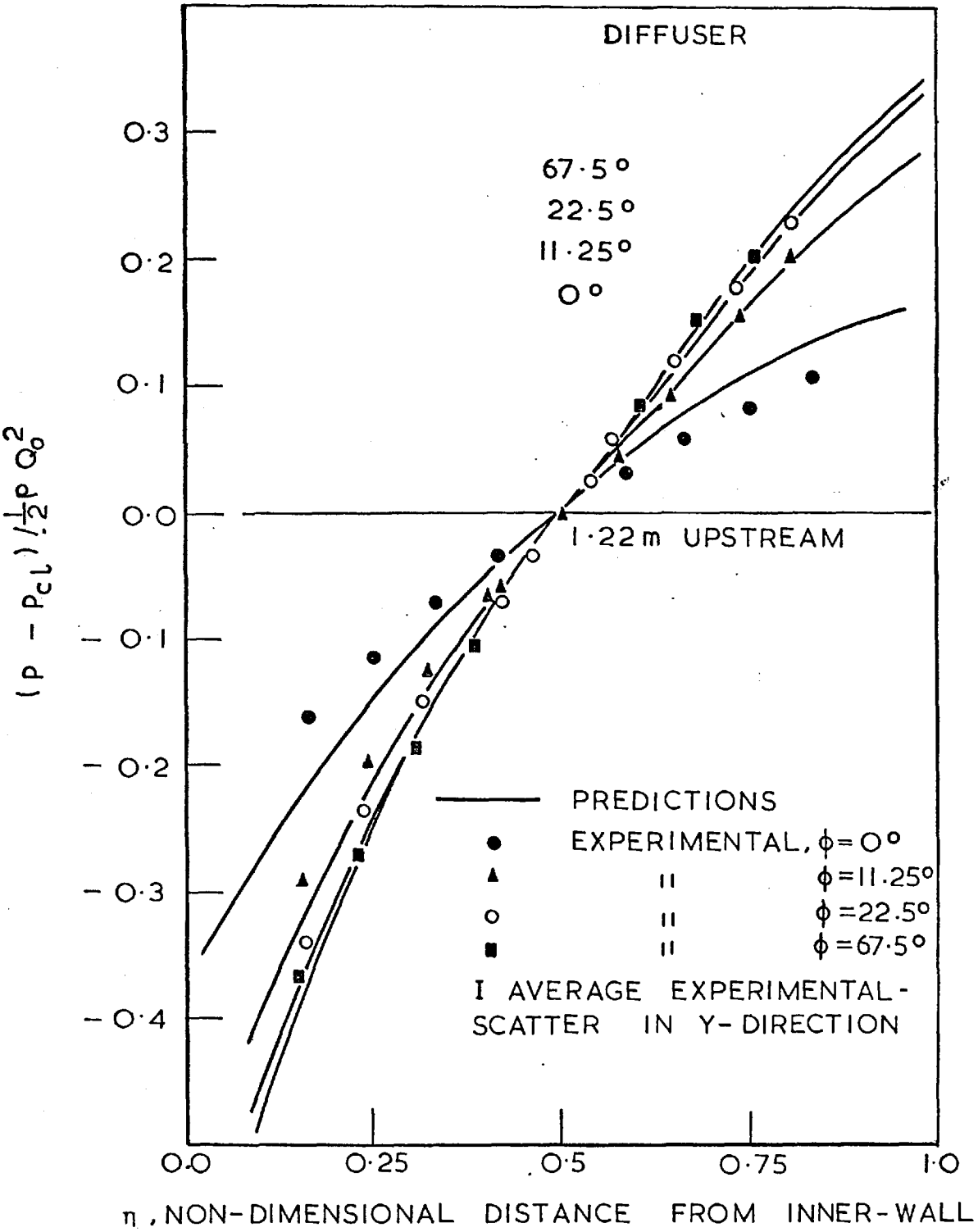

Fig. (8.5.8): Development of static-pressure distribution along the diffuser.

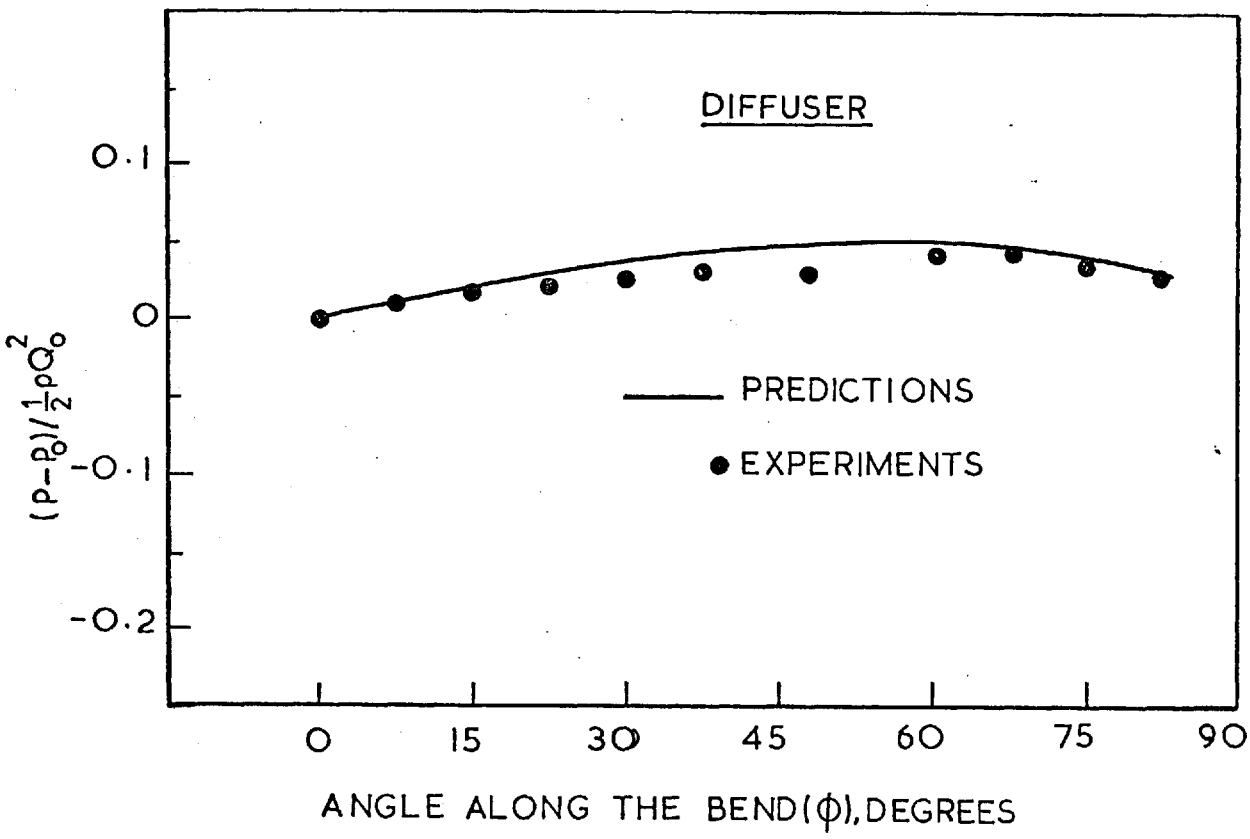

Fig. (8.5.9): Development of static pressure along the centreline of the diffuser.

8.6 Discussion

The comparisons presented above show that the flow in strongly-curved ducts is partially-parabolic in its nature; that is the flow is significantly influenced by the effects of the transmission of downstream events through the pressure field. The origin of the elliptic effects can be better understood by examining the flow situation in somewhat more detail. As described in Sec. (7.2.4), the flow in a curved duct is associated with cross-stream variations in the pressure field which are generated as a result of the centrifugal forces acting on the fluid. The consequence of these cross-stream pressure-variations are two fold: Firstly, they give rise to transverse velocities, i.e. velocities along the x and y directions, as shown in Figure (8.6.1) (in the present case, because of large width of the duct, the y-direction velocities are confined only to the regions near the side walls and are negligible elsewhere). Second, the cross-stream variations accelerate certain regions of flow relative to the other by creating differential amounts of longitudinal pressure gradients over the cross-section. The elliptic effects arise because of this later consequence. It is through the variations in the longitudinal pressure gradients that events at a downstream station are transmitted to upstream regions. The flow region which is most influenced by these downstream effects is that where the cross-stream

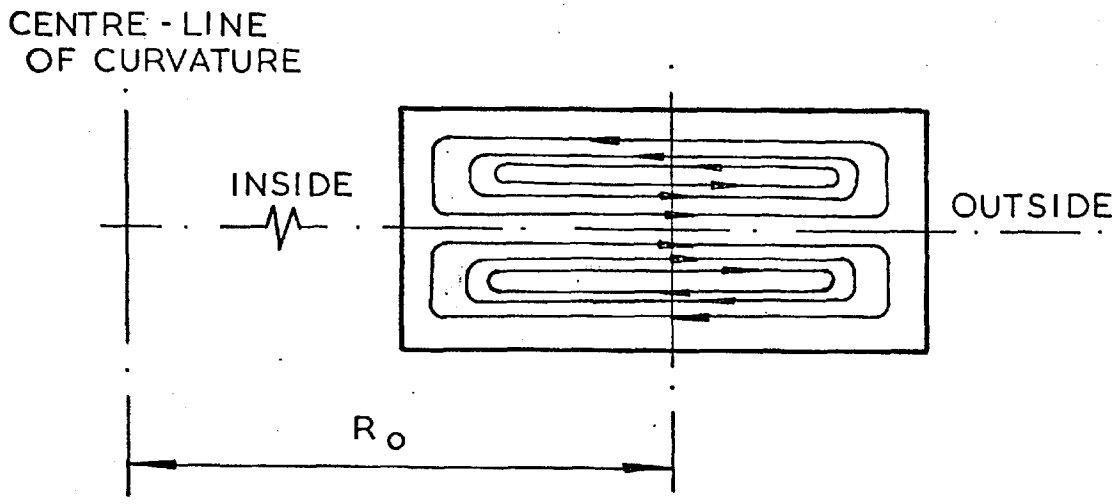

Fig. (8.6.1): Secondary flow pattern in a curved duct.

pressure variations are changed rapidly; in the present case this happens at the inlet of the curved duct. In this region, the flow from the straight section is suddenly accelerated on the inner side and retarted on the outer side as it encounters the pressure variations in the curved duct. The profile of longitudinal velocity is hence distorted, with a velocity maximum at the inside, even before the flow enters the curved duct. The flow pattern produced in the straight section continues to develop further in the curved duct; and is influenced then by the centrifugal forces. The effect of the centrifugal forces is to drive the fluid outwards to shift the maximum to the outside; but the extent to which they overtake the inlet effects depends on the curvature of the duct, the state of flow (laminar or turbulent), and the duct length provided for the flow development. In strongly curved ducts, since the radial pressure variations are large the distortion of the flow field at 0^{o} of the bend is substantially large; and therefore the effects of the inlet ellipticity prevail over a large region of the flow domain. In mildly-curved ducts, on the other hand, the cross-stream pressure gradients are relatively small; and the effects of the inlet ellipticity are quickly dominated.

The need for a partially-parabolic calculation procedure depends on the length of flow region influenced by the elliptic effects in the pressure field. From

Figures (8.4.8) and (8.5.8) it may be seen that after about 20 degrees of the bend, there are no large changes in the cross-stream pressure-gradients; this means that the region after about this distance in the curved duct is parabolic; and can safely be computed using the parabolic procedure, provided the starting conditions for the marching integration are prescribed correctly. In mildly-curved ducts since the flow field at the 0^{o} position is relatively unaffected it is safe to assume that the flow at the 0^{o} location is the same as that in the straight pipe; such an approximation will not give correct results for flow in strongly-curved ducts, as has been evident from the present calculations. The partially-parabolic nature of the flow in strongly-curved ducts is also evident from the contours of total pressure which show regions of equal total-pressure on the inside and outside. The static pressure at the outside is higher than that at inside but since the velocity is smaller, the total pressures at inside and at outside are nearly the same. But in mildly-curved ducts it is the opposite; the regions of high velocity and high static pressure are both at outside.

Two aspects of the present calculations need further discussion. First, the conditions at the exit. In the present computations, the exit boundary was prescribed to be of uniform pressure i.e. with no variations across the duct cross-section. But in

reality, the pressure field is not changed suddenly to the atmospheric conditions; but some variations will be present at the end of the test section. Since these variations were not measured at present, a uniform-pressure was prescribed at the exit. The effect of this wrong prescription of exit-boundary condition is however small on the calculations made in regions away from the exit. In the present calculations comparisons with experiments upto 67.5^{o} of the bend have been good; but since no comparisons have been made farther than this position the precise extent of region influenced by the exit-boundary condition is not known. In any case, it is possible in the present calculation procedure also to prescribe a desired variation of exit pressure without additional difficulty.

Second, the present calculations using the partially-parabolic procedure, although show good agreement in axial-velocity profiles, under-predict the transverse velocities by about 10-15 percent. It may be recalled that a similar discrepancy between predicted and measured values was also observed in the case of turbulent flow in mildly-curved pipes (Sec. 7.3). The discrepancies observed earlier and in the calculations of the present chapter are probably due to the turbulence-model currently used. From a few measurements of Vermeulen (1971) in a curved duct, it appears that the turbulent viscosity for flow in curved ducts is not isotropic as has been assumed

in the present turbulence model; for the viscosity in the transverse directions was observed to be about half of that in the longitudinal direction. It may therefore be necessary to discard the effective viscosity approach for calculation of flow in curved ducts; and employ more complex turbulence models; alternatively, it is also possible to make empirical modifications to the $k\sim\varepsilon$ model, based on experimental findings such as that of Vermeulen (1971).

8.7 Concluding remarks

The computations reported in this chapter have shown that for the calculation of flows in strongly-curved ducts, the partially-parabolic procedure is greatly superior; it gives good agreement with experimental data, whereas the fully-parabolic procedure is even qualitatively at variance with the measurements. From the view point of economics, the partially-parabolic procedure is however, about three times more expensive than the parabolic one; but when compared with a fully-elliptic procedure, it is significantly cheaper, not least in computer storage.

CHAPTER 9

CONCLUDING REMARKS

9.1 Main results of the present study

The main achievements of the present study and the conclusions thereof may be summarised as follows:

1) The parabolic calculation procedure has been successfully applied to predict the laminar flow and heat transfer in mildly-curved circular pipes. The computed distributions of mean velocity, static pressure, temperature etc. displayed good agreement with experimental data.

2) The capabilities of the two-equation ($k\sim\varepsilon$) turbulence-model to predict the turbulent flow in curved ducts have been assessed. Predictions for turbulent flow and heat transfer in a 180^{o} bend agreed reasonably well with experiments but the agreement has not been as good as that observed for the case of laminar flows. The turbulence model, it is concluded, therefore requires modifications to account for the effects of secondary flow on the turbulence-structure.

3) A calculation procedure has been developed for economical handling of partially-parabolic flow situations. In this procedure, account is taken of the influences of downstream events which travel upstream via the pressure field. The distinctive features of this procedure are:

(a) it stores the pressure field as a three-dimensional array; and

(b) it performs several marching sweeps through the flow domain

In each sweep, the guessed pressure field is corrected so as ultimately to satisfy the momentum and continuity equations over the complete flow domain. The procedure has been successfully validated for turbulent flow in a strongly-curved rectangular duct. The predictions using this procedure have been observed to be in close agreement with experimental data; the results from the parabolic procedure, on the other hand, were at qualitative variance with measurements.

4) An experimental program has been successfully completed; measurements have been made of the distributions of velocity and pressure

for turbulent flow in a strongly-curved duct. The data obtained from this investigation have been useful in validating the partially-parabolic calculation procedure. Further, the measurements made close to the bottom wall of the duct have suggested that, in this region, the component of velocity along the wall-shear-stress direction varies in a logarithmic manner with distance from the wall.

5) The computing times required for the present calculations have been modest. The partially-parabolic procedure has been observed to be more economical than a fully-elliptic procedure; but in comparison with the parabolic procedure, the partially-parabolic procedure requires computing times three times as large.

9.2 Suggestions for future work

The present investigation suggests a few areas where further research is needed to improve the present capabilities to predict flows in curved ducts; these areas are as follows.

1) First, it shall be beneficial from view point of economy if the convergence rate of the partially-parabolic calculation

procedure can be further improved. At this stage, the author is not aware of any specific improvements to the procedure, except those discussed in Section 4.7; but it is recommended that in future studies concerning the partially-parabolic calculation procedure, attention may be focussed also on this aspect.

2) A second observation from the present study is concerned with the turbulence model currently employed to predict flows in curved ducts. It appears from the present calculations that turbulence models based on the concept of turbulent viscosity do not completely represent the turbulence structure in curved ducts. Further testing of the turbulence model needs to be made to establish that the present conclusions are sound, by predicting other experimental data in curved ducts and in similar flow situations (e.g. flows with rotation, buoyancy etc). If the present conclusions are firmly proved, it is necessary then to develop either more-complex turbulence-models, such as the Reynolds-stress models, or to devise empirical modifications to the current two-equation turbulence model.

Both these refinements to the turbulence model will need some experimental information on the turbulence structure in curved ducts which, at the moment is lacking; it is therefore also necessary to make measurements of the turbulence structure in curved ducts.

LIST OF REFERENCES

1. ADLER M (1934): "Stromung in gerkrummten Rohren", Z. ang. Mathemati u Mechani , 14, 257.

2. AKIYAMA M and CHENG K C (1971): "Boundary-vorticity method for laminar forced convection heat transfer in curved pipes", International Journal of Heat and Mass Transfer, 14, 1659.

3. AMSDEN A A and HARLOW F H (1970): "The SMAC method: a numerical technique for calculating incompressible fluid flows", Los Almos Scientific Laboratory, LA-4370.

4. AUSTIN L R (1971): "The development of viscous flow within helical coils", Ph.D. Thesis, University of Utah, Utah.

5. AUSTIN L R and SEADER J D (1973): "Fully-developed viscous flow in coiled circular pipes", AIChE Journal, 19, 1, 85.

6. BARUA S N (1962): "On secondary flow in stationary curved pipes", Quarterly Journal of Mechanics and Applied Mathematics, 16, 61.

7. CARETTO L S, CURR R M and SPALDING D B (1972): "Two numerical methods for three-dimensional boundary layers", Computer Methods in Applied Mechanics and Engineering, 1, 39.

8. CARETTO L S, GOSMAN A D, PATANKAR S V and SPALDING D B (1972): "Two calculation procedures for steady three-dimensional flows with recirculation", Proceedings of the third International Conference on Numerical Methods in Fluid Mechanics, II, 60.

9. CHORIN A J (1968): "Numerical solution of the Navier-Stokes equations", Math. Computation, 22, 745.

10. DEAN W R (1927): "Note on the motion of fluid in a curved pipe", Philosophical Magazine, 4, 208.

11. DEAN W R (1928): "The stream-line motion in a curved pipe", ibid., 5, 673.

12. DETRA R W (1953): "The secondary flow in curved pipes", Mitt. aus dem Institut fur Aerodynamik, E.T.H. Zürich, No. 20.

13. DRAVID A N, SMITH K A, MERILL E W and BRIAN P L T (1971): "Effect of secondary-fluid motion on laminar flow heat transfer in helically-coiled tubes, AIChE Journal, 17, 5, 1114.

14. EDE A J (1960): "Effect of an abrupt disturbance of the flow on a local heat transfer coefficient in a pipe. Right-angled bend: radius ration 21:1", National Engineering Laboratory Report No. Heat 181.

15. EDE A J (1963): "Effect of an abrupt disturbance of the flow on the local heat transfer coefficient in a pipe. 180^{o} hairpin bend: radius ratio 22:1", National Engineering Laboratory Report No. 104.

16. EDE A J (1966): "The effect of a 180^{o} bend on heat transfer to water in a tube", National Engineering Laboratory Report No. 257.

17. EICHENBERGER H P (1953): "Shear flow in bends", Journal of Mathematics and Physics, 32, 34.

18. FISH P E J (1970): "Three-dimensional flow of fluids in ducts", Ph.D. Thesis, London University.

19. FRANCIS G P (1965): "Incompressible flow of the three-dimensional turbulent boundary layer on the floor of curved channels", Ph.D. Thesis, Cornell University.

20. GOSMAN A D, PUN W M, RUNCHAL A K, SPALDING D B and WOLFSHTEIN M (1969): "Heat and mass transfer in recirculating flows", Academic Press, London.

21. GOSMAN A D and SPALDING D B (1971): "The prediction of confined three-dimensional boundary layers", Proceedings of a conference on internal flows, held at Universtiy of Salford, England, 1971.

22. GREENSPAN D (1973): "Secondary flow in a curved tube, Journal of Fluid Mechanics, 57, 167.

23. GRUSCHWITZ E (1935): "Turbulent reibungsschichten mit sekundarstromung", Ingenieur-Archiv, 6, 355.

24. HARLOW F H and WELCH J E (1965): "Numerical calculation of time-dependent viscous incompressible flow of fluid with free surface", The Physics of Fluids, 8, 2182.

25. HARLOW F H and NAKAYAMA P (1968): "Transport of turbulence energy decay rate", Los Almos Scientific Lab., University of California Report LA-3854.

26. HARLOW F H (1973): "Turbulence transport modelling", AIAA Selected Reprint Series, 15.

27. HAWES W B (1932): "Some sidelights of the heat transfer problem", Transactions Institution of Chemical Engineers, 10, 162.

28. HAWTHORNE W R (1951): "Secondary circulation in fluid flow", Proceedings of the Royal Society, 206A, 374.

29. HAWTHORNE W R (1963): "Flow in bent pipes", Proceedings of Seminar in Aeronautical Sciences, National Aeronautical Laboratory, Bangalore, India, 305.

30. HAWTHORNE W R (1965): Chapter 1 in "Research frontiers in fluid dynamics", ed. R J Seeger and G Temple, Interscience, New York.

31. HAWTHORNE W R (1966): "The applicability of secondary flow analyses to the solution of internal flow problems" in Fluid Mechanics of Internal Flow, ed. G Sovran, Elsevier, Amsterdam.

32. HOGG G W (1968): "The effect of secondary flow on point heat transfer coefficients for turbulent flow inside curved tubes", Ph.D. Thesis, University of Idaho.

33. HOGG G W and SEADER J D (1969): "Prediction of point heat-transfer coefficients for turbulent flow inside curved tubes", paper presented at the AIChE 62nd Annual meeting, Washington, D.C.

34. HOGG G W and SEADER J D (1970): "The peripheral secondary-velocity components for turbulent flow inside curved tubes", paper presented at the AIChE 67th National meeting, Atlanta, Georgia.

35. HORLOCK J H (1956): "Some experiments on secondary flow in pipe bends", Proceedings of the Royal Society, A234, 335.

36. ITO H (1969): "Laminar flow in curved pipes", Z. Angnew Mathematics u Mechanics, 49, 653.

37. ITO H (1959): "Friction factors for turbulent flow in curved pipes", Transactions ASME, J. Basic Engineering, D81, 123.

38. JERIE J (1971): "An investigation of the flow in a 90 degree rectangular duct with special emphasis on the three-dimensional boundary layer", M.A.Sc. Thesis, University of Waterloo.

39. JONES W P and LAUNDER B E (1972): "The prediction of laminarisation with a 2-equation model of turbulence", International J. Heat and Mass Transfer, 15, 301.

40. JOY W (1950): "Experimental investigation of flow in rectangular bends", M.S. Thesis, Massachusetts Institute of Technology.

41. KALB C E and SEADER J D (1972): "Heat and mass transfer phenomena for viscous flow in curved circular pipes", International Journal of Heat and Mass Transfer, 15, 801.

42. KULEGAN G H and BEIJ K H (1937): "Pressure losses for fluid flow in curved pipes", Bureau of Standards, 18, 89.

43. LAUNDER B E (1971): "An improved modelling of the Reynolds stresses", Imperial College, Mechanical Engineering Department, Report TM/TN/A/9.

44. LAUNDER B E and SPALDING D B (1972): "Mathematical models of turbulence", Academic Press, London.

45. LAUNDER B E, MORSE A, RODI W and SPALDING D B (1972): "The prediction of free shear flows - A comparison of the performance of six turbulence models", Proceedings of NASA Conference on Free Shear Flows, Langely, USA.

46. LAUNDER B E and SPALDING D B (1973): "The numerical computation of turbulent flows", Computer Methods for Applied Mechanics and Engineering, 3, 269.

47. McMILLAN F A (1957): "Experiments on Pitot tubes in shear flow", British Aeronautical Research Council, R & M No. 3028.

48. McCONALOGUE D J (1969): "Motion of a fluid in a curved tube", Ph.D. Thesis, London University.

49. MELLOR G L and HERRING H J (1973): "A survey of mean turbulent field closure models", AIAA Journal, 11, 5, 590.

50. MORI Y and NAKAYAMA W (1965): "Study on forced convective heat transfer in curved pipes", International Journal of Heat and Mass Transfer, 8, 67.

51. MORI Y and NAKAYAMA W (1967): "Study on forced convective heat transfer in curved pipes", International Journal of Heat and Mass Transfer, 10, 37.

52. NASH J F and PATEL V C (1972): "Three-dimensional turbulent boundary layers", SBC Technical books Inc., Atlanta.

53. OLSON D E (1971): "Fluid mechanics relevant to respiratory flow within curved or elliptical tubes and bifurcating systems", Ph.D. Thesis, London University.

54. PATANKAR S V and SPALDING D B (1972): "Heat and mass transfer in boundary layers", Intertext Books, London.

55. PATANKAR S V and SPALDING D B (1972): "A calculation procedure for heat, mass and momentum transfer in three-dimensional parabolic flows", International Journal of Heat and Mass Transfer, 15, 1787.

56. PATANKAR S V, PRATAP V S and SPALDING D B (1974): "Prediction of laminar flow and heat transfer in helically-coiled pipes", Journal of Fluid Mechanics, 62, 3, 539.

57. PATANKAR S V, PRATAP V S and SPALDING D B (1975): "Prediction of turbulent flow in curved pipes", Journal of Fluid Mechanics, 67, 3, 595.

58. PATEL V C (1965): "Calibration of Preston tube and limitations on its use in pressure gradients", Journal of Fluid Mechanics, 23, 1, 185.

59. PRANDTL L (1925): "Veber die ausgebildete turbulenz", ZAMM, 15, 136.

60. PRATAP V S and SPALDING D B (1975): "Numerical computations of the flow in curved ducts", Imperial College, Mechanical Engineering Department, Report No. HTS/75/3.

61. ROWE M (1966): "Some secondary flow problems in fluid dynamics", Ph.D. Thesis, Cambridge University.

62. SEBAN R A and McLAUGHLIN E F (1963): "Heat transfer in tube coils with laminar and turbulent flow", International Journal of Heat and Mass Transfer, 6, 387.

63. SHARMA D (1974): "Turbulent convective phenomena in straight rectangular-sectioned diffusers", Ph.D. Thesis, London University.

64. SINGH M P (1974): "Entry flow in a curved pipe", Journal of Fluid Mechanics, 65, 517.

65. SPALDING D B (1971): Unpublished notes at Imperial College.

66. SPALDING D B (1972): "A novel finite-difference formulation for differential expressions involving both first and second derivatives", Int. J. Numerical Methods in Engg., 4, pp. 551-559.

67. SPALDING D B (1974): Private communication.

68. SPALDING D B (1975): Private communication.

69. SQUIRE H B (1954): "Note on secondary flow in a curved circular pipe", British Aeronautical Research Council Report no. 16,601.

70. SQUIRE H B and WINTER K G (1951): "The secondary flow in a cascade of airfoils in a non-uniform stream", Journal of Aeronautical Sciences, 18, 271.

71. SRINIVASAN P S, NANDAPURKAR S S and HOLLAND F A (1968): "Pressure drop and heat transfer in coils", The Chemical Engineer, CE 113.

72. STUART A R and HETHERINGTON R (1970): "The solution of the three-variable duct flow equations", Proceedings of Symposium held at Pennsylvania State University on fluid mechanics, acoustics and design of turbo-machinery, August 1970.

73. TARBELL J M and SAMUELS M R (1973): "Momentum and heat transfer in helical coils", Chemical Engineering Journal, 5, 117.

74. TATCHELL D G (1975): "Convection processes in confined, three-dimensional boundary layers", Ph.D. Thesis, London University.

75. TRUESDELL L C (Jr) and ADLER R J (1970): "Numerical treatment of fully-developed laminar flow in helically-coiled tubes", AIChE Journal, 16, 6, 1010.

76. VERMEULEN A J (1971): "Measurements in three-dimensional turbulent boundary-layers", Ph.D. Thesis, Cambridge University.

77. YAO L and BERGER S A (1975): "Entry flow in a curved pipe", Journal of Fluid Mechanics, 67, 1, 177.

78. YOUNG J W S (1973): "Three-dimensional turbulent boundary layers - an investigation in the curved duct environment", Ph.D. Thesis, University of Waterloo.

79. YOUNG J W S (1972): "Calibration report and user's guide for the aspect ratio $\frac{1}{4}$, 90 degree bend", Internal report on laboratory procedures, Department of Mechanical Engineering, University of Waterloo.

80. YOUNG J W S, HOWARD J H G and JERIE J (1972): "A zero-streamwise-pressure-gradient three-dimensional turbulent boundary layer in a 90° curved rectangular duct", Transactions of the CSME, 1, 2, 87.

NOMENCLATURE

Symbol	Meaning	Location of first appearance
A	coefficient in the discretised equation.	Eqn. (4.2.8)
a	radius of pipe.	Sec. (2.2.2)
B	coefficient in the finite-difference equation; represents contribution from upstream and source terms.	Eqn. (4.2.8)
C	cell areas for calculating mass fluxes.	Eqn. (4.2.14)
C_1, C_2, C_μ	constants in the turbulence model.	Eqns. (5.3.2-5.3.4)
c_p	specific heat.	Eqn. (5.4.6)
c_f	coefficient of skin friction ($\tau_W / \frac{1}{2} \rho Q^2$).	Eqn. (6.6.1)
D^u, D^v, D^w	coefficients of pressure gradient terms.	Eqns. (4.2.10-4.2.12)
d	diameter of pitot probe.	
E	constant in the log law.	Eqn. (5.4.1)
F	coefficient in the discretised equation.	Eqn. (4.2.3)
f	friction factor ($dp/dz \; / \; \frac{1}{2}\rho w_{av}^2$); also interpolation factor in Eqn. (4.2.4).	Sec. (7.2.2)
G	generation of turbulence energy.	Eqn. (5.3.3)
$J_{\phi,i}$	flux of ϕ in the i^{th} direction.	Eqn. (3.2.5)

Symbol	Meaning	Location of first appearance
K	Dean number.	Sec. (2.2.2)
k	kinetic-energy of turbulence.	Sec. (5.1)
L	convection coefficients in the derivation of the discretised equation.	Eqn. (4.2.2)
$\dot{m}$	residual mass source.	Eqn. (4.2.18)
$\bar{m}$	total mass into the flow domain through inlet and boundaries.	Eqn. (4.3.7)
P_T	P function in the wall functions for the energy equation.	Eqn. (5.4.6)
p	pressure.	Eqn. (3.2.2)
$\bar{p}$	average pressure field, used in the parabolic procedure.	Eqn. (3.2.7)
Q	total velocity at the centre of the cross-sectional plane.	Eqn. (6.6.1)
q	total velocity at a point.	Eqn. (5.4.1)
R	radius of curvature.	Eqn. (3.2.8)
r	coordinate in the cylindrical polar system.	Eqn. (3.2.8)
s	source/sink term.	Eqn. (3.2.2)
T	temperature; also used to represent diffusion terms, in equation (4.2.2).	Eqn. (5.4.6)
u,v,w	the three velocity components.	Eqn. (3.2.1)
x,y,z	coordinates in the cartesian system.	Eqn. (3.2.1)

Symbol	Meaning	Location of first appearance
y^+	non-dimensional distance used in a relation $u^+=f(y^+)$ to express the velocity-variation.	Sec. (5.3)
y_N	distance from wall to the interface of the near-wall control volume.	Eqn. (5.4.5)

Greek symbols

α	relaxation factor.	Sec. (4.2.6)
β	reduction factor; defined by equation (A2.).	Eqn. (4.4.3)
δ,Δ	difference of	Fig. (4.2.4)
ϵ	dissipation rate of turbulence kinetic-energy.	Sec. (5.1)
Γ	exchange coefficient.	Eqn. (3.2.9)
ρ	density of fluid.	Eqn. (3.2.2)
η,ζ,ξ	coordinates in the (η,ζ,ξ)system.	Eqn. (3.2.12)
θ	coordinate in the cylindrical-polar system.	Eqn. (3.2.8)
μ	coefficient of viscosity.	Eqn. (5.3.5)
κ	constant in the logarithmic law for variation of near-wall-velocity.	Eqn. (5.4.1)
ν	kinematic viscosity.	Eqn. (6.6.1)
λ	dimensionless wavelength.	Sec. (7.2.2)
Φ	general flow variable.	Eqn. (3.2.5)

Symbol	Meaning	Location of first appearance
ϕ	coordinate in the (r,θ,ϕ) and (x,y,ϕ) systems.	Eqn. (3.2.8)
τ	shear stress.	Eqn. (3.2.2)
σ	Prandtl/Schmidt number.	Eqn. (5.3.6)

Subscripts

av	average over the cross section; also denotes peripheral average in Fig. (7.2.21).	Fig. (7.2.3)
cl	centre line.	Fig. (7.3.5(a))
D	downstream.	Eqn. (4.2.12)
E	east grid-node; also east boundary in eqn. (3.2.12).	Eqn. (4.2.2)
e	east interface.	Eqn. (4.2.2)
eff	effective value.	Eqn. (A1.2.15)
f	frictional component.	Eqn. (6.6.1)
k	kinetic-energy of turbulence.	Eqn. (5.3.3)
ℓ	laminar value.	Eqn. (5.3.5)
m	mean value; average of outside and inside.	Fig. (7.2.21)
N	north grid-node; also north boundary in eqn. (3.2.12).	Eqn. (4.2.2)
n	north interface	Eqn. (4.2.2)
new	new value.	Eqn. (4.4.3)
O	inlet.	Fig. (8.4.9)

Symbol	Meaning	Location of first appearance
old	old value.	Eqn. (4.4.3)
P	at point P.	Eqn. (4.2.2)
r	r coordinate direction.	Eqn. (A1.2.2)
S	south grid node; also south boundary in eqn. (3.2.12).	Eqn. (4.2.2)
s	south interface.	Eqn. (4.2.2)
T	temperature.	Eqn. (5.3.6)
t	turbulent.	Eqn. (5.3.5)
U	upstream.	Sec. (4.2.5)
u	u velocity.	Eqn. (3.2.2)
v	v velocity.	Eqn. (3.2.3)
W	west grid node; also wall.	Eqn. (4.2.2)
w	w velocity; also west interface in eqn. (4.2.2).	Eqn. (3.2.4)
x,y,z	coordinate directions.	Eqn. (3.2.2)
Φ	general variable.	Eqn. (3.2.5)
ε	dissipation rate of kinetic-energy of turbulence.	Eqn. (5.3.4)
θ	coordinate.	Eqn. (A1.2.2)
η,ζ,ξ	coordinates.	Eqn. (A1.4.6)

Superscripts

Symbol	Meaning	Location of first appearance
p	pressure correction.	Eqn. (4.2.17)
u,v,w	velocity components.	Eqn. (4.2.10-4.2.12)
x,y	coordinate directions.	Eqn. (4.2.2)
*	approximate value.	Eqn. (4.2.15)
'	denotes corrections in Chapter 4 and fluctuating component in Chapter 5 and elsewhere.	Eqn. (4.2.15)

APPENDIX A1

THE GOVERNING DIFFERENTIAL EQUATIONS

A1.1 Introduction

In this appendix, the partial-differential equations governing the steady, three-dimensional incompressible flow and heat-transfer phenomena in curved ducts are described in their full form. The equations are expressed in the three coordinate systems mentioned in Chapter 3, namely the (r,θ,ϕ), the (x,y,ϕ) and the (η,ζ,ξ) systems. The equations stated here are identical for laminar and turbulent flow situations except that for turbulent flows, the shear stresses are calculated from an 'effective' exchange-coefficient which is the sum of the laminar and turbulent exchange-coefficients; also, for laminar flows the equations for the kinetic-energy of turbulence and its dissipation rate are not solved. The following sets of equations are stated in their partially-parabolic form; if their parabolic form is desired, only the longitudinal momentum equation needs to be rewritten using a $\bar{p}$ pressure field.

A1.2 The (r,θ,ϕ) coordinate system

The partial-differential equations governing flow and heat-transfer phenomena in a flow situation

described by the (r, θ, ϕ) coordinate system are as follows:

Continuity:

$$\frac{\partial u}{\partial r} + \frac{\partial v}{r\partial\theta} + \frac{u}{r} + \frac{\partial w}{R\partial\phi} + \frac{(u\cos\theta - v\sin\theta)}{R} = 0 \qquad \text{(A1.2.1)}$$

r-momentum:

$$\rho\left(u\frac{\partial u}{\partial r} + \frac{v}{r}\frac{\partial u}{\partial\theta} - \frac{v^2}{r} + \frac{w}{R}\frac{\partial u}{\partial\phi} - \frac{w^2}{R}\cos\theta\right) = -\frac{\partial p}{\partial r} + \frac{\partial\tau_{rr}}{\partial r} + \frac{1}{r}\frac{\partial\tau_{r\theta}}{\partial\theta} - \frac{\tau_{\theta\theta}}{r} + \frac{1}{r}\tau_{rr} + \frac{\tau_{rr}}{R}\cos\theta - \frac{\tau_{r\theta}}{R}\sin\theta \qquad \text{(A1.2.2)}$$

θ-momentum:

$$\rho\left(u\frac{\partial v}{\partial r} + \frac{u}{r}\frac{\partial v}{\partial\theta} + \frac{uv}{r} + \frac{w}{R}\frac{\partial v}{\partial\phi} + \frac{w^2}{R}\sin\theta\right) = -\frac{\partial p}{r\partial\theta} + \frac{\partial\tau_{\theta r}}{\partial r} + \frac{\partial\tau_{\theta\theta}}{r\partial\theta} + \frac{2}{r}\tau_{r\theta} + \frac{\tau_{\theta r}}{R}\cos\theta - \frac{\tau_{\theta\theta}}{R}\sin\theta \qquad \text{(A1.2.3)}$$

ϕ-momentum:

$$\rho \left(u \frac{\partial w}{\partial r} + \frac{v}{r} \frac{\partial w}{\partial \theta} + \frac{w \partial w}{R \partial \phi} + \frac{w}{R} (u \cos\theta - v \sin\theta)\right)$$

$$= - \frac{\partial p}{R \partial \phi} + \frac{\tau_{\phi r}}{\partial r} + \frac{\tau_{\phi r}}{r} + \frac{\tau_{\phi r}}{R} \cos\theta - \frac{\tau_{\phi\theta}}{R} \sin\theta + \frac{\partial \tau_{\phi\theta}}{r \partial \theta}$$

(A1.2.4)

Kinetic-energy of turbulence (k):

$$\rho \left(u \frac{\partial k}{\partial r} + \frac{v}{r} \frac{\partial k}{\partial \theta} + \frac{w}{R} \frac{\partial k}{\partial \phi}\right) = \frac{\partial}{\partial r} \left(\Gamma_{eff,k} \frac{\partial k}{\partial r}\right) + \frac{1}{r} \Gamma_{eff,k} \frac{\partial k}{\partial r}$$

$$+ \frac{1}{R} \left(\Gamma_{eff,k} \frac{\partial k}{\partial r} \cos\theta - \Gamma_{eff,k} \frac{\partial k}{r \partial \theta} \sin\theta\right)$$

$$+ \frac{\partial}{r^2 \partial \theta} \left(\Gamma_{eff,k} \frac{\partial k}{\partial \theta}\right) + G - \rho\varepsilon$$

(A1.2.5)

Rate of dissipation of k(ε):

$$\rho \left(u \frac{\partial \varepsilon}{\partial r} + \frac{v}{r} \frac{\partial \varepsilon}{\partial \theta} + \frac{w}{R} \frac{\partial \varepsilon}{\partial \phi}\right) = \frac{\partial}{\partial r} \left(\Gamma_{eff,\varepsilon} \frac{\partial \varepsilon}{\partial r}\right) + \frac{1}{r} \Gamma_{eff,\varepsilon} \frac{\partial \varepsilon}{\partial r}$$

$$+ \frac{1}{R} \left(\Gamma_{eff,\varepsilon} \frac{\partial \varepsilon}{\partial r} \cos\theta - \Gamma_{eff,\varepsilon} \frac{\partial \varepsilon}{r \partial \theta} \sin\theta\right)$$

$$+ \frac{\partial}{r^2 \partial \theta} \left(\Gamma_{eff,\varepsilon} \frac{\partial \varepsilon}{\partial \theta}\right) + C_1 \frac{\varepsilon}{k} G - C_2 \frac{\rho \varepsilon^2}{k}$$

(A1.2.6)

Energy, h:

$$\rho \left(u \frac{\partial h}{\partial r} + \frac{v}{r} \frac{\partial h}{\partial \theta} + \frac{w}{R} \frac{\partial h}{\partial \phi}\right) = \frac{\partial}{r \partial r} \left(r \Gamma_{eff,h} \frac{\partial h}{\partial r}\right) + \frac{\partial}{r^2 \partial \theta} \left(\Gamma_{eff,h} \frac{\partial h}{\partial \theta}\right)$$

$$+ \frac{\Gamma_{eff,h}}{R} \left(\frac{\partial h}{\partial r} \cos\theta - \frac{\partial h}{r \partial \theta} \sin\theta\right)$$

(A1.2.7)

The shear stresses in equations (A1.2.2) to (A1.2.4) are expressed below, after they have been simplified by the neglect of gradients in ϕ-direction.

$$\tau_{rr} = 2\mu \frac{\partial u}{\partial r} ; \qquad \text{(A1.2.8)}$$

$$\tau_{r\theta} = \mu \left(\frac{\partial u}{r\partial\theta} - \frac{v}{r} + \frac{\partial v}{\partial r}\right) = \tau_{\theta r} \qquad \text{(A1.2.9)}$$

$$\tau_{\theta\theta} = 2\mu \left(\frac{\partial v}{r\partial\theta} + \frac{u}{r}\right) \qquad \text{(A1.2.10)}$$

$$\tau_{\phi r} = \mu \left(\frac{\partial w}{\partial r} - \frac{w}{R}\cos\theta\right) \qquad \text{(A1.2.11)}$$

$$\tau_{\phi\theta} = \mu \left(\frac{\partial w}{r\partial\theta} + \frac{w}{R}\sin\theta\right) \qquad \text{(A1.2.12)}$$

where $\mu = \mu_\ell$ for laminar flows (A1.2.13(a))

$\mu = \mu_{eff} = (\mu_\ell + \mu_t)$ for turbulent flows (A1.2.13(b))

and $\mu_t = C_\mu \rho k^2/\varepsilon$ (A1.2.14)

The effective exchange coefficient for transport of a variable, Φ is

$$\Gamma_{eff,\Phi} = \frac{\mu_\ell}{\sigma_{\Phi,\ell}} + \frac{\mu_t}{\sigma_{\Phi,t}} \qquad \text{(A1.2.15)}$$

where the subscripts ℓ and t refer to the laminar and turbulent values and the subscript 'eff' refers to the

effective value. The expression for the generation of kinetic energy of turbulence is expressed as follows:

$$G = \mu_t \Bigg[2 \{ \left(\frac{\partial U_r}{\partial r}\right)^2 + \left(\frac{\partial U_\theta}{r\partial\theta}\right)^2 + \left(\frac{U_r}{r}\right)^2 + \frac{2}{r^2} U_r \frac{\partial U_\theta}{\partial\theta} - \frac{U_\theta}{r} \left(\frac{\partial U_r}{r\partial\theta} + \frac{\partial U_\theta}{\partial r}\right)\} + \left(\frac{\partial U_r}{r\partial\theta} + \frac{\partial U_\theta}{\partial r}\right)^2 + \left(\frac{\partial U_\phi}{\partial r}\right)^2 + \left(\frac{\partial U_\phi}{r\partial\theta}\right)^2 + \frac{U_\theta^2}{r^2} + \frac{U_\phi^2}{R^2} + \frac{2}{R} U_\phi \left(\frac{\partial U_\phi}{r\partial\theta} \sin\theta - \frac{\partial U_\phi}{\partial r} \cos\theta\right) \Bigg] \qquad \text{(A1.2.16)}$$

The terms which were treated in the form of source terms, from viewpoint of the computational procedure, can be obtained by subtracting, from the above equation, terms represented by the following equation:

$$\text{div}\ (G\Phi) = \text{div}\ (\Gamma_{eff}\ \text{grad}\ \Phi) \qquad \text{(A1.2.17)}$$

where G is the mass velocity vector;

Φ is the dependent variable of the equation;

Γ_{eff} is the effective exchange coefficient;

and the divergence and gradient operators have the following expressions in the present coordinate system:

$$\text{div } \vec{V} = \frac{\partial V_1}{\partial r} + \frac{\partial V_2}{r\partial\theta} + \frac{V_1}{r} + \frac{\partial V_3}{R\partial\phi} + \left(\frac{V_1 \cos\theta - V_2 \sin\theta}{R}\right) \qquad \text{(A1.2.18)}$$

where $\vec{V} = V_1\, i + V_2\, j + V_3\, k$;

and i, j, k are the unit vectors along r, θ, ϕ directions.

$$\text{grad } \Phi = \frac{\partial \Phi}{\partial r} + \frac{\partial \Phi}{r\partial\theta} + \frac{1}{R}\frac{\partial \Phi}{\partial \phi} \qquad \text{(A1.2.19)}$$

A1.3 The (x,y,ϕ) coordinate system

The governing differential equations for the (x,y,ϕ) coordinate system have been derived in a similar manner as those in Sec. (A1.2); the equations in the (x,y,ϕ) system are:

Continuity:

$$\frac{\partial u}{\partial x} + \frac{\partial v}{\partial y} + \frac{1}{R}\frac{\partial w}{\partial \phi} + \frac{u}{R} = 0 \qquad \text{(A1.3.1)}$$

x-momentum:

$$\rho\left(u\frac{\partial u}{\partial x} + v\frac{\partial u}{\partial y} + \frac{w}{R}\frac{\partial u}{\partial \phi} - \frac{w^2}{R}\right) = -\frac{\partial p}{\partial x} + \frac{\partial \tau_{xx}}{\partial x} + \frac{\partial \tau_{xy}}{\partial y} + \frac{\tau_{xx}}{R}$$

(A1.3.2)

y-momentum:

$$\rho \left(u \frac{\partial v}{\partial x} + v \frac{\partial v}{\partial y} + \frac{w}{R} \frac{\partial v}{\partial \phi}\right) = - \frac{\partial p}{\partial y} + \frac{\partial \tau_{yx}}{\partial x} + \frac{\partial \tau_{yy}}{\partial y} + \frac{\tau_{yx}}{R}$$

(A1.3.3)

ϕ-momentum:

$$\rho \left(u \frac{\partial w}{\partial x} + \frac{uw}{R} + v \frac{\partial w}{\partial y} + \frac{w}{R} \frac{\partial w}{\partial \phi}\right) = - \frac{\partial p}{R \partial \phi} + \frac{\partial \tau_{\phi x}}{\partial x}$$

$$+ \frac{\partial \tau_{\phi y}}{\partial y} + \frac{2}{R} \tau_{\phi x} \qquad \text{(A1.3.4)}$$

Kinetic energy of turbulence (k):

$$\rho \left(u \frac{\partial k}{\partial x} + v \frac{\partial k}{\partial y} + w \frac{\partial k}{R \partial \phi}\right) = \frac{\partial}{\partial x} \left(\Gamma_{eff,k} \frac{\partial k}{\partial x}\right) + \frac{\partial}{\partial y} \left(\Gamma_{eff,k} \frac{\partial k}{\partial y}\right)$$

$$\Gamma_{eff,k} \cdot \frac{1}{R} \frac{\partial k}{\partial x} + G - \rho \varepsilon \qquad \text{(A1.3.5)}$$

Rate of dissipation of k (ε):

$$\rho \left(u \frac{\partial \varepsilon}{\partial x} + v \frac{\partial \varepsilon}{\partial y} + w \frac{\partial \varepsilon}{R \partial \phi}\right) = \frac{\partial}{\partial x} \left(\Gamma_{eff,\varepsilon} \frac{\partial \varepsilon}{\partial x}\right) + \frac{\partial}{\partial y} \left(\Gamma_{eff,\varepsilon} \frac{\partial \varepsilon}{\partial y}\right)$$

$$\Gamma_{eff,\varepsilon} \frac{1}{R} \frac{\partial \varepsilon}{\partial x} + \frac{C_1 \varepsilon}{k} G - \frac{C_2 \rho \varepsilon^2}{k}$$

(A1.3.6)

The expressions for the shear stresses, after neglect of terms representing gradients in ϕ-direction are as follows:

$$\tau_{xx} = 2\mu \frac{\partial u}{\partial x} \qquad \text{(A1.3.7)}$$

$$\tau_{xy} = \mu \left(\frac{\partial u}{\partial y} + \frac{\partial v}{\partial x}\right) = \tau_{yx} \qquad \text{(A1.3.8)}$$

$$\tau_{yy} = 2\mu \frac{\partial v}{\partial y} \qquad \text{(A1.3.9)}$$

$$\tau_{\phi x} = \mu \left(\frac{\partial w}{\partial x} - \frac{w}{R}\right) \qquad \text{(A1.3.10)}$$

$$\tau_{\phi y} = \mu \left(\frac{\partial w}{\partial y}\right) \qquad \text{(A1.3.11)}$$

The expressions for μ are the same as in (A1.2.13) and (A1.2.14).

The term G, which represents the generation of turbulence kinetic-energy, is given by the following expression:

$$G = \mu_t \left[2 \left\{ \left(\frac{\partial u}{\partial x}\right)^2 + \left(\frac{\partial v}{\partial y}\right)^2 \right\} + \left(\frac{\partial u}{\partial y} + \frac{\partial v}{\partial x}\right)^2 + \left(\frac{\partial w}{\partial y}\right)^2 + \left(\frac{\partial w}{\partial x}\right)^2 - \frac{2}{R} w \frac{\partial w}{\partial x} + \frac{w^2}{R^2} + 2 \frac{u^2}{R^2} \right] \qquad \text{(A1.3.12)}$$

The divergence and gradient operators for the present coordinate system have the following forms:

$$\text{div } \vec{V} = \frac{\partial V_1}{\partial x} + \frac{\partial V_2}{\partial y} + \frac{1}{R}\frac{\partial V_3}{\partial \phi} + \frac{V_1}{R} \qquad \text{(A1.3.13)}$$

$$\text{grad } \Phi = \frac{\partial \Phi}{\partial x} + \frac{\partial \Phi}{\partial y} + \frac{\partial \Phi}{R\partial \phi} \qquad \text{(A1.3.14)}$$

The expression for $\vec{V}$ is the same as that described in (A1.2.18).

A1.4 The (η,ζ,ξ) system

The governing differential equations in the (η,ζ,ξ) coordinate system were derived by transforming the equations of (A1.3) using the following transformations:

$$\eta \equiv \frac{x - x_W}{x_E - x_W}$$

$$\zeta \equiv \frac{y - y_S}{y_N - y_S} \qquad \text{(A1.4.1)}$$

$$\xi \equiv \phi$$

The subscripts N, S, E and W refer respectively to the North, South, East and West boundaries in the x-y plane of the calculation domain, as illustrated in Figure (3.2.2(c)). In the above transformation, the coordinates η and ζ are mutually orthogonal for all values of ξ; and planes of constant-ξ are approximated as planes of constant-ϕ. The velocity components u and v are defined as before, to be normal to the y-z and x-z planes

respectively, i.e. to be aligned with the η and ζ coordinates. The w-component of velocity however, is defined to be along the grid lines joining two adjacent ($\eta \sim \zeta$) planes and thus is not <u>exactly</u> normal to the constant-ϕ direction. The coordinates (η,ζ,ξ) defined above satisfy the following relationships:

$$\frac{\partial}{\partial x} = \frac{\partial}{\partial \eta} \cdot \frac{\partial \eta}{\partial x} + \frac{\partial}{\partial \zeta} \cdot \frac{\partial \zeta}{\partial x} + \frac{\partial}{\partial \xi} \cdot \frac{\partial \xi}{\partial x}$$

$$\frac{\partial}{\partial y} = \frac{\partial}{\partial \eta} \cdot \frac{\partial \eta}{\partial y} + \frac{\partial}{\partial \zeta} \cdot \frac{\partial \zeta}{\partial y} + \frac{\partial}{\partial \xi} \cdot \frac{\partial \xi}{\partial y} \qquad \text{(A1.4.2)}$$

$$\frac{\partial}{\partial \phi} = \frac{\partial}{\partial \eta} \cdot \frac{\partial \eta}{\partial \phi} + \frac{\partial}{\partial \zeta} \cdot \frac{\partial \zeta}{\partial \phi} + \frac{\partial}{\partial \xi} \cdot \frac{\partial \xi}{\partial \phi}$$

These relations and the definitions of η, ζ, ξ given in (A1.4.1), when substituted in the equations for a (x,y,ϕ) system result in the following set of differential equations, which govern the three-dimensional flow in a curved diffuser of rectangular cross-section.

<u>Continuity</u>:

$$\frac{1}{(x_E - x_W)} \left\{ \frac{\partial u}{\partial \eta} - \frac{\partial w}{\partial \eta} \left(\frac{\partial x_W}{R \partial \xi} + \eta \frac{\partial}{R \partial \xi} (x_E - x_W) \right) \right\}$$

$$+ \frac{1}{(y_N - y_S)} \left\{ \frac{\partial v}{\partial \zeta} - \frac{\partial w}{\partial \zeta} \left(\frac{\partial y_S}{R \partial \xi} + \zeta \frac{\partial}{R \partial \xi} (y_N - y_S) \right) \right\}$$

$$+ \frac{1}{R} \frac{\partial w}{\partial \xi} + \frac{u}{R} = 0 \qquad \text{(A1.4.3)}$$

η-momentum:

$$\rho\left[\frac{1}{(x_E-x_W)}\frac{\partial u}{\partial \eta}\{u - w\,(\frac{\partial x_W}{R\partial \xi} + \eta\,\frac{\partial}{R\partial \xi}\,(x_E-x_W))\}\right.$$

$$+\frac{1}{(y_N-y_S)}\frac{\partial u}{\partial \zeta}\{u - w\,(\frac{\partial y_S}{R\partial \xi} + \xi\,\frac{\partial}{R\partial \xi}\,(y_N-y_S))\}$$

$$\left.+\frac{w}{R}\frac{\partial w}{\partial \xi} - \frac{w^2}{R}\right] = -\frac{1}{(x_E-x_W)}\frac{\partial p}{\partial \eta} + \frac{1}{(x_E-x_W)}\frac{\partial \tau_{\eta\eta}}{\partial \eta}$$

$$+\frac{1}{(y_N-y_S)}\frac{\partial \tau_{\eta\eta}}{\partial \zeta} + \frac{\tau_{\eta\eta}}{R}$$

(A1.4.4)

ζ-momentum:

$$\rho\left[\frac{1}{(x_E-x_W)}\frac{\partial v}{\partial \eta}\{u - w\,(\frac{\partial x_W}{R\partial \phi} + \eta\,\frac{\partial}{R\partial \phi}\,(x_E-x_W))\}\right.$$

$$+\frac{1}{(y_N-y_S)}\frac{\partial v}{\partial \zeta}\{v - w\,(\frac{\partial y_S}{R\partial \phi} + \zeta\,\frac{\partial}{R\partial \phi}\,(y_N-y_S))\}$$

$$\left.+\frac{w}{R}\frac{\partial w}{\partial \xi}\right] = -\frac{1}{(y_N-y_S)}\frac{\partial p}{\partial \zeta} + \frac{1}{(x_E-x_W)}\frac{\partial \tau_{\zeta\eta}}{\partial \eta}$$

$$+\frac{1}{(y_N-y_S)}\frac{\partial \tau_{\zeta\zeta}}{\partial \zeta} + \frac{\tau_{\zeta\eta}}{R}$$

(A1.4.5)

ϕ-momentum:

$$\rho \left[\frac{1}{(x_E - x_W)} \frac{\partial w}{\partial \eta} \{u - w \left(\frac{\partial x_W}{R \partial \phi} + \eta \frac{\partial}{R \partial \phi} (x_E - x_W) \right)\} \right.$$

$$+ \frac{1}{(y_N - y_S)} \frac{\partial w}{\partial \zeta} \{v - w \left(\frac{\partial y_S}{R \partial \phi} + \zeta \frac{\partial}{R \partial \phi} (y_N - y_S) \right)\}$$

$$\left. + \frac{w}{R} \frac{\partial w}{\partial \xi} + \frac{uw}{R} \right] = - \frac{\partial p}{R \partial \xi} + \frac{1}{(x_E - x_W)} \frac{\partial \tau_{\xi\eta}}{\partial \eta} + \frac{1}{(y_N - y_S)} \frac{\partial \tau_{\xi\zeta}}{\partial \zeta}$$

$$+ \frac{2}{R} \tau_{\xi\eta}$$

(A1.4.6)

Kinetic energy of turbulence (k):

$$\rho \left[\frac{1}{(x_E - x_W)} \frac{\partial k}{\partial \eta} \{u - w \left(\frac{\partial x_W}{R \partial \phi} + \eta \frac{\partial}{R \partial \phi} (x_E - x_W) \right)\} \right.$$

$$+ \frac{1}{(y_N - y_S)} \frac{\partial k}{\partial \zeta} \{v - w \left(\frac{\partial y_S}{R \partial \phi} + \zeta \frac{\partial}{R \partial \phi} (y_N - y_S) \right)\}$$

$$\left. + w \frac{\partial k}{R \partial \xi} \right] = \frac{1}{(x_E - x_W)^2} \frac{\partial}{\partial \eta} \left(\frac{\mu_{eff}}{\sigma_k} \frac{\partial k}{\partial \eta} \right)$$

$$+ \frac{1}{(y_N - y_S)^2} \frac{\partial}{\partial \zeta} \left(\frac{\mu_{eff}}{\sigma_k} \frac{\partial k}{\partial \zeta} \right)$$

$$+ \frac{1}{(x_E - x_W)} \frac{\mu_{eff}}{\sigma_k} \frac{1}{R} \frac{\partial k}{\partial \eta} + G - \rho \varepsilon$$

(A1.4.7)

Rate of dissipation of k (ε):

$$\rho\Bigg[\frac{1}{(x_E-x_W)}\frac{\partial\varepsilon}{\partial\eta}\{u - w\,(\frac{\partial x_W}{R\partial\phi} + \eta\,\frac{\partial}{R\partial\phi}\,(x_E-x_W))\}$$

$$+\frac{1}{(y_N-y_S)}\frac{\partial\varepsilon}{\partial\zeta}\{v - w\,(\frac{\partial y_S}{R\partial\phi} + \zeta\,\frac{\partial}{R\partial\phi}\,(y_N-y_S))\}$$

$$+ w\,\frac{\partial\varepsilon}{\partial\xi}\Bigg] = \frac{1}{(x_E-x_W)^2}\frac{\partial}{\partial\eta}\,(\frac{\mu_{eff}}{\sigma_\varepsilon}\frac{\partial\varepsilon}{\partial\eta})$$

$$+\frac{1}{(y_N-y_S)^2}\frac{\partial}{\partial\zeta}\,(\frac{\mu_{eff}}{\sigma_\varepsilon}\frac{\partial\varepsilon}{\partial\zeta})$$

$$+\frac{1}{(x_E-x_W)}\frac{1}{R}\frac{\partial\varepsilon}{\partial\eta} + \frac{C_1\varepsilon}{k}\,G - \frac{C_2\,\rho\varepsilon^2}{k} \qquad \text{(A1.4.8)}$$

The expressions for the shear stresses can be derived in a similar way by transforming equations (A1.3.7) to (A1.3.11), which thereupon result in the following expressions.

$$\tau_{\eta\eta} = 2\mu\,\frac{1}{(x_E-x_W)}\frac{\partial u}{\partial\eta} \qquad \text{(A1.4.9)}$$

$$\tau_{\eta\zeta} = \mu\{(\frac{1}{(y_N-y_S)})\,\frac{\partial u}{\partial\zeta} + \frac{1}{(x_E-x_W)}\frac{\partial v}{\partial\eta}\} = \tau_{\zeta\eta} \qquad \text{(A1.4.10)}$$

$$\tau_{\zeta\zeta} = 2\mu\,\frac{1}{(y_N-y_S)}\,(\frac{\partial v}{\partial\zeta}) \qquad \text{(A1.4.11)}$$

$$\tau_{\xi\eta} = \mu\,\{\,\frac{1}{(x_E-x_W)}\frac{\partial w}{\partial\eta} - \frac{w}{R}\,\} \qquad \text{(A1.4.12)}$$

$$\tau_{\xi\zeta} = \mu\,\{\,\frac{1}{(y_N-y_S)}\frac{\partial w}{\partial\zeta}\,\} \qquad \text{(A1.4.13)}$$

The generation of kinetic-energy of turbulence, G is transformed into the following form:

$$G = \mu_t \Bigg[2 \left\{ \frac{1}{(x_E - x_W)^2} \left(\frac{\partial u}{\partial \eta}\right)^2 + \frac{1}{(y_N - y_S)^2} \left(\frac{\partial v}{\partial \zeta}\right)^2 \right\} + \left(\frac{1}{(x_E - x_W)} \frac{\partial u}{\partial \eta} + \frac{1}{(y_N - y_S)} \frac{\partial v}{\partial \zeta}\right)^2 + \frac{1}{(y_N - y_S)^2} \left(\frac{\partial w}{\partial \zeta}\right)^2 + \frac{1}{(x_E - x_W)^2} \left(\frac{\partial w}{\partial \eta}\right)^2 - \frac{1}{(x_E - x_W)} \frac{2w}{R} \frac{\partial w}{\partial \eta} + \frac{w^2}{R^2} + \frac{2\,u^2}{R^2} \Bigg] \qquad \text{(A1.4.14)}$$

The expressions for the divergence and gradient operators for the (η, ζ, ξ) coordinate system are as follows:

$$\text{div } \vec{V} = \frac{1}{(x_E - x_W)} \left\{ \frac{\partial V_1}{\partial \eta} - \frac{\partial V_3}{\partial \eta} \left(\frac{\partial x_W}{R \partial \xi} + \eta \frac{\partial}{R \partial \xi} (x_E - x_W)\right)\right\} + \frac{1}{(y_N - y_S)} \left\{ \frac{\partial V_2}{\partial \zeta} - \frac{\partial V_3}{\partial \zeta} \left(\frac{\partial y_S}{R \partial \xi} + \zeta \frac{\partial}{R \partial \xi} (y_N - y_S)\right)\right\} + \frac{1}{R} \frac{\partial V_3}{\partial \xi} + \frac{V_1}{R} \qquad \text{(A1.4.15)}$$

$$\text{grad } \Phi = \frac{1}{(x_E - x_W)} \frac{\partial \Phi}{\partial \eta} \left\{1 - \frac{\partial x_W}{R \partial \xi} - \eta \frac{\partial}{R \partial \xi} (x_E - x_W)\right\} + \frac{1}{(y_N - y_S)} \frac{\partial \Phi}{\partial \zeta} \left\{1 - \frac{\partial y_S}{R \partial \xi} - \zeta \frac{\partial}{R \partial \xi} (y_N - y_S)\right\} + \frac{1}{R} \frac{\partial \Phi}{\partial \xi} \qquad \text{(A1.4.16)}$$

APPENDIX A2

A MODIFICATION TO THE PARTIALLY-PARABOLIC CALCULATION PROCEDURE

A2.1 Introduction

In this appendix, a modification to the calculation procedure for partially-parabolic flows is described. This modification, suggested by Spalding (1974), has been observed to improve the rate of convergence (i.e. rate of diminution of the pressure-corrections) of the calculation procedure. In this modification parts of the pressure-corrections calculated at a downstream location are applied to the pressure field at the upstream stations, the purpose being to compensate for the mass imbalances caused by the downstream pressure-corrections. Details of this modification are as follows.

A2.2 Details of the modification

The central idea in the modification is to apply parts of the pressure corrections calculated at any location to all upstream stations. The reason for correcting the upstream pressures is as follows. In the unmodified procedure, the equation for pressure corrections was derived by assuming that the pressure field at adjacent cross-sectional planes remains unaltered; and thus p_U' and p_D' in equation (4.2.8) were put equal to

zero. This assumption was necessary to make the pressure-correction equation two-dimensional* so as to reduce the necessary computer-storage.

However this practice, although advantageous has two shortcomings. First, since the corrections made at any downstream location disturb the mass balance at the upstream locations, and since p_U' is assumed to be zero these imbalances are not compensated. Second, the influences of the downstream events are not quickly disseminated upstream; for the influences travel only at the rate of one plane per sweep through the flow domain. Both these disadvantages decrease the rate of convergence of the calculation procedure.

The present modification is introduced to overcome the above defects. The aim is to compensate the mass imbalances at the upstream locations without changing the existing practices for calculating the pressure-corrections, i.e. without changing the two-dimensional form of the pressure-correction equation. This is achieved by once again correcting the upstream pressures, the amounts of which are calculated in the following manner.

Consider the control volume shown in Figure (A2.1). In this diagram, the point P is the location

---

*By two-dimensional it is meant that the corrections are calculated for one cross-sectional plane at any time.

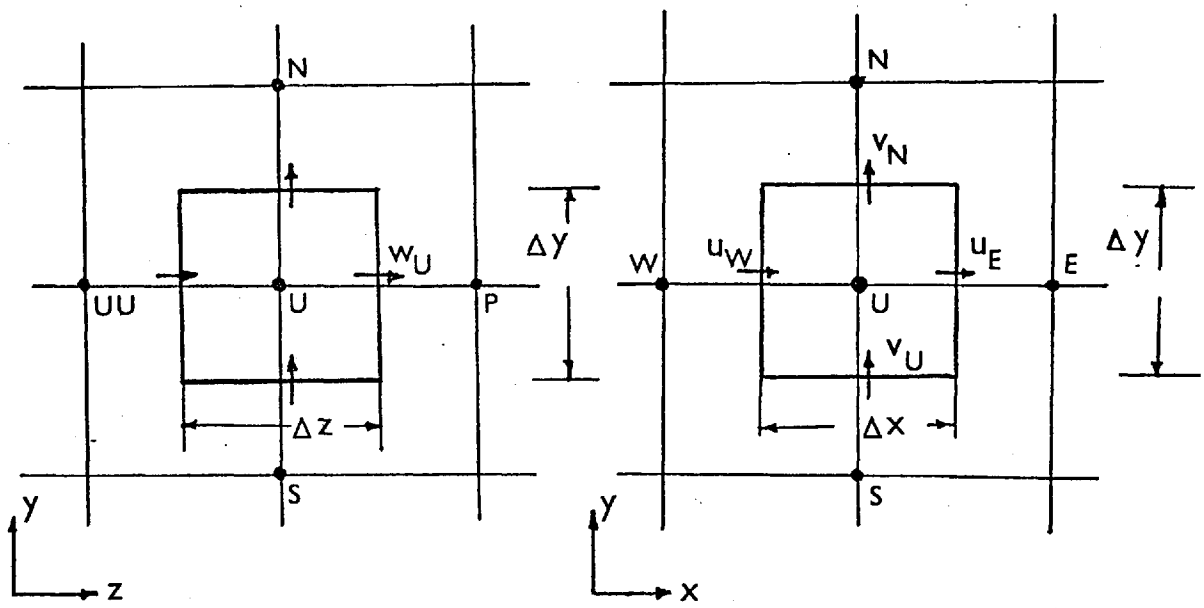

y-z plane x-y plane

where a pressure-correction p' is just applied. The grid node U is situated one plane upstream of P; and the nodes N, S, E and W are neighbours to U in the same cross-sectional plane. UU is located one plane further upstream to U.

The pressure correction p'_P applied at P alters the velocity w_U; and thus introduces a mass imbalance at U. The expression for this mass imbalance, $\dot{m}$, is given by:

$$\dot{m} = D_P^W \cdot p'_P \cdot \Delta x . \Delta y \qquad \text{(A2.2.1)}$$

where Δx and Δy are the areas of the control volume normal to the w-velocity and D^W is the coefficient linking the velocity change to the pressure change. The purpose of the present analysis is to obtain expressions for correcting the upstream pressures so as annihilate the mass imbalance $\dot{m}$; the way these expressions are derived is as follows. First, it is assumed that the pressures at locations N, S, E, W and UU remain unchanged; i.e. no corrections are made at these locations to counteract the effects of p_P'. Thus the mass imbalance $\dot{m}$ is assumed to be corrected solely by changing the pressure at U. If the correction to this pressure is denoted by p_U'', the expressions for the velocity changes may be expressed as follows.

$$u_E' = - p_U'' \, D_E^u \qquad \text{(A2.2.2)}$$

$$u_U' = p_U'' \, D_U^u \qquad \text{(A2.2.3)}$$

$$v_N' = - p_U'' \, D_N^v \qquad \text{(A2.2.4)}$$

$$v_U' = p_U'' \, D_U^v \qquad \text{(A2.2.5)}$$

$$w_P' = - D_P^w \, p_U'' \qquad \text{(A2.2.6)}$$

and

$$w_U' = D_U^w \, p_U'' \qquad \text{(A2.2.7)}$$

The above expressions follow from the linearised momentum equations derived in sec. (4.2). The quantities D^u, D^v, D^w are the coefficients which link the velocity-changes to the pressure corrections.

A mass balance is now made for the control volume shown in Figure (A2.1). The mass-balance equation, incorporating the velocity-changes, is written as

$$\Delta z\ \Delta y\ (u_E' - u_U') + \Delta x\ \Delta z\ (v_N' - v_U')$$

$$+ \Delta x\ \Delta y\ (w_P' - w_U') = \dot{m} \qquad \text{(A2.2.8)}$$

where Δx, Δy, Δz are the dimensions of the control volume. The expressions for velocity changes are now substituted into the above equation; and the following expression for p_U'' is obtained.

$$p_U'' = \frac{p_P' \cdot \Delta x\ \Delta y\ D_P^w}{(\Delta y\ \Delta z)\ (D_E^u + D_U^u) + \Delta x\ \Delta z\ (D_N^v + D_U^v) + (\Delta x\ \Delta y)\ (D_P^w + D_U^w)} \qquad \text{(A2.2.9)}$$

Or, in short,

$$p_U'' = \beta \cdot p_P' \qquad \text{(A2.2.10)}$$

Where,

$$\beta \equiv \frac{\Delta x \Delta y \; D_P^{\,w}}{(\Delta y\, \Delta z)\,(D_E^{\,u} + D_U^{\,u}) + (\Delta x\, \Delta z)\,(D_N^{\,v} + D_U^{\,v}) + (\Delta x\, \Delta y)\,(D_P^{\,w} + D_U^{\,w})} \qquad \text{(A2.2.11)}$$

The quantity β in the above expression represents the fraction of p_p' which is applied to the pressure at U to compensate for the mass imbalance $\dot{m}$.

It can be seen easily that the corrections made at U will also now introduce new mass imbalance at UU; and will therefore necessitate pressure corrections at UU. The corrections at UU will in turn effect other upstream locations; and therefore it turns out that all upstream pressures need to be adjusted to compensate for the effects of p_p'. However, since the value of β reduces in a geometric way with distance from the point P, it is usually necessary to consider only about 5 or 6 planes, at any time. For a location 'n' planes upstream of P, the appropriate correction is calculated from the following relation

$$p_n'' = \beta_n\, p_{n-1}'' = \beta_{n-1} \cdot \beta_n \cdot p_{n-2}'' = \beta_1 \cdot \beta_2 \cdot \beta_3 \cdots \beta_n \cdot p_p' \qquad \text{(A2.2.12)}$$

where the 'β's have the expression given in (A2.2.9) It is necessary to note that the values of D^u, D^v and D^w used in the expression for β need to be approximated by the corresponding values at the location P; this approximation is necessary because the coefficients D^u, D^v, D^w are not stored in a three-dimensional array; and are available for only one cross-sectional plane at any time.

The modification described in this appendix was tested in the calculation of two different partially-parabolic flows situations. In both flows, it has been observed that the present modification gave savings in computer time to the extent of 25 percent.

APPENDIX A3

CORRECTIONS TO THE EXPERIMENTAL DATA

This appendix lists the various corrections applied to the experimental data obtained in the present investigation. These corrections have been obtained by calibrating the measuring devices against standard instruments. The calibration experiments from which the present corrections have been derived were performed by Young (1972). The various corrections applied to the present experimental data are as follows.

1) Correction to the measured angles

(a) For measurements with pitot-directional probe = 0.5^{o}.

(b) For measurements with total-head probe = 0.5^{o}.

2) Corrections to static pressure measured by the pitot-directional probe

(a) Correction for blocked static-holes.

It was observed (Young (1972)) that the static pressure measured by the pitot-directional probe was in slight error when compared against that measured by a standard pitot static probe. This discrepancy was attributed to the blockage of one of the static-pressure

holes (total 8 in number) on the pitot-directional probe. The correction to this end to the measured static pressure was 0.02796 lbf/ft^2 in a nominal value of 1 lbf/ft^2.

(b) Correction for displaced position of the static pressure holes

It may be seen, from the construction of the probes that the location where the static pressure is measured is slightly different from that where the total pressure is measured. For this reason, in calculating the velocity, the measured static pressure was corrected to be appropriate to the location where the total pressure was measured. This correction is given approximately by the relation

$$\Delta p = \frac{0.85}{12} \cdot \frac{dp}{dx} \qquad \text{(A3.1)}$$

where $\frac{dp}{dx}$ is the pressure gradient along the transverse direction (x). The nominal value of this correction was 0.12 lbf/ft^2.

3) Displacement correction to the Pitot tube height

The pitot-tube heights were corrected to account for the displacement of the pressure centre of a pitot probe, when it is placed in a shear flow. This correction was calculated from the following relation (McMillan (1957)):

$$\Delta h = 0.15\ d \qquad \text{(A3.2)}$$

where,

Δh is the correction to the pitot tube height and d is the diameter of the pitot tube.

4) Correction to the wall static pressure

The wall static pressures were observed to be in slight error; the necessary correction was - .00822 lbf/ft^2 in a nominal value of 1 lbf/ft^2.

5) Corrections due to temperature effects on the transducer

Following correction was recommended by the manufacturer, to compensate for the effect of room temperature T on the voltage output of the transducer.

For 35° F $< T <$ 75° F correction (in volts)

$$= .03894 - .0005125 * T$$

For 75° F $< T <$ 135° F correction (in volts)

$$= .008 - .0001 * T.$$